



UNIVERSITY OF  
LIVERPOOL

**COMPUTATIONAL ANALYSIS OF DYNAMICS WITHIN THE  
NUCLEAR FACTOR-KAPPA $\beta$  SIGNALLING SYSTEM**

*Thesis submitted in accordance with the requirements of the University of Liverpool  
for the degree of Doctor in Philosophy*

*by*

**Simon Peter West**

**July 2012**

## **Declaration**

This thesis is the result of my own work, unless otherwise stated, and it is based upon the results from experimental and theoretical work performed as a PhD student between October 2009 and July 2012 in the department of Biological Sciences within the University of Liverpool.

Neither this thesis nor any part of it has been submitted in support of an application for another degree or qualification at this or any other University or other institute of learning.

Simon West

July 2012

## Acknowledgements

There are many people who have aided me in the completion of this task - a big thank you to all of you. Firstly, I'd like to thank my supervisors Prof Chris Sanderson, Dr Rachel Bearon and Prof Mike White. Thanks for all the support and opportunities you have given me, and everything you have done to help me to complete this thesis on an accelerated schedule.

In addition to my supervisors there are many people that I have worked with and without their advice and encouragement I would not have reached this point. A very BIG thanks to Pawel Paszek, while his criticism has been plentiful it is always constructive and without his guidance over the last three years I would not have completed my PhD. Thanks must also go to Prof Vadim Biktashev who helped to make a reluctant student more rigorous and has put me on the path to my first publication. Thanks to Dan Woodcock (aka #2) for all his help and suggestions when the NF- $\kappa$ B world was getting a little hotter. Thanks to Cath Heyward my diclofenac buddy and neighbour, who in addition to dealing with my many questions over the last year also proof read this tome – yes typos are her fault! Many thanks to Dave Spiller for his A20 suggestions, mad microscope skills and the occasional pint! I would also like to thank John 'the Daddy' Ankers, James 'the actual daddy' Bagnall and Damon Daniels for all their advice and generally listening to my complaining. There are many other people both in Liverpool and Manchester who have helped over the years. Dr Violaine See for giving me a home for the last 18 months. Many thanks to Anne H, Haleh, Carol and Sarah for the delicious cake and the gossip. Thank you to Anne M, Anthony, Claire, Connie, David T, Louise, Nisha, Sheila, Steph, and Raheela for you lab help, friendship and advice over the last three years. To everybody else who has been a part of the See and White groups thank you very, very much, unfortunately I can't list you all as I'm trying to keep this to a page. Finally a big heads up to my fellow SABR students Karen and James who have been with me from the beginning. It has been a memorable four years and that is thanks to you guys and your unconventional attitude towards life!

Beyond work thanks to everyone who has been a friend over the years. The PhD students at Liverpool who I've enjoyed lunching with over the last three years, those include Jane, Louise, Jen, Jo and many more. Thanks to my housemates Jenna, Tash and Indy. The 'House of Hot' has been an epic place to live and I will miss you lots. All the tramps for giving such good banter over the years and keeping me young in spirit if not in body! Everyone who was part of the MSc at Warwick especially Jo, Joe and Mrs Lewis. Dominic Francis Graham Holdaway for the red wine, Mario Kart and TV cookery backup plan. My Bath buddies Gen, James, Jess, Jo, Laura, Rees and Tam. Many thanks to Sean for everything, but mainly dealing with a moodier Simon than everyone else! Finally thank you to Mum, Dad, Phil, Teresa, Nina, Jay and the Grandparents for all your help and support both financial and emotional over the last 25 years, and for not saying too much when I told you I was going to do another 4 year study!

Lastly, thanks to NF- $\kappa$ B for being a VERY important protein!

## Abstract

The Nuclear Factor kappaB (NF- $\kappa$ B) proteins are a very important family of transcription factors. The signalling system of the NF- $\kappa$ B transcription factors drives cellular inflammation and immune responses, playing a central role in cell proliferation and apoptosis. NF- $\kappa$ B regulates the transcription of over 300 target genes including several negative feedback genes, such as the Inhibitory kappaBs (I $\kappa$ Bs) and zinc-finger protein A20. Disruption to NF- $\kappa$ B signalling has been implicated in many autoimmune diseases and cancers. The ever growing list of diseases in which NF- $\kappa$ B is deregulated has made this one of the most intensely studied eukaryotic transcription factors.

In response to continuous TNF $\alpha$  stimulation the system exhibits nuclear-cytoplasmic oscillations in the localisation of NF- $\kappa$ B with a robust period. Pulsatile stimulation causes nuclear translocations of NF- $\kappa$ B that are entrained to the pulse frequency. The altered frequency of these oscillations results in a different pattern of NF- $\kappa$ B dependent gene expression. This suggests the hypothesis that altering the frequency of NF- $\kappa$ B oscillations could provide a novel means to control the output of the system, allowing the exploitation of this system as a therapeutic target.

The complex nonlinear dynamics in the NF- $\kappa$ B system make it an ideal candidate for a systems level analysis. Throughout this thesis a Systems Biology approach has been used to elucidate, both computationally and experimentally, how the period of NF- $\kappa$ B oscillations can be altered. This involved the development of a computational framework to characterise core network topology and parameter sensitivities of a recent deterministic model of the NF- $\kappa$ B system. Within this framework a model reduction algorithm has been described that has general applications to many other biochemical models. Bifurcation theory has been employed to characterise the system's sensitivities.

Computational analyses provided a basis to relate new experimental insights to our existing understanding of the system. Ectopic expression of the negative feedbacks I $\kappa$ B $\alpha$  and A20 showed different effects on the NF- $\kappa$ B oscillatory period. Computational analysis demonstrated that the manipulation of the delay in their transcriptional initiation could markedly change their influence on the oscillations. Single cell imaging also revealed a portion of A20 localised in perinuclear compartments. Two novel perturbations to the NF- $\kappa$ B dynamics are also considered: the effect after treatment with the non-steroidal anti-inflammatory drug (NSAID) diclofenac, and the effect of altered temperature. Theoretical analyses of these data lead to a number of hypotheses about how such perturbations influence the system.

Ultimately, this thesis presents a number of new insights into modulating the period of NF- $\kappa$ B oscillations and computational tools to aid in the analysis of biochemical networks.

---

## Table of Contents

<b>Declaration</b> .....	<b>i</b>
<b>Acknowledgements</b> .....	<b>ii</b>
<b>Abstract</b> .....	<b>iii</b>
<b>Table of Contents</b> .....	<b>iv</b>
<b>List of Abbreviations</b> .....	<b>ix</b>
<b>List of Figures</b> .....	<b>xii</b>
<b>List of Tables</b> .....	<b>xv</b>
<b>Chapter 1 – Introduction</b> .....	<b>1</b>
<b>1.1 Systems Biology</b> .....	<b>2</b>
<b>1.1.1 The Complexity of Biological Signalling Systems</b> .....	<b>2</b>
<b>1.1.2 Systems Biology to Unravel the Complexity</b> .....	<b>6</b>
<b>1.2 Computational Modelling</b> .....	<b>9</b>
<b>1.2.1 Model Building and Deterministic Representations</b> .....	<b>9</b>
<b>1.2.2 Stochastic Representations</b> .....	<b>13</b>
<b>1.2.3 Spatial and Multi-scale Modelling</b> .....	<b>15</b>
<b>1.3 Analysis Methods for Computational Models</b> .....	<b>16</b>
<b>1.3.1 Sensitivity Analysis</b> .....	<b>16</b>
<b>1.3.2 Phase Portrait and Bifurcation Analysis</b> .....	<b>19</b>
<b>1.3.3 Model Reduction Methods</b> .....	<b>22</b>
<b>1.4 Biological Oscillators</b> .....	<b>24</b>
<b>1.5 The NF-<math>\kappa</math>B Signalling Network</b> .....	<b>26</b>
<b>1.5.1 Core Components of the NF-<math>\kappa</math>B System</b> .....	<b>26</b>
<b>1.5.2 Dynamic Behaviour within the NF-<math>\kappa</math>B System</b> .....	<b>29</b>
<b>1.5.3 Computational Models of the NF-<math>\kappa</math>B System</b> .....	<b>31</b>
<b>1.6 Project Motivation and Aims</b> .....	<b>35</b>
<b>1.6.1 Project Motivation</b> .....	<b>35</b>

---

---

1.6.2 Aims and Objectives.....	36
<b>Chapter 2 – Materials and Methods.....</b>	<b>37</b>
2.1 Computational Methods.....	38
2.2 Experimental Techniques.....	38
2.2.1 Reagents.....	38
2.2.2 Plasmids.....	38
2.2.3 Restriction Endonuclease Digestion and Agarose Gel Electrophoresis... .....	39
2.2.4 Cell Culture.....	39
2.2.5 Transfection.....	40
2.2.6 Confocal Microscopy.....	40
2.2.7 Image Analysis.....	40
2.2.8 Western Blotting.....	41
2.2.9 Quantitative RT-PCR.....	42
2.2.10 Microarray.....	43
2.2.11 Cell Treatments.....	44
2.2.11.1 Diclofenac.....	44
2.2.11.2 Temperature.....	44
<b>Chapter 3 – A Minimal Model of the NF-<math>\kappa</math>B System .....</b>	<b>45</b>
3.1 Minimal Models: A Systems Biology Tool.....	46
3.2 A Method of “Speed Coefficients”.....	48
3.2.1 Perturbation Theory.....	48
3.2.2 Method of Speed Coefficients for Model Reduction.....	50
3.3 Minimal Model of the NF- $\kappa$ B System with respect to Continuous TNF $\alpha$ Stimulation.....	52
3.3.1 Initial Model Simplification.....	52
3.3.2 Outline of Key Reduction Steps.....	55
3.4 Effect of the Method on Dynamic Properties of the NF- $\kappa$ B Model.....	60

---

---

3.5	Model Reduction with Respect to Pulsed TNF $\alpha$ Input .....	63
3.6	Discussion.....	66
<b>Chapter 4 – Computational Analysis of Period Modulation in the NF-<math>\kappa</math>B System</b> .....		<b>70</b>
4.1	Introduction .....	71
4.2	Period Sensitivity .....	73
4.3	The Effect of Multiple Parameter Changes.....	86
4.4	Discussion.....	95
<b>Chapter 5 – Investigating the Role of the Negative Feedbacks I<math>\kappa</math>B<math>\alpha</math> and A20 .....</b> .....		<b>98</b>
5.1	Introduction.....	99
5.2	Analysis of the Effects of I $\kappa$ B $\alpha$ and A20 Feedback on NF- $\kappa$ B Dynamics . .....	101
5.2.1	Computational Analysis of I $\kappa$ B $\alpha$ and A20 Transcription .....	101
5.2.2	Robustness of the Period to I $\kappa$ B $\alpha$ Transcription.....	105
5.2.3	Characterising NF- $\kappa$ B and I $\kappa$ B $\alpha$ Dynamics Using BAC Constructs..... .....	108
5.2.4	Developing a Model Robust to I $\kappa$ B $\alpha$ Transcription Rate.....	110
5.2.5	The Effect of A20 Feedback on NF- $\kappa$ B Oscillations.....	116
5.2.6	One and Two-dimensional Bifurcation Analysis for A20.....	119
5.2.7	Perinuclear Speckling of A20.....	121
5.3	Discussion.....	127
5.3.1	Implications of A20 Expression Data on Future Modelling .....	127
5.3.2	General Discussion.....	128
<b>Chapter 6 – Pharmacological and Temperature Perturbations to the NF-<math>\kappa</math>B System.....</b>		<b>134</b>
6.1	Introduction.....	135
6.2	Pharmacological Modulation of the NF- $\kappa$ B System.....	135

---

---

<b>6.2.1</b>	<b>Pharmacological Introduction .....</b>	<b>135</b>
<b>6.2.2</b>	<b>Pharmacological Results.....</b>	<b>137</b>
<b>6.2.2.1</b>	<b>Characterisation of RelA Oscillations After Treatment with Diclofenac .....</b>	<b>137</b>
<b>6.2.2.2</b>	<b>The Effect of Diclofenac Treatment on the Degradation and Phosphorylation of I<math>\kappa</math>B<math>\alpha</math>.....</b>	<b>140</b>
<b>6.2.2.3</b>	<b>Computational Analysis of the IKK Module.....</b>	<b>142</b>
<b>6.2.2.4</b>	<b>Delayed Activation of IKK.....</b>	<b>146</b>
<b>6.2.3</b>	<b>Conclusions &amp; Future Outlook .....</b>	<b>152</b>
<b>6.3</b>	<b>The Effect of Temperature on the NF-<math>\kappa</math>B System .....</b>	<b>155</b>
<b>6.3.1</b>	<b>Temperature Introduction .....</b>	<b>155</b>
<b>6.3.2</b>	<b>Temperature Results.....</b>	<b>157</b>
<b>6.3.2.1</b>	<b>Characterisation of RelA Oscillations at Different Temperatures .....</b>	<b>157</b>
<b>6.3.2.2</b>	<b>Understanding the Temperature influence on NF-<math>\kappa</math>B Dynamics Using the Balance Equations .....</b>	<b>159</b>
<b>6.3.2.3</b>	<b>I<math>\kappa</math>B<math>\alpha</math> and A20 mRNA Expression Profiles at Different Temperatures .....</b>	<b>162</b>
<b>6.3.2.4</b>	<b>A Temperature Sensitive NF-<math>\kappa</math>B Model.....</b>	<b>164</b>
<b>6.3.2.5</b>	<b>Validating the Temperature Sensitive NF-<math>\kappa</math>B Model .....</b>	<b>166</b>
<b>6.3.2.6</b>	<b>Refinement of the Temperature Sensitive Model .....</b>	<b>168</b>
<b>6.3.2.7</b>	<b>The Effect of Pulsatile and Low Dose TNF<math>\alpha</math> Stimulation on the Dual Delay Model.....</b>	<b>170</b>
<b>6.3.2.8</b>	<b>The Role of I<math>\kappa</math>B<math>\alpha</math> and A20 Feedback in the Dual Delay Model .....</b>	<b>173</b>
<b>6.3.3</b>	<b>Conclusions &amp; Future Outlook .....</b>	<b>176</b>
<b>6.4</b>	<b>Discussion.....</b>	<b>181</b>
<b>Chapter 7 – Final Discussion .....</b>		<b>183</b>
<b>7.1</b>	<b>Introduction .....</b>	<b>184</b>
<b>7.2</b>	<b>Reflection on Project Aims.....</b>	<b>185</b>
<b>7.3</b>	<b>Computational Methods for Analysis of Biological Models.....</b>	<b>186</b>

---



---

<b>7.4</b>	<b>The Importance of Negative Feedbacks in Oscillatory Systems .....</b>	<b>189</b>
<b>7.5</b>	<b>Modulation of the NF-<math>\kappa</math>B Period .....</b>	<b>190</b>
<b>7.6</b>	<b>Future Perspective .....</b>	<b>193</b>
<b>7.7</b>	<b>Final Comment.....</b>	<b>195</b>
	<b>Chapter 8 – Bibliography .....</b>	<b>197</b>
	<b>Appendix 1 – Ashall Model Representations .....</b>	<b>211</b>
<b>A1.1</b>	<b>Ashall Model Equations and Parameters .....</b>	<b>212</b>
<b>A1.2</b>	<b>11-Variable Representation of the Ashall Model .....</b>	<b>215</b>
	<b>Appendix 2 – Minimal Models .....</b>	<b>217</b>
<b>A2.1</b>	<b>Equations for the <math>z_0p_1y_1v_1s_1w_1</math> Model.....</b>	<b>218</b>
<b>A2.2</b>	<b>Equations for the <math>z_0p_0y_0v_0</math> Model.....</b>	<b>221</b>
	<b>Appendix 3 – Delay Models .....</b>	<b>222</b>
<b>A3.1</b>	<b>Delayed IKK Activation.....</b>	<b>223</b>
<b>A3.2</b>	<b>Delayed A20 Transcription .....</b>	<b>226</b>
<b>A3.3</b>	<b>Delayed I<math>\kappa</math>B<math>\alpha</math> Transcription.....</b>	<b>229</b>
<b>A3.4</b>	<b>Dual Delay Model .....</b>	<b>232</b>

## List of Abbreviations

Abbreviations used as per SI unit conventions with the following additions:

ARD	Ankyrin Repeat Domain
BAC	Bacterial Artificial Chromosome
CA	Cellular Automata
CBP	CREB-Binding Protein
CCI	Centre for Cell Imaging, University of Liverpool
ChIP	Chromatin Immunoprecipitation
CME	Chemical Master Equation
CMV	Cytomegalovirus
CYLD	Cylindromatosis
DDE	Delay Differential Equation
DSIF	DRB Sensitivity Inducing Factor
DNA	Deoxyribose Nucleic Acid
dsRedXP	DsRed-Express
EGFP	Enhanced Green Fluorescent Protein
ELIE	Elongation Inhibitory Element
EMSA	Electrophoretic Mobility Shift Assay
FADD	Fas-Associated Death Domain
FBS	Fetal Bovine Serum
FCS	Fluorescent Correlation Spectroscopy
HB	Hopf Bifurcation
HeLa	Human Cervical Carcinoma
IKK	I $\kappa$ B Kinase
I $\kappa$ B	Inhibitory $\kappa$ B

LHS	Left-Hand Side
LMB	Leptomycin B
LPS	Lipopolysaccharide
LSM	Laser Scanning Microscopy
MAPK	Mitogen-Activated Protein Kinase
MCP-1	Monocyte chemotactic protein-1
mRNA	Messenger Ribose Nucleic Acid
mins	Minutes
N:C	Nuclear-cytoplasmic
NEMO	NF- $\kappa$ B Essential Modifier (also called IKK $\gamma$ )
NES	Nuclear Export Sequence
NF- $\kappa$ B	Nuclear Factor kappaB
NLS	Nuclear Localisation Sequence
ODE	Ordinary Differential Equation
PDE	Partial Differential Equation
Pol II	RNA Polymerase II
pp	Proximal Promoter
p-TEFb	Positive Transcription Elongation Factor - b
QSSA	Quasi-steady State Approximation
RHS	Right-Hand Side
ROI	Region of Interest
RT-PCR	Reverse Transcriptase Polymerase Chain Reaction
RANTES	Regulated upon Activation Normal T Cell Expressed and Secreted
Rel	Reticuloendotheliosis oncogene
RHD	Rel Homology Domain

RIP	Receptor Interacting Protein
RRE	Reaction Rate Equation
SD	Standard Deviation
SEM	Standard Error of the Mean
SM	Simplified Model
SMC	Systems Microscopy Centre, University of Manchester
siRNA	Small Interfering Ribose Nucleic Acid
SK-N-AS	Human S-Type Neuroblastoma
Sp1	Specificity Protein 1
TAK1	TGF- $\beta$ Activated Kinase
TNF-R	Tumour Necrosis Factor Receptor
TNF $\alpha$	Tumour Necrosis Factor Alpha
TRADD	TNF-R Associated Death Domain
TRAF	TNF-R Associated Factor
USF1	Upstream Transcription Factor 1
YFP	Yellow Fluorescent Protein

## List of Figures

### Chapter 1 - Introduction

Figure 1.1	Three example motifs from cellular signalling pathways.	-4-
Figure 1.2	Interdisciplinary research cycle.	-7-
Figure 1.3	Abstraction of transcription for model building.	-10-
Figure 1.4	A series of phase planes demonstrating fixed points and limit cycles solutions of ODEs.	-20-
Figure 1.5	Schematic of the NF- $\kappa$ B signalling system.	-28-
Figure 1.6	Example of NF- $\kappa$ B nucleo-cytoplasmic oscillations.	-30-

### Chapter 3 – A Minimal Model of the NF- $\kappa$ B System

Figure 3.1	Semi-logarithmic plot of the speed coefficients for the Simplified Model.	-49-
Figure 3.2	Comparison of the SM solution with the $z_0$ model solutions.	-55-
Figure 3.3	Comparison of the $z_0$ , $z_0p_0$ , and $z_0p_1$ models.	-56-
Figure 3.4	Semi-logarithmic plot of the speed coefficients for the $z_0p_0y_0v_0s_0$ model.	-56-
Figure 3.5	Comparison of the $z_0p_0y_0v_0s_0$ , $z_0p_0y_0v_0s_0w_0$ and $z_0p_0y_0v_0s_0w_1$ models.	-57-
Figure 3.6	Comparison of the SM, $z_0p_0y_0v_0s_0w_1$ and $z_0p_1y_1v_1s_1w_1$ models.	-59-
Figure 3.7	Bifurcation analysis for each stage of the model reduction process.	-60-
Figure 3.8	Comparison of the reduced model and the minimal model of Krishna <i>et al.</i>	-61-
Figure 3.9	Comparison of different minimal models response to a pulsed TNF $\alpha$ input.	-65-
Figure 3.10	Speed coefficients for the $z_0p_0y_0$ model calculated using pulsed or continuous TNF $\alpha$ input.	-65-
Figure 3.11	Network diagrams of the SM and the two 4-variable reduced model.	-66-

### Chapter 4 – Computational Analysis of Period Modulation in the NF- $\kappa$ B System

Figure 4.1	Control coefficients for the Ashall model.	-74-
Figure 4.2	Example output from XPPAUT.	-77-
Figure 4.3	Example of the measurements taken from a period bifurcation.	-79-
Figure 4.4	Global analysis of the period bifurcations of the Ashall model.	-80-
Figure 4.5	Period bifurcation with respect to I $\kappa$ B $\alpha$ translation rate and I $\kappa$ B $\alpha$ mRNA degradation.	-82-
Figure 4.6	Local analysis of the period bifurcations of the Ashall model.	-83-

Figure 4.7	The effect of multiple random parameter changes on the period of the Ashall model solution.	-86-
Figure 4.8	Period bifurcation diagrams with respect to A20 transcription and translation rates.	-88-
Figure 4.9	The number of non-oscillating solutions after multiple parameter changes.	-88-
Figure 4.10	Correlation between predicted solution period and the simulated solution period after multiple parameter changes.	-90-
Figure 4.11	Distribution of the parameter values that resulted in solutions with substantially altered periods.	-92-
Figure 4.12	Bifurcation analysis with respect to the level of IKK as multiple parameters are changed.	-94-

## Chapter 5 – Investigating the Role of the Negative Feedbacks $I\kappa B\alpha$ and A20

Figure 5.1	The change in the solution period as $I\kappa B\alpha$ or A20 transcription rate is varied.	-101-
Figure 5.2	The change in the solution period as $I\kappa B\alpha$ and A20 transcription rates are co-varied.	-103-
Figure 5.3	The change in the solution period as $I\kappa B\alpha$ transcription rate and NF- $\kappa B$ levels are co-varied.	-106-
Figure 5.4	Comparison of NF- $\kappa B$ oscillation periods using different reported constructs.	-110-
Figure 5.5	(A) The change in model period as $I\kappa B\alpha$ transcription rate is varied. (B) Control coefficients for the Ashall model with altered parameters.	-111-
Figure 5.6	Exploration of the effect of changing $I\kappa B\alpha$ -related on the bifurcation structure with respect to $I\kappa B\alpha$ transcription rate.	-112-
Figure 5.7	The change in the solution period as $I\kappa B\alpha$ transcription and degradation rates are co-varied.	-114-
Figure 5.8	Properties of the Ashall model after alteration to make it robust to $I\kappa B\alpha$ transcription rate.	-115-
Figure 5.9	Fluorescence confocal images of cell transfected with RelA and A20 reporters.	-117-
Figure 5.10	Characterisation of RelA dynamics in cells transfected with RelA and A20 reporters.	-119-
Figure 5.11	Bifurcation analysis with respect to A20 transcription rate.	-120-
Figure 5.12	The change in the solution period as A20 transcription rate and NF- $\kappa B$ levels are co-varied.	-121-
Figure 5.13	Fluorescence confocal images of perinuclear speckling of A20.	-123-
Figure 5.14	Analysis of the dynamics of the A20 perinuclear speckles.	-125-
Figure 5.15	Fluorescence confocal images showing an example of excretion of A20 speckles.	-126-

---

## Chapter 6 – Pharmacological and Temperature Perturbations to the NF- $\kappa$ B System

Figure 6.1	Example RelA dynamics in cells treated with diclofenac.	-137-
Figure 6.2	Characterisation of RelA dynamics in cells treated with diclofenac.	-139-
Figure 6.3	Western blot analysis of I $\kappa$ B $\alpha$ and phospho-I $\kappa$ B $\alpha$ in cells treated with diclofenac.	-141-
Figure 6.4	The effect of co-varying IKK-related parameters on the period of the limit cycle.	-144-
Figure 6.5	Analysis of the change in the IKK-related parameters required to alter the model period by 60%.	-146-
Figure 6.6	Analysis of the solution of the Ashall model with delayed IKK activation.	-149-
Figure 6.7	Period of the limit cycle for different lengths of delay in the activation of IKK.	-150-
Figure 6.8	Comparison of the original solution of the Ashall model and the model adapted to recapitulate treatment with diclofenac.	-151-
Figure 6.9	Example RelA dynamics in cells imaged at different temperatures.	-157-
Figure 6.10	Summary of the RelA peak-to-peak timings at different temperatures.	-159-
Figure 6.11	Logarithmic control coefficients for the Ashall model.	-161-
Figure 6.12	RelA, I $\kappa$ B $\alpha$ , I $\kappa$ B $\epsilon$ and A20 expression profiles at 37 and 40°C.	-163-
Figure 6.13	Solutions of the model with delayed A20 transcription.	-165-
Figure 6.14	Quantitative RT-PCR for I $\kappa$ B $\alpha$ and A20 at 37 and 40°C.	-167-
Figure 6.15	Analysis of the model with delayed I $\kappa$ B $\alpha$ and A20 transcription.	-169-
Figure 6.16	Comparison of the Ashall and dual delay models' response to pulsed TNF $\alpha$ input.	-170-
Figure 6.17	Bifurcation analysis with respect to TNF $\alpha$ dose for the Ashall, Low dose TNF $\alpha$ and dual delay models.	-172-
Figure 6.18	The change in the period of the solution of the dual delay model as I $\kappa$ B $\alpha$ or A20 transcription is varied.	-173-
Figure 6.19	The effect of increasing the delay in I $\kappa$ B $\alpha$ transcription on the period bifurcation with respect to I $\kappa$ B $\alpha$ transcription rate.	-175-

## List of Tables

### Chapter 1 – Introduction

Table 1.1	Examples of biological systems that show oscillatory behaviour	-25-
-----------	--	------

### Chapter 2 – Materials and Methods

Table 2.1	Common tissue culture vessels, cell densities and medium volumes.	-39-
Table 2.2	Summary of Western blot antibodies.	-42-
Table 2.3	Quantitative RT-PCR primer sequences.	-43-
Table 2.4	Quantitative RT-PCR cycle conditions.	-43-

### Chapter 3 – A Minimal Model of the NF- $\kappa$ B System

Table 3.1	Reassignment of variable and parameters in the Ashall <i>et al.</i> model.	-53-
Table 3.2	Key dynamic features of each reduced model.	-59-

### Chapter 4 – Computational Analysis of Period Modulation in the NF- $\kappa$ B System

Table 4.1	Comparison of the most sensitive parameters in the Ashall model identified by different sensitivity analysis methods.	-85-
-----------	---	------

### Chapter 6 – Pharmacological and Temperature Perturbations to the NF- $\kappa$ B System

Table 6.1	Summary of RelA peak-to-peak timings at different temperatures.	-158-
Table 6.2	Summary of the delay parameters required to recapitulate the NF- $\kappa$ B dynamics at all temperatures in the dual delay model.	-170-



# **Chapter 1 – Introduction**

## **1.1 – Systems Biology**

Biological systems are extremely complex. Most cellular processes are governed by large numbers of functionally diverse components, which interact selectively and nonlinearly to produce coherent outcomes (Kitano, 2002b). In recent years molecular biology has generated a wealth of information about the components of these biological systems. However, knowledge of the components alone is not sufficient to understand the emergent function of the overall system. It is important to understand how these parts interact with each other and their environment. The interactions of these components often give rise to nonlinear dynamical effects. Yet the large number of components in dynamic biological systems (Meng *et al.*, 2004) - often incorporating complex feedback mechanisms – means that this is not a trivial task.

Systems Biology aims to address this complexity by integrating biological experiments with computational modelling to gain an insight into how the system functions as a whole. There are many definitions of Systems Biology; a common theme among these is the idea of integrating experimental data with theoretical analysis in re-enforcing cycles. The concept of applying mathematical models to solve biological problems is by no means novel (Hodgkin and Huxley, 1952). However, with the current developments in biological techniques and the ability to generate high-throughput data sets there is now a “golden opportunity for systems level analysis” (Kitano, 2002b). Computational modelling can be used within the experimental cycle to understand these complex, nonlinear interactions and direct future experimental design.

### **1.1.1 – The Complexity of Biological Signalling Systems**

Intracellular signalling pathways control cellular responses to external physiological signals. The components of these pathways control the flow of information from the external environment to an effector resulting in a response, such as changes in gene expression, morphology or movement (Alberts, 2002). In general, cells receive a signal at a receptor - a transmembrane protein that receives extracellular stimuli through ligands binding to an extracellular domain, which then transmits this signal to intracellular components by conformational change, dimerization or

---

internalisation (Klipp and Liebermeister, 2006). Upon receptor activation a coordinated series of events ensues, causing the transduction of this signal and the production of an effective response. The steps in these pathways form complex biochemical circuits consisting of protein-protein interactions and modification cascades, which process, encode and integrate signals within a network (Kholodenko, 2006).

Signals are transduced through protein interactions, modifications or a combination of these events. Proteins can be covalently modified in a number of ways including phosphorylation, acetylation and ubiquitination. These modifications can occur collectively on the same protein at multiple sites to change their activity or specificity for binding partners (Alberts, 2002). Signalling proteins are also regulated by degradation. Activation of the pathway can result in the stabilisation of an activator or degradation of an inhibitor, often through the ubiquitin-proteasome pathway (Alberts, 2002). The localisation of signalling components can also affect their function, by enabling their interaction with targets. Components of signalling pathways often form complexes with scaffold proteins to ensure physical vicinity or correct molecular orientation (Klipp and Liebermeister, 2006).

Specific programmes of gene expression are often required in response to environmental or pathogenic stresses. Therefore, signalling pathways frequently result in the activation of transcription factors that can alter gene expression. This can include the expression of genes that feedback to the signalling circuit forming positive or negative feedback loops. Transcription and translation form additional points of regulation through chromatin remodelling, the recruitment of activators and transcription factors to the promoter, mRNA processing and protein folding (Alberts, 2002).

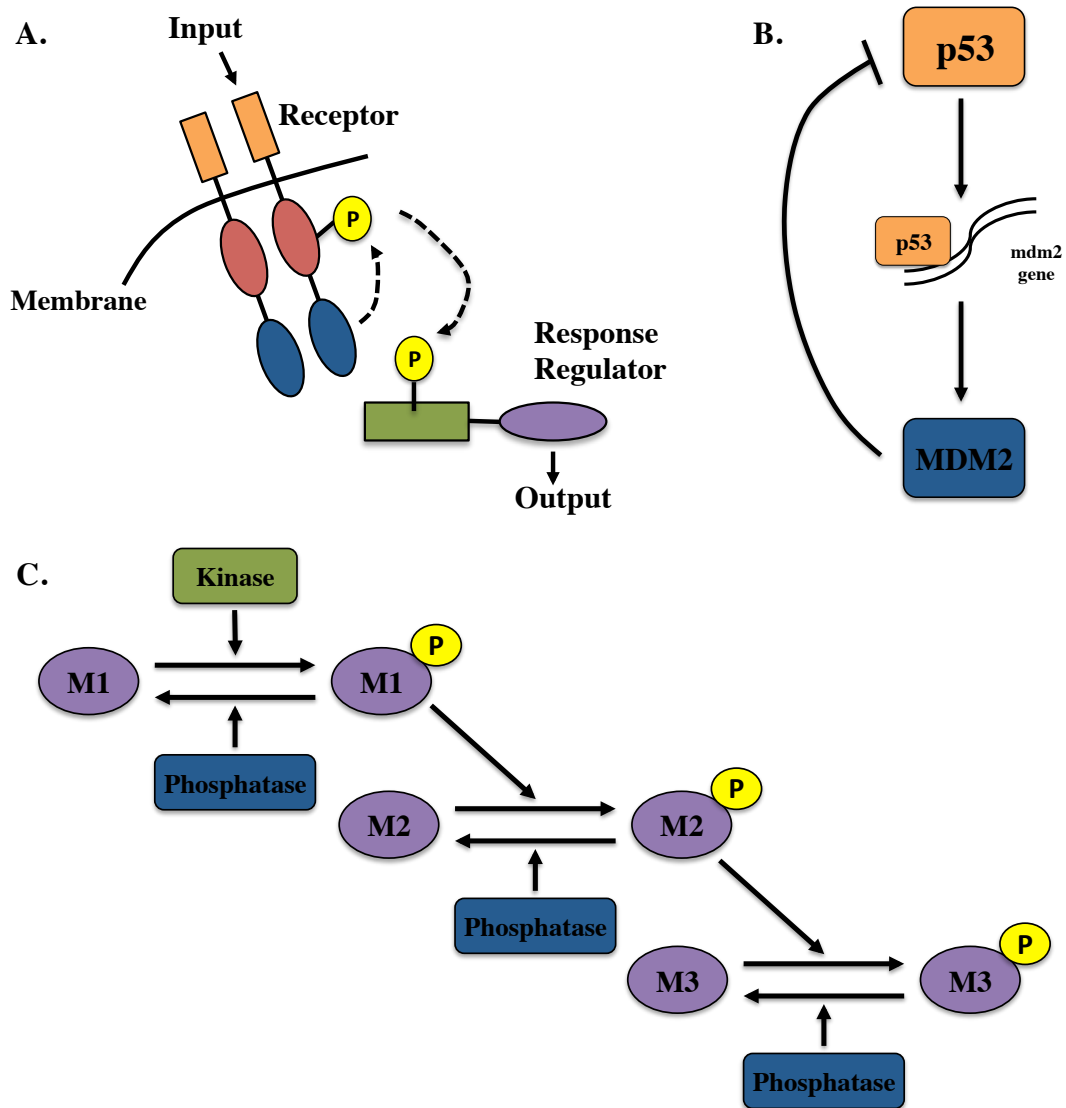


**Figure 1.1** - Three example motifs from cellular signalling pathways. (A) An example of a linear chain, in this case two-component signal transduction adapted from Skerker *et al.* (2008). (B) A negative feedback loop, in this case the p53-MDM2 auto-regulatory loop. Upon stimulation p53 induces transcription of MDM2, which once translated inhibits p53 through protein-protein interaction, adapted from Oren (1999). (C) A general example of a multi-layered phosphorylation cascade this motif is present in the MAPK pathway, adapted from Kholodenko (2006).

The simplest example of a signalling pathway is a linear chain, where the first component or link in the chain receives a signal from an external source and relays this along the chain to the final link, which is capable of eliciting a biological response (Weng *et al.*, 1999). One biological example of this motif is bacterial two-component signal transduction (figure 1.1a). These pathways typically consist of a receptor that auto-phosphorylates in response to a signal and then transfers this

phosphoryl group to a cognate response regulator, which can effect changes in cell physiology or behaviour (Skerker *et al.*, 2008). Signalling networks in mammalian systems tend to be far more complex as they are comprised of multiple components with varying levels of interaction. As the number of components in a system is increased, the number of possible interactions also increases. Numerous network motifs have been shown to exist in signalling systems and sensory transcriptional networks. Starting from the simplest example of a linear signal cascade (figure 1.1a), additional layers of complexity include negative feedback (figure 1.1b), feed-forward and auto-regulatory loops (Alon, 2007). In addition, biological networks are often multi-layered, involving multiple steps in the transduction of the signal from receptor to effector (figure 1.1c). One such example is the Mitogen-Activated Protein (MAP) kinase cascade (Kolch *et al.*, 2005). The MAPK cascade consists of three or four different proteins that specifically catalyse the phosphorylation of the subsequent protein (Klipp and Liebermeister, 2006). Further to the complexity conferred from the network's topology, spatial distribution, thresholds of activation, compartmentalisation and isoforms with partially overlapping function all serve to increase the complexity of these signalling and sensory transcription systems (Weng *et al.*, 1999).

Further complexities in biological systems arise through crosstalk between signalling pathways. Crosstalk can occur in pathways that use a common intermediate to transduce signals, or when signals from one pathway modulate another (Klipp and Liebermeister, 2006). Crosstalk can happen at both the intra- and intercellular level and has been identified between multiple pathways. In signalling networks these points of crosstalk may act as junctions, which integrate signals, or nodes, which split the signal and route it to multiple outputs (Jordan *et al.*, 2000). Crosstalk between systems can help to ensure a cell responds correctly depending on its position in the cell cycle or in the event of multiple stimuli (Brady *et al.*, 2011). For example, crosstalk has also been observed between the pro-inflammatory transcription factor NF- $\kappa$ B and the tumour suppressor p53, where one can effect the transactivation of the other in response to different stimuli. This has been proposed to be through competition for the same co-activator proteins p300 and CREB-binding

protein (CBP) (Webster and Perkins, 1999). Crosstalk results in combined and expanded networks with an even greater number of components.

From an evolutionary perspective complexity in biological signalling helps to ensure the fidelity of the signal is maintained and that the cell can differentiate between the many signals it receives, therefore allowing the cell to mount a robust and appropriate response and negate the impact of noise within the system. However, network complexity poses a huge challenge in developing an understanding of the system and how to effectively modulate a system when considering it as a therapeutic target.

### **1.1.2 – Systems Biology to Unravel the Complexity**

Classical ‘reductionist’ approaches to biology endeavour to build an understanding of a system by determining the function of each component one by one. However, as has been stated, signalling networks and other biological systems can be composed of a large number of components which can have partially overlapping functions and interact with several other factors. To understand such a system via single-component analysis would be a huge combinatorial challenge. Moreover, many biological networks display emergent properties that are the result of the interactions of multiple components of the network and cannot be understood by studying isolated reactions (Bhalla and Iyengar, 1999). One example of an emergent property is the nuclear-cytoplasmic oscillations in the localisation of the NF- $\kappa$ B transcription factor (Nelson et al., 2004). These oscillations are the result of the interactions between multiple components; in this case the transcription factor and its inhibitors.

Systems level approaches endeavour to analyse the behaviour of a given system as a whole, relating our knowledge of the components and their interactions to its overall function. There are different definitions of Systems Biology, but a common theme among many is the use of an interdisciplinary approach to integrate experimental data with theoretical analysis. Interdisciplinary research provides a new step in the iterative cycle of biological research that classically involves hypothesis generation, experimentation and validation; namely, the development and refinement of computational models (figure 1.2). Computational models can be developed based on

current biological understanding to generate non-intuitive hypotheses and direct future experimental design (Kitano, 2002b). These models are usually ‘disproven’ by the experimental data, which leads to refinement of the model and the generation of new hypotheses to be tested. This work proceeds in iterative cycles to continually build our knowledge of the system.

With the advent of high-throughput data collection methods such as genomics, transcriptomics and proteomics, interdisciplinary techniques are more vital than ever to aid in the analysis and dissection of these large data sets. With the production of these data it has become apparent that the magnitude of complexity of interactions in a cell is too vast to be understood by intuition alone (Ideker *et al.*, 2001). Therefore, computational modelling has becoming a necessary tool in biological research.

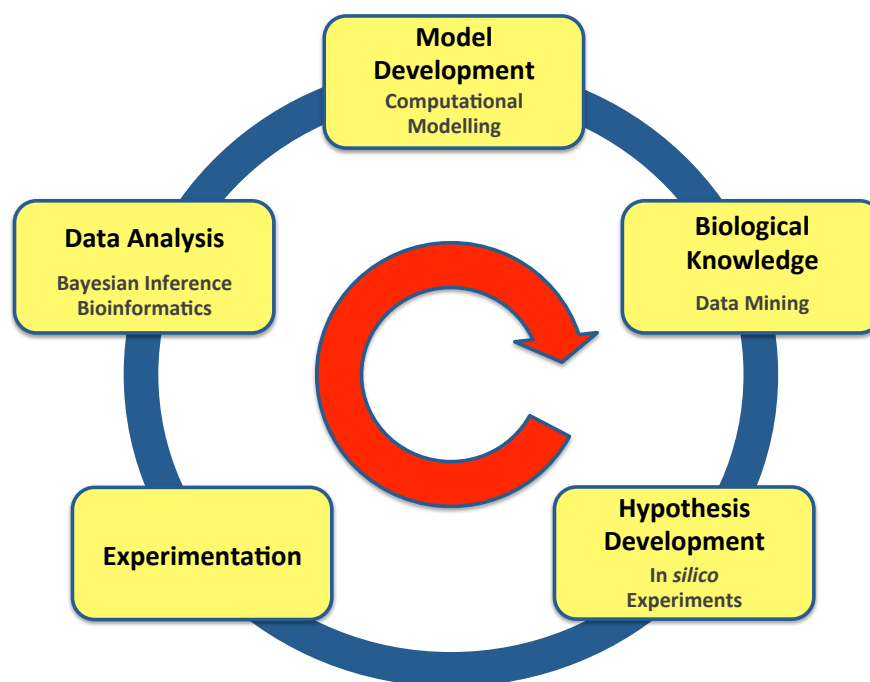


**Figure 1.2** - The cycle of interdisciplinary work showing the stages for a systems analysis. The grey text highlights possible interdisciplinary approaches that can aid in the development of biological understanding.

It has been argued that one of the ultimate goals of systems biology is to “develop detailed simulations of human physiology at all levels of biological organisation” (Dubitzky, 2006). While such simulations are quite far-off, a number of computational models have been developed for numerous biological systems including signalling pathways like NF- $\kappa$ B and p53, regulatory networks such as the cell cycle, circadian clock and metabolism (Kell, 2006, Novak and Tyson, 2008). However, multicellular organisms are composed of numerous cell types all with adapted and specific functions; these models may not be able to recapitulate the appropriate behaviour for all cell types. Moreover, the different cell types are integrated into tissues and different organs to form a whole functioning organism. Therefore, the challenges of modelling biology don't end at the cellular level.

It is important to be aware that all models are only approximations of their mimicked systems. Models are designed to be as simple as possible while still being able to accurately represent the desired, usually experimentally measured, output of a system. One linchpin quote of the systems biology community summarises this point “essentially, all models are wrong, but some are useful” Box and Draper (1987). In systems biology a model that is insufficient to fit new experimental data can often be used to inform our understanding of the system. While it is important to be aware of the assumptions and limitations of computational models, they provide a valuable tool to further understanding of complex biological systems. Models provide a means to realise non-linear and high dimensional systems in a dynamic context and allow us to probe them for insight and understanding in a way network diagrams cannot.



## **1.2– Computational Modelling**

There is a huge breadth of modelling approaches that have been applied to biological systems; these include stochastic, deterministic and spatial modelling, these approaches have even been combined into hybrid and multi-scale models. Fundamental properties within a biological system include temporal and spatial scales, compartmentalisation, noise and nonlinearity; different modelling approaches can represent these better than others. The choice of modelling approach depends on the biological question that is being addressed and the available data that can be used to parameterise and validate a model.

### **1.2.1 – Model Building and Deterministic Representations**

It has been proposed that no single model can be: applicable to all systems, precise in its predicted output, and realistic in its depiction of the model structure (Haefner, 2005, Levins, 1966). In a biological context, this would mean that no single model could recapitulate a dynamic process correctly for all cell types and include a representation of all the components of that process. Therefore, when designing biological models there must be a trade-off between abstraction of the system and an appropriate level of complexity so that the fundamental questions can be addressed.

Once a suitable level of abstraction has been established the first step of model building is to decide which species to include within a model and what function these will have. Their localisation, association with other species or post-translational modifications will determine this choice. In addition to the list of species a set of reactions is required to define the interactions of each component with the rest of the system. This process of building a descriptive framework and identifying the key species to include in a model can help to elucidate gaps in knowledge (van Riel, 2006).

A tool often employed to represent biochemical reactions is the Law of Mass Action. This states the rate of the reaction is proportional to the concentration of the substrates (Murray 2002). The law of mass action can be used in conjunction with the description framework to produce a system of reaction rate equations (RREs). For example, consider the process of transcription where an activator *A* binds to

---

DNA and causes the transcription of pre-mRNA (*pRNA*), which after splicing becomes mRNA with a rate  $k_s$ . This mRNA is then translated into a protein *P* with a rate  $k_t$  (figure 1.3).

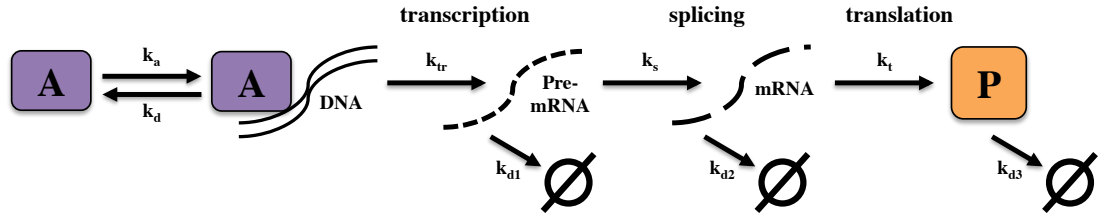


**Figure 1.3** - Simple example of transcription of a protein *P* by a transcription factor *A*. The transcription factor *A* binds the DNA causing transcription of the pre-mRNA with rate  $k_{tr}$ . This is spliced into mRNA with rate  $k_s$ , which is in turn translated into a protein *P* with rate  $k_t$ . The pre-mRNA, mRNA and protein are all degraded with rates  $k_{d1}$ ,  $k_{d2}$ , and  $k_{d3}$  respectively. The level of the transcription factor *A* is assumed constant,  $k_a$  and  $k_d$  are the association and disassociation rates of *A* with the DNA. Example adapted from Bolouri and Davidson (2002).

If the law of mass action is assumed true then the evolution of this system over time can be represented as a set of coupled ordinary differential equations (ODEs)

$$\frac{dpRNA}{dt} = \frac{k_{tr}A}{k_{diss}+A} - k_{d1}pRNA, \quad (1.1)$$

$$\frac{dmRNA}{dt} = k_t pRNA - k_{d2}mRNA, \quad (1.2)$$

$$\frac{dP}{dt} = k_s mRNA - k_{d3}P, \quad (1.3)$$

where  $k_{d1}$ ,  $k_{d2}$ , and  $k_{d3}$  are the degradation rates of the pre-mRNA, mRNA and protein respectively. The first term is an example of a Michaelis-Menten rate equation assuming the reaction is in equilibrium (Britton, 2003). If  $k_a$  and  $k_d$  are the association and disassociation rates of *A* with the DNA then  $k_{diss} = k_d/k_a$  is the equilibrium constant representing complex formation between *A* and the DNA. The parameter  $k_{tr} = k_{tr\_max}A_0$ , the maximum rate of transcription ( $k_{tr\_max}$ ) multiplied by the total concentration of *A* ( $A_0$ ). These kinetics assume that the concentration of *A* is large enough that the concentration of unbound *A* is approximately equal to the total concentration of *A*, and that *A* is a conserved quantity (Bolouri and Davidson, 2002, Britton, 2003). These are the general principles employed to define a set of coupled ordinary differential equations (ODEs) for a particular system of interest.

A system of  $n$  ordinary differential equations representing the variables  $x_1, \dots, x_n$  and dependent on the parameters  $k_1, \dots, k_m$ , usually rate constants, has the general mathematical representation

$$\begin{cases} \frac{dx_i}{dt} = f_i(t, x_1, \dots, x_n, k_1, \dots, k_m), \\ x_i(0) = x_{i_0} \end{cases}, \quad (1.4)$$

where  $t$  is time,  $i = 1, \dots, n$  and  $(x_{1_0}, \dots, x_{n_0})$  is a vector of initial conditions. The function  $f_i: [0, \infty) \times \mathbb{R}^n \rightarrow \mathbb{R}$  maps a subset of  $\mathbb{R}^n$  to  $\mathbb{R}$ . There is a wealth of literature to prove the existence of a unique solution of these systems. One common theorem, the Picard-Lindelöf theorem, states: there exists a unique solution to the system described by (1.4) if the function  $f$  is Lipschitz continuous (Vries, 2006). This is often true for biochemical models as the functions used to describe biological reactions are usually linear or logistic and, in general, continuous. It is sometimes also convenient to write these systems using a vector notation

$$\begin{cases} \frac{d\mathbf{x}}{dt} = f(\mathbf{x}, t, \mathbf{k}), \\ \mathbf{x}(0) = \mathbf{x}_0 \end{cases}, \quad (1.5)$$

where  $\mathbf{x} = \{x_1, \dots, x_n\}$ ,  $\mathbf{k} = \{k_1, \dots, k_m\}$  and  $f: [0, \infty) \times \mathbb{R}^n \rightarrow \mathbb{R}^n$ . A system of ODEs can be solved using analytic or numerical methods to predict the evolution of the system in time, for a given set of initial conditions.

ODEs are an example of a ‘deterministic’ model. This nomenclature is used as the entire system is defined by its equations and initial conditions and therefore the outcome is pre-determined. Other examples of deterministic models include partial differential equations (PDEs), delay differential equations (DDEs) and difference equations. Deterministic models have been used to study a diverse range of biological processes including population dynamics, neuron firing and cellular signalling (Murray, 2002). ODE and PDE representations are commonly used as the dynamic properties of such systems have been very well characterised and as a result there is a wealth of techniques that can be used to analyse these system.

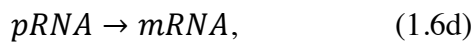
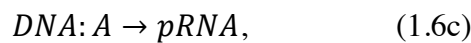
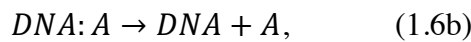
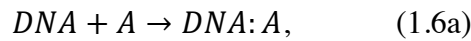
ODEs make two fundamental assumptions and are therefore not always an appropriate method. ODEs assume that the reacting spaces, in this case cellular

compartments, are homogeneous and well stirred and therefore do not account for the spatial distribution of the variables. If space cannot be treated as homogenous PDEs can be used to represent the system evolution in space and time, however, this considerably increases the complexity of the mathematics involved (Haefner, 2005). In addition, as the number of reacting molecules decreases the spatial and rate assumptions of ODEs can become invalid.

Deterministic model representation does not account for biological noise in the rate of a reaction. However, interactions between molecules follow the basic laws of thermal physics and therefore biological processes are inherently stochastic in nature. One derivation in theoretical statistical physics states that the fluctuations in a system are inversely proportional to the square root of the number of molecules, this was named the ' $\sqrt{n}$  law' (Schrodinger, 1948). More recent studies have defined a measure of the noise to be the variance in molecule number divide by the mean molecule number. If a system is in equilibrium the noise is inversely proportional to the mean molecule number (Bruggeman *et al.*, 2009). This implies that if the number of molecules involved in a reaction is sufficiently large, then the noise becomes less significant and the process can be well approximated by a deterministic representation (Meng *et al.*, 2004). However, biological processes, such as gene transcription, often involve few molecules and can be subject to relatively large stochastic variations (McAdams and Arkin, 1999).

## 1.2.2 – Stochastic Representations

Stochastic models can be used to simulate the discrete nature of molecular interactions over time and account for the random nature of collisions between reacting molecules. The application of stochastic modelling begins from a similar abstraction of the system and description of elementary reactions. However, in this case the rate controlling processes are representative of probabilities per unit time. Consider the example of transcription above (figure 1.3), this can be decomposed into 5 species: A, DNA, DNA:A, pre-mRNA, mRNA and P. Associated with these species are 8 reactions:



In a given time step each of these reactions can occur with a different probability, these reactions and probabilities define the change in the state of the system over time. Stochastic systems are reviewed more formally in Gillespie (2007), below key points of this review are briefly outlined. Assuming a well-stirred system of  $n$  chemical species interacting through  $m$  chemical reactions, in a constant volume at a constant temperature. The state vector  $\mathbf{X}(t) = \{X_1(t), \dots, X_n(t)\}$  represents the number of molecules of each species at time  $t$ , given the system is initially in some state  $\mathbf{X}(t_0) = \mathbf{x}_0$ . The system is defined by two quantities the stoichiometric matrix  $\{v_{ij}\}$ , which describes the change in species  $i$  given reaction  $j$  occurs. Associated with each reaction is a propensity function  $a_j(\mathbf{x})$ , where  $a_j(\mathbf{x})dt$  is defined to be: the probability, given  $\mathbf{X}(t) = \mathbf{x}$ , that reaction  $j$  will occur somewhere in the volume in the next infinitesimal time interval  $[t, t + dt)$ . In the transcription example reactions

(1.6a)-(1.6h) will define the stoichiometry matrix and the associated probabilities the propensity functions. These can then be used to form a set of Chemical Master Equations (CMEs) that define the evolution of the system over time. The CME is

$$\frac{\partial P(\mathbf{x}, t | \mathbf{x}_0, t_0)}{\partial t} = \sum_{j=1}^M [a_j(\mathbf{x} - \mathbf{v}_j)P(\mathbf{x} - \mathbf{v}_j, t | \mathbf{x}_0, t_0) - a_j(\mathbf{x})P(\mathbf{x}, t | \mathbf{x}_0, t_0)], \quad (1.7)$$

where  $\mathbf{v}_j = (v_{1j}, \dots, v_{nj})$  is a vector of length  $n$ . For unimolecular reactions, (1.6d)-(1.6h),  $a_j(\mathbf{x}) = c_j x_i$ , where  $x_i$  is the species involved, in this case the  $c_j$ s are equivalent to the reaction rates. If the expected number of reactions in a time step is sufficiently large the CME can be approximated as a continuous stochastic process. The thermodynamic limit is the point where the species number and volume approach infinity, but their ratio remains constant. In the thermodynamic limit continuous stochastic processes can be approximated as continuous deterministic processes (Gillespie, 2007). In computational modelling, this implies that as the number of molecules increases the solution of a stochastic model tends towards the deterministic solution (Gillespie, 2007, Meng *et al.*, 2004). Therefore, the choice between a stochastic or deterministic representation will depend upon the molecule number and stochastic nature of the process being represented.

Stochastic modelling can be used to understand the role of noise in biochemical systems and how this can result in different functional outputs. A downside of stochastic modelling approaches is that they are generally far more computationally intensive and less intuitive to implement. Stochastic models have been used to study population dynamics, signalling pathways and gene transcription (Harper *et al.*, 2011, McKane and Newman, 2004, Puszynski *et al.*, 2008). One approach to develop a model that balances computational efficiency with appropriate representation of biological process is hybrid stochastic modelling. This approach combines both deterministic and stochastic representation of reactions within a model. Reactions that are well approximated by continuous processes, such as phosphorylation and translocation, can be represented by deterministic equations and stochastic processes, such as gene transcription, can be represented using CMEs (Ashall *et al.*, 2009, Lipniacki *et al.*, 2006, Paszek *et al.*, 2010b).

### 1.2.3 – Spatial and Multi-scale Modelling

Stochastic and deterministic models make the assumption that cellular compartments can be regarded as well-stirred containers, thus ignoring spatial distribution in cells and representing the processes as only time dependent (Wilkinson, 2009). Spatial distribution of molecules can be of critical importance to cellular pathways, segregation of molecules through localisation or association with scaffold complexes is a common mechanism of regulating pathway activity (Kholodenko, 2006). Recently, there has been a development of spatial models to understand the role of spatial organisation in signalling pathways (Walker and Southgate, 2009). Two approaches to this include cellular automata (CA) and agent-based modelling. CAs represent spatial elements in a 2D- or 3D-lattice. Each point on the lattice is updated iteratively using simple logic rules that depend on its previous state, the state of its neighbours and local environmental variables. CA methods are useful for representing cellular behaviour in cases when cell shape and size can be ignored (Takahashi *et al.*, 2005). Agent-based modelling represents systems as a composition of interacting, autonomous ‘agents’ (Macal and North, 2010). Unlike CA this approach has more generic applications as cells are not constrained to a particular point in space and cell shape can be included as a parameter (Walker and Southgate, 2009).

Beyond the single cell, multi-scale models have been developed to understand biological processes on the scale of tissues and organs (Eissing *et al.*, 2011). At their simplest, these models are a CA where each point of the lattice represents a cell and each cell has a biochemical circuit associated with it; this could be a system of ODEs or CMEs to represent a cellular process. These circuits will have an input and output to influence and be influenced by their local environment, usually through the diffusion of factors such as cytokines or nutrients. These modelling approaches have been developed to include non-regular lattices and account for irregular cell shape (Bernabeu *et al.*, 2009, Pitt-Francis *et al.*, 2009). Multi-scale models have been used to study tumour growth and angiogenesis, signal propagation in tissues and to model whole organs such as the heart (Dada and Mendes, 2011, Yde *et al.*, 2011).

## 1.3– Analysis Methods for Computational Models

The large number of variables and reactions in dynamics models often make them analytically intractable. As a result a number of methods have been developed to aid in the analysis of computational models. These include metabolic analysis, sensitivity analysis, and dynamic analysis methods such as phase portraits and bifurcation analysis. Model reduction methods have also been developed to extract the core network topology responsible for the system dynamics.

### 1.3.1 – Sensitivity Analysis

Model behaviour may be strongly dependent on the parameters (van Riel, 2006). Sensitivity analysis methods characterise the effect of perturbations of the parameters on the solution. One of the best known examples of sensitivity analysis is the use of metabolic control analysis (MCA), which defines coefficients to quantitatively measure the effect of various reactions in the pathway on the fluxes or metabolite concentration (Wildermuth, 2000). In general biological systems, the parameter sensitivity is defined as the change of a dependent variable due to a change in a parameter (Wu *et al.*, 2008). For the system defined by (1.5) with a solution  $\mathbf{x}(t, \mathbf{k})$  a general representation of parameter sensitivity is

$$S_k^M = \frac{\delta M(\mathbf{x})/M(\mathbf{x})}{\delta k_j/k_j}, \quad (1.8)$$

where  $k_j$  represents the parameter that is varied and  $M(\mathbf{x})$  is some characteristic of the system's solution, e.g., amplitude or period, (van Riel, 2006). For the system of ODEs defined by (1.4) the effect of a small change  $\Delta k_j$  of the  $j^{\text{th}}$  parameter on the solution for a variable of interest,  $x_i$ , can be expressed as a Taylor series expansion:

$$x_i(t, k_i + \Delta k_i) = x_i(t, k_j) + \sum_{l=1}^m \frac{\partial x_i}{\partial k_l} \Delta k_l + \frac{1}{2} \sum_{l=1}^m \sum_{s=1}^m \frac{\partial^2 x_i}{\partial k_l \partial k_s} \Delta k_l \Delta k_s + \dots \quad (1.9)$$

The partial derivatives  $\partial x_i / \partial k_l$  are known as the first-order local sensitivity coefficients (Yue *et al.*, 2006). A variety of methods have been developed to determine these sensitivity coefficients at each time-step of the solution (Yue *et al.*,



2006). The concepts of MCA and sensitivity analysis have also been generalised to provide a framework for analysis of stochastic systems (Irving, 1992).

Many of the methods developed for MCA address the sensitivities of the system's stationary steady states (Rand, 2008). However, in many systems the transient or periodic behaviour is of primary interest. This has led to the development of dynamic sensitivity analysis (Rand, 2008, Wu *et al.*, 2008). In oscillatory systems, a key goal is to understand how parameter variations affect properties of the limit cycle, such as period or amplitude. One of the most straightforward ways to address this is to follow how the model solution changes as a single parameter is varied and others are kept fixed. The sensitivity can then be measured by the difference in the solution characteristics. The definition of a sensitivity coefficient can be extended to periodic solutions. For example, if after a transient phase the solution of (1.4) oscillates with a period  $P = \omega$ , then there exists a periodic solution

$$x_i(t) = g_i(t, k_1, \dots, k_n) = g_i(t + \omega, k_1, \dots, k_n), \quad (1.10)$$

for all  $i = 1, \dots, n$ . For a parameter of interest  $k_j$  Rand (2008) defines the sensitivity coefficients for periodic solutions to be the partial derivative of the periodic function (1.10) with respect to the parameter  $k_j$ ,

$$\frac{\partial g(t, k_j)}{\partial k_j}. \quad (1.11)$$

This definition can be used to define a control coefficient for a particular feature of the limit cycle, such as period, this will be seen in Chapter 4. Various tools have been developed to aid in the derivation of sensitivity measures for a given system of equations and initial conditions. One such tool is the global sensitivity analysis software (Rand, 2008). This software allows for the calculation of control coefficients for all the model parameters. Thus, providing a measure of what model variables are most sensitive to which parameters, and at what point in the limit cycle the variable is sensitive.

In many systems a lack of sensitivity has been shown to be evolutionarily advantageous, this is called “Robustness” (Morohashi *et al.*, 2002). Biological systems must operate under varying internal and environmental conditions that can cause changes in the internal ‘parameters’ of the system (Kitano, 2002a). Robustness to perturbations has been observed in sensory signalling networks, such as the chemotactic pathway in *E.coli* (Alon *et al.*, 1999). This network governs the migration of bacteria towards chemical attractants. A key feature of this is exact adaptation: a change in the concentration of an attractant induces a rapid change in the bacteria’s movement, or tumbling, which gradually adapts to precisely its pre-stimulation value. The ‘precision’ of this adaptation was observed to be extremely robust to multiple perturbations of the network (Alon *et al.*, 1999). Since signalling pathways have been identified to be robust it is logical to extend this criteria to the mathematical models thereof. This has led to the use of robustness as a criterion for selection between competing models. Robustness can be assayed using parameter sensitivity and application of this method has been successful in identifying known weakness in models of the biochemical oscillator underlying the *Xenopus* cell cycle (Morohashi *et al.*, 2002). However, systems also need to be sensitive to certain parameter changes in order to respond to signals; therefore there is a trade-off between robustness and sensitivity. Robustness and sensitivity to variation of the input has been observed in signalling systems, such as the NF- $\kappa$ B signalling pathway, whose oscillatory period but not persistence of response is robust to stimulating dose (Ashall *et al.*, 2009, Tay *et al.*, 2010, Turner *et al.*, 2010). This is an important consideration when using robustness as a criterion for model validation and development.

### 1.3.2 – Phase Portrait and Bifurcation Analysis

Phase space is defined to be the set whose elements present all possible states of a system at any moment in time (Hale and Koçak, 1991). The phase space for the system defined by (1.4) would be the  $n$ -dimensional space consisting of all possible values of the set  $(x_1, x_2, \dots, x_n)$ . A phase portrait is a 2- or 3-dimensional representation of the solutions of the ordinary differential equations as curves, where each dimension corresponds to one variable and time is a parameter (Britton, 2003). If  $n > 3$  then this portrait is a projection of the system's solutions into lower dimensions. Consider the 2-dimensional system of ODEs defined by

$$\begin{aligned} \dot{x}_1 &= \mu x_1 - x_2 - x_1(x_1^2 + x_2^2), \\ \dot{x}_2 &= x_1 + \mu x_2 - x_2(x_1^2 + x_2^2). \end{aligned} \quad (1.12)$$

A plot of the curve defined by the solution to these equations in the  $(x_1, x_2)$ -plane for a given set of initial conditions is a phase portrait. Figure 1.4 shows a series of phase portraits for this dynamic system, where the  $y$ - and  $z$ -axis correspond to  $x_1$  and  $x_2$ , and the  $x$ -axis corresponds to the parameter  $\mu$ . The portrait changes from a stable focus (attracting to a fixed point, red) to a limit cycle (purple) as the parameter value is increased. Analysis of the phase plane can identify key aspects of a dynamic system like hysteresis, points of stability, and limit cycles (figure 1.4, purple line) (Kuznetsov, 2004). A limit cycle or periodic solution is defined to be a closed trajectory in phase space, which is the limit of other solutions as time approaches infinity (Britton, 2003). A stable limit cycle attracts all neighbouring trajectories; in dynamic systems this is equivalent to showing sustained oscillations (Kuznetsov, 2004).

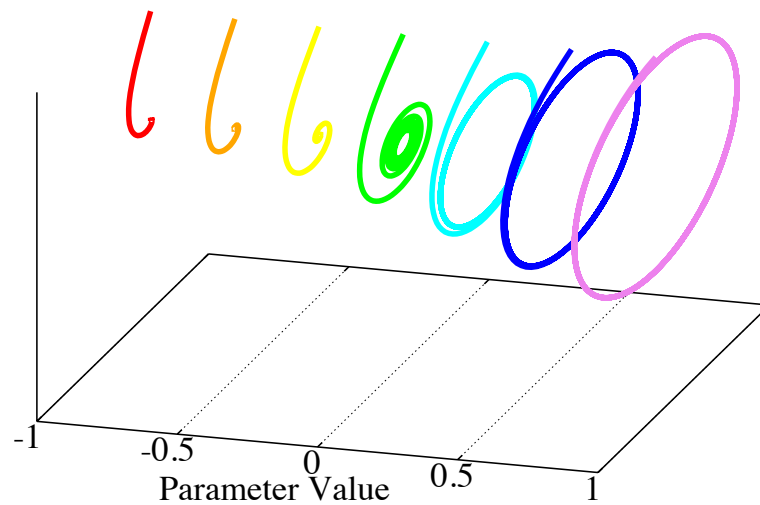


**Figure 1.4** - A series of phase planes showing a bifurcation from a fixed point to limit cycle oscillations for the system defined by (1.12). The  $y$ - and  $z$ -axes correspond to  $x_1$  and  $x_2$ , and the  $x$ -axis corresponds to the parameter  $\mu$ . The colour lines represent the phase plane trajectory as the parameter  $\mu$  is increased from -1 to 1. For negative parameter values the trajectories approach a fixed point. For positive values they exhibit a limit cycle. This system undergoes a bifurcation at the parameter value 0; in this case an Andronov-Hopf bifurcation. Example adapted from Kuznetsov (2004)

Bifurcation theory is a well-established branch of mathematics that explains many of the phenomena that have been discovered in the natural sciences, such as oscillations and hysteresis (Kielhöfer, 2003). Bifurcation analysis traces time varying changes in the state of the system in multi-dimensional space where each dimension represents a parameter (Kitano, 2002b). A differential equation is said to have a stable solution with respect to a parameter if the qualitative nature of the solution does not change for small variations of the parameter. A bifurcation occurs in a dynamic system when the phase portraits become topologically non-equivalent due to variation of system parameters (Kuznetsov, 2004). In short, a bifurcation occurs if the stable steady state loses stability and the system reorganises into a new stable steady state. A parameter value for which the orbit is not stable is called a bifurcation value and the system is said to be at a bifurcation point (Hale and Koçak, 1991). A diagram of the solution behaviour (steady states, periodic orbit) against a parameter is a bifurcation diagram (Britton, 2003).

The stability of the solution of a system of ODEs depends on the eigenvalues of the Jacobian matrix. For the system of ODEs defined by (1.4) the Jacobian matrix  $J$  is the  $n$ -by- $n$  matrix

$$J = \begin{bmatrix} \frac{\partial f_1}{\partial x_1} & \cdots & \frac{\partial f_1}{\partial x_n} \\ \vdots & \ddots & \vdots \\ \frac{\partial f_n}{\partial x_1} & \cdots & \frac{\partial f_n}{\partial x_n} \end{bmatrix}. \quad (1.13)$$

The characteristic polynomial is defined to be the determinant of the matrix  $(J - \lambda I)$ , where  $I$  is the identity matrix. The roots of this polynomial are the eigenvalues of the Jacobian matrix (Hale and Koçak, 1991). In systems with a dimension higher than 1, a steady state loses stability when a pair of eigenvalues cross the imaginary axis due to parameter variation. If all the eigenvalues have negative real part then the system has a stable focus, attracting to a fixed point. If any eigenvalue has a positive real part the system has an unstable focus, moving away from a fixed point (Britton, 2003). The Andronov-Hopf Bifurcation Theorem states: for a system of differential equations with a given set of parameter values if the Jacobian has a pair of conjugate nonzero purely imaginary eigenvalues then the system has a nontrivial periodic orbit (Hale and Koçak, 1991). The point at which these eigenvalues cross the imaginary axis and become purely imaginary conjugate values, or vice versa, is called a Hopf bifurcation (HB) (Kuznetsov, 2004). A HB is of particular relevance as it occurs when the solution branches from a stable steady state, where variables remain constant, to a stable limit cycle where the solutions oscillate or vice versa. For example, the system defined by (1.12) has the Jacobian matrix

$$\begin{bmatrix} \mu & -1 \\ 1 & \mu \end{bmatrix}, \quad (1.14)$$

after linearization about the origin (Kuznetsov, 2004). The eigenvalues of this system are the solution of the polynomial  $\lambda^2 - 2\mu\lambda + \mu^2 = 0$ , namely,

$$\lambda = \mu \pm i. \quad (1.15)$$

Therefore, if  $\mu < 0$  there is a stable focus, if  $\mu > 0$  there is an unstable focus. At  $\mu = 0$  a Hopf bifurcation may occur, as the eigenvalues are purely imaginary. Numerical analysis of the system (figure 1.4) shows a HB does occur, as the phase

portraits change from a stable focus for  $\mu < 0$  to a limit cycle for  $\mu > 0$ . For large systems analysis of the dynamics is performed numerically and HBs determined by consideration of the eigenvalues as the parameters are varied. Examples of bifurcation analysis software include XPPAUT and MatCont (Dhooge *et al.*, 2003, Doedel *et al.*, 2000, Ermentrout, 2002).

The application of bifurcation analysis provides detailed information about the behaviour of a dynamical system and has been applied effectively to biological models (Borisuk and Tyson, 1998, Wang *et al.*, 2012b). Bifurcation analysis quantifies the change in the period and amplitude of a limit cycle as a parameter is varied. This can be done over the entire parameter range for which the stable limit cycle exists, unlike sensitivity analysis that considers only a small range of the parameter. Bifurcation theory can also be generalised into higher dimensions allowing for the analysis of simultaneous parameter changes on the properties of the system solutions (Kuznetsov, 2004).

### **1.3.3 – Model Reduction Methods**

The dynamical systems that arise from biological networks can often have high-dimensional state space and depend on a large number of parameters. Model reduction approaches provide an avenue to extract the core reactions and variables responsible for the key dynamical features of the system. These approaches include modularisation to break large systems down into more tractable functional units (Saez-Rodriguez *et al.*, 2004). However, there is no standard definition of a module, so this becomes a heuristic technique. Other techniques include using *a posteriori* analysis and characteristic timescales. Based on error analysis, the former method identifies, for different time intervals, the components of the model required for accurate representation of the solution and uses this information to guide model simplification (Whiteley, 2010). The latter utilises the fact that many biological systems incorporate markedly different time-scales ranging from seconds to hours. Relevant approaches employ the use of partial-equilibria (PE), quasi-steady-state approximations (QSSA), or grouping variables with equivalent time-scales (Krishna *et al.*, 2006, Maeda *et al.*, 1998, Schneider and Wilhelm, 2000). These methods often rely on intuition to determine the successive reduction steps. A more rigorous

Computational Singular Perturbation (CSP) method allows for a guided reduction through QSSA or PE based on timescale coefficients, defined by the inverse of the eigenvalues of the Jacobian matrix (Lam and Goussis, 1994). Similarly, the Intrinsic Low-Dimensional Manifolds (ILDM) decomposes the system into fast and slow subsets according to a chosen time-scale of interest (Surovtsova *et al.*, 2009). Although both these methods are more rigorous than the classical PE and QSSA techniques, they are also more abstract and thus more challenging to apply than their predecessors.

## 1.4– Biological Oscillators

Oscillatory dynamics have been observed in numerous biological systems from the circadian clock to signalling pathways like p53 and NF- $\kappa$ B (Novak and Tyson, 2008). An oscillation can be defined as a cyclic change in a measurable quantity of a system, which exhibits a relatively constant waveform and period (Friesen and Block, 1984). The most important characteristics of an oscillator include period and in the case of more than one oscillating species phase, other characteristics can include amplitude and waveform (Friesen and Block, 1984). Oscillations are an example of emergent behaviour; therefore they cannot always be fully understood through biochemical assays alone and require a systems level approach (Novak and Tyson, 2008).

One of the earliest observed biochemical oscillators was the concentration of reduced pyridine nucleotide in yeast cells (Chance *et al.*, 1964). Oscillations have subsequently been observed in a number of biochemical systems with periods that span multiple timescales, from seconds in the case of Calcium oscillations to hours in the case of the cell cycle (table 1.1). Moreover, it has been shown that the frequency and amplitude of some such oscillations can encode information and have vital physiological functions. For example, the frequency of  $\text{Ca}^{2+}$  oscillations can influence the dilation of arteries and changes their amplitude can alter gene transcription (Berridge *et al.*, 1998). In the NF- $\kappa$ B system, the frequency of oscillations affects the expression profile of NF- $\kappa$ B dependent genes (Ashall *et al.*, 2009). Therefore, it is important to understand the mechanisms that cause and control these oscillations.

In order for a system to have stable oscillations there are certain requirements that should be present in the network topology. The first is a negative feedback to return a reaction to its starting point. Second, this feedback must be delayed in order to perturb the system from its steady state. Finally, there must be sufficient nonlinearity in the system to destabilise the steady state (Friesen and Block, 1984, Novak and Tyson, 2008). Figure 1.1b is a simplified example of the p53 auto-regulatory loop - this system has the design principles required for oscillations. There is negative feedback from MDM2, which inhibits p53 activity, and the intermediary steps of



transcription and translation of MDM2 provide the delay required for oscillations. Theoretical studies have demonstrated it is possible to generate oscillations using this circuit (Lev Bar-Or *et al.*, 2000) and time-lapse fluorescence imaging has shown oscillations in the level of nuclear p53 in response to gamma irradiation (Geva-Zatorsky *et al.*, 2006). This transcriptional negative feedback loop is a key motif that is also present in NF- $\kappa$ B and cell cycle oscillatory models (Krishna *et al.*, 2006, Lahav *et al.*, 2004, Novak and Tyson, 2004).

It has been proposed that the addition of a positive feedback to an oscillatory system offers a means to tune the frequency of oscillations (Tsai *et al.*, 2008). A more recent study has demonstrated that the presence of nested negative feedback loops provides an alternative avenue to control characteristic of the oscillations (Nguyen, 2012). Analysis of oscillatory systems has shown that in addition to the feedbacks driving oscillations other components of the system can serve to influence the limit cycle, therefore all components should be considered equally (Gerard *et al.*, 2009, Reijenga *et al.*, 2005).

**Table 1.1** - Example of biological systems that show oscillatory behaviour. This table has been adapted from Novak and Tyson (2008) and Tsai *et al.*, (2008).

Function	Core Components	Period	Reference
Metabolism	Glucose, ATP, phospho-fructokinase	2-mins	(Goldbeter and Lefever, 1972)
Signalling	Ca <sup>2+</sup> , Ins(1,3,5)P <sub>3</sub>	>1-s	(Meyer and Stryer, 1988)
Signalling	NF- $\kappa$ B, IKK, I $\kappa$ B	~2-h	(Nelson <i>et al.</i> , 2004)
Signalling	p53, MDM2	5-h	(Monk, 2003)
Cell Proliferation	Cell Cycle	10-mns - >24-h	(Tyson and Novak, 2001)
Circadian Rhythm	PER, TIM, CLOCK, CYC	24-h	(Goldbeter, 1995, Tyson <i>et al.</i> , 1999)

## **1.5 – The NF- $\kappa$ B Signalling Network**

The Nuclear Factor  $\kappa$ B (NF- $\kappa$ B) transcription factor signalling pathway drives cellular inflammation and immune responses, playing key roles in cell proliferation and apoptosis. It is a central regulator of many of the genes induced in response to inflammatory cytokines and pathogen-derived substances. Disruption of NF- $\kappa$ B signalling has been implicated in many autoimmune diseases and cancers, inviting broad interest in the regulation of this transcription factor (Hayden and Ghosh, 2008).

### **1.5.1 – Core Components of the NF- $\kappa$ B System**

The NF- $\kappa$ B system conveys extracellular signals from cell surface receptors to the nucleus through the interaction of a number of proteins. Central to this system is the NF- $\kappa$ B family of transcription factors and the Inhibitor kappaB (I $\kappa$ B) proteins. The NF- $\kappa$ B proteins are dimeric transcription factors, composed of homo- and heterodimers of NF- $\kappa$ B family members (Chen and Greene, 2004). NF- $\kappa$ B family members are characterised by a conserved N-terminal Rel homology domain (RHD). The RHD is ~300 amino acids in length and is responsible for DNA binding, interaction with inhibitory  $\kappa$ B proteins (I $\kappa$ Bs) and contains a nuclear localisation sequence (NLS). In mammalian cells five NF- $\kappa$ B family members are known: p50, p52, p65/RelA, c-Rel and RelB. The proteins p50 and p52 are derived from precursor proteins p105 and p100 respectively (Hayden and Ghosh, 2008). The composition of NF- $\kappa$ B dimers in the cell varies depending on the state of the cell. Therefore the NF- $\kappa$ B system is able to respond to a wide variety of stimuli (Thanos and Maniatis, 1995). The NF- $\kappa$ B system is usually divided into the canonical and non-canonical pathways. The non-canonical pathway primarily involves the RelB:p52 complex and is involved in lymphoid organogenesis, B-cell survival and maturation, and dendritic cell activation (Sun, 2011). The canonical pathway is associated with inflammation and the immune response. In the canonical pathway NF- $\kappa$ B is prototypically a dimer of RelA and p50, which is the most prevalent complex. In unstimulated cells the NF- $\kappa$ B dimers are sequestered in the cytoplasm bound to I $\kappa$ B proteins.

The I $\kappa$ B proteins are a family of regulators of the NF- $\kappa$ B dimers, which share multiple copies of an ankyrin-like repeat domain (ARD) required for their interaction with the NF- $\kappa$ B RHD (Beg and Baldwin, 1993). The I $\kappa$ Bs regulate the DNA binding and subcellular localisation of the NF- $\kappa$ B transcription factors (Baldwin, 1996). The I $\kappa$ B family consists of multiple members including I $\kappa$ B $\alpha$ , I $\kappa$ B $\beta$  and I $\kappa$ B $\epsilon$ . The precursor proteins p100 and p105 also contain similar ARD and can function as I $\kappa$ B like proteins (Li and Verma, 2002). Different I $\kappa$ Bs tend to associate with different NF- $\kappa$ B dimers, with I $\kappa$ B $\alpha$  and I $\kappa$ B $\epsilon$  predominantly associating with the RelA:p50 heterodimer. Several of the I $\kappa$ Bs are under the transcriptional control of NF- $\kappa$ B leading to regulatory feedback, these include I $\kappa$ B $\alpha$  and I $\kappa$ B $\epsilon$  (Kearns *et al.*, 2006, Sun *et al.*, 1993). I $\kappa$ B $\alpha$  is believed to sequester NF- $\kappa$ B in the cytoplasm, however, live cell imaging following treatment with leptomycin-B (LMB) to block nuclear export shows a nuclear accumulation of NF- $\kappa$ B (Birbach *et al.*, 2002, Nelson *et al.*, 2002, Sung *et al.*, 2009). This suggests that there is in fact a steady state between NF- $\kappa$ B nuclear-cytoplasmic localisation that is weighted towards a cytoplasmic localisation.

NF- $\kappa$ B activation is achieved through signal induced degradation of the I $\kappa$ Bs in the cytoplasm. Activating stimuli, like Tumour Necrosis Factor alpha (TNF $\alpha$ ), initiate a signalling cascade leading to the activation of the I $\kappa$ B kinase (IKK) complex. The IKK complex is composed of two highly homologous kinases (IKK $\alpha$  and IKK $\beta$ ) and a regulatory subunit IKK $\gamma$  (NEMO) (Karin, 1999). The IKK complex phosphorylates the I $\kappa$ B proteins resulting in their ubiquitination and proteasome-mediated degradation (Ghosh *et al.*, 1998). This allows uninhibited NF- $\kappa$ B to translocation to the nucleus where it regulates the transcription of over 300 target genes through specific binding to  $\kappa$ B site in promoter/enhancer regions (Hoffmann and Baltimore, 2006). NF- $\kappa$ B dependent genes can be subdivided into early, middle and late genes depending on the time of their induction after TNF $\alpha$  stimulation (Tian *et al.*, 2005). Subsequent studies have shown the number of TNF $\alpha$  dependent genes in macrophages to be in the thousands (Sun *et al.*, 2008). These data highlight the potential scale and complexity of NF- $\kappa$ B dependent gene regulation.

One NF- $\kappa$ B target gene is I $\kappa$ B $\alpha$ . Newly synthesised I $\kappa$ B $\alpha$  can bind to NF- $\kappa$ B in the nucleus and return it to the cytoplasm via the I $\kappa$ B nuclear export sequence (NES) (Arenzana-Seisdedos *et al.*, 1997), thus creating a negative feedback within the system which drives nucleo-cytoplasmic (N:C) oscillations in NF- $\kappa$ B localisation (Nelson *et al.*, 2004). In addition to I $\kappa$ B $\alpha$ , NF- $\kappa$ B regulates the transcription of several other feedbacks such as I $\kappa$ B family member I $\kappa$ B $\epsilon$ , IKK inhibitor A20 and cytokines like TNF $\alpha$  (Kearns *et al.*, 2006, Krikos *et al.*, 1992, Tian *et al.*, 2005).

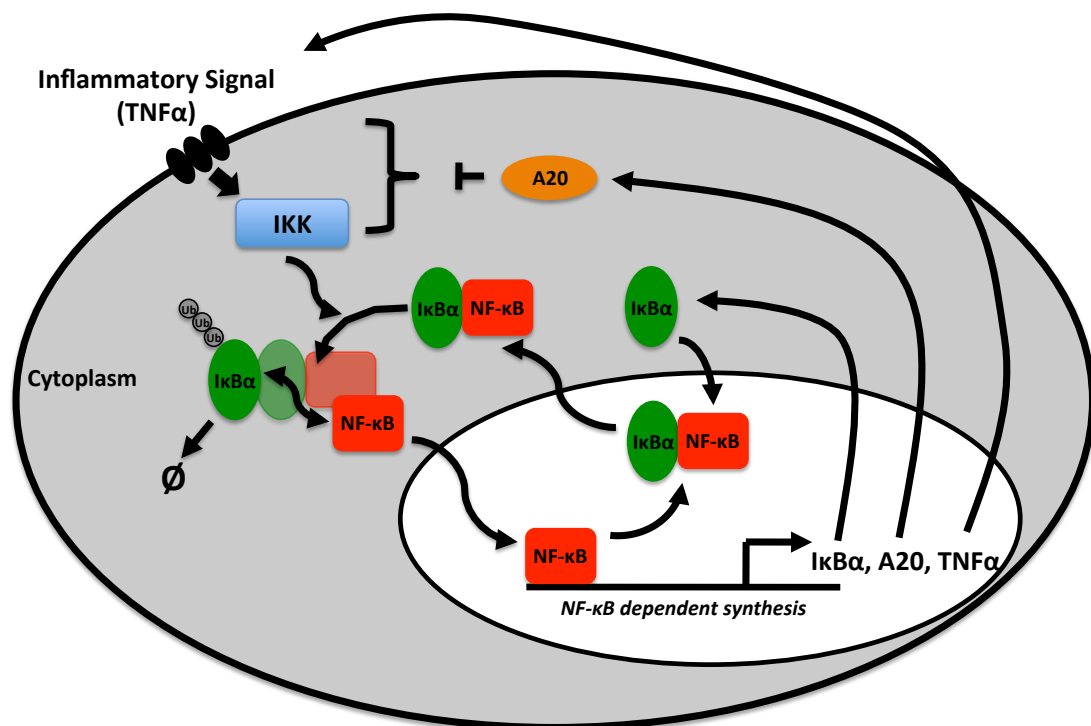


**Figure 1.5** - Schematic of some of the core components of the NF- $\kappa$ B signalling system and their interactions. Inflammatory signals, such as TNF $\alpha$  bind to the receptor resulting in activation of the IKK complex. This causes the phosphorylation and proteasome-mediated degradation of the I $\kappa$ Bs resulting in nuclear translocation of RelA to the nucleus. Here NF- $\kappa$ B induces the transcription of a number of genes including the negative feedbacks I $\kappa$ B $\alpha$  and A20. Once transcribed I $\kappa$ B $\alpha$  binds to nuclear NF- $\kappa$ B returning it to the cytoplasm and A20 inhibits IKK activity. NF- $\kappa$ B can also transcribe many positive feedbacks including pro-inflammatory cytokines, such as TNF $\alpha$ .

One key regulator of NF- $\kappa$ B signalling is the zinc-finger protein A20. Upon TNF $\alpha$  stimulation A20 mRNA is induced by NF- $\kappa$ B, once synthesised A20 is able to inhibit NF- $\kappa$ B activity (Verstrepen *et al.*, 2010). The exact method of A20 action has not been completely elucidated and various inhibitory mechanisms have been proposed. Co-expression experiments have demonstrated that A20 can interact with several intermediaries upstream of the IKK complex, such as TRAF1 and TRAF2, as well as IKK $\alpha$  and NEMO. These data suggest that A20 regulates IKK activation after TNF $\alpha$  stimulation (Verstrepen *et al.*, 2010). It has further been shown that A20 binding to NEMO can block IKK phosphorylation (Skaug *et al.*, 2011). A20 contains both deubiquitinating and ubiquitin ligase domains, which can target RIP, an essential mediator of TNF $\alpha$  signalling, for proteasomal degradation (Wertz *et al.*, 2004). A20 activity can also be regulated by phosphorylation, which can increase the ability of A20 to inhibit NF- $\kappa$ B signalling, this has been hypothesised to be a mechanism to tailor A20's down regulation of NF- $\kappa$ B activity (Hutti *et al.*, 2007, Verstrepen *et al.*, 2010). A20 has a predominantly cytoplasmic localisation, however, it has also been observed that a fraction of A20 co-localises with lysosome-interacting compartments (Li *et al.*, 2008). Moreover, it was demonstrated that A20 could target TRAF2 to the lysosome for degradation (Li *et al.*, 2009). In addition to A20 there are several additional known negative feedbacks in the NF- $\kappa$ B system including Cezanne and Cyldromatosis (CYLD) (Enesa *et al.*, 2008, Jono *et al.*, 2004)

### **1.5.2 – Dynamic Behaviour within the NF- $\kappa$ B System**

Bulk-cell analysis of the NF- $\kappa$ B system revealed stimulus induced movement of NF- $\kappa$ B to the nucleus. This was seen as a biphasic response resulting from the degradation and re-synthesis of the I $\kappa$ B proteins (Baeuerle and Baltimore, 1988, Hoffmann *et al.*, 2002). More recent studies using live cell fluorescence imaging have seen nucleo-cytoplasmic (N:C) oscillations in NF- $\kappa$ B protein localisation in single cells (Nelson *et al.*, 2004). TNF $\alpha$  treatment of neuroblastoma (SK-N-AS) and cervical carcinoma (HeLa) cells expressing fluorescently tagged RelA showed N:C oscillations in RelA with a period of 100-minutes that persisted for several hours (figure 1.6). Oscillations in RelA localisation have subsequently been seen in

numerous studies (Sung *et al.*, 2009, Tay *et al.*, 2010). Co-expression with the fluorescently tagged inhibitor I $\kappa$ B $\alpha$  driven by a  $\kappa$ B (5x consensus) promoter resulted in N:C oscillations in the level of I $\kappa$ B $\alpha$  out of phase with RelA oscillations (Nelson *et al.*, 2004). There is a large degree of heterogeneity in the timing of oscillations between cells, therefore cellular averaging could suggest why these oscillations are not evident at the population level. Further it has been suggested that this heterogeneity is important to maintain a robust tissue level phenotype in response to stimuli (Paszek *et al.*, 2010b). Detailed analysis of quantified RelA fluorescence in SK-N-AS cells showed a highly synchronised first translocation of RelA followed by a variable time between the first and second peak of nuclear movement, the average time between subsequent peaks then settled to be approximately 100-minutes (Ashall *et al.*, 2009, Horton, 2006).

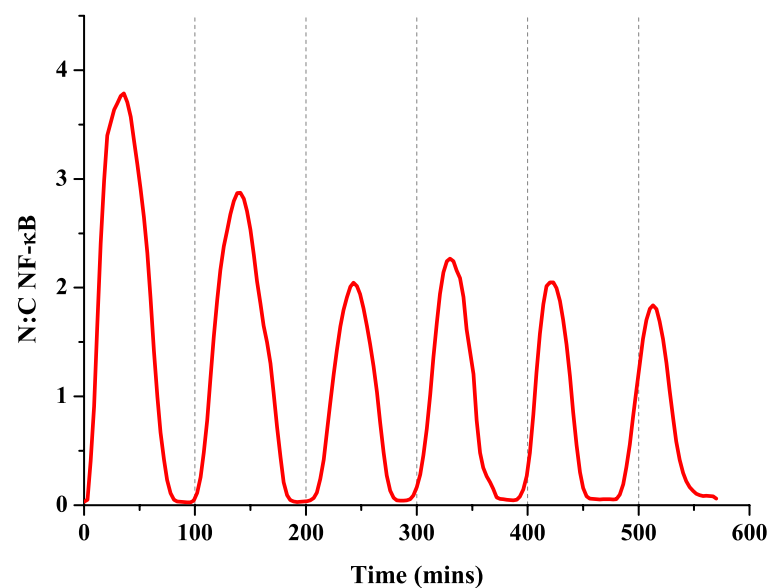


**Figure 1.6** - Example of oscillations in the nucleo-cytoplasmic ratio (N:C) of RelA fluorescence in SK-N-AS cells. SK-N-AS cells were transiently transfected with a RelA fluorescent reporter and treated with 10ng/ml TNF $\alpha$ . These data are taken from Nelson *et al.* (2004).

To understand the role of frequency in the NF- $\kappa$ B system further studies were performed using pulses of TNF $\alpha$  at various intervals (Ashall *et al.*, 2009). SK-N-AS cells expressing fluorescently tagged RelA were exposed to 5-minute pulses of TNF $\alpha$  followed by washing. When stimulated at 200-minute intervals cells showed a single synchronous translocation of equal magnitude in response to each pulse. Stimulation at 100- or 60-minute intervals also caused a synchronous timing in cell responses, however, there was a reduction in the amplitude after the first peak (Ashall *et al.*, 2009). This demonstrates that the system can be forced to oscillate at different frequencies. Moreover, RT-PCR analysis of cells stimulated with pulses of TNF $\alpha$  at the different frequencies exhibited different transcriptional profiles of various NF- $\kappa$ B target genes (Ashall *et al.*, 2009). Therefore, altering the frequency of NF- $\kappa$ B oscillations could be a novel tool to influence the downstream effects of the system.

### **1.5.3 – Computational Models of the NF- $\kappa$ B System**

The central role of the NF- $\kappa$ B system in cell fate decisions and its nonlinear dynamic behaviour make it an ideal candidate to study using a Systems Biology approach. This has resulted in the development of numerous mathematical models of the system to elucidate the function of many of its components. The first model of the NF- $\kappa$ B system aimed to understand how the association and disassociation rates of NF- $\kappa$ B with the I $\kappa$ Bs kept the majority of NF- $\kappa$ B in its inactive state in unstimulated cells (Carlotti *et al.*, 2000). However, this model only allowed for the simulation of the first phase of the NF- $\kappa$ B response.

The earliest models to address the full NF- $\kappa$ B response to stimulation, simulating the NF- $\kappa$ B biphasic dynamics seen in bulk-cell assays was a representation of NF- $\kappa$ B and its inhibitors I $\kappa$ B $\alpha$ , - $\beta$  and - $\epsilon$  by Hoffmann *et al.* (2002). This model predicted distinct roles for the three different inhibitors: I $\kappa$ B $\alpha$  acted as a negative feedback producing nuclear-cytoplasmic oscillations in NF- $\kappa$ B, while I $\kappa$ B $\beta$  and - $\epsilon$  acted to dampen these oscillations. This model identified the network topology to be crucial in driving the dynamics, however it also had limitations. The model assumed constitutive expression of I $\kappa$ B $\epsilon$ , which has subsequently been shown to be NF- $\kappa$ B

---

responsive (Kearns *et al.*, 2006). This constitutive expression was integral for the dampening of NF- $\kappa$ B oscillations; oscillatory solutions were only simulated in the I $\kappa$ B $\epsilon$  knockout case. However, NF- $\kappa$ B oscillations have been observed in single-cells with I $\kappa$ B $\epsilon$  and I $\kappa$ B $\beta$  present (Ashall *et al.*, 2009). In the subsequent years this model has been refined and developed based upon new data and biological insight. This has resulted in the inclusion of inducible I $\kappa$ B $\epsilon$  expression, alteration of rates based on new experimental data and the inclusion of additional stimuli (Cheong *et al.*, 2008).

The most substantial alteration to the initial model in Hoffmann *et al.* (2002) was by Lipniacki *et al.* (2004). The feedback from all the I $\kappa$ B isoforms was approximated by I $\kappa$ B $\alpha$  the most active and abundant one, the knockout of which is lethal (Gerondakis *et al.*, 1999). The model was compartmentalised to consider the nuclear and cytoplasmic volumes, and the I $\kappa$ B $\alpha$  parameters were re-fitted to have more realistic mRNA and protein levels. In the Hoffmann *et al.* model the coefficient for I $\kappa$ B $\alpha$  transcription rate was equivalent to hundreds of transcripts per second, which is physiologically unrealistic. Finally, the A20 inhibitory protein was included and the IKK kinetics developed. This model highlighted the interplay of the A20 and I $\kappa$ B $\alpha$  negative feedbacks for normal NF- $\kappa$ B dynamics. Their different mechanism allowed for the effective nuclear translocation of NF- $\kappa$ B. This model also highlighted the importance of a consideration of nuclear and cytoplasmic volumes when modelling NF- $\kappa$ B. Similarly, this model has been further developed over the years through re-fitting of parameters, the representation of the TNF $\alpha$  receptor and stochastic representations of transcription (Lipniacki *et al.*, 2007).

Concurrently, there was also the development of a model that can recapitulate the single-cell NF- $\kappa$ B dynamics seen through live cell imaging. This model began as a derivative of the model in Hoffmann *et al.* (2002) with a re-parameterisation to capture the single cell oscillations seen by Nelson *et al.* (2004). However, the model has further been revised drawing on the refinements of the other NF- $\kappa$ B models. This model recreated the NF- $\kappa$ B dynamics seen in single cell in response to continuous and pulsed TNF $\alpha$  stimulation (Ashall *et al.*, 2009). Many of the alterations from its predecessor are similar to those made by Lipniacki *et al.* (2004), including the

---



nuclear and cytoplasmic compartmentalisation, removal of  $I\kappa B\beta$  and  $-\varepsilon$  feedbacks and the inclusion of the inducible A20 negative feedback. However, the IKK structure was modified to allow the model to respond to both continuous and pulsed  $TNF\alpha$  stimulation. This model required a cyclic structure of the IKK module with a sufficient delay between inactivation and reactivation to allow for oscillations in its activity. The model suggested that IKK activation and deactivation happens on a faster timescale than production and degradation. One inaccuracy in this model is the relative instability of the A20 protein. The half-life of A20 in this model is approximately 5 minutes, however, the half-life of the protein has been measured to be around 8 hours in the Human Cervical Carcinoma (HeLa) cell line (Werner *et al.*, 2008). This coefficient was hypothesised to be representative of A20 activity and degradation. While, A20 is a stable protein it is not necessarily actively inhibiting  $NF-\kappa B$  signalling for the entirety of its lifetime. For example, A20 sequestration has been observed, with a portion of A20 co-localising with the lysosome (Li *et al.*, 2008, Li *et al.*, 2009). Further it has been hypothesised that post-translation modifications, such as phosphorylation, are required for full A20 activity (Verstrepen *et al.*, 2010). A20 in the Ashall *et al.* model is also, in part, representative of a number of other negative feedbacks such as CYLD and Cezanne. These factors were all hypothesised to contribute to the physiologically unrealistic parameter value.

More recently spatial models have been developed.  $NF-\kappa B$  regulates the transcription of many pro-inflammatory cytokines suggesting it plays an important role in autocrine and paracrine signalling. In one example a spatial distributed lattice of cells each containing a minimal model the  $NF-\kappa B$  system was used to probe the spatial effects of  $NF-\kappa B$  signalling. This model suggested the  $NF-\kappa B$  system could produce waves of cytokines to propagate the inflammatory signal (Yde *et al.*, 2011).

One of the key differences in models of the  $NF-\kappa B$  system is the nature of the data that has been used to develop them.  $NF-\kappa B$  dynamics have been studied using single-cell and population assays in numerous cell types and different cells types display differing signalling characteristics. For example HeLa cells show damped oscillations in comparison to SK-N-AS cells (Nelson *et al.*, 2004). Moreover, population data can show different dynamics to those of single cells. The

deterministic model in Ashall *et al.* (2009) was further developed to include a stochastic representation of gene transcription and included the addition of delayed feedback from the inhibitor I $\kappa$ B $\epsilon$ . This model had a variable period, when multiple simulations were averaged the result was NF- $\kappa$ B dynamics similar those seen in bulk-cell assays. Ashall *et al.* (2009) showed the delay in the transcription of I $\kappa$ B $\epsilon$  delay served to increase cell-to-cell heterogeneity and that a delay of 45 minutes was optimal to cause intercellular variation. This was hypothesised to be important in mediating chronic inflammation by maintaining a robust tissue phenotype (Paszek *et al.*, 2010b).

Another reason for this diversity in models of the NF- $\kappa$ B system was proposed by Wong *et al.* (2012) in a recent paper. The authors defined a concept of ‘tension’ for biochemical networks that are able to perform multiple tasks or which can exhibit markedly different dynamics, this was the existence of different parameter spaces to represent the distinct dynamics of a system. Moreover, the authors hypothesise that a model that is able to fit all criteria will not be sufficiently robust and there exists a trade-off between tension and robustness. In the case of the model presented by Ashall *et al.* (2009) the idea of tension was explored to understand the continuous and pulsatile response. This concept could have applications to the NF- $\kappa$ B system suggesting there is no model that will be able to recapitulate all dynamics seen in response to different stimuli, stimulation protocols and in different cell lines, without the use of distinct parameter sets.

Current NF- $\kappa$ B models remain limited in certain aspects. Many of these limitations are the result of a lack of appropriate data to make alterations to the model. Very few models consider the different dimers of NF- $\kappa$ B or post-translational modifications. For example, IKK phosphorylation at the 536<sup>th</sup> serine residue on RelA has been shown to effect nuclear translocation (Perkins, 2007). Different stimuli have also been seen to influence the temporal profile of IKK activity (Werner *et al.*, 2005), which could influence different components of the pathway. Models representations also seldom represent other feedbacks in the system, both positive and negative.

## **1.6– Project Motivation and Aims**

### **1.6.1 – Project Motivation**

The NF- $\kappa$ B pathway has been seen to be deregulated in a number of human illnesses, including autoimmune disorders such as cachexia and Alzheimer's disease (Tergaonkar, 2006). In addition NF- $\kappa$ B has a central role in cancer, controlling the expression of genes that are involved in tumour promotion, angiogenesis and metastasis (Garg and Aggarwal, 2002). This has motivated a great deal of research into exploring the NF- $\kappa$ B pathway as a therapeutic target. However, NF- $\kappa$ B is activated by a number of stimuli and its target genes number in the hundreds if not thousands (Garg and Aggarwal, 2002, Sun *et al.*, 2008, Tian *et al.*, 2005). Moreover, genetic deletions of RelA result in embryonic lethality in mice (Beg and Baltimore, 1996). Therefore therapeutic exploitation is more complex than simply inhibiting NF- $\kappa$ B activity.

Mutations often reside in genes that encode upstream regulators of NF- $\kappa$ B (Baud and Karin, 2009) and there are a number of known inhibitors of these components, including proteasome, I $\kappa$ B $\alpha$  and IKK inhibitors (Tergaonkar, 2006). However, many upstream targets, such as the proteasome, are also valuable parts of other pathways required for normal physiological function (Karin *et al.*, 2004). Thus for effective drug development, targeting NF- $\kappa$ B must focus on specific inhibition (Garg and Aggarwal, 2002). Specific inhibitors of TNF $\alpha$  and IL-1 $\beta$  are currently used to treat autoimmune disorders (Dhimolea, 2010, Wong *et al.*, 2008) and inhibitors of specific kinases, such as IKK $\beta$ , are in development (Karin *et al.*, 2004).

An understanding of how different aspects of the NF- $\kappa$ B network affect its activity will be of paramount importance in future drug discovery. Moreover, recent studies have shown that altering the oscillation frequency of NF- $\kappa$ B results in differential NF- $\kappa$ B-dependent gene expression (Ashall *et al.*, 2009). Therefore, modulation of NF- $\kappa$ B activity could provide an alternative avenue to exploit this transcription factor for therapeutic benefit while bypassing the toxic side effects that can be a result of inhibition.

## 1.6.2 – Aims and Objectives

The primary aim of this thesis is to use a Systems Biology approach to generate and test predictions about how the period of NF- $\kappa$ B oscillations can be controlled. The central hypothesis being that period modulation can alter the output of the NF- $\kappa$ B system helping to inform drug development.

Towards achieving this goal a range of computation analysis methods will be employed to understand how the different aspects of the system control NF- $\kappa$ B dynamics. These analyses will be undertaken in one of the most recent models of the canonical NF- $\kappa$ B pathway presented in Ashall *et al.* (2009), which will subsequently be referred to as the Ashall model. The methods used will include model reduction, to elucidate the core network topology, in conjunction with sensitivity and bifurcation analyses to address how different reactions influence the period. This solid computational framework will allow for the development of hypotheses regarding period control of the NF- $\kappa$ B system.

Negative feedbacks are central to generating sustained oscillations. Therefore, a key focus will be to understand the effect of the I $\kappa$ B $\alpha$  and A20 feedbacks, both computationally and experimentally. This will include an analysis of RelA single cell dynamics after co-transfection with constructs expressing I $\kappa$ B $\alpha$  and A20 from part, or all, of their endogenous promoter regions. These data will be used to further develop the *in silico* representation of the NF- $\kappa$ B system.

In addition, experimental analysis of perturbations that can potentially alter the oscillatory period will be undertaken. These new data will then be related to the existing NF- $\kappa$ B model to elucidate the mechanism responsible for their effect. Hopefully, this will allow for model development and new predictions to be generated regarding the function of the NF- $\kappa$ B system and how its dynamic behaviour can be altered.

# **Chapter 2 – Materials and Methods**

## **2.1 – Computational Methods**

Computational modelling was implemented using MATLAB (release 14 or later). Systems of ODEs were solved using the MATLAB function ODE15s, unless otherwise stated. Simulated time series data was analysed using MATLAB. All deterministic simulations and analysis were run off a single laptop. XPPAUTO was used to perform bifurcation analysis on the systems of ODEs studied (Doedel *et al.*, 2000, Ermentrout, 2002). MAPLE 13 was used for symbolic mathematics manipulation and the output converted to MATLAB for simulation.

## **2.2 – Experimental Techniques**

The majority of experimental data presented in this thesis has been collected by members of the Centre for Cell Imaging (CCI), University of Liverpool or the Systems Microscopy Centre (SMC), University of Manchester. Those people's contributions have been cited where appropriate. References are provided for all published experimental data used. This section outlines methods used for any unpublished data presented in this thesis.

### **2.2.1 – Reagents**

Non-essential amino acids and tissue culture medium were purchased from Gibco Life Technologies (UK). Foetal Bovine Serum (FBS) was from PAA Laboratories (UK). Human recombinant TNF $\alpha$  was supplied by Calbiochem (UK). All other reagents were supplied by Sigma-Aldrich unless otherwise stated.

### **2.2.2 – Plasmids**

The CMV-p65-DsRedXP and CMV-I $\kappa$ B $\alpha$ -EGFP constructs have been described previously (Nelson *et al.*, 2004). C. Gibney at the CCI created the pA20-EGFP-A20 construct using Invitrogen's Gateway<sup>TM</sup> cloning system. Plasmids were propagated using *E. coli* DH5 $\alpha$  and purified using Qiagen Maxiprep kits (Qiagen, UK).

### 2.2.3 – Restriction Endonuclease Digestion and Agarose Gel

#### Electrophoresis

0.5µg of DNA was combined with the appropriate restriction endonuclease (1U/µg DNA) in the presence of a supplied 1X buffer (Roche), and made to a total reaction volume of 20µl then incubated for 1.5h at the appropriate temperature (usually 37°C). Digested plasmids were combined with 1X DNA loading buffer (Bioline) and resolved by 1% agarose gel electrophoresis containing 1mg/µl SYBRsafe using HyperLadder 1 (Bioline) for 1h at 100V/s. Products were visualised by UV illumination using a Gel Doc (BioRad).

### 2.2.4 – Cell Culture

SK-N-AS (human S-type neuroblastoma, ECACC No. 94092302) cells were grown in Minimal Essential Medium with Earle's salts plus 10% (v/v) Foetal Bovine Serum and 1% (v/v) non-essential amino acids and maintained at 37°C, 5% CO<sub>2</sub>. Cells were grown as a monolayer culture in 75cm<sup>2</sup> tissue culture flasks (Corning, UK) and passaged when the monolayer reached 80% confluency. The media was removed, cells washed with Mg<sup>2+</sup>/Ca<sup>2+</sup> phosphate buffered saline (PBS) and then incubated with 1ml of 1x trypsin/EDTA (Invitrogen) for 2-5 minutes to detach the cells from the flask. Cells were re-suspended in 9ml of medium, centrifuged at 1000rpm for 5 minutes and the supernatant aspirated to remove traces of trypsin. The cell pellet was re-suspended in 10ml of fresh medium. A sample from the cell suspension was counted using a Z2 Coulter counter (Coulter, UK), the remaining cells diluted in medium and seeded as required (table 2.1).

**Table 2.1** - Commonly used tissue culture vessels, typical plating densities and corresponding volume of medium.

Cell Culture Vessel	Number of Cells Plated	Total Medium Volume
35mm dish	1x10 <sup>5</sup>	3ml
60mm dish	5x10 <sup>5</sup>	5ml
750ml flask	1x10 <sup>6</sup>	15ml

### **2.2.5 - Transfection**

Cells were transfected using FeuGene®6 transfection reagent as per manufacturer's instructions. For a 35mm dish a ratio of 2µl reagent to 1µg DNA was used for transient transfection of SK-N-AS cells, in 100µl of serum-free medium.

### **2.2.6 – Confocal Microscopy**

Imaging of transfected cells proceeded 24-48h post transfection. Microscopy was carried out in a humidified CO<sub>2</sub> incubator (at 37°C, 5% CO<sub>2</sub>) using a Zeiss LSM510 or LSM710 confocal microscope with a Plan-Apochromat 63x 1.4 NA or Fluar 40x 1.4 NA oil objective. Images were recorded approximately every 5 minutes for the duration of the experiment. After an initial period of time-lapse imaging (~1h) cells were stimulated with 10ng/ml TNFα. DsRedXP tagged proteins were visualised by excitation with a green helium neon laser (543nm) and emitted light was then reflected off a 545nm dichroic mirror and collected through a 560nm long-pass filter. EGFP and EYFP tagged proteins were visualised by excitation with a 488nm or 514nm argon ion laser. EGFP and EYFP emitted light was reflected from a 505-550nm band-pass filter from a 545nm dichroic mirror. Cyan tagged proteins were excited using the 458nm line of an argon ion laser and emitted light passed through a 475-510nm band-pass filter. Data capture was performed on the LSM510 using version AIM Version 4.2 of the LSM510 software and on the LSM710 using the ZEN2010B software.

### **2.2.7 – Image Analysis**

Fluorescence intensities were calculated using CellTracker version 0.6 or later (Du *et al.*, 2010, Shen *et al.*, 2006). Two methods of CellTracker were employed, whole-cell tracking and region of interest (ROI) tracking. Whole-cell tracking involved drawing accurate boundaries around the nucleus and cytoplasm, whilst ROI tracking involved drawing a circle in the area of interest in the cell. ROI tracking is more prone to noise but still provides largely similar data (Turner, 2010). CellTracker data was exported as mean intensity or total intensity into Microsoft Excel format. Microsoft Excel was used to analyse the imaging data.



CellTracker was also used to track speckled fluorescence. A small ROI was placed around the speckles of interest at intervals of approximately 3 frames (~3s). The distance between the centroid of ROIs was then calculated to follow their movement. In addition speckles were analysed using AQM Kinetic to filter out low intensity fluorescence and create a time stack of images.

### **2.2.8 – Western Blotting**

SK-N-AS cells were seeded into 60mm dishes at a density of  $5 \times 10^5$ , incubated for 24h and then subjected to experimental conditions. At the appropriate times cells were washed with PBS and lysed in 200 $\mu$ l lysis buffer [50mM Tris-HCl pH 7.5, 50mM NaCl, 0.5% Triton X-100, 0.5mM EDTA, 1mM DTT, 1xEDTA Free Protease Inhibitor Cocktail (Roche, UK), 1xPhosphatase Inhibitor Cocktail (Sigma-Aldrich, UK)]. Lysates were centrifuged for 10 minutes at 4°C (13,000rpm) and the protein concentration of the supernatant was measured using Pierce BCA Protein Assay Kit (Thermo-Fischer, USA). Samples were diluted into loading buffer [8M urea, 5% SDS, 10%  $\beta$ -mercaptoethanol], heated at 100°C for 5 minutes, and 35 $\mu$ g of protein was loaded into each well of a 10% SDS-PAGE gel. Samples were separated by electrophoresis and electro-transferred onto nitrocellulose membrane. Membranes were incubated in blocking buffer [5% dried skimmed milk in 0.1% Tween 20 supplemented Tris-buffered saline (TTBS)] for 1h at room temperature, followed by washing with TTBS. Detection of the protein was carried out using the appropriate primary and secondary antibodies as per manufacture's instructions (Cell Signaling, USA, Sigma-Aldrich, UK, see table 2.2). Nitrocellulose membranes were incubated for 1-2 minutes in ECL reagent (SuperSignal West Dura Extended Duration Substrate, Thermo-Scientific, USA). The membranes were exposed on CL-Xposure films (Thermo-Scientific, USA) according to manufacturers instructions and the integrated intensity of protein bands were quantified using AQM Advanced6 (Andor, UK).

**Table 2.2** - Summary of the antibodies used in Western blotting, showing the protein of interest, supplier, dilution and the species.

Probe	Supplier	Typical Dilution	Species
Phospho – p65	Cell Signalling, UK	1:1000	Rabbit
Phospho – IκBα	Cell Signalling, UK	1:1000	Mouse
IκBα	Cell Signalling, UK	1:1000	Rabbit
Histone 3	Sigma-Aldrich, UK	1:1000	Rabbit

### 2.2.9 – Quantitative RT-PCR

Cells were seeded into 60mm dishes at a density of  $1 \times 10^6$  and incubated for 24h prior to stimulation with 10ng/ml TNF $\alpha$  (Calbiochem, UK) for the required duration. The RNeasy Mini Kit (Qiagen, Germany) was used to extract mRNA from cells. Prior to lysis the media was removed and the cells were washed with ice cold PBS. 600 $\mu$ l of lysis buffer RLT containing  $\beta$ -mercaptoethanol (1% (v/v)) was added to lyse the cells. Homogenisation of the lysate was performed using a QIAshredder (Qiagen, Germany), as detailed in the protocol. Samples were eluted into 30 $\mu$ l of RNase free water and stored at -80°C. The mRNA quantity and purity was assessed using a Nanodrop 1000 spectrophotometer (Thermo Scientific).

Reverse transcription of extracted RNA (to cDNA) was carried out using SuperScript® VILO cDNA Synthesis Kit (Invitrogen). 2 $\mu$ g of mRNA was used according to the manufacturer's protocol then the cDNA was diluted 1 in 20 with RNase free water.

Q-PCR reactions were carried out in triplicates. 20 $\mu$ l mixtures were made using 1 $\mu$ l of cDNA, 300nM of primer (sequences table 2.3), 1x LightCycler 480 SYBR Green PCR mastermix (Roche) with RNase free H<sub>2</sub>O. Temperature cycling was performed using a LightCycler 480 (Roche) using the parameters in table 2.4. Results were analysed using the LightCycler 480 software to calculate the fold changed based on the threshold cycle (CT) value for each PCR reaction using the  $2^{-\Delta\Delta CT}$  method (Pfaffl *et al.*, 2002). The target gene was normalised to the reference gene cyclophilin A,

with time 0-min used as a calibrator. *Quantitative RT-PCR experiments were performed by Dr L. Ashall at the Systems Microscopy Centre, University of Manchester.*

**Table 2.3** - Quantitative RT-PCR primer sequences.

Target cDNA	Forward Primer (5' to 3')	Reverse Primer (5' to 3')
IκBα	TGGTGCCTTGGGTGCTGAT	GGCAGTCCGGCCATTACA
A20	CACAAGCTTCCGGACTTCTC	GCCCTCATCGACAGAAACAT
Cyclophilin A	GCTTTGGGTCCAGGAATGG	GTTGTCCACAGTCAGCAATGGT

**Table 2.4** - Quantitative RT-PCR cycle conditions.

Step	Temperature (°C)	Duration
Initial denaturation	95	5-min
Denaturation	95	10s
Annealing & elongation	60	30s

### 2.2.10 - Microarray

Cell lysis and mRNA extraction were performed according to the protocol in section 2.2.9. 300ng RNA was converted to cDNA using the TransPlex® Whole Transcriptome Amplification (WTA1) kit (Sigma). The protocol was carried out according to manufacturer's instructions with 17 cycles for the amplification stage. The NimbleGen™ (Roche) human gene expression microarray service was used and cDNA was sent for hybridisation and analysis according to their protocol. *Experiments were performed by Dr C. Harper and Dr L. Ashall at the Systems Microscopy Centre, University of Manchester. Analysis to determine differentially expression genes was performed by Dr B. Noyvert at the Systems Biology Centre, University of Warwick, and D. Daniels at the Systems Microscopy Centre, University of Manchester.*

## **2.2.11 - Cell Treatments**

### **2.2.11.1 – Diclofenac**

Diclofenac (Sigma-Aldrich, UK) was administered 90 minutes before stimulation at doses of 300 $\mu$ M or 500 $\mu$ M, before being used for western blot analysis of confocal microscopy.

### **2.2.11.2 - Temperature**

For experimental conditions at temperatures other than 37°C cells were incubated at the appropriate temperature (35°C, 39°C or 40°C) at 5% CO<sub>2</sub> 1 hour prior to analysis.

For experimental conditions at temperatures other than 37°C cells were incubated at the appropriate temperature (35°C, 39°C or 40°C) and 5% CO<sub>2</sub> for 1h prior to experimentation.

**Chapter 3 –  
A Minimal Model of the NF- $\kappa$ B  
System**

### 3.1 – Minimal Models: A Systems Biology Tool

The dynamical models that represent biological systems can often have high-dimensional state space and depend on a large number of parameters. Understanding the relationship between structure, parameters and function of such large systems is often a challenging and computationally intensive task. A prime example of such a complex and high-dimensional system is the signalling network of the Nuclear Factor kappa B (NF- $\kappa$ B) transcription factor. Sensitivity analysis is often employed to understand these models, assessing how individual parameters influence model dynamics in a local and global context (Ihekwaba *et al.*, 2005, Ihekwaba *et al.*, 2004, Rand, 2008). Model reduction approaches provide an alternative avenue to extract the core reactions and variables responsible for the key dynamical features of the system.

There are various methods to reduce the complexity of biochemical models. These include modularisation, separation of timescale and error analysis methods. These methods have been defined with varying degrees of rigour. Modularisation involves separating a system into functional units (Saez-Rodriguez *et al.*, 2004), however, there is no clear definition of a module so this remains a heuristic technique. Timescale methods utilise the fact that systems often incorporate markedly different timescale ranging from seconds to hours. These approaches include the application of partial-equilibriums (PE), quasi-steady-state approximations (QSSA), or grouping variables with equivalent timescales (Krishna *et al.*, 2006, Maeda *et al.*, 1998, Schneider and Wilhelm, 2000). However, these methods often rely on intuition to determine reduction steps. More rigorous methods have also been defined, such as the Computational Singular Perturbation (CSP) and Intrinsic Low-Dimensional Manifold Methods (Lam and Goussis, 1994, Surovtsova *et al.*, 2009). These methods include rules to determine the variable to remove based on the timescales of the system. However, these methods are more abstract and therefore not necessarily accessible to interdisciplinary researchers. Model reduction methods have been successfully applied to numerous biochemical systems including neuronal models, NF- $\kappa$ B and calcium signalling (Krishna *et al.*, 2006, Maeda *et al.*, 1998, Surovtsova *et al.*, 2009).

This chapter outlines a QSSA method for the reduction of a biochemical reaction system using an application of Tikhonov's theorem (Tikhonov, 1952). "Speed coefficients" are defined that enable ranking of variables according to how quickly they approach their momentary steady-state. This allows a straightforward and rigorous elimination of variables through asymptotic expansion around a QSSA for each variable removed, while preserving dynamic characteristics of the system. This method is used to derive a minimal model of the NF- $\kappa$ B signalling network from the model presented in Ashall *et al.* (2009).

## 3.2 – A Method of “Speed Coefficients”

### 3.2.1 – Perturbation Theory

The application of steady-state approximation (QSSA) to biochemical reaction systems typically argues that some of the reagents are highly reactive, so are used as quickly as they are made. Therefore, after the initial transient phase, the concentration of such a reagent is always close to what would be its steady state, if concentrations of other reagents were maintained constant. In the simplest form, this means that in the kinetic equations, the corresponding rate of change can be set to zero. This provides a general procedure for simplifying biochemical systems, based on the difference of characteristic time-scales (Klonowski, 1983). The basic mathematical justification of the formal procedures stems from the work by (Tikhonov, 1952). More refined results justifying higher-order approximations based on the same idea have also been described (Fenichel, 1979). In the real-life kinetic equation it is not always obvious which reagents can be suitable for the QSSA. To identify such reagents, a formal method of “parametric embedding” can be followed (Biktasheva *et al.*, 2006, Suckley and Biktashev, 2003). Our procedure is described in terms of a generic system of  $N$  ordinary differential equations (ODEs),

$$\frac{dx_i}{dt} = f_i(x_1, \dots, x_N), i = 1, \dots, N. \quad (3.1)$$

The “speed coefficients” are defined for each dynamic variable  $x_i$  as

$$\lambda_i(x_1, \dots, x_N) = \left| \frac{\partial f_i}{\partial x_i} \right|. \quad (3.2)$$

By definition, these coefficients depend on the dynamic variables, or, for a selected solution, they depend on time  $t$ . They can be used to rank the variables according to how quickly they approach their momentary steady states (figure 3.1). Once the fastest variable has been identified, the system can be formulated in terms of an artificial small parameter  $\varepsilon$ :

$$\begin{aligned} \frac{df}{dt} &= f(x, z, t), \\ \varepsilon \frac{dg}{dt} &= g(x, z, t), \end{aligned} \quad (3.3)$$



where  $x$  is a vector of slow variables and  $z$  is the fast variable. This is termed a one-parametric embedding of the system, discussed in detail in (Suckley and Biktashev, 2003). Briefly, the idea is that if the variable is indeed the fastest, then the solution will only slightly change if it made even faster. Hence although the original problem corresponds to  $\varepsilon = 1$ , a good approximation can be obtained in the limit  $\varepsilon \rightarrow 0$ . In this limit, the system (3.3) becomes

$$\begin{aligned} \frac{df}{dt} &= f(x, z, t), \\ z &= \phi(x, t), \end{aligned} \quad (3.4)$$

where  $\phi(x, t)$  is the solution of  $g(x, z, t) = 0$ . If  $\varepsilon$  is small, the solutions to the original system (3.3) differ from solutions of (3.4) only slightly; this is true both for solutions of an initial-value problem for a finite interval (Tikhonov, 1952) and for long-term solutions, say limit cycles (Fenichel, 1979).

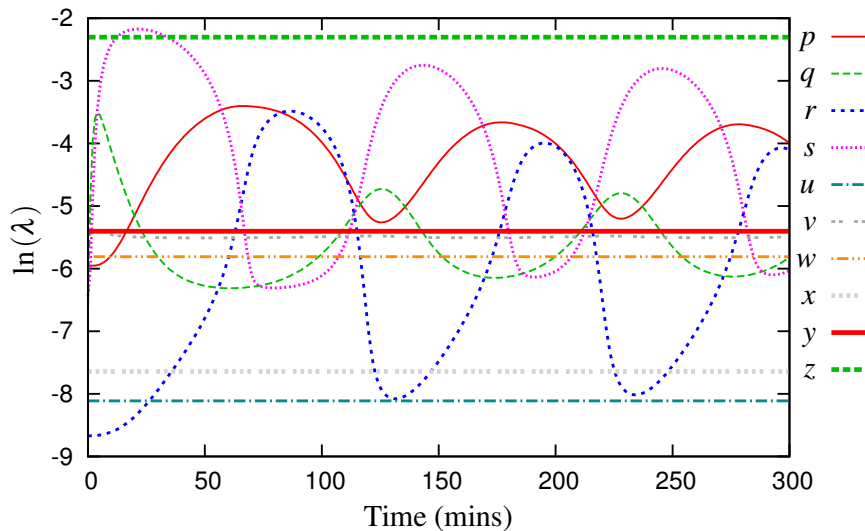


**Figure 3.1** – Semi-logarithmic plot of speed coefficients for the Simplified Model (see section 3.3). A larger speed coefficient means the variable is approaching its steady state faster. These coefficients identify the variable  $z$  as the fastest, and therefore most appropriate candidate for elimination.

### 3.2.2 – Method of Speed Coefficients for Model Reduction

Based on Tikhonov's and Fenichel's theorems and the definition the speed coefficients a general method can be defined for reducing the dimension of a biochemical reaction system. The method is illustrated using an example where the right-hand side of its ordinary differential equation is linear with respect to the same variable. Suppose the variable  $x_j$  has been identified as the fast variable in the system (3.1). With account of the artificial small parameter, this gives

$$\varepsilon \frac{dx_j}{dt} = \alpha_j(t) - \beta_j(t)x_j, \quad (3.5)$$

where coefficients  $\alpha_j(t)$  and  $\beta_j(t)$  are presumed to depend on time via other dynamic variables. A solution is sought in the form of an asymptotic series  $x_j = x_j^0 + \varepsilon x_j^1 + \varepsilon^2 x_j^2 + \mathcal{O}(\varepsilon^3)$ . Substituting this into (3.5) gives

$$\varepsilon \dot{x}_j^0 + \varepsilon^2 \dot{x}_j^1 + \varepsilon^3 \dot{x}_j^2 = \alpha - \beta x_j - \varepsilon \beta x_j^1 - \varepsilon^2 \beta x_j^2 + \mathcal{O}(\varepsilon^3). \quad (3.6)$$

The simplest approximation for  $x_j$  is obtained by considering the terms in (3.6) proportional to  $\varepsilon^0$ ,

$$0 = \alpha(t) - \beta(t)x_j^0, \quad (3.7)$$

which results in the zeroth-order QSSA for variable  $x_j$ :

$$\bar{x}_j^0 = x_j^0 = \frac{\alpha_j(t)}{\beta_j(t)}. \quad (3.8)$$

This approximation  $x_j^0$  is then substituted into the original system of equations for the variable  $x_j$ . If the variable is sufficiently fast then this steady-state expression should be a good approximation of the fast variable and the substitution will cause minimal change to the solution.

In general, the zeroth-order QSSA provides a reasonable approximation of the original variable. However, if such approximation is not good enough, it can be improved by calculating an additional correction term.

This is done by considering terms in (3.6) proportional to  $\varepsilon^1$ :

$$\varepsilon \dot{x}_j^0 = -\varepsilon \beta x_j^1. \quad (3.9)$$

Substituting our earlier result (3.8) into equation (3.9) and solving for  $x_j^1$  gives the first-order correction in the form

$$x_j^1 = -\frac{1}{\beta} \dot{x}_j^0 = \frac{\alpha_j \dot{\beta}_j - \beta_j \dot{\alpha}_j}{\beta_j^3}. \quad (3.10)$$

This results in the first-order QSSA  $\bar{x}_j^1 = x_j^0 + \varepsilon x_j^1$  in the form

$$x_j^1 = \frac{\alpha_j(t)}{\beta_j(t)} + \frac{\alpha_j(t)\dot{\beta}_j(t) - \beta_j(t)\dot{\alpha}_j(t)}{\beta_j^3(t)}, \quad (3.11)$$

since the original problem corresponds to  $\varepsilon = 1$ . This method can then be formulated into a general algorithm to reduce the dimension of a biochemical system defined by ordinary differential equations. The algorithm reads:

1. Using numerical methods, find a representative solution of the system of ODEs for the chosen time interval.
2. Calculate the expressions for the time scale coefficients ( $\lambda$ 's), using equation (3.2) from the system of ODEs (this can be assisted by a symbolic calculations software, e.g. Maple).
3. Substitute the numerical solution of the system into the expressions for the  $\lambda$ 's to find the speed for each variable at each time point.
4. Plot the speed coefficients vs. time and identify the fastest variable.
5. Calculate the expression for the zeroth-order QSSA using (3.8).
6. Substitute this QSSA into the system of ODEs to eliminate the fastest variable, thus obtaining a reduced system.
7. Compare the solution of the reduced system with the solution of the original system.
8. *If the zeroth-order QSSA is insufficient to maintain a suitable accuracy, calculate the first-order QSSA using equation (3.11).*
9. Repeat the process above for the new reduced system.

### 3.3 – Minimal Model of the NF- $\kappa$ B System with respect to Continuous TNF $\alpha$ Stimulation

#### 3.3.1 – Initial Model Simplification

The “two-feedback” deterministic model of the NF- $\kappa$ B system presented in Ashall *et al.* (2009) form the starting point of this process. It is a system of 14 ordinary differential equations representing NF- $\kappa$ B and the negative feedbacks I $\kappa$ B $\alpha$  and A20 (figure 3.11a). For this chapter a brief notation for variables and parameters is used as given in table 3.1. A minimal model has been sought with respect to a representative solution that was obtained for initial conditions as described in table 3.1 and  $k_{24} \equiv 1$ . In a biological context this corresponds to continuous stimulation of the system with a high dose of 10ng/ml TNF $\alpha$  (Ashall *et al.*, 2009).

Before employing the reduction algorithm the system was simplify by elementary means. It was noticed that  $\frac{d}{dt}(v + w + a) = 0$ , so there is a conserved quantity  $v + w + a = k_2 = const$ , which represents the total amount of IKK in the cell. This allows to eliminate  $a$  via substitution  $a = k_3 - v - w$ . Likewise,  $p + r + z + c + d = k_3 = const$  is the conserved total amount of NF- $\kappa$ B in all its five forms, which we used to eliminate  $d$ . Further, that variable  $b$  is “decoupled”: it is only present in its own equation, and the dynamics of other variables do not depend on it. So it can be removed from the analysis, as the solution for it, if necessary, can be obtained by post factum by integration from solution of the remaining system. Finally, for this representative solution it was observed that some of the terms in the equation consistently remain so small that their elimination does not visibly change the solution. Then variable  $c$  becomes decoupled in the same sense after elimination of the small terms.

**Table 3.1** – Variables and parameters: their names as in Ashall *et al.* (2009), alternative short names and values. The initial conditions were obtained by equilibrating the system without stimulus ( $k_{24}=0$ ), with  $v$  and  $r$  set to  $k_2$  and  $k_3$  respectively, and other variables set to zero. \* IKK =  $v + w + a$ . † NF $\kappa$ B =  $p + r + z + c + d$ .

Variables			
NF $\kappa$ B	Cytoplasmic NF- $\kappa$ B	$p$	$3.81 \times 10^{-3}$
I $\kappa$ B $\alpha$	Cytoplasmic I $\kappa$ B $\alpha$	$q$	$1.58 \times 10^{-2}$
nNF $\kappa$ B	Nuclear NF- $\kappa$ B	$r$	$9.79 \times 10^{-3}$
nI $\kappa$ B $\alpha$	Nuclear I $\kappa$ B $\alpha$	$s$	$5.44 \times 10^{-3}$
tI $\kappa$ B $\alpha$	I $\kappa$ B $\alpha$ mRNA	$u$	$2.07 \times 10^{-5}$
IKK $n$	Neutral IKK	$v$	0.08
IKK $a$	Active IKK	$w$	0
tA20	A20 mRNA	$x$	$6.49 \times 10^{-6}$
A20	A20 protein	$y$	$7.19 \times 10^{-4}$
pI $\kappa$ B $\alpha$ o NF $\kappa$ B	Phospho I $\kappa$ B $\alpha$ complexed with NF- $\kappa$ B	$z$	0
IKK $i$	Inactive IKK	$a$	0
pI $\kappa$ B $\alpha$	Phosphorylated I $\kappa$ B $\alpha$	$b$	0
nI $\kappa$ B $\alpha$ o nNF $\kappa$ B	Nuclear I $\kappa$ B $\alpha$ complexed with NF- $\kappa$ B	$c$	$7.95 \times 10^{-4}$
I $\kappa$ B $\alpha$ o NF $\kappa$ B	Cytoplasmic I $\kappa$ B $\alpha$ complexed with NF- $\kappa$ B	$d$	$7.30 \times 10^{-2}$
Parameters			
$k_v$	Ratio of nuclear to cytoplasmic volume	$k_1$	3.3
TIKK*	Total amount of IKK	$k_2$	0.08 $\mu$ M
TNF- $\kappa$ B†	Total amount of NF- $\kappa$ B	$k_3$	0.08 $\mu$ M
$ka1a$	I $\kappa$ B $\alpha$ and NF- $\kappa$ B association in cytoplasm	$k_4$	0.5
$c1a$	I $\kappa$ B $\alpha$ transcription	$k_5$	$1.4 \times 10^{-7}\mu\text{M}^{-1}\text{s}^{-1}$
$c2a$	I $\kappa$ B $\alpha$ mRNA translation	$k_6$	$0.5\text{s}^{-1}$
$c3a$	I $\kappa$ B $\alpha$ mRNA degradation	$k_7$	$0.0003\text{s}^{-1}$
$c4a$	I $\kappa$ B $\alpha$ protein degradation	$k_8$	$0.0005\text{s}^{-1}$
$c1$	A20 transcription	$k_9$	$1.4 \times 10^{-7}\mu\text{M}^{-1}\text{s}^{-1}$
$c2$	A20 mRNA translation	$k_{10}$	$0.5\text{s}^{-1}$
$c3$	A20 mRNA degradation	$k_{11}$	$0.00048\text{s}^{-1}$
$c4$	A20 protein degradation	$k_{12}$	$0.0045\text{s}^{-1}$
$ki3a$	I $\kappa$ B $\alpha$ nuclear import	$k_{13}$	$0.00067\text{s}^{-1}$
$ke3a$	I $\kappa$ B $\alpha$ nuclear export	$k_{14}$	$3.35 \times 10^{-4}\text{s}^{-1}$
$ki1$	NF- $\kappa$ B nuclear import	$k_{15}$	$0.0026\text{s}^{-1}$
$ke1$	NF- $\kappa$ B nuclear export	$k_{16}$	$0.00052\text{s}^{-1}$
$kc1a$	I $\kappa$ B $\alpha$ phosphorylation by IKK	$k_{17}$	$0.074\text{s}^{-1}$
$kc2a$	I $\kappa$ B $\alpha$ :NF- $\kappa$ B phosphorylation by IKK	$k_{18}$	$0.185\text{s}^{-1}$
$kt2a$	Phospho-I $\kappa$ B $\alpha$ :NF- $\kappa$ B degradation	$k_{19}$	$0.1\text{s}^{-1}$
$kp$	IKK recycling	$k_{20}$	$0.0006\text{s}^{-1}$
$kbA20$	A20 inhibition rate	$k_{21}$	0.0018 $\mu$ M
$ka$	IKK activation	$k_{22}$	$0.004\text{s}^{-1}$
$ki$	IKK inactivation	$k_{23}$	$0.003\text{s}^{-1}$
$TR$	TNF $\alpha$ stimulation	$k_{24}$	1/0
$k$	Order of the Hill function for transcription		0.065 $\mu$ M
$h$	Half-max constant of the Hill function		2

This resulted in a system of 10 equations, which shall be referred to as the Simplified Model (SM):

$$\frac{dp}{dt} = k_{19}z - k_4qp - k_{15}p + k_{16}r \quad (3.12a)$$

$$\frac{dq}{dt} = k_6u - k_4qp - k_8q - k_{13}q + k_{14}s - k_{17}wq \quad (3.12b)$$

$$\frac{dr}{dt} = k_{15}k_1p - k_4sr - k_{16}k_1r \quad (3.12c)$$

$$\frac{ds}{dt} = k_{13}k_1p - k_4sr - k_8s - k_{14}k_1s \quad (3.12d)$$

$$\frac{du}{dt} = k_5 \frac{r^h}{r^h+k^h} - k_7u \quad (3.12e)$$

$$\frac{dv}{dt} = k_{20} \frac{k_{21}}{k_{21}+k_{24}v} (k_2 - v) - k_{24}k_{22}v \quad (3.12f)$$

$$\frac{dw}{dt} = k_{24}k_{22}v - k_{23}w \quad (3.12g)$$

$$\frac{dx}{dt} = k_9 \frac{r^h}{r^h+k^h} - k_{11}u \quad (3.12h)$$

$$\frac{dy}{dt} = k_{10}x - k_{12}y \quad (3.12i)$$

$$\frac{dz}{dt} = k_{18}w \left( k_3 - p - \frac{r}{k_1} \right) - k_{19}z \quad (3.12j)$$

This model is very close to the original, as can be seen from (figure 3.2 and table 3.2), and makes the starting point of the reduction procedure. The reduction algorithm is applied iteratively, eliminating a sequence of fast variables and employing different orders of approximation for them. To keep track of these, a nomenclature for the reduced models is introduced. The model variants are named according to the variables that have been removed, each with a subscript showing if a zeroth- or first-order QSSA has been used, 0 or 1 respectively. For example, the first variable eliminated is  $z$ , therefore the model with this variable replaced with a zeroth-order QSSA is titled  $z_0$  and the same with a first-order QSSA is titled  $z_1$ . A model where the variables  $z$  and  $p$  have been replaced in turn with their zeroth- and first-order QSSAs respectively will be denoted as  $z_0p_1$ , etc.

### 3.3.2 – Outline of Key Reduction Steps

In this section key points of the reduction sequence are explained to demonstrate the application of the method. However, in the interest of brevity not all steps are explained fully. Figure 3.1 shows the speed coefficients calculated for the simplified model. From these it can be seen that the fastest variable to eliminate in the first iteration is  $z$ . Application of the method, using zeroth-order approximation, results in a 9-variable model with comparable solution trajectories to those of the simplified model, as illustrated in figure 3.2.

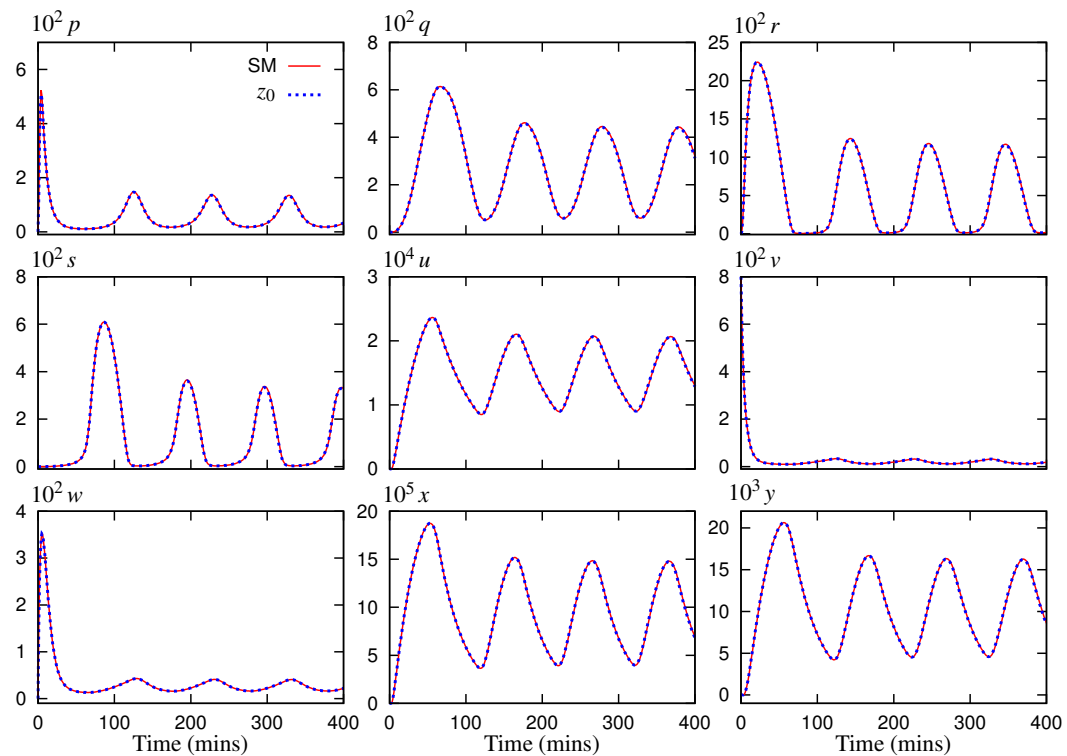


**Figure 3.2** - Components of the representative solution for the 10-variable Simplified Model (SM, solid lines) and reduced 9-variable model  $z_0$  (dashed lines). The lines visually coincide in all cases, indicating that zeroth-order approximation is sufficient for  $z$ .

Addition of a first-order correction to some of the QSSAs improved the model fit in comparison to respective predecessors. Figure 3.3 shows that a first-order correction in the variable  $p$  markedly improved the accuracy of the 8-variable reduced model. However, addition of these corrections can also increase the algebraic complexity of the system and it must be considered whether the improvement of the model outweighs the added complexity.

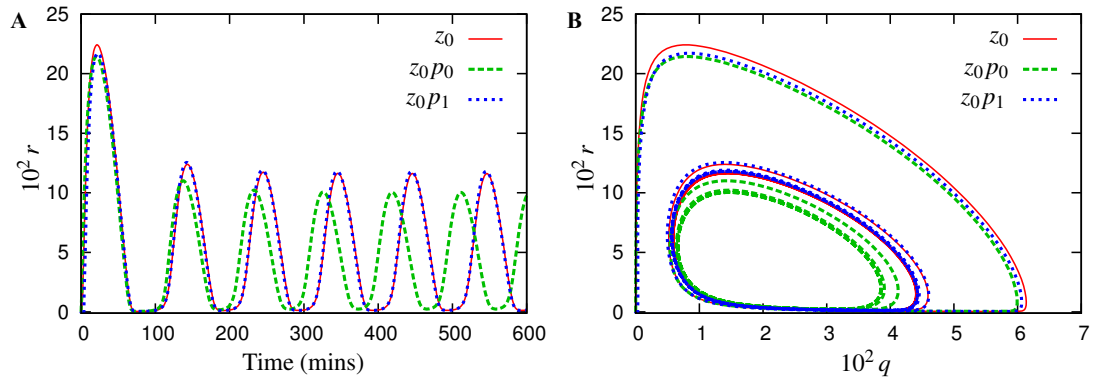


**Figure 3.3** – Comparison of the representative solution for the 9-variable model  $z_0$  (solid lines) and its two 8-variable reductions, with the zeroth-order (dashed lines) and the first-order (dotted lines) approximations for  $p$ . (A) Shows a solution for the variable nuclear NF- $\kappa$ B,  $r$ . (B) Shows a phase plane for the variables  $q$  and  $r$ . Use of the first-order approximation gives a marked improvement in accuracy of the reduced model.

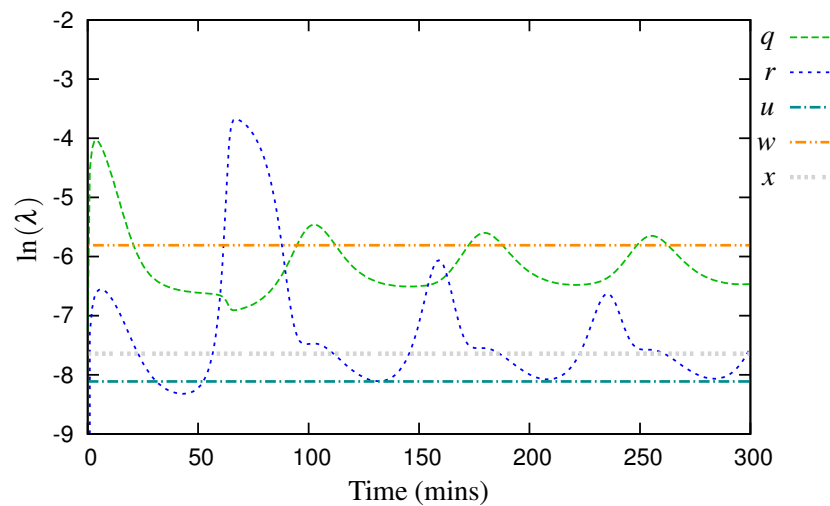


**Figure 3.4** – Semi-logarithmic plot of speed coefficients for dynamic variables of the  $z_0 p_0 y_0 v_0 s_0$  model. The variable  $w$  has the largest minimum compared to other variables, identifying it as the most appropriate candidate for the next elimination.



As the reduction progressed, there was an increasing overlap in the ranges of the speed coefficients. For elimination of any ambiguity a rule was adopted to select for elimination the variable that is fastest at its slowest. This means the variable that has the maximal of the minimum values of the speed coefficients over the simulated time interval. For example in figure 3.4, this rule identifies the variable  $w$  for elimination during reduction to the 4-variable model, even though two other variables,  $r$  and  $q$ , are at times faster.

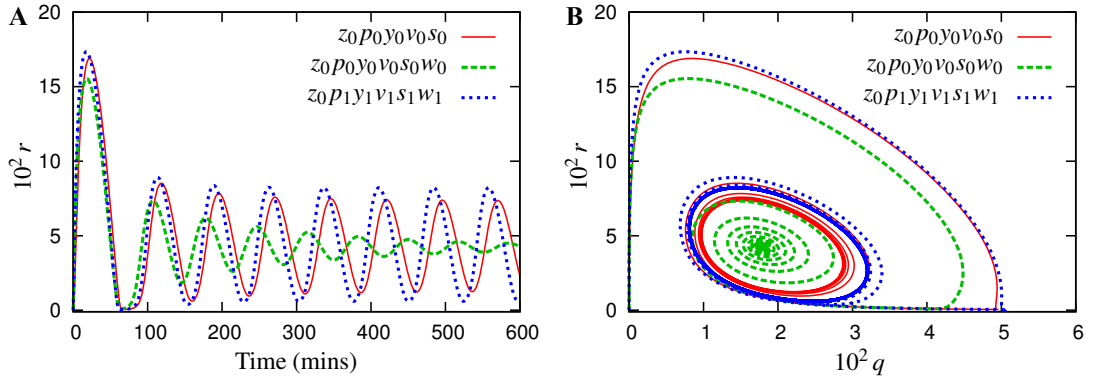


**Figure 3.5** – Comparison of the representative solution for the 5-variable model  $z_0 p_0 y_0 v_0 s_0$  (solid lines) and its two possible 4-variable reductions, with the zeroth-order (dashed lines) and the first-order (dotted lines) approximations for  $w$ . Use of the first-order approximation not only improved the accuracy of the 4-variable model, but also maintained a stable limit cycle.

Successive cycles of the algorithm were applied to ultimately reduce this system to four differential equations. The method maintained the important qualitative features of the system, such as the limit cycle. However, through each stage of the reduction, the resulting limit cycle had a slightly reduced period and amplitude (table 3.2). Using only the zeroth-order QSSAs was sufficient to reduce the model to five ODEs ( $z_0 p_0 y_0 v_0 s_0$ ), while maintaining the limit cycle. In order to reduce the system further, the use of a first-order QSSA was necessary (figure 3.5). A suitable zeroth- or first-order QSSA could not be calculated to reduce the model beyond this and therefore the model,  $z_0 p_0 y_0 v_0 s_0 w_1$ , of four differential equations was chosen as the end point of this analysis. This minimal model is given by (3.13), where  $A = k_{24} k_{22} k_{20} k_{21} k_{12} k_3$  and  $B = k_{20} k_{21} k_{12} + k_{24} k_{22} k_{21} k_{12} + k_{24}^2 k_{22} k_{10} k_{23} x$ .

$$\frac{dq}{dt} = k_6 u - k_4 q \bar{p}(q, r, x) - k_8 q - k_{13} q + k_{14} \bar{s}(q, r) - k_{17} \bar{w}(r, x) q \quad (3.13a)$$

$$\frac{dr}{dt} = k_{15} k_1 \bar{p}(q, r, x) - k_4 \bar{s}(q, r) r - k_{16} k_1 r \quad (3.13b)$$

$$\frac{du}{dt} = k_5 \frac{r^h}{r^h + k^h} - k_7 u \quad (3.13c)$$

$$\frac{dx}{dt} = k_9 \frac{r^h}{r^h + k^h} - k_{11} u \quad (3.13d)$$

$$\bar{w}(r, x) = \frac{A}{B(x)} + \frac{k_{24}^2 k_{22} k_{10} A \left( \frac{k_9 r^h}{k^h + k^h} - k_{11} x \right)}{B(x)^2} \quad (3.13e)$$

$$\bar{s}(q, r) = \frac{k_1 3q}{k_4 r + k_1 k_{14} + k_8} \quad (3.12f)$$

$$\bar{p}(q, r, x) = \frac{k_{16} r + k_{18} \bar{w}(r, x) \left( k_3 - \frac{r}{k_1} \right)}{k_4 q + k_{15} + k_{18} \bar{w}(r, x)} \quad (3.13g)$$

It was possible to add first-order corrections to all of the dynamic variables during the model reduction, producing a minimal model  $z_l p_l y_l v_l s_l w_l$  with a far improved fit in comparison to the original. However, the  $z_0$  approximation was so accurate that  $z_l$  did not make a noticeable improvement. Figure 3.6 shows comparison of the “simplest” and “the most accurate” 4-variable models to the original 10-variable one (the  $z_0 p_l y_l v_l s_l w_l$  model is presented in Appendix 2.1).

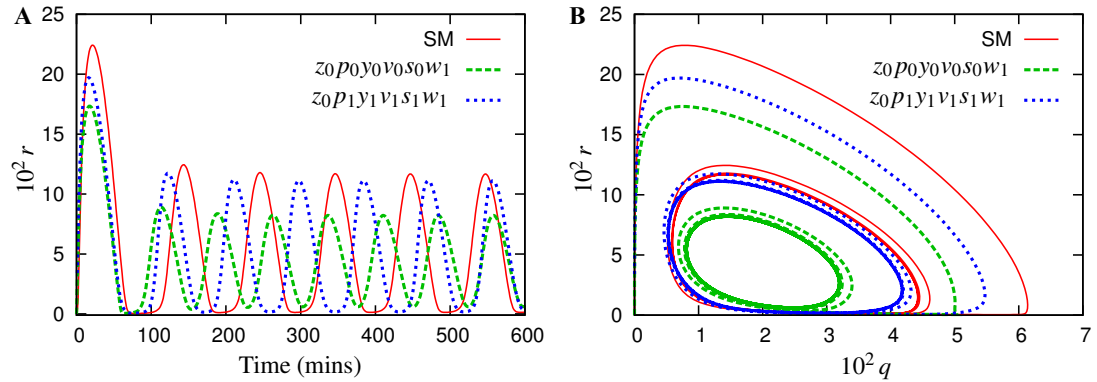


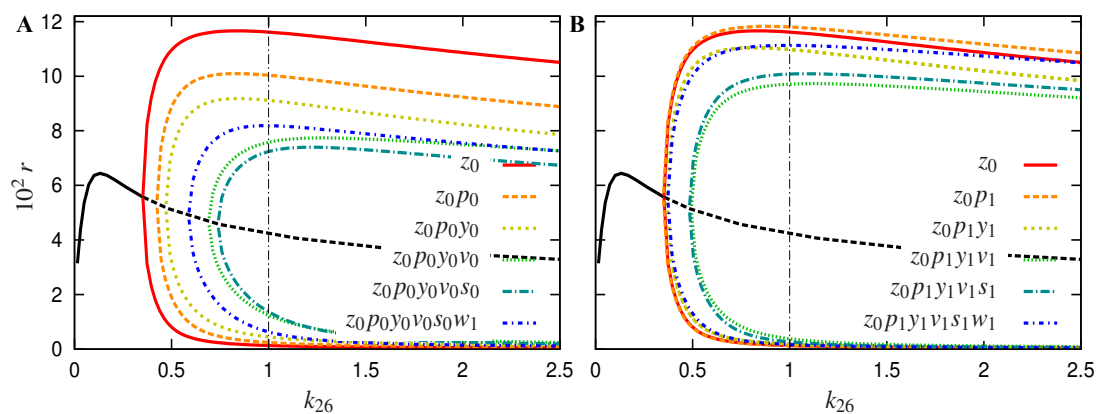
**Figure 3.6** – Comparison of the representative solution for the Simplified Model (solid lines) and the two four-variable reductions, the cruder  $z_0 p_0 y_0 v_0 s_0 w_1$  model (dashed lines) and the more accurate  $z_0 p_1 y_1 v_1 s_1 w_1$  (dotted lines). (A) Shows a time course for the variable  $r$  (nuclear NF-κB) (B) shows a phase-plane for the variables  $r$  and  $q$  (nuclear NF-κB and IκBα).

**Table 3.2** - Key dynamic features of the NF-κB system for each of the model variants. Fold change in period and amplitude was calculated relative to the period and amplitude of the original model in Ashall *et al.* (2009). MSE was calculated after the model had been scaled to have the same period to determine the qualitative differences in solutions.

Model	Variable Removed at this stage	Period (mins)	Fold change in period	Fold change in amplitude	Shape MSE $\times 10^5$
Original Model	N/A	99.5	1	1	N/A
Simplified Model	$a, b, c, d$	100.5	1.01	1.06	1.24
$z_0$	$z$	100	1.01	1.06	10.5
$z_0 p_0$	$p$	92.5	0.93	0.92	2.47
$z_0 p_0 y_0$	$y$	85.5	0.86	0.83	9.42
$z_0 p_0 y_0 v_0$	$v$	77.7	0.78	0.65	32.4
$z_0 p_0 y_0 v_0 s_0$	$s$	75.0	0.75	0.62	38.6
$z_0 p_0 y_0 v_0 s_0 w_1$	$w$	73.8	0.74	0.71	22.3
$z_0 p_1 y_0 v_0 s_0 w_1$	As above	80.3	0.80	0.90	5.28
$z_0 p_1 y_1 v_1 s_1 w_1$	As above	86.6	0.87	1.01	6.31

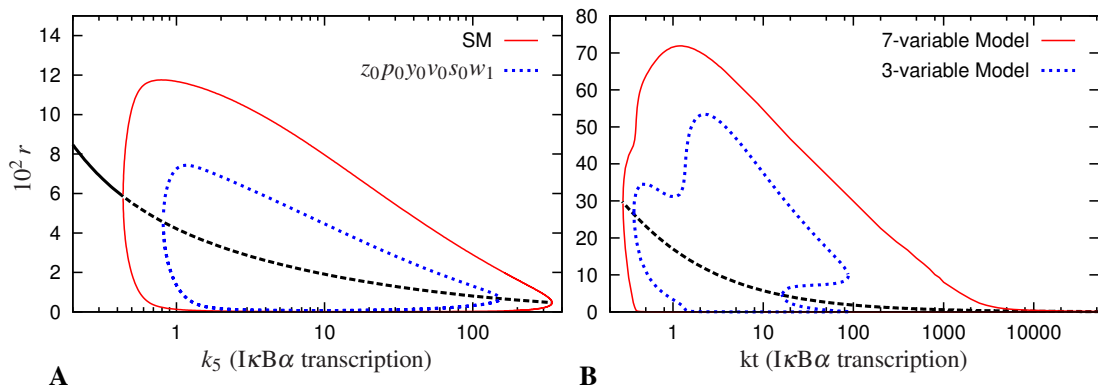
### 3.4 – Effect of the Method on Dynamic Properties of the NF- $\kappa$ B Model

Figure 3.7 shows how some of the dynamic properties of the model change through the reduction process. It represents the steady state solution and continuation for the variable  $r$  as the parameter  $k_{24}$  is varied (calculated using XPPAUT), showing the effect of altering the TNF $\alpha$  dose (Turner *et al.*, 2010). In the original model, there is a supercritical Hopf bifurcation (HB) at  $k_{24}=0.36$  above which the limit cycle is observed. Successive elimination of the fastest variables causes the HB point to move up closer to the  $k_{24} = 1$ , which corresponds to a saturating dose of TNF $\alpha$ . Reduction from five to four differential equations using zeroth-order QSSA for  $w$  would move the HB point further to the right (Hopf bifurcation at  $k_{24} = 3.105$ ), killing off the limit cycle at the standard value  $k_{24} = 1$ . As a value of 1 represents a saturating dose of TNF $\alpha$ , limit cycle behaviour at this point is key dynamic feature of the system. However, first-order QSSA for  $w$  moves the HB point in the opposite direction. Figure 3.7 also demonstrates that use of the first-order correction terms dramatically reduces the loss in limit cycle amplitude and change in location of the HB point.



**Figure 3.7** – Bifurcation analysis for the different stages of the model reduction, with respect for the parameter  $k_{24}$ , representing the dose of TNF $\alpha$  stimulation. The lines described in the legends represent minimal and maximal values achieved in limit cycles in the corresponding models. Otherwise, the solid lines going through the middle represent the stable equilibrium and the dashed lines represent the unstable equilibrium. (A) Bifurcation analysis for the models generated when using zeroth-order approximations. (B) Bifurcation analysis for the models generated when using first-order approximations.

Many mathematical models have been developed to investigate feedback control of the NF- $\kappa$ B system (Hoffmann *et al.*, 2002, Lipniacki *et al.*, 2004, Sung *et al.*, 2009). Of particular relevance to this work is the 3-variable minimal model developed by Krishna *et al.* (2006). This model was based on a previously published one-feedback (I $\kappa$ B $\alpha$  only) model of the system (Hoffmann *et al.*, 2002). It was reduced with respect to continuous TNF $\alpha$  input by eliminating any decoupled reactions, coarse-graining over fast variables and then the application of two partial equilibriums. The final step of the reduction exploited a feature present in the NF- $\kappa$ B system to eliminate the final variable. In comparison with the minimal model derived in this chapter (3.13), the model by Krishna *et al.* relies on similar variables to describe the system. However the resulting equations and system characteristics are different. In particular, the Krishna model exhibited “spiky oscillations” of the nuclear NF- $\kappa$ B, whereas this model shows a much more symmetric oscillation pattern.



**Figure 3.8** - Analysis of alternatively reduced models of the NF- $\kappa$ B system. Shown are bifurcation diagrams with respect to the rate of the I $\kappa$ B $\alpha$  transcription. Simulations performed for a continuous TNF $\alpha$  input. (A) The minimal  $z_0p_0y_0v_0s_0w_1$  model developed herein (3.13) in comparison to the SM. The I $\kappa$ B $\alpha$  transcription rate was normalised to its nominal value (as in Table 3.1). (b) The 3-variable reduced model and its 7-variable predecessor developed in Krishna *et al.* (2006), the transcription rate was normalised to its nominal value of 1.03. Branches of the solution in colour represent minimal and maximal values of the limit cycle. Solid and dashed black lines correspond to stable and unstable equilibria, respectively.

Figure 3.8 shows the bifurcation diagrams with respect to the rate of  $I\kappa B\alpha$  transcription for the two minimal models and their predecessors. The Krishna minimal model demonstrates features that are not present in the corresponding full model. These include variation of the limit cycle amplitude for values of the  $I\kappa B\alpha$  transcription around 1, and a subcritical Hopf bifurcation, with unstable limit cycles and hysteresis for the values of that parameter between 20 and 100. On the contrary, the minimal model developed in this chapter preserves the properties of the full model at least at the qualitative level, even for the values of the parameter very different from the one corresponding to the representative solution. This shows that application of the method of speed coefficients can produce a reduced model of comparable dimensionality while better preserving the dynamic properties of the original system than other less rigorous techniques.

### 3.5 – Model Reduction with Respect to Pulsed TNF $\alpha$

#### Input

Previously, the minimal models were derived with respect to a solution that corresponded to a constant value of the TNF $\alpha$  input,  $k_{24} \equiv 1$ . The universality of such models depends on how representative that solution actually is. In this subsection an example is given where a different selection of the representative solution leads to a different reduced model.

For the NF- $\kappa$ B system there is another experimentally relevant case, where the TNF $\alpha$  input is varied:  $k_{24} = 0$  except for 5-minute pulses of  $k_{24} = 1$  delivered every 100 minutes. Under such stimulation, the system exhibits pulses of the nuclear NF- $\kappa$ B entrained to the input frequency (Ashall *et al.*, 2009). Despite the same 100-minute period, these pulses are markedly different than oscillations induced with the continuous TNF $\alpha$  input. The Simplified Model reproduces this property (figure 3.2 vs. figure 3.9). However, the 6-variable variant,  $z_0 p_0 y_0 v_0$  (see Appendix 2.2 for equations), does not respond with a full-size nuclear NF- $\kappa$ B translocation to each pulse, and the solution is of a double period (figure 3.9).

To understand this, an alternative minimal model was developed, choosing the periodically entrained solution as the representative one. For the periodically entrained solution, the hierarchy of speeds of the variables associated with the IKK module is different from the  $k_{24} \equiv 1$  case. Specifically, the first three fastest variables are  $z$ ,  $p$  and  $y$  as before. However, when choosing the 4<sup>th</sup> variable for elimination, the neutral form of IKK,  $v$ , becomes one of the slowest, and the algorithm identified the active IKK,  $w$ , for approximation (figure 3.10). In the continuous case,  $v$  and  $w$  were the first and second fastest variables, respectively (figure 3.10). Ultimately, application of the algorithm with respect to the pulsed input resulted in a different model, which showed a much better agreement with the SM and did not display a period doubling (figure 3.9). This alternative 6-variable, ( $*z_0 p_0 y_0 w_0$ ) model is given by:

$$\frac{dq}{dt} = -k_4 q \bar{p} + k_6 u - k_8 q - k_{13} q + k_{14} s - k_{17} \bar{w} q \quad (3.14a)$$

$$\frac{dr}{dt} = k_{15} k_1 \bar{p} - k_4 s r - k_{16} k_1 r \quad (3.14b)$$

$$\frac{ds}{dt} = k_{13} k_1 \bar{p} - k_4 s r - k_8 s - k_{14} k_1 s \quad (3.14c)$$

$$\frac{du}{dt} = k_5 \frac{r^h}{r^h + k^h} - k_7 u \quad (3.14d)$$

$$\frac{dv}{dt} = k_{20} \frac{k_{21}}{k_{21} + k_{24} y} (k_2 - v) - k_{24} k_{22} v \quad (3.14e)$$

$$\frac{dx}{dt} = k_9 \frac{r^h}{r^h + k^h} - k_{11} x \quad (3.14f)$$

$$\bar{p}(q, r, v) = \frac{k_{16} k_1 r + k_{18} k_3 k_1 \bar{w} - k_{18} \bar{w} r}{k_1 (k_4 q + k_{15} + k_{18} \bar{w})} \quad (3.14g)$$

$$\bar{y}(x) = \frac{k_{10} x}{k_{12}} \quad (3.14h)$$

$$\bar{w}(v) = \frac{k_{24} k_{22} v}{k_{23}} \quad (3.14i)$$

The difference in the  $v$  speed for alternative TNF $\alpha$  stimulation can be easily understood by analysing the dynamic equation for  $v$ . The last term in its right-hand side,  $-k_{24} k_{22} v$ , directly contributes towards decay of  $v$ , but only when  $k_{24}$  is switched on. So when  $k_{24}$  is off, the  $v$  variable is much slower and its adiabatic elimination is not justified.



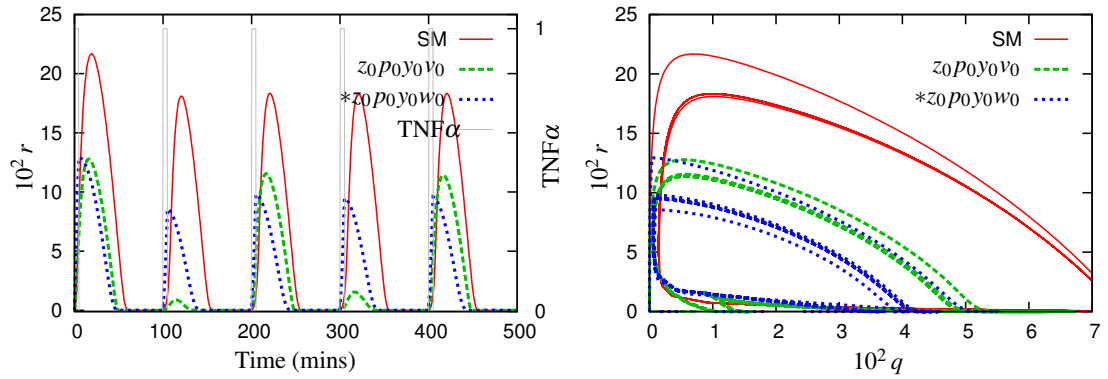


**Figure 3.9** - Models' response to a pulsed TNF $\alpha$  input. Shown are solution of the Simplified Model (SM, solid line), the 6-variable model  $z_0 p_0 y_0 v_0$  (dashed line), and the alternative 6-variable model  $*z_0 p_0 y_0 w_0$  (3.14) (dotted line). The TNF $\alpha$  input is varied:  $k_{24} = 0$  except for 5-minute pulses of  $k_{24} = 1$  delivered every 100 minutes (shown in grey lines on the left panel). (A) Solution for nuclear NF- $\kappa$ B,  $r$ . (B) Phase plane for  $r$  and  $q$ .

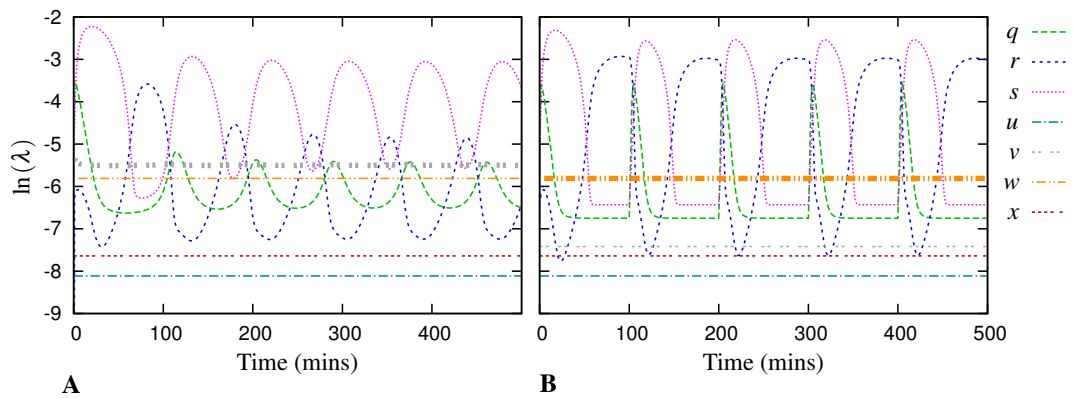


**Figure 3.10** - Comparison of the speed coefficients for the  $z_0 p_0 y_0$  model calculated with respect to different solutions. (a) Constant input ( $k_{24} \equiv 1$ ). (b) Pulsed input;  $k_{24} = 0$  except for 5-minute pulses of  $k_{24} = 1$  delivered every 100 minutes. Depicted in bold are the fourth fastest variables:  $v$  in (A) and  $w$  in (A).

### 3.6 – Discussion

A key problem in computational and systems biology is to understand how dynamical properties of a system arise via the underlying biochemical networks. However, as these networks involve many components this task becomes analytically intractable and computationally challenging. This chapter presents a clearly defined and accessible QSSA algorithm for reduction of such biochemical reaction systems. The method proposed relies on the derivation of speed coefficients to rank system variables according to how quickly they approach their momentary-steady state. This enables a systematic method for selection of variables for steady state approximation at each step of the algorithm.

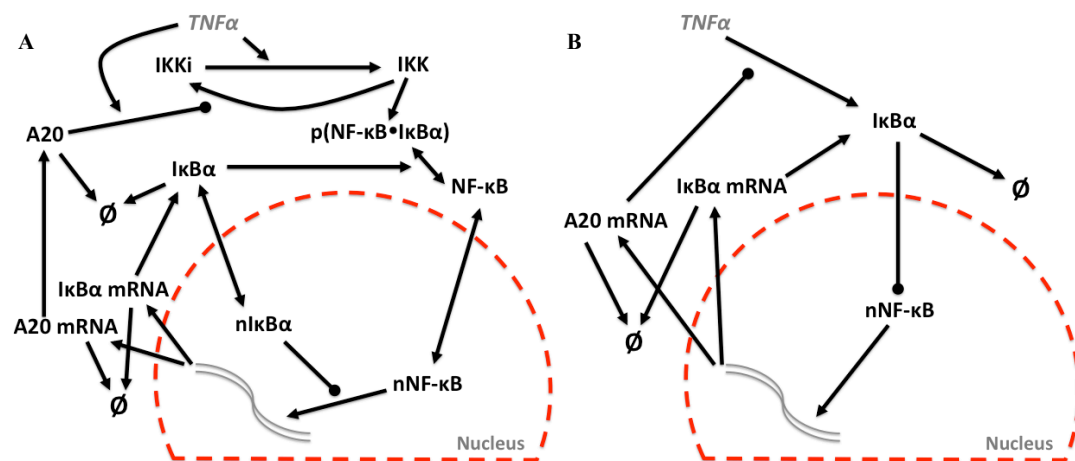


**Figure 3.11** – Network diagram of the Simplified Model (derived from Ashall et al., 2009) and the minimal model of the NF- $\kappa$ B system. Time-dependent variables present in each model are depicted with black colour. Pointed and round arrowheads represent activating and inhibitory reactions, respectively. In unstimulated conditions NF- $\kappa$ B is sequestered in the cytoplasm by association with I $\kappa$ B $\alpha$  inhibitors. Stimulation with  $TNF\alpha$  (by changing  $k_{24} = 1$  from 0) causes activation of the IKK kinase, and subsequently degradation of I $\kappa$ B $\alpha$  and translocation of free NF- $\kappa$ B to the nucleus. Nuclear NF- $\kappa$ B induces transcription of I $\kappa$ B $\alpha$  and A20. Once synthesised I $\kappa$ B $\alpha$  is able to bind to NF- $\kappa$ B and return it to the cytoplasm, while A20 inhibits the IKK activity.

This method was used to derive a minimal model of the NF- $\kappa$ B signalling network, a key regulator of the immune response that uses oscillatory dynamics (Ashall et al, 2009). Starting from a 14-variable model (figure 3.11a), the method succeeded in closely representing dynamics of the NF- $\kappa$ B network in response to constant TNF $\alpha$  input by a set of four variables (figure 3.11b and (3.13)). The minimal model included the nuclear NF- $\kappa$ B and its cytoplasmic inhibitor I $\kappa$ B $\alpha$ , as well as two negative feedback loops via transcription of the I $\kappa$ B $\alpha$  and A20 genes. The latter variables were consistently ranked the slowest during successive reduction steps (figure 3.1 and figure 3.4). This suggested that the timescale of transcription relative to other processes generates the key delayed negative feedback motif that drives oscillations in the system (Novak and Tyson, 2008). While reducing the model, it was observed that the period as well as the amplitude of oscillations was decreased with each reduction (table 3.2). Replacing those variables with the respective QSSAs decreased the effective delay time in the system, and thus reduced the system's propensity for oscillations. This effect was reversed by using first-order QSSA for some of the eliminated variables, namely cytoplasmic NF- $\kappa$ B, nuclear I $\kappa$ B $\alpha$  and the active form of IKK kinase. A more accurate representation of those variables is thus important to faithfully represent NF- $\kappa$ B dynamics (figure 3.5 –figure 3.7).

The reduced model derived in this chapter was also compared with another minimal model of the NF- $\kappa$ B system. In this case it was a model derived from the model of Hoffmann *et al.* (2002), which includes negative feedback from I $\kappa$ B $\alpha$  (Krishna *et al.*, 2006). There is a high degree of similarity between the model derived by Krishna *et al.* and the model derived herein. The reduced model of Krishna *et al.* has 3-variables, nuclear NF- $\kappa$ B, cytoplasmic I $\kappa$ B $\alpha$  and I $\kappa$ B $\alpha$  transcript. The model derived in this chapter includes the same three species plus the additional feedback from the transcription of A20, which is not present in the Hoffmann *et al.* (2002) model. This similarity suggests the method was successful in identifying the core network topology responsible for NF- $\kappa$ B dynamics. Theoretically, it should be possible to further reduce both models to remove one of the two representations of I $\kappa$ B $\alpha$ , however, in practice this was not possible. This could be for two possible reasons, first, the representation of cytoplasmic I $\kappa$ B $\alpha$  is vital to generate the delay necessary

for the system to oscillate. Another reason can be seen in analysis of the speed coefficients for the variables  $q$  and  $r$  (figure 3.1 and figure 3.4). The speed coefficients appear to be in anti-phase, one is slow while the other is fast, the overlap between them increases as the reduction progresses. This high degree of overlap suggests it may not be possible to remove the variable cytoplasmic I $\kappa$ B $\alpha$  as the topology of its interaction with NF- $\kappa$ B is paramount to drive oscillations in this system. In this way, analysis of the speed coefficients can be used to gain additional insight into the system.

Bifurcation analysis with respect to TNF $\alpha$  dose and I $\kappa$ B $\alpha$  transcription rate demonstrated that this method was able to qualitatively preserve the dynamic properties of the system (figure 3.7 and figure 3.8). This is because the method, in most cases, replaces a variable with a suitable approximation and therefore does not change the system only the timescale. This is not necessarily true for all model reduction methods, for example, analysis of the model by Krishna *et al.* showed that their method did not preserve the dynamic properties of the system through the stages of reduction (figure 3.8). This is most likely as the technique is heuristic in nature and doesn't follow a defined set of rules. Moreover, the final reduction step applied by Krishna *et al.* exploited a property unique to the NF- $\kappa$ B system that is not well defined. Figure 3.8 shows that this lack of rigour in the method results in a loss of stability in the dynamic structure of the model; this instability occurs at a distance from the parameterised value and therefore it could be argued that it is not of great importance. As this chapter has demonstrated model reduction is an essentially local technique based on a representative solution of interest generated from a specific parameter set or input, therefore one derived model is not necessarily applicable to all of parameter space.

A model derived with respect to a specific solution is not necessarily able to reproduce the same breadth of responses as its forebear. However, by applying the algorithm with respect to a different solution one might try to potentially extract other key features of the system. Here, it was demonstrated that the reduction of the model with respect to a pulsed and continuous TNF $\alpha$  input resulted in a different order of elimination of the variables and ultimately a different minimal model (figure

3.9). The differences unravelled specific component of the IKK module responsible for NF- $\kappa$ B dynamics in response to different stimulation protocols. With a pulsed input the amplitude of the subsequent peaks is determined by the “refractory period”, i.e. the time it takes for the active IKK to return to its neutral state. This requires a very accurate, i.e. a temporal representation of the neutral form of IKK,  $v$ , in the model. However, in response to continuous TNF $\alpha$  input, both IKK-related variables became less important, and their steady-state approximation is sufficient to support the limit cycle.

Similarly to other such approximation methods, there is a trade-off between simplicity and accuracy of the end-point models. Even if errors introduced by one reduction step are small, for many steps they can accumulate. The approximations can be improved by using higher-order asymptotics, which increases algebraic complexity of the resulting reduced model but retains the dimensionality. In practically interesting cases, the increased algebraic complexity may be overcome by appropriate approximation of the functions in the resulting models. Another way to improve the accuracy of reduced models is to adjust parameters to match the solutions of the full model; a semi-empirical model resulting from such adjustment would still have an advantage over a fully empirical model in that at least its structure is not arbitrary postulated. In addition to a lower dimensionality, the reduced problems are less stiff, as by definition, the variables with fastest characteristic timescales are eliminated first. The reduced dimensionality and stiffness allow, in principle, more efficient computations which may be important, for example, in large scale models including interactions of many cells. Last but not least, systems of lower dimensionality are more amenable for qualitative study and intuitive understanding.

**Chapter 4 –  
Computational Analysis of  
Period Modulation in the  
NF- $\kappa$ B System**

## 4.1 – Introduction

The frequency of biochemical oscillation has been indicated to be important in encoding biological responses. For example, the frequency of calcium  $\text{Ca}^{2+}$  oscillations can influence muscle cell contraction and gene expression (Berridge *et al.*, 1998). Live cell imaging of fluorescently labelled RelA has shown that the prototypic NF- $\kappa$ B dimer oscillates between the nucleus and cytoplasm with a robust period of 100 minutes in response to continuous high-dose TNF $\alpha$  stimulation (Nelson *et al.*, 2004). The duration and dose of TNF $\alpha$  stimulation has been observed to influence the persistence of NF- $\kappa$ B oscillations and resulting gene expression (Ashall *et al.*, 2009, Tay *et al.*, 2010). Studies have also demonstrated that 5-minute pulses of TNF $\alpha$  administered at different frequencies, from 60- to 200-minutes, can elicit NF- $\kappa$ B nuclear translocations entrained to the pulsing frequency. Moreover, the frequency of NF- $\kappa$ B oscillations was demonstrated to control downstream gene expression (Ashall *et al.*, 2009). These data highlight the importance of NF- $\kappa$ B dynamics in coordinating cellular responses to inflammatory signals.

There are far-reaching clinical implications of NF- $\kappa$ B dysregulation, moreover, it has proved difficult to exploit as a therapeutic target due to its multitude of inputs and effects (Garg and Aggarwal, 2002). Constitutive nuclear NF- $\kappa$ B activity has been described in many tumour cell lines (Aggarwal, 2004). The cause of constitutive NF- $\kappa$ B activation is incompletely understood but I $\kappa$ B $\alpha$  dysregulation, enhanced proteasome activity and enhanced cytokine expression have all been implicated (Aggarwal, 2004). In multiple myeloma, genetic analysis has identified loss of function mutations in the negative regulator of NF- $\kappa$ B, CYLD (Baud and Karin, 2009). Similarly to A20, CYLD is an NF- $\kappa$ B-inducible inhibitor of IKK activity (Jono *et al.*, 2004). Oncogenic mutations often reside in genes that encode upstream regulators of NF- $\kappa$ B activity and tumour cell lines have been shown to be sensitive to inhibition of components of the NF- $\kappa$ B pathway, including the proteasome, IKK complex and I $\kappa$ B $\alpha$  (Baud and Karin, 2009). These insights coupled with the observations of Ashall *et al.* (2009), who demonstrated frequency to encode response, suggest modulation of NF- $\kappa$ B dynamics could provide a new avenue to control the

resulting output of the system. However, to alter the NF- $\kappa$ B dynamics in a physiological context will require a deeper understanding of the system.

Ashall *et al.* (2009) demonstrated the importance of the frequency in encoding output of the NF- $\kappa$ B system using pulsatile stimulation. However, this experimental regime would be difficult to recreate in a physiological context. Using the deterministic model presented in Ashall *et al.* (2009), which shall be referred to as the “Ashall model”, a comprehensive analysis of the sensitivity of the model’s period to different parameter perturbations has been carried out. Model evaluation techniques such as sensitivity and bifurcation analysis can be used to understand how altering reactions rates within the system can influence the period, amplitude and existence of the limit cycle. These analyses in conjunction with the minimal model developed in Chapter 3 provide a basis to understand how the period of NF- $\kappa$ B oscillations can be changed. This information can then be used to make predictions about which points of the system to target in order to change the predominant NF- $\kappa$ B dynamic, which could result in differential NF- $\kappa$ B function. Ultimately, this analysis can help to inform new decisions when considering this system as a therapeutic target.

The Ashall model was originally presented as a system of 14 ODEs (Appendix 1.1). However, the system is equivalent to one of 11 variables and 29 parameters (Wang *et al.*, 2012a). This is in part due to the existence of linear dependent and decoupled variables (Section 3.3.1, Chapter 3). If required, the eliminated variables can be recovered post factum by integration of the solution of the remaining variables. This reduced system will form the basis for analysis in this Chapter. The same parameter notation as Ashall *et al.* has been used; the model and equations are presented in Appendix 1.2.



## 4.2 – Period Sensitivity

A classical way to analyse the sensitivity of dynamic systems is by calculation of the control coefficients (Section 1.2, Chapter 1). Control coefficients represent how a change in a parameter perturbs the solution or a particular performance measure of the solution (Rand, 2008). Consider a system of  $n$  ODEs (as described by (1.4) and (1.5))

$$\frac{dx}{dt} = f_i(t, \mathbf{x}, \mathbf{k}), \quad (4.1)$$

where  $t$  is time,  $\mathbf{x} = \{x_1, \dots, x_n\}$  are the dynamic variables and  $\mathbf{k} = \{k_1, \dots, k_m\}$  are the parameters. If the system is assumed to oscillate with a period  $P = \omega$  after a transient phase there will exist a periodic solution  $\mathbf{x}(t) = \mathbf{g}(t, \mathbf{k}) = \mathbf{g}(t + \omega, \mathbf{k})$ .

The parameter sensitivities measure how the solution changes with respect to a given parameter change (Section 1.2, Chapter 1). For a periodic solution this is represented by the derivative of the periodic function with respect to the parameter  $k_j$ ,

$$\frac{\partial \mathbf{g}(t, k_j)}{\partial k_j}. \quad (4.3)$$

In this analysis the performance measure of interest is the period  $P$ . The period is a function of the parameters and therefore the period at the original parameter values  $k_0$  can be defined to be  $\omega_0$ . Rand (2008) defines a control coefficient  $c_j$  to relate the change in the limit cycle period with respect to a change in the  $j^{\text{th}}$  parameter  $k_j$  to be

$$c_j := \frac{\partial P}{\partial k_j} = \frac{1}{f_m(\mathbf{x}_0)} \frac{\partial g_m}{\partial k_j}(\omega_0). \quad (4.3)$$

for values of  $k$  near to  $k_0$  and for all  $m \in \{1, \dots, n\}$ , where the initial condition  $\mathbf{x}_0$  is assumed to be  $\mathbf{x}_0(\mathbf{k}) = \mathbf{g}(0, \mathbf{x}, \mathbf{k})$ . The derivation of this relationship can be found in Rand (2008). These quantities can be calculated numerically in MATLAB using the Global Sensitivity Analysis Software (Rand, 2008). This software builds a matrix of  $m$  columns where the  $j^{\text{th}}$  column is a concatenation of the vectors that represent the derivative of the each variable with respect to the  $j^{\text{th}}$  parameter for all time points simulated i.e. a concatenation of the vectors  $\partial x_i(t)/\partial k_j$  for all  $i$  (see Section

equation (1.9), Chapter 1). This matrix represents the change in the entire system for a change in a parameter, from this matrix (4.3) can be calculated. In addition Singular Value Decomposition can be performed on this matrix to identify the sensitive variables and the parameters to which these variables are sensitive.

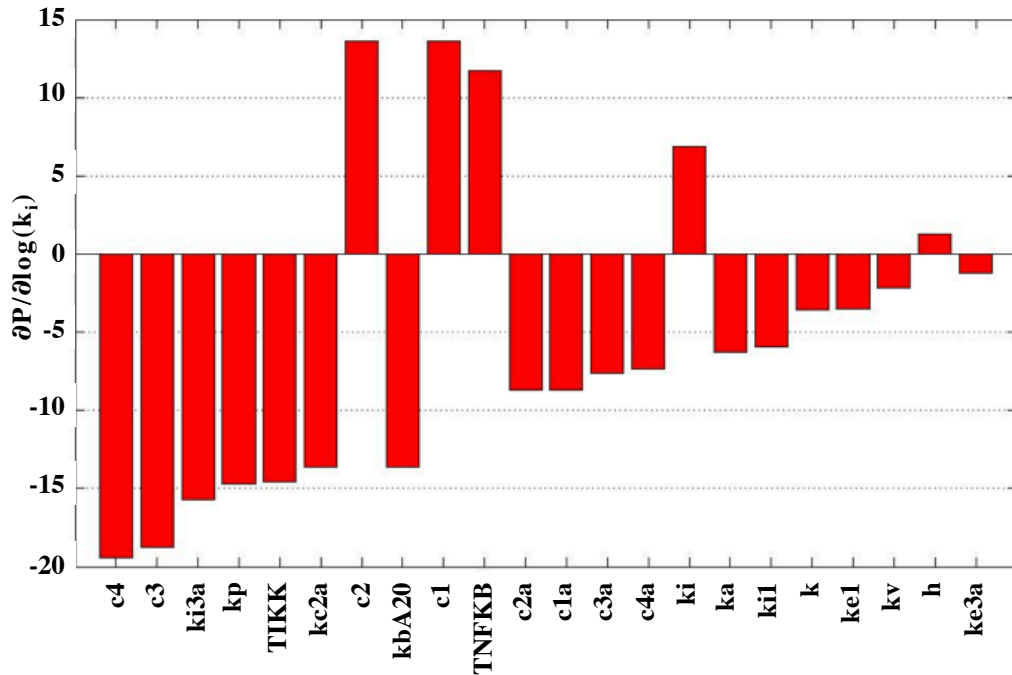


**Figure 4.1** – Control coefficients for the Ashall model calculated using the Global Sensitivity Analysis software (Rand, 2008). The parameters are ordered in terms of their sensitivity from most to least, those parameter with small coefficients are not shown to aid visualisation.

Figure 4.1 depicts the control coefficients for the parameters in the Ashall model, they show that a subset of the parameters have the majority of influence on the period of the model. The sum of the absolute value of the coefficients is  $\sim 215.4$ , this can be considered a measure of the total control exerted by all the parameters on the system. The first 10 parameters of the model contribute to approximately 70% of this sum; therefore over two-thirds of the sensitivity is as a result of 10 of the 29 model parameters. These parameters are: those related to the A20 variable (c4, c3),  $\text{I}\kappa\text{B}\alpha$  nuclear import (ki3a), IKK activity (kp), and the total level of IKK (TIKK) and

NF- $\kappa$ B (TNF $\kappa$ B). A number of parameters related to the negative feedbacks had large control coefficients, highlighting the importance of these species. The minimal model analysis identified I $\kappa$ B $\alpha$  and A20 transcription as central to the system dynamics, therefore it could be expected that the system would be sensitive to the parameters in these equations, namely  $c_{1a}$ ,  $c_{3a}$ ,  $c_1$ ,  $c_3$ ,  $k$  and  $h$ . While some of these have large control coefficients ( $c_3$  and  $c_1$ ), others have relatively small coefficients ( $h$  and  $k$ ) and a number of parameters with large control coefficients are not included in these equations. This implies that while the mRNA species are key to generating oscillations in this model, a number of other parameters are central to controlling the properties of these oscillations.

To gain a deeper insight into the effects on the period of those parameters with large period derivatives bifurcation analysis with respect to each of the model parameters was performed. The HB is of particular relevance to this analysis as it occurs when the solution branches from a stable steady state, where variables remain constant, to a stable limit cycle, where the solutions oscillate or vice versa. The majority of parameters in the Ashall model have at least two HB points that flank the parameter values for which the system exhibits a stable limit cycle. For example, bifurcation analysis with respect to the A20 protein degradation rate ( $c_4$ ) identified two HB points at  $c_4 \approx 0.0072$  and  $c_4 \approx 0.75$ . Therefore, assuming all other parameters remain fixed, for values of  $c_4$  less than 0.0072 and greater than 0.75 any set of initial conditions will give a solution that is exhibiting damped oscillations converging to constant concentrations of the variables. However, if  $0.0072 < c_4 < 0.75$  the system will evolve into sustained oscillations. It should be noted that it is possible to have several HBs. Bifurcation analysis, in general, is a local technique performed for a given interval of the parameter value. If analysis were extended to the entire range of possible parameter values, in this case the positive real line, it may be possible to find more distal regions of the parameter space where the system also displays a limit cycle. However, if the system is constrained by measured parameters this is a minor consideration as it is likely to involve unrealistic parameter values.

Using the software package XPPAUT (Doedel *et al.*, 2000, Ermentrout, 2002) the location of these HB points can be found numerically and properties of the limit cycle between these points analysed, namely amplitude and period (figure 4.2a and figure 4.2b respectively). Figure 4.2a is an example XPPAUT output detailing how the limit cycle amplitude changes between the two HB points. Figure 4.2b shows a corresponding XPPAUT output detailing how the period of the limit cycle changes between the HB points, this shall be referred to as a period bifurcation.

Bifurcation theory has previously been used to analyse the Ashall model to understand the response of the model to TNF $\alpha$  stimulation (Wang *et al.*, 2012a). The primary focus of their analysis was on the effect of parameter perturbations on the location of the HB with respect to the parameter TR (TNF $\alpha$  dose). However, the authors also used numerical bifurcation analysis to understand the effect of parameter changes on the limit cycle period. The period bifurcation was calculated in a range 10% above and below the nominal parameter value and these points were used to derive a sensitivity score that was a normalised average gradient of the period bifurcation curve (figure 4.2b) in this range. This analysis identified parameters with a strong influence on the period similar to those in figure 4.1, namely  $c_4$ ,  $c_3$ ,  $c_2$ , TIKK,  $k_p$ ,  $k_{i3a}$ . However, the author's definition of period sensitivity is not intuitive and cannot be easily applied to understand the quantitative effect of a parameter change. Here an alternative analysis of the period bifurcations is performed, which unlike control coefficients can be applied locally and globally and is more intuitive than the analysis of Wang *et al.* (2012a).

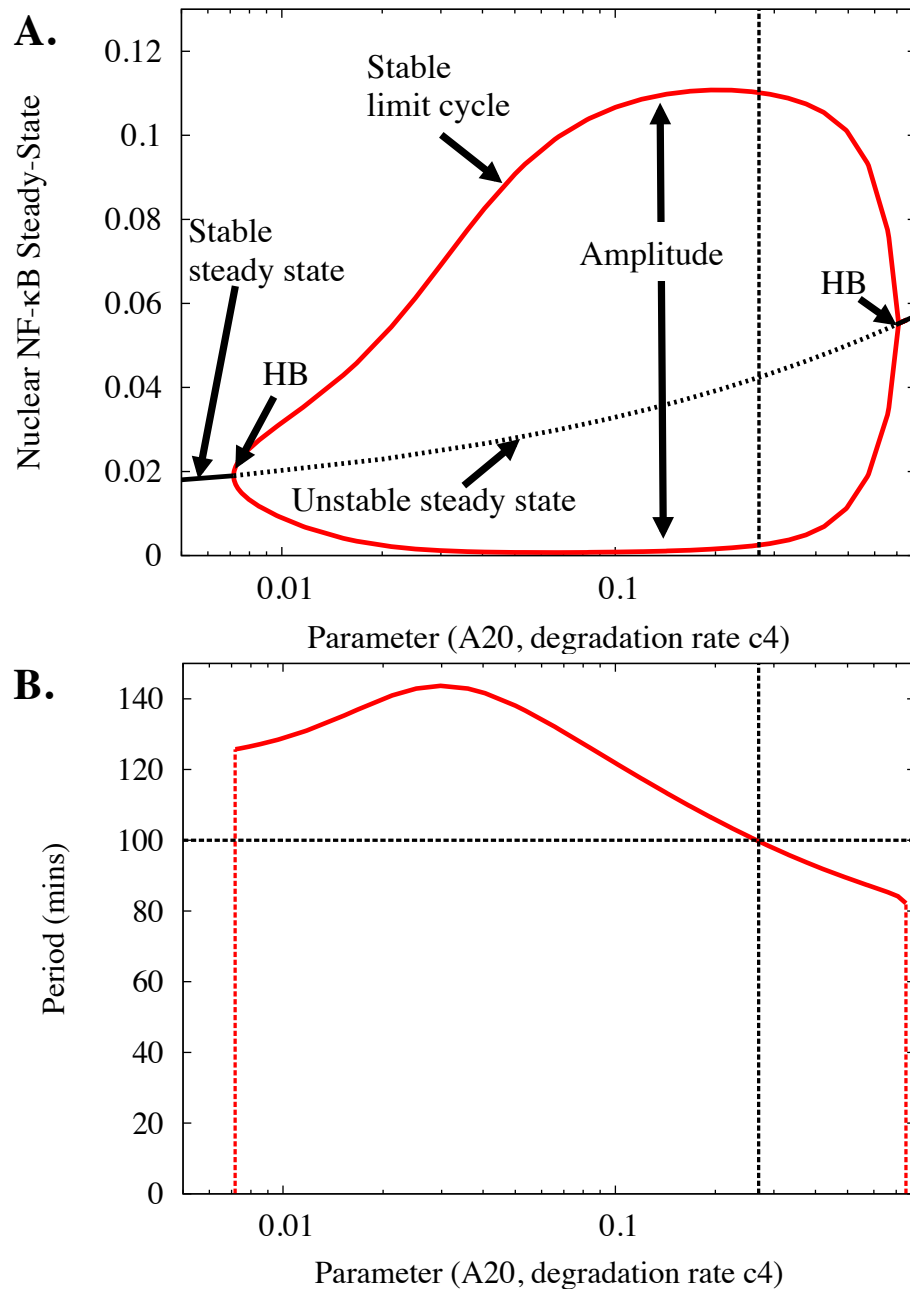


**Figure 4.2** - Example bifurcation analysis output from the XPPAUT software with respect to the parameter  $c_4$  (A20 degradation, see Table 4.1), plotted on the log scale. (A) Amplitude properties: the red line represents the maximum and minimum of the limit cycle amplitude, solid black line represents a stable steady-state, dashed black line an unstable steady state, and the vertical dashed black line shows the original parameter value. (B) Period properties: solid red line represents the period of the limit cycle for the corresponding parameter value, dashed vertical red lines represent the two HB points, dashed vertical black line represents the original parameter value and the dashed horizontal line shows the original period value.

For a system of ODEs with a periodic solution (4.1) the period of this system at the original parameter values can be defined to be  $P_0$ . For a given parameter, say  $k_j$ , we can define the period of the system for a perturbation of that parameter, say  $k_j = \delta k_j$ , to be  $P_{k_j=\delta k_j}$ . To determine the maximum possible period increase and decrease for a parameter increase or decrease the following quantities can be defined. For a parameter increase:

$$P_{k_j+}^+ = \max \left( P_{k_j \leq \delta k_j \leq HB^+} \right) \quad (4.5)$$

$$P_{k_j+}^- = \min \left( P_{k_j \leq \delta k_j \leq HB^+} \right). \quad (4.6)$$

Similarly for a parameter decrease:

$$P_{k_j-}^+ = \max \left( P_{HB^- \leq \delta k_j \leq k_j} \right) \quad (4.7)$$

$$P_{k_j-}^- = \min \left( P_{HB^- \leq \delta k_j \leq k_j} \right), \quad (4.8)$$

where  $HB^+$  and  $HB^-$  are the upper and lower HB points for the given parameter. These quantities define the maximum and minimum limit cycle period values that can be obtained by variation of the parameter between its HB points. The notation  $k_j +$  and  $k_j -$  denote if the parameter has been increased or decreased, and the  $P^+$  and  $P^-$  denote a period increase or decrease. The addition of this notation allows for the consideration of non-monotonic period bifurcations and the different magnitude of effect if the parameter is increased or decreased.

This analysis of the period bifurcation can then be used to characterise the effect of parameter changes on the limit cycle. Figure 4.4a charts the change in period that can be achieved for the parameters identified to have large control coefficients. It can be seen that some of the parameters identified as having weaker control coefficients appear, in this analysis, to have a large influence on the period. For example, the parameters  $c1a$  and  $c2a$ , which represent  $\text{IkB}\alpha$  transcription and translation. This is because this form of analysis does not consider the size of the parameter change that is required to induce such a change in period. To understand this better the period change should be normalised to the parameter change. Given a parameter change

$k_j = \delta k_j$  and the associated period  $P_{k_j = \delta k_j}$  the sensitivity measure associated with this parameter change is defined as

$$S_{\delta k_j}^{\pm} = \frac{(P_{\delta k_j} - P^*)}{\log \eta_j}, \quad (4.9)$$

where  $\eta_j = \delta k_j / k_j$ , the + and – notation has been added to identify if it is a measure for a parameter increase or decrease. This measure normalises the period change to the relative parameter change, it can be applied to the maximum and minimum periods identified by (4.5)-(4.8), where the period changes are normalised to the associated parameter change. In the case where these extrema are not unique the smallest parameter change required for the altered period was used.

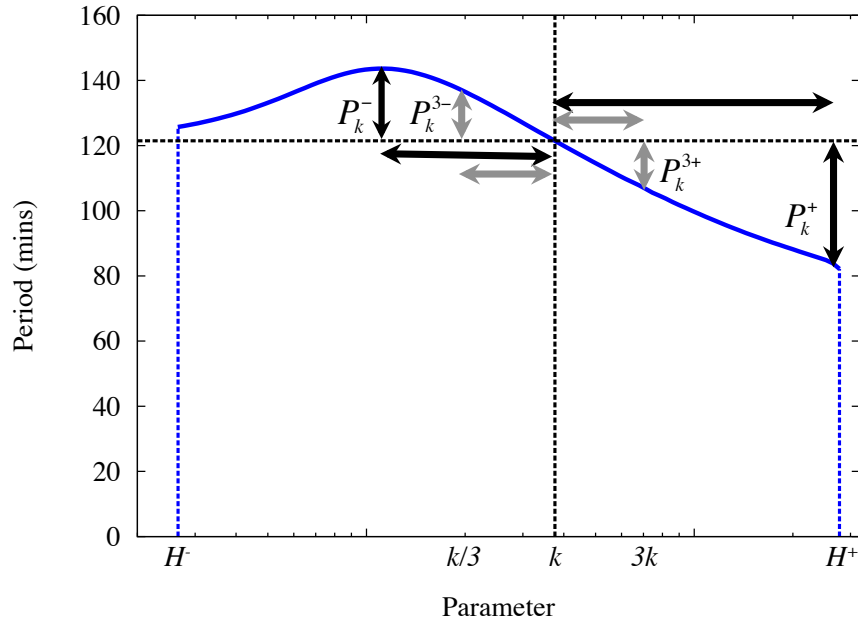


**Figure 4.3** – Schematic of the measures taken for the analysis defined by (4.2)-(4.5) and (4.10)-(4.13), for an example period bifurcation of the fictitious parameter  $k$ . The values  $k/3$  and  $3k$  demonstrate a three-fold increase or decrease of this parameter, respectively. The corresponding maximum or minimum period in this range would be the  $P_k^{3-}$  or  $P_k^{3+}$  values respectively. Similarly,  $H$  and  $H^+$  represent the lower and upper HB points, respectively. The maximum or minimal period change in these ranges would correspond to the  $P_k^-$  or  $P_k^+$  values.

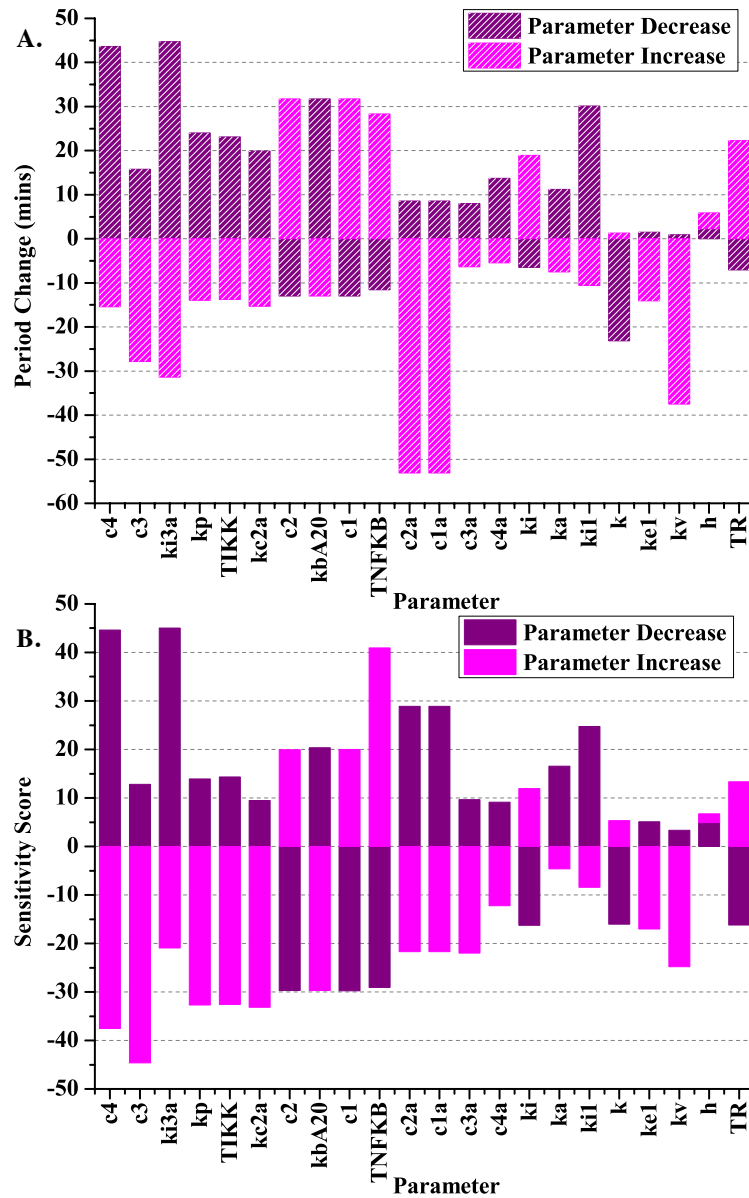


**Figure 4.4** – Global Analysis of the period bifurcations of the Ashall *et al.* (2009) model. (A) Period change calculated as  $P_{\delta k_j}^+ - P_0$  or  $P_{\delta k_j}^- - P_0$  using equations (4.5) to (4.8). (B) Sensitivity measure  $S^+$  and  $S^-$  calculated using equation (4.9) and (4.5)-(4.8). The pink colour represents the effect for increasing the parameter and purple colour represents the effect for reducing the parameter.



Application of this sensitivity measure (equation 4.9) to the quantities defined by (4.5)-(4.8) resulted in parameter sensitivities that are in better agreement with the control coefficients (figure 4.1 and figure 4.4b). After use of this normalisation the parameters with a propensity to alter the period by a substantial amount did not necessarily have high sensitivity scores (c1a and c2a in figure 4.4b). This can be seen from closer analysis of the parameter c2a. Although altering c2a can change the period by up to 50 minutes, to do this requires over 100-fold change in the parameter resulting in the parameter having a relatively small sensitivity measure (figure 4.4b). This can be seen more clearly in figure 4.5a, which shows the whole period bifurcation for the parameter c2a, a small change about c2a's original value results a relatively small change in the period (~10 minutes).

Figure 4.5b represents the period bifurcation for the parameter c3a and highlights another consideration when performing this analysis or sensitivity analyses in general. The period bifurcation for this parameter is not monotonic; decreasing the parameter attains the maximum and minimum possible limit cycle periods. For this parameter the highest sensitivity measure with respect to reducing the period is attained by increasing the parameter value and the highest sensitivity measure with respect to increasing the period is attained by reducing the parameter. Therefore, these two measurers have been included in the analysis presented in figure 4.4a. It must be noted that the sensitivity measure assumes a linear relationship between parameter change and resulting period, which has already been seen to not always be the case (figure 4.2 and figure 4.4). For a specific parameter of interest it will always be prudent to analyse the bifurcation diagrams with respect to this parameter to fully understand its influence on the system dynamics.

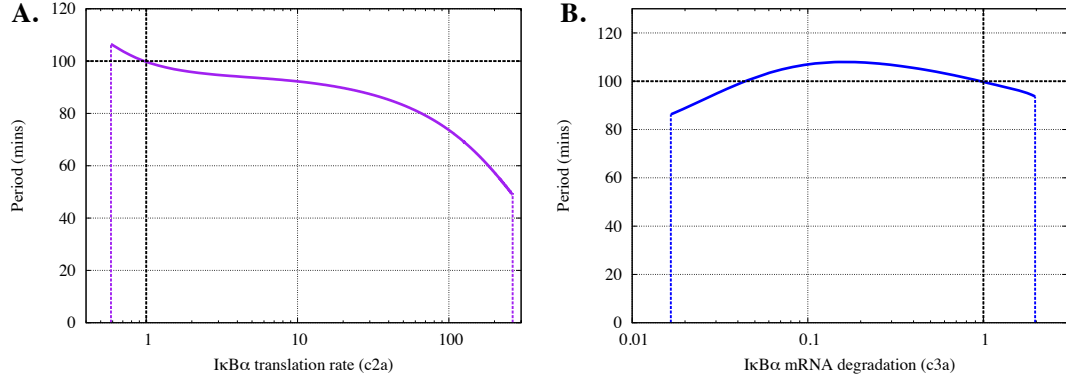


**Figure 4.5** - Period bifurcation diagrams for the parameters  $c2a$  (I $\kappa$ B $\alpha$  translation rate) and  $c3a$  (I $\kappa$ B $\alpha$  mRNA degradation), (A) and (B) respectively. Parameters have been normalised to their nominal value, the vertical black dashed line represent the nominal parameter value and the horizontal black dashed line represents the nominal period of 100 minutes.

For some parameter large changes in the period can only be achieved by extremely large parameter variations, which in some cases could correspond to a physiologically improbable rate. This global analysis method can be adapted to consider a local range of the parameter value. The quantities defined by (4.5)-(4.8) can be altered to consider a limited range of the parameter values  $k_j/\mu \leq \delta k_j \leq \mu k_j$ .

$$P_{k_j^+}^{\mu} = \max \left( P_{k_j \leq \delta k_j \leq \mu k_j} \right), \quad (4.10)$$

$$P_{k_j^-}^{\mu} = \max \left( P_{k_j/\mu \leq \delta k_j \leq k_j} \right), \quad (4.11)$$

$$P_{k_j^+}^{\mu^-} = \min \left( P_{k_j \leq \delta k_j \leq \mu k_j} \right), \quad (4.12)$$

$$P_{k_j^-}^{\mu^-} = \min \left( P_{k_j/\mu \leq \delta k_j \leq k_j} \right). \quad (4.13)$$

Again the quantities have been defined as to keep track of the sign of the change in parameter value and to account for a lack of monotonicity in the parameter range considered. For the analysis performed in this chapter a 3-fold range has been considered ( $\mu=3$ ). Equation (4.9) can then be applied to (4.10)-(4.13) to get a new sensitivity score.

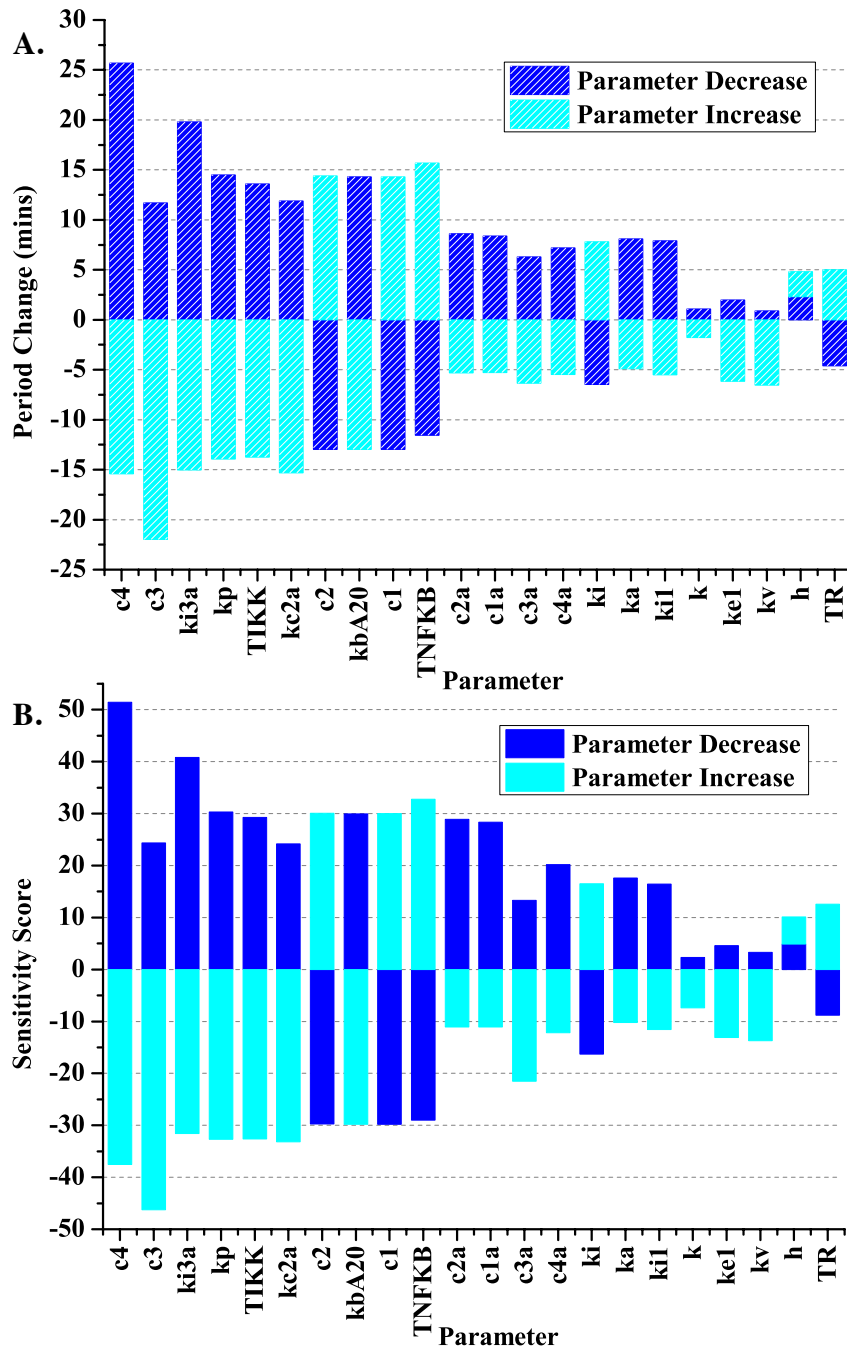


**Figure 4.6** - Local analysis of the period bifurcations of the Ashall model, over a 3-fold range of the original parameter values. (A) Period changes calculated using equations (4.10)-(4.13). (B) Sensitivity measure  $S^+$  and  $S^-$  calculated using equation (4.9) and (4.10)-(4.13). The cyan colour represents the effect for increasing the parameter and blue colour represents the effect for reducing the parameter.

Considering a limited range of the parameter value resulted in a better agreement between the control coefficients, bifurcation analysis of Wang *et al.* (2012a) and the sensitivity scores calculated herein. Considering a 3-fold change also meant that the application of the sensitivity measure is more justified, as the bifurcation structure in this range was more linear. The parameters that can elicit the greatest period change are the A20 related parameters  $c_4$ ,  $c_3$ ,  $c_2$  and  $c_1$ , I $\kappa$ B $\alpha$  nuclear import  $ki3a$ , and the IKK related parameters  $k_p$ , TIKK and  $kbA20$  (figure 4.6). Figure 4.6a demonstrates that it is only possible to achieve a change in period of approximately 25 minutes in either direction and over half the parameters give less than a 10-minute change in period. This demonstrates that the model is robust to the majority of parameter variations. Wang *et al.* (2012a) hypothesised the parameters of the Ashall model can be divided into two groups, those that have a strong influence on the period and those that do not. Analysis of the control coefficients and this bifurcation analysis support their hypothesis.

This analysis demonstrated that increasing and decreasing the parameter value does not necessarily have the same scale of effect on the period. The parameter that gives the greatest increase in the period ( $c_4$ ) is not the same as the parameter that gives the greatest reduction ( $c_3$ ). This is not considered by the control coefficients or the analysis performed by Wang *et al.* (2012), which assume a constant gradient over the interval of interest. For example, reducing the parameter  $c_3$  by up to 2-fold can give a 22-minute reduction of the period but an up to 2-fold increase only gives a 12-minute increase.

Table 4.1 summarises the most sensitive parameters identified by all three analysis methods. For the analysis performed in this chapter, two values have been used: the maximum possible measure for an increase or decrease of a parameter but not both, denoted  $\max(|S^+|, |S^-|)$ , and the sum of the measures for both increasing and decreasing a parameter, denoted  $|S^+| + |S^-|$ , where  $S^+$  is the sensitivity measure for increasing the parameter and  $S^-$  is the measure for decreasing the parameter. It can be seen that there is a great degree of similarity between all three methods, the five most sensitive parameters are the same for each analysis and nine of the top ten parameters are the same for each. These analyses can be used as a starting point to

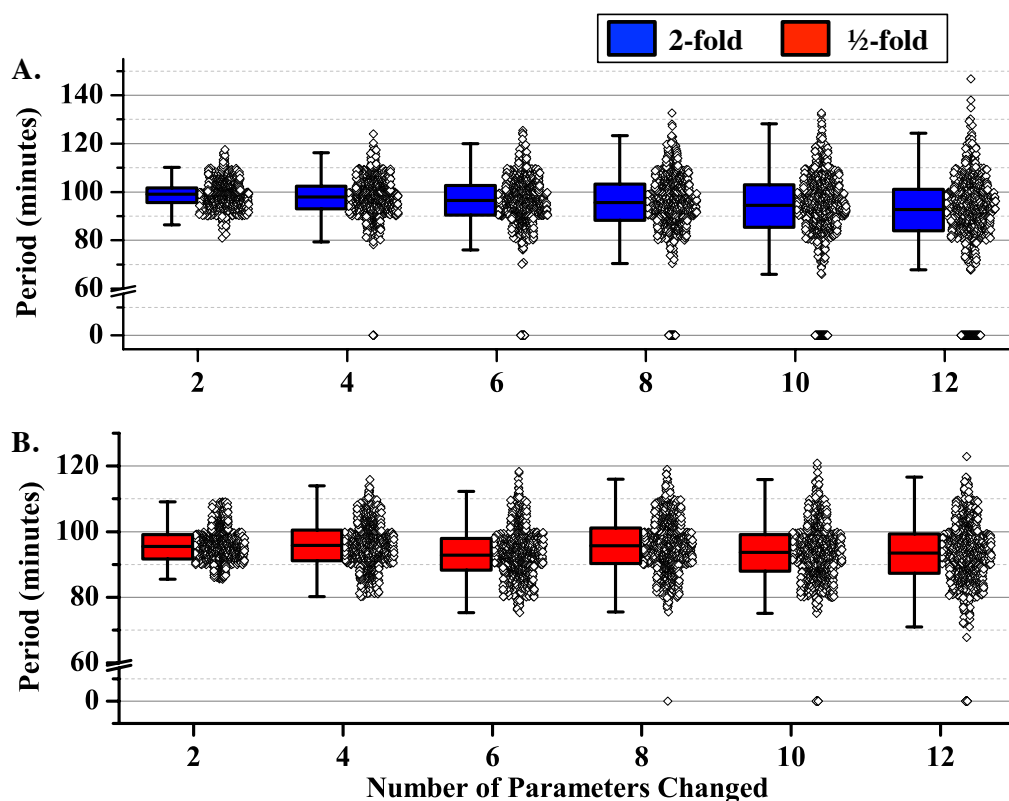
understand how changes to different aspects of the system can influence the dynamics. In advantage to the period derivatives the bifurcation analysis highlights the non-linear nature of parameter changes where increasing or decreasing the parameters may not have the same magnitude of effect.

**Table 4.1** – Comparison of the top 10 most sensitive parameters for the three analysis methods discussed in this Chapter. Those being the control coefficients, the bifurcation analysis of Wong *et al.* (2012) and the sensitivity measure defined herein. The maximum absolute measure for either a parameter increase or decrease (column 4), and the sum of measures for both a parameter increase and decrease (column 5) have been calculated. Highlighted parameters represent deviation from the order defined by the control coefficients.

	<b>Control Coefficient</b>	<b>Wang <i>et al.</i> (2012)</b>	<b><math>\max( S^+ ,  S^- )</math></b>	<b><math> S^+  +  S^- </math></b>
1 <sup>st</sup>	<i>c4</i>	<i>c4</i>	<i>c4</i>	<i>c3</i>
2 <sup>nd</sup>	<i>c3</i>	<i>c3</i>	<i>c3</i>	<i>c4</i>
3 <sup>rd</sup>	<i>ki3a</i>	<i>ki3a</i>	<i>ki3a</i>	<i>ki3a</i>
4 <sup>th</sup>	<i>kp</i>	<i>kp</i>	<i>kp</i>	<i>kp</i>
5 <sup>th</sup>	<i>TIKK</i>	<i>TIKK</i>	<i>TIKK</i>	<i>TIKK</i>
6 <sup>th</sup>	<i>kc2a</i>	<i>kc2a</i>	<i>kc2a</i>	<i>TNF<math>\kappa</math>B</i>
7 <sup>th</sup>	<i>c2</i>	<i>c1</i>	<i>c2</i>	<i>c2</i>
8 <sup>th</sup>	<i>kbA20</i>	<i>c2</i>	<i>kbA20</i>	<i>kbA20</i>
9 <sup>th</sup>	<i>c1</i>	<i>TNF<math>\kappa</math>B</i>	<i>c1</i>	<i>c1</i>
10 <sup>th</sup>	<i>TNF<math>\kappa</math>B</i>	<i>c2a</i>	<i>TNF<math>\kappa</math>B</i>	<i>kc2a</i>

### 4.3 – The Effect of Multiple Parameter Changes

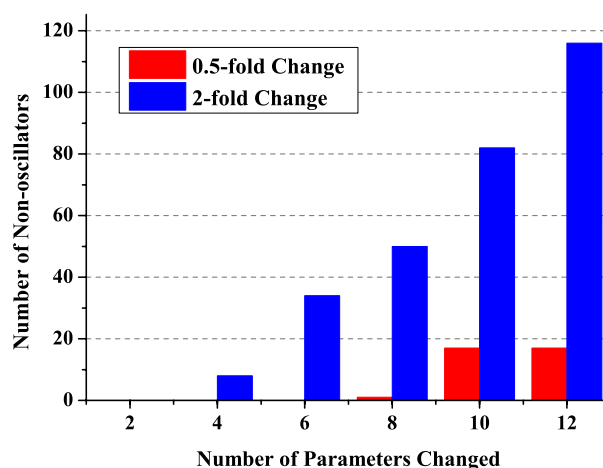
The sensitivity and bifurcation analyses illustrate that a subset of parameters has the majority of the influence on the limit cycle properties. To address how the system responds to changes in a number, or all, of these parameters a series of simulations were performed. Up to 12 parameters were sequentially altered by sampling from a uniform distribution over a 2-fold or half-fold range of their original value (figure 4.7a and figure 4.7b respectively). The parameters were ranked according to their control coefficients (figure 4.1) and the parameter with the highest absolute coefficient was altered first, then the next highest and so on.



**Figure 4.7** – Multiple parameter variations and the distribution of the resulting model periods, calculated using MATLAB. Using a uniform distribution over a 2-fold or half-fold range of the parameter value an increasing number of parameters were altered by sampling from this distribution. (A) 2-fold, (B) half fold. The x-axis gives the number of parameters altered and y-axis represents the corresponding model period. The parameters were chosen in order, starting with the most sensitive as identified by figure 4.1. 1000 simulations were performed for each fold change and parameter set chosen, the resulting distribution of periods shown. The box represents the 2<sup>nd</sup> and 3<sup>rd</sup> quartiles, the whisker the 1<sup>st</sup> and 4<sup>th</sup>, the central bar represents the median value. Models that did not achieve a limit cycle are shown as having 0-minute periods. The distribution of the data is shown to the right of the box.

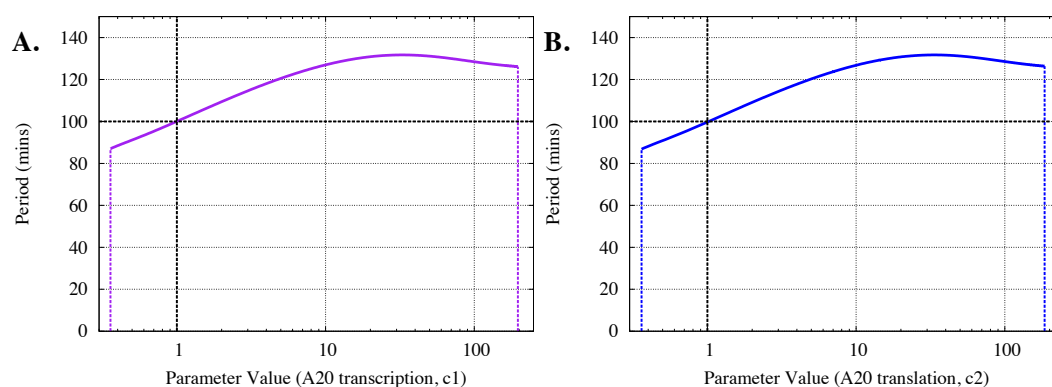
The results of this analysis for 1000 simulations for each fold change and parameter set are shown in figure 4.7, as expected the distribution of the solution periods increased with the number of parameters varied and the size of the fold change used. In figure 4.7 it can be seen that the majority of model periods are clustered between 80 and 120 minutes. In the half-fold simulations only 2 parameter sets gave solutions with periods greater than 120 minutes and less than 6% of the parameter sets gave periods less than 80 minutes. In the 2-fold simulations using 12 parameters less than 10% of parameter sets gave a period change  $\pm 20$  minutes and for 10 parameters or fewer this reduced to 3%. In this set of simulations there were substantially more solutions that did not oscillate than gave a large change in period, demonstrating the model is extremely robust to half-fold changes in parameters and maintains robustness when this range is increased to 2-fold. As the number of parameters altered increased the median period shortened, but remained close to the 100-minutes and within the bounds of experimental noise which was observed to be  $\sim 25$  minutes in SK-N-AS cells (Horton, 2006). In all cases there were more solutions with shorter periods than longer periods. However, from the bifurcation analysis (figure 4.6a) the sum of the total period increase for these 12 parameters is greater than the sum of the total period decrease (+172.9mins vs. -106.5mins), which would imply the period is more likely to increase. This promotes the hypothesis that the effect of multiple parameter changes is not predicted by the sum of their individual contributions.

Figure 4.8 represents the number of non-oscillating solutions associated with each simulation set. As the size or number of parameters changes increases there is an increased chance that the model does not oscillate (figure 4.8a), this was more likely than the parameter changes substantially altering the period ( $\pm 20\%$  either way). This could imply that there is a bound to the periods that can be realised in this model without resorting to a complete scaling of parameters. This supports the hypothesis, discussed in Section 1.4.3, that there is tension in biochemical models and independent parameter sets are required to evolve markedly different dynamics (Wong *et al.*, 2012). This analysis demonstrates that in order to exploit NF- $\kappa$ B oscillations for clinical means an in depth understanding of how individual perturbations alter the period is required.



**Figure 4.8** – The number of non-oscillating cells when an increasing number of parameters are varied sampling from a uniform distribution 2-fold or a half-fold about the nominal parameter value. Results are from 1000 simulations and the 12 most sensitive parameters identified by the period derivatives were used.

Figure 4.6 demonstrates that each parameter can increase and decrease the period depending upon the nature of the change therefore, it is reasonable to hypothesise that multiple changes could cancel each other out. This is further complicated by the fact that some parameters in the model are linked; this can be seen from analysis of the bifurcation structure. For example, the period bifurcations with respect to A20 transcription and translation rates are identical after normalisation of the parameter value (figure 4.9); this behaviour is also true for  $\text{I}\kappa\text{B}\alpha$  production.



**Figure 4.9** - Period bifurcations for the parameters related to A20 transcription (c1) and translation (c2), (A) and (B) respectively. The parameters have been normalised to their nominal parameter value. The vertical black dashed line represents the nominal parameter value, horizontal black dashed line shows the nominal period.



To understand if the effect of multiple parameter changes could be predicted from each parameter's individual bifurcation analysis, the simulation protocol was repeated for a larger sample size ( $n=2000$ ). The 10 parameters with the largest control coefficients (figure 4.1) were altered through sampling from a uniform distribution over a 2-fold range of the original value and the corresponding limit cycle period was found, should it exist. The sensitivity measure relates the period change in minutes to the relative change in a parameter. Therefore, if it is assumed that the effect of a parameter on the period is linear for the interval on which the measure was calculated, the sensitivity measure represents the period change per unit parameter change. Thus, multiplying a relative change in the parameter by this measure can be used to predict the period change for a particular parameter change. The summation of these predicted changes for all 10 parameter can then be used to predict the overall period change for a particular simulation.

Figure 4.10a illustrates a comparison between the period change predicted using the sensitivity measure and the simulated period for each of the randomly sampled parameter sets. The red line has a gradient of 1 and therefore depicts the location of parameter sets that have similar predicted and simulated periods. There are a number of points near this line, which demonstrate additive changes based on the individual parameter analyses. However, there are far more points where this is clearly not the case, this can be seen by their distance from the red line. A number of parameter sets predicted to have a very little effect on the period give a large change and vice versa. There are also a number of parameter sets where the predicted change is negative yet they result in a model with a longer period and vice versa, this can be seen from the points in quadrants not occupied by the red line.

The distribution of predicted periods for the parameter sets that did not result in a periodic solution is summarised in figure 4.10b. Some of the predicted changes are sizable and therefore it is reasonable to assume that they involve large parameter changes which move the system past a HB point, however, other predicted changes are smaller and therefore this assumption has less credence. The parameter sets that gave no limit cycle were searched to see if any only contained small parameter changes. A threshold in the relative parameter change of  $|\eta_j| < 0.2$  was set, where

$\eta_j = \log_{10}(\partial k_j/k_j)$ . This value was chosen as it encompasses two thirds of the total interval sampled. Only two parameter sets were found that resulted in no limit cycle and had parameter changes below this threshold; within these two sets there was at least one change that was very close to the threshold value. This suggest that while not all parameter changes need to be large, a large change is required in at least one parameter to result in a non-periodic solution.

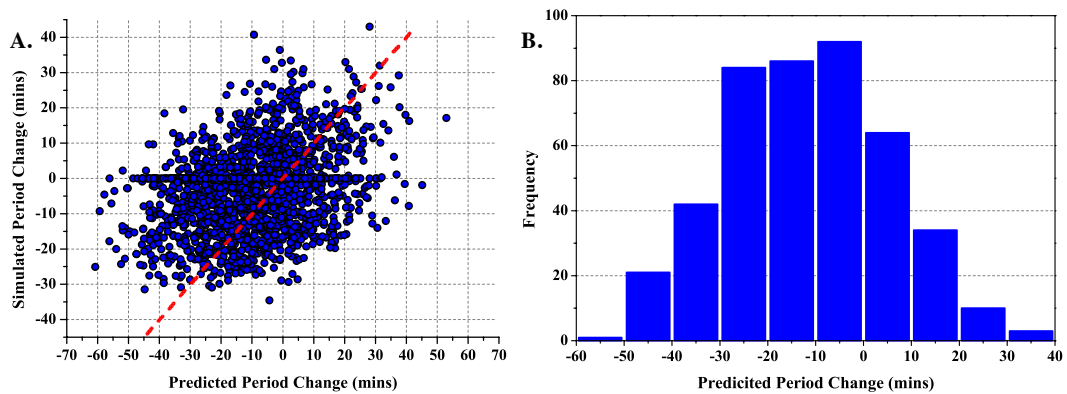


**Figure 4.10** - Correlation between predicted solution period and the simulated solution period after multiple parameter changes. The 10 parameters with the largest control coefficients (Figure 4.1) were altered by sampling from a uniform distribution over a 2-fold range of the original parameter value. (A) The sensitivity measure (4.6) was used to define a vector that corresponds to period change for a relative change in the parameter. This was used to predict a change in period assuming the 1-dimensional effects were additive, this is compared to the actual period change determined from simulation of the parameter set. (B) The distribution of predicted period changes for the parameter sets that did not result in a periodic solution.

The distribution of parameter values that resulted in solutions with substantially altered period ( $\pm 20$ mins) or no limit cycles were further analysed to determine if there was any discernable pattern. The parameters were normalised to their original value and the relative change determined through taking the logarithm, figure 4.11 depicts a box plot for each parameter summarising key statistics of these distributions. For parameter sets that increased the period there was a striking parallel between the signs of the average parameter value and the control coefficients (figure 4.9a and figure 4.1). The parameters with negative control coefficients had negative mean and median values, and vice versa. These data also suggest that a large increase in the parameters with positive control coefficients is required to give a longer period, this is evidenced by the tight distributions around large positive

changes in these parameters ( $c_2$ ,  $c_1$  and TNF $\kappa$ B). Interestingly, this pattern was less apparent in the parameter sets that shortened the period (figure 4.9b). In this case the changes that resulted in shorter periods were predominantly increases in the parameter value, with the exception of TNF $\kappa$ B. This pattern might be representative of a scaling effect; of these 10 parameters all but TNF $\kappa$ B, TIKK and kbA20 are linear. It has previously been established that these 10 parameters have the majority of control in the system and therefore an increase in all of them might be sufficient to scale the system. This is further evidenced by the fact that the three most influential parameters have large median increases ( $c_4$ ,  $c_3$  and  $ki_3a$ ). Figure 4.11c shows the distributions of parameter values in set that resulted in non-oscillating solutions; in this case a particular pattern is less evident. All of the parameter distributions appear far more uniform across the entire range of possible changes, in comparison to the other cases (figure 4.11a and figure 4.11b). This could imply that large changes are contained within these sets, which are moving the system past a Hopf bifurcation.

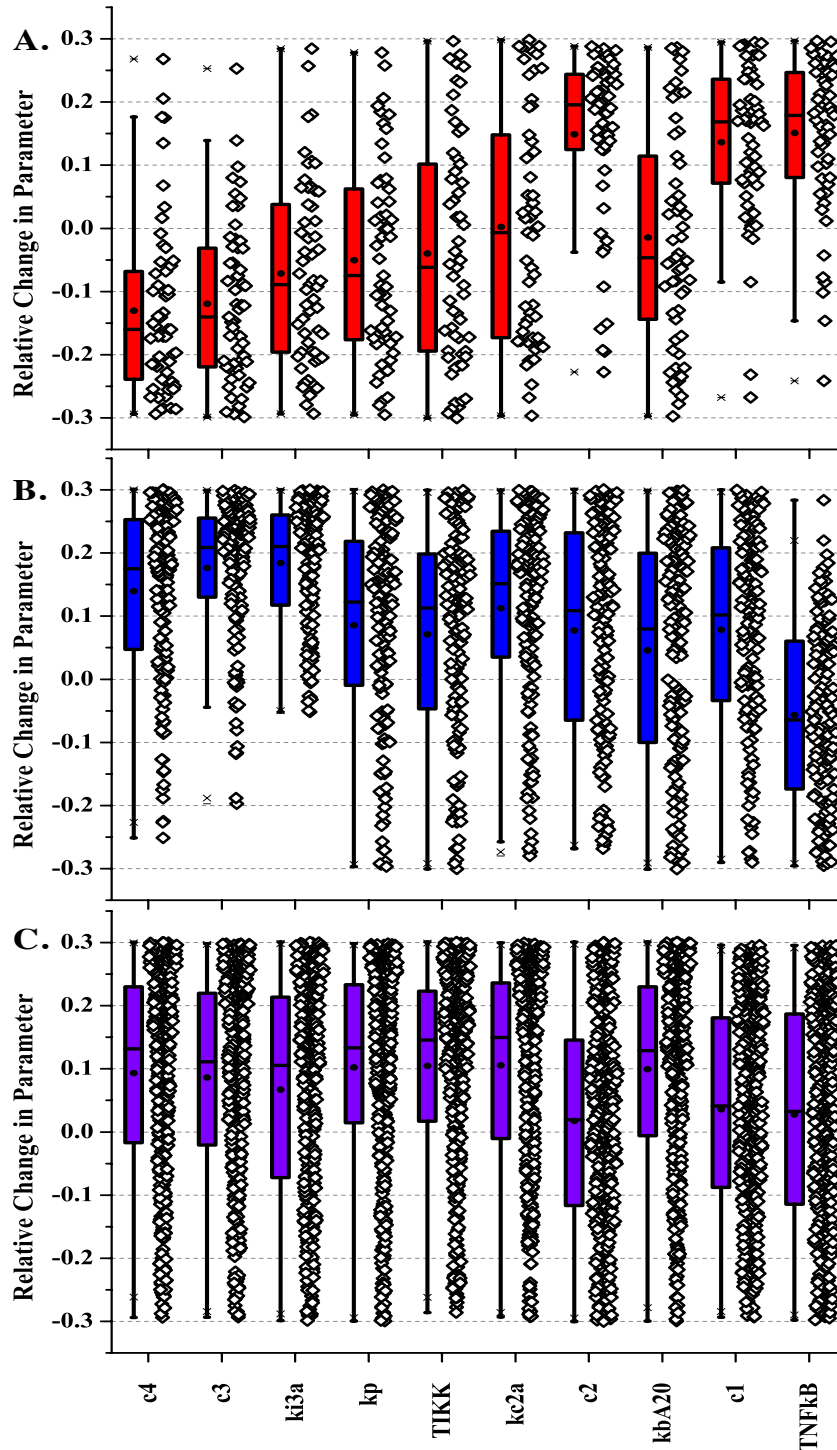


**Figure 4.11** - Distribution of the parameter values that resulted in models with a substantially altered limit cycle. The 10 parameters with the largest control coefficients (figure 4.1) were sampled from a uniform distribution over a 2-fold range of the original value; these are the results from 2000 simulations. (A) Parameter sets giving limit cycle periods greater than 120 minutes, (B) less than 80 minutes, (C) no limit cycle or amplitudes  $< 0.001 \mu\text{M}$ . Boxes show the 2<sup>nd</sup> and 3<sup>rd</sup> quartiles, central bars represent the median, points in the boxes show the mean and whiskers represent the 1<sup>st</sup> and 4<sup>th</sup> quartile. The distribution of the data is shown to the right of the box.

To more quantitatively explore these non-additive effects a series of bifurcation analyses with respect to the level of IKK (TIKK) were performed. Using figure 4.6 as a guide the model parameters were altered sequentially 2-fold to increase the period, starting from the parameter identified to have the greatest sensitivity score, then moving to the next most influential parameter, and so on (order taken from figure 4.6). After each parameter was changed the period bifurcation for TIKK was calculated using XPPAUT; these are shown in figure 4.12. Using this analysis method it is possible to follow the changes in the period bifurcation with respect to a parameter, in this case TIKK, as an increasing number of other parameters are changed. The parameter changes have been chosen to always increase the period, based on the bifurcation analysis performed in Section 4.2.

As the first seven parameters changed (c4 to c1), the period at the original TIKK value increases with each step and the gradient of the period bifurcation about the parameter value remains negative. These effects correlate with the relationships identified in figure 4.6. However, as further parameters are changed the gradient of the period bifurcation at the original TIKK value changes from positive to negative. Moreover, for the last parameter changed (kc2a) the period at the nominal parameter value decreases. These results contradict the relationships identified by all three analyses methods detailed in section 4.2. This highlights that the effect of multiple parameter changes is not predictable from the single parameter analysis. Therefore, it is only possible to move so far in parameter space before the local period-parameter relationships identified by sensitivity and bifurcation analyses are no longer valid.

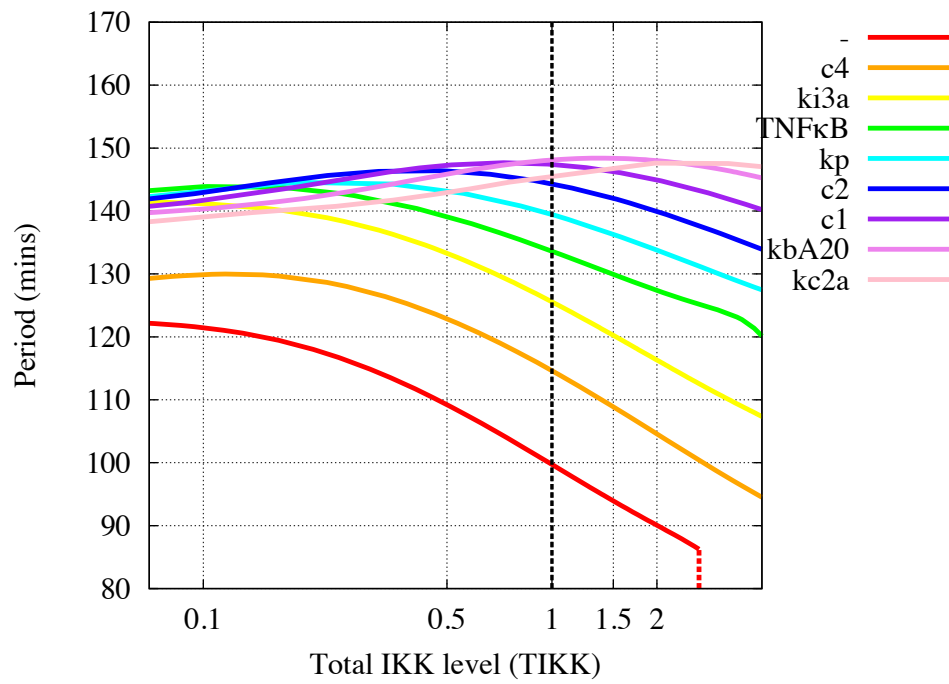


**Figure 4.12** – Period bifurcation analysis for the parameter TIKK (level of IKK), demonstrating how the bifurcation structure varies as the number of parameters changed is increased. The red line depicts the original bifurcation for the parameter set in Ashall *et al.* (2009). For each iteration of the line (red to violet) one parameter is changed 2-fold in the appropriate direction to increase the period using an order defined by the sensitivities in figure 4.6. The legend charts the order in which parameters are changed from top to bottom. The TIKK parameter has been normalised to its nominal value, the vertical black dashed line represents this nominal value.

## 4.4 – Discussion

This chapter has applied sensitivity analysis and bifurcation theory to develop an insight into how the model of NF- $\kappa$ B signalling presented in Ashall *et al.* (2009) can be perturbed to alter the period of oscillations. Three methods were compared: the control coefficients defined by Rand (2008), a bifurcation analysis by Wang *et al.* (2012) and an analysis of the period bifurcation defined herein. All three methods resulted in period sensitivities that are highly correlated (table 4.1). They identified the A20 feedback mechanism to be extremely important in controlling the period of NF- $\kappa$ B oscillations, in all cases the system was most sensitive to the parameters  $c_4$  and  $c_3$ , representing A20 protein and mRNA degradation. It is unsurprising that the A20 negative feedback loop is of central importance as it also represents several other negative feedbacks in the system. One example is CYLD, which has been implicated in constitutive NF- $\kappa$ B activation in multiple myeloma (Baud and Karin, 2009). In addition, I $\kappa$ B $\alpha$  nuclear import ( $ki3a$ ) and IKK recycling ( $kp$ ) were also demonstrated to be important. IKK recycling is important in oscillations as it delays the reset of the IKK complex giving rise to oscillation in the IKK activity; this was demonstrated when deriving a minimal model to a pulsed input (Section 3.5, Chapter 3). These results suggest that the effect of I $\kappa$ B $\alpha$ , A20 and IKK on the NF- $\kappa$ B dynamics warrant further investigation; this will be seen in Chapter 5 for I $\kappa$ B $\alpha$  and A20, and Chapter 6 for IKK.

The method of analysis used herein has been designed to give a large amount of information about the system. It can be used to understand the effect of small and large parameter changes and to consider the effect of increasing and decreasing parameters independently. Figure 4.4 and figure 4.6 demonstrates the interval about the parameter analysed can change the sensitivity scores and limit the extent to which dynamic properties of the system can be altered. Moreover, figure 4.6 demonstrates that parameters have different effects depending on whether the value is increased or decreased. This concept is not accounted for by control coefficients or the analysis of Wang *et al.* (2012a). Bifurcation analysis is more time consuming than some classical analysis methods where software has been designed to automate the analysis (Rand, 2008). However, as has been demonstrated it can yield a greater

amount of information about the system. This trade-off between information and analysis time is something that must be considered based on the nature of the question being addressed. In addition, the software packages used for this analysis are relatively straightforward and it would be possible to develop a programme capable of automating this process.

One advantage of bifurcation analysis over control analysis is that the nonlinear effect of parameter changes can be addressed over the whole range of parameter values for which a limit cycle exists. As a result it can be used to understand properties such as monotonicity. Consider the parameter  $h$ , the order of the Hill function. The period derivative for this parameter has a positive sign (figure 4.1) implying the period increases as the parameter is increased, however, analysis of the bifurcation structure with respect to this parameter (figure 4.4 and figure 4.6) showed that both increasing and decreasing the parameter resulted in lengthening of the period. This suggests that the parameter value actually lies near a local minimum of the bifurcation, something that is not highlighted by the period derivatives. This example is for a parameter that has relatively little influence on the period and as it represents the order of the Hill function, this parameter is seldom a consideration for perturbation. However, this example highlights that analysis of the bifurcation structure can yield more information than control coefficients.

Many of the reactions or parameters in biochemical reaction systems can be related. For example, in the Ashall model an increase in A20 transcription can be offset by the same relative decrease in translation, this can be seen as bifurcation analyses with respect to these parameters have the same structure (figure 4.9). In the Ashall model there is a linear reaction representing  $I\kappa B\alpha$  and A20 translation, which explains the identical bifurcation structures. In reality there is probably far more non-linearity due to splicing, translation, folding and post-transcriptional modifications, which the Ashall model does not capture. The related parameters all have the same control coefficients and sensitivity measures, which makes it difficult to de-convolve the effect each process has on the system.

Robustness is an important measure of the validity of biochemical models. A degree of variation in internal and environmental conditions is expected, which will have an



effect on the parameters of the system. The period sensitivities demonstrated that the majority of influence on the limit cycle is the result of a subset of parameters. The multiple parameter variations in Section 4.3 gave additional insight into the robustness of the Ashall model. These simulations implied that random perturbations of the parameters over a reasonable interval around the parameter value, in general, did not substantially alter the period of the limit cycle. This is most likely due to parameter variations having opposing effects and therefore cancelling each other out. Further analysis of parameter sets showed that the period change is not necessarily equivalent to the sum of the contributions from the individual parameters (figure 4.10). Analysis of the parameter sets that did not result in a periodic solution identified them to contain large parameter changes. This suggested that large uninformed parameter changes are more likely to result in a non-oscillating system than a considerably altered limit cycle. The non-additive nature of multiple parameter changes was further evidenced by figure 4.12, which shows the period bifurcation changes as the number of parameters changed increases.

The analysis methods presented in this chapter consider local perturbations with respect to a single parameter. However, the parameter space associated with many biochemical models is of a high dimension and the relationships identified at one point in parameter space do not necessarily hold true everywhere. Figure 4.12 demonstrates this for the Ashall model, the local relationships remain qualitatively true close to the original parameterisation but alter as the parameter changes move the system further away from the original point in parameter space. Sensitivity and bifurcation analysis method can be extended into higher dimensions to address the effect of co-varying multiple parameters in a system. Multi-dimensional bifurcation analysis is applied in Chapter 5 and Chapter 6 to analyse the effect of multiple perturbations on the NF- $\kappa$ B system.

**Chapter 5 –  
Investigating the Role of the  
Negative Feedbacks I $\kappa$ B $\alpha$  and  
A20**

## 5.1 – Introduction

Negative feedbacks not only terminate cellular responses, they can modulate the dynamics of cellular signalling (Kholodenko, 2006). The presence of a negative feedback loop in the network topology is a key requirement in order for a biological system to exhibit stable oscillations. Other requirements include sufficient delay in this feedback and non-linearity in the system (Friesen and Block, 1984, Novak and Tyson, 2008). Studies have shown interlinked positive and negative feedbacks generated robust oscillations with a tuneable frequency (Tsai *et al.*, 2008) and increase adaptability to extra-cellular signals (Ma *et al.*, 2009, Paszek *et al.*, 2010a). More recently, an analysis of the effect of multiple negative feedbacks acting at different levels in the pathway has been conducted (Nguyen, 2012). This analysis found, similarly, that the presence of nested feedback structures provided robust control of oscillation dynamics and their basic characteristics, such as period and amplitude. Moreover, the analysis found the dual feedbacks often had opposite effects on oscillation characteristics.

I $\kappa$ B $\alpha$  and A20 are vital negative feedbacks for normal NF- $\kappa$ B function. On a physiological level I $\kappa$ B $\alpha$  genetic deletion in mice resulted in perinatal lethality (Beg *et al.*, 1995), and in the case of A20 deletion the mice died at a few weeks of age (Lee *et al.*, 2000). On a cellular level inhibition of I $\kappa$ B $\alpha$  and A20 feedback results in the loss of NF- $\kappa$ B oscillations and a predominantly nuclear localisation of the transcription factor (Baldwin, 1996, Werner *et al.*, 2008).

Computational analysis of the NF- $\kappa$ B system has demonstrated that negative feedback from I $\kappa$ B $\alpha$  and A20 is integral to the NF- $\kappa$ B dynamics and a core part of the network topology. The model of Hoffmann *et al.* (2002) demonstrated that inducible I $\kappa$ B $\alpha$  feedback generates oscillations in NF- $\kappa$ B. This was further elucidated in the minimal NF- $\kappa$ B model developed by Krishna *et al.* (2006), which identified the core network to consist of the variable nuclear NF- $\kappa$ B and two representations of its negative feedback I $\kappa$ B $\alpha$ . Further analysis of this model, which included the addition of A20 negative feedback, demonstrated that nested feedback loops allowed for independent control of the period (Mengel *et al.*, 2012). Moreover,

adjusting the expression of A20 could change the period by up to a factor of 2. The minimal model developed in Chapter 3 consisted of the same three variables as the model of Krishna *et al.* plus a representation of the negative feedback A20. Throughout the model reduction process the differential equations related to I $\kappa$ B $\alpha$  and A20 transcription remained unchanged, and the speed coefficients associated with the I $\kappa$ B $\alpha$  and A20 mRNA variables were consistently the slowest. This relationship is further supported by sensitivity and bifurcation analyses, which identified the parameters related to A20 and I $\kappa$ B $\alpha$  to have a strong influence on the model's dynamics (Wang *et al.*, (2012a) and Chapter 4). NF- $\kappa$ B dynamics are important to control cellular function and an understanding of how to modulate these dynamics could have far-reaching implications when considering the NF- $\kappa$ B system as a therapeutic target. This chapter explores the central role of these negative feedback loops in generating and controlling oscillations.

## 5.2 – Analysis of the Effects of I $\kappa$ B $\alpha$ and A20 Feedback on NF- $\kappa$ B Dynamics

### 5.2.1 – Computational Analysis of I $\kappa$ B $\alpha$ and A20 Transcription

The transcription rates of the I $\kappa$ B $\alpha$  and A20 variables were chosen for analysis based upon several reasons. First, the minimal model identified the mRNA species of these variables to be integral in maintaining oscillations. Second, experimental changes such as siRNA inhibition and over-expression through transient transfection can be related to changes in the *in silico* transcription rates. It is also possible to relate these changes to protein production. The high reaction rate and linear term that represents translation of mRNA in the Ashall model results in bifurcations with respect to the translation rates that are equivalent to the bifurcations with respect to the corresponding transcription rates (figure 4.8, Chapter 4). Therefore, in the case of this model both analyses are equivalent.

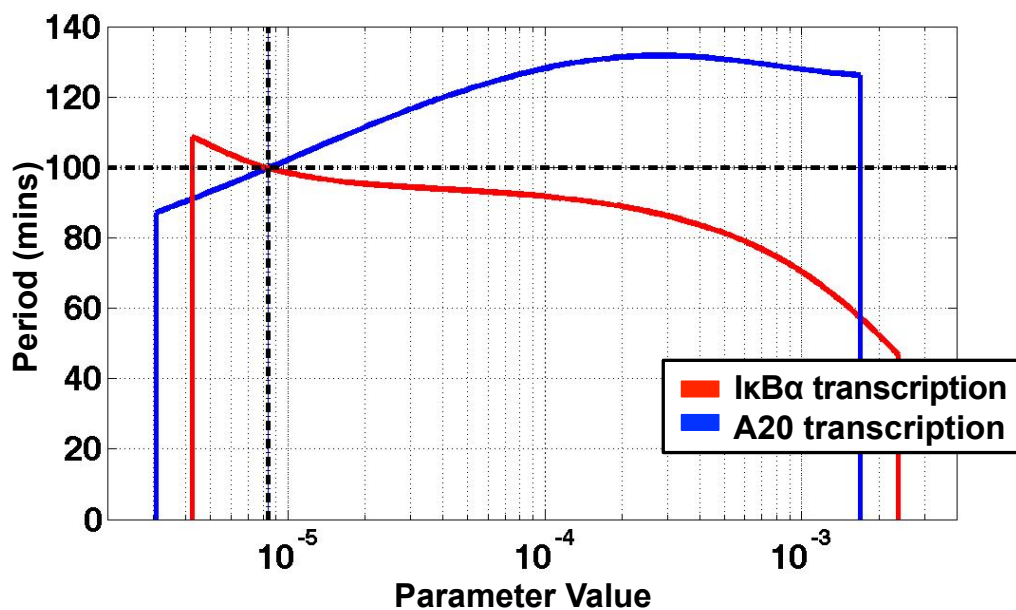


**Figure 5.1** –Semi-logarithmic plot showing how the limit cycle period changes as the parameters related to I $\kappa$ B $\alpha$  (c1a) and A20 (c1) transcription are varied, red and blue lines respectively. Vertical dashed black line represents the parameter value used in Ashall *et al.* (2009). The horizontal dashed black line represents the experimentally observed 100-minute period. Analysis performed using XPPAUT.

Figure 5.1 represents the period bifurcations for the  $I\kappa B\alpha$  and A20 transcription parameters,  $c1a$  and  $c1$  respectively. The parameters have opposite effects on the period; this is in agreement with observations regarding dual negative feedback models (Nguyen, 2012). These opposite effects could suggest that the system has evolved to be robust to fluctuation in the parameters due to environmental changes, such as temperature, where the effect of an increase in one rate is offset by an opposite effect in the increase of another. This phenomenon has been observed in circadian oscillations, which are temperature-compensated (this will be discussed further in Chapter 6).

To further understand the impact of these negative feedbacks on the period a 2-dimensional bifurcation analysis was undertaken. Using XPPAUT bifurcation analysis with respect to two model parameters can be performed. This analysis gives a 2-dimensional surface, with each parameter representing a dimension, for which the model has a stable limit cycle. This analysis was conducted for the parameters representing  $I\kappa B\alpha$  and A20 transcription rate,  $c1a$  and  $c1$  respectively (figure 5.2a). The x- and y-axes represents the  $I\kappa B\alpha$  and A20 transcription parameter values, and the z-axis shows the change in limit cycle period (from the nominal 100-minutes) that corresponds to the (x,y) parameter pair. This analysis indicated by changing two parameters it is possible to manipulate the period over a considerable range of values with up to a 59-minute shortening or 49-minute lengthening. By only changing one of these parameters it is possible to increase the period by 8.6 minutes in the case of  $I\kappa B\alpha$  or 31.7 minutes for A20, therefore the increase in the period by varying two parameters is super-additive. However, when reducing the period single parameter changes can give a 12- or 46.9-minute change for A20 and  $I\kappa B\alpha$ , respectively. Therefore in this case the effect is additive. This analysis demonstrates that by altering multiple parameters it is possible to attain greater period changes than when using a single parameter. Moreover, that these changes can be greater than the sum of the individual parameter effects. It must be noted that to attain such a considerable change in the period requires parameter changes up to  $\sim 100$ -fold, which may not be considered plausible from a physiological perspective. As an aside, it is interesting to note that by varying both parameters, it is possible to reduce a parameter value

beyond its 1-dimensional HB and still maintain a limit cycle, if this change is balanced with a suitable change in the other parameter.

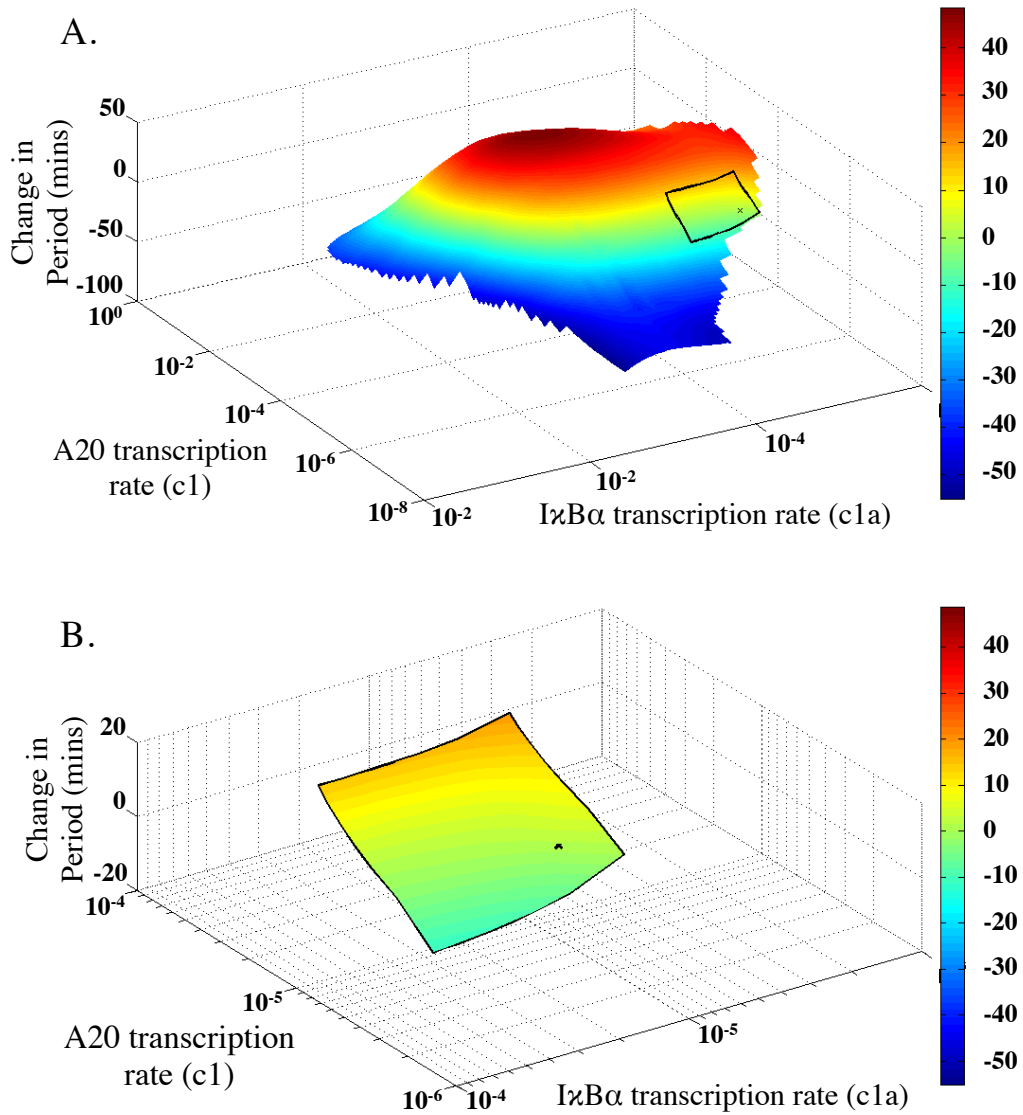


**Figure 5.2** – 2-dimensional bifurcation analysis for the parameters related to  $I\kappa B\alpha$  and A20 transcription ( $c1a$  and  $c1$  respectively) performed using XPPAUTO and MATLAB. Values on the z-axis show the corresponding period change for each pair of parameter values relative to the nominal values of 100-minutes. (A) Analysis for the range of parameter pairs where limit cycle oscillations exist. (B) A zoomed segment showing the corresponding period change when limiting parameter variations to up to a 5-fold increase or decrease.

The parameters  $c_{1a}$  and  $c_1$  represent the maximum possible rate of mRNA production for I $\kappa$ B $\alpha$  and A20 assuming two gene copies. The transcription rate for I $\kappa$ B $\alpha$  was fitted using constraints found in the literature (Ashall *et al.*, 2009). The fitted parameter for I $\kappa$ B $\alpha$  transcription rate corresponds to approximately 10 mRNA molecules per minute and the rate for A20 was assumed to be the same. The constraints bounded the rate of transcription between 1.1 and 3.3 kilobases per minute, with a minimum spacing between polymerases of approximately 100 nucleotides (Cheong *et al.*, 2006, Femino *et al.*, 1998). Assuming these constraints the maximum transcription rate is approximately 30 mRNA molecules per minute for I $\kappa$ B $\alpha$  and 50 for A20 as it is a shorter gene. However, these maximal rates were measured in *E.coli* and it would be sensible to assume a slower transcription rate in eukaryotic cells due to more complicated transcriptional architecture. These values imply that the physiological rate of transcription would not vary more than 5-fold above the parameter value without the inclusion of additional gene copies.

The 2-dimensional analysis limited to a 5-fold range of the parameter values can be seen in figure 5.2b. This range is sufficient to encompass the maximum bounds of I $\kappa$ B $\alpha$  and A20 transcription without the inclusion of additional transgenes. If the parameter values are restricted to this more realistic level the surface is considerably flatter, showing only a ~25-minute increase and a ~15-minute decrease at the extremes. When the analysis is limited to this range of parameter values the effects seen through co-variation are additive. This leads to the hypothesis that within the bounds of physiological transcription rates the period is robust, as the model predicts changes similar to the variability seen in the experimental data (Ashall *et al.*, 2009, Nelson *et al.*, 2004).

Transient transfection demonstrates another means to increase the transcription rate of a gene. If the rate of 10 mRNA molecules per minute for the two alleles were assumed true, then each additional copy of the gene would increase the rate by up to 5 mRNA molecules per minute. Bian and Belmont (2010) generated a number of stable cell lines transfected with a red fluorescent reporter constitutively expressed from the cytomegalovirus (CMV) promoter. Of the 12 cell lines 10 had a copy number less than 20, one clone had a copy number of ~30 and another of ~125. The



data regarding NF- $\kappa$ B dynamics was generated using a similar construct expressing RelA from a CMV promoter. Therefore, the data from Bian and Belmont can be used as an estimate for the copy number in cells transiently transfected with NF- $\kappa$ B reporter plasmids. However, transfection protocol and efficiency, cell line, and plasmid size can influence copy number, as such this is only a crude estimate. Assuming a high copy number of 20, this would result in a transcription rate of  $\sim$ 100 mRNA molecules per minute or a 10-fold increase in transcription. From figure 5.1 it can be seen that this could result in a  $\sim$ 30-minute increase in period for A20 and a  $\sim$ 10-minute decrease in the period for I $\kappa$ B $\alpha$ . One caveat to this analysis is that studies have demonstrated a poor correlation between expression level and copy number due to site integration effects in cells stably transfected with plasmid constructs (Bian and Belmont, 2010). Moreover, this is a comparison between stably and transiently transfected cells. It is more appropriate to experimentally determine relative expression levels of individual clones or cells when relating this computational analysis to experimental data.

### **5.2.2 – Robustness of the Period to I $\kappa$ B $\alpha$ Transcription**

The period of NF- $\kappa$ B oscillations was seen to be approximately 100 minutes in cells transiently transfected with only CMV driven RelA-dsRedXP, or with both CMV driven RelA-dsRedXP and CMV driven I $\kappa$ B $\alpha$ -EGFP (Ashall *et al.*, 2009, Horton, 2006, Nelson *et al.*, 2004). When the cells were transfected with CMV-RelA-dsRedXP and an I $\kappa$ B $\alpha$ -EGFP reporter whose transcription was driven by a promoter containing five  $\kappa$ B binding sites (NF-I $\kappa$ B $\alpha$ -EGFP), the period appeared considerably extended (Nelson *et al.*, 2004). These data are in contradiction to the computational analysis shown in figure 5.1 and figure 5.3.

As has been stated, transient transfection systems like these often result in the uptake of multiple copies of the plasmid and over-expression of the protein of interest in comparison to physiological levels. From the sensitivity analysis in Chapter 4 it can be seen that the level of NF- $\kappa$ B (prototypically p65:p50, parameter TNFKB) and I $\kappa$ B $\alpha$  expression (parameter c1a) have opposite effects on the system, suggesting the requirement of a balance between their levels in the system in order to maintain a

limit cycle. To understand the effect of over-expression through transient co-transfection of these two reporters a 2-dimensional bifurcation analysis of the system was performed with respect to NF- $\kappa$ B level and I $\kappa$ B $\alpha$  transcription rate (figure 5.3).

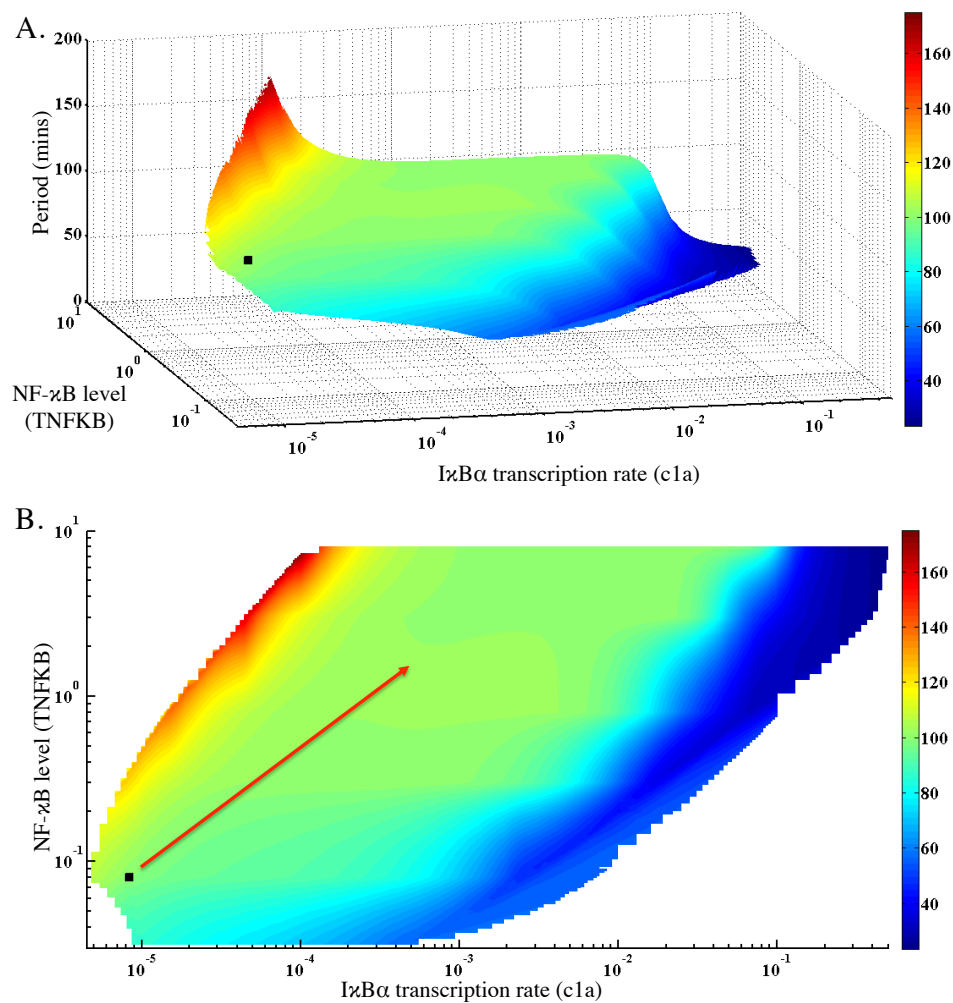


**Figure 5.3** – 2-dimensional bifurcation analysis for the parameters related to I $\kappa$ B $\alpha$  transcription (c1a) and the level of NF- $\kappa$ B (TNFKB). (A) The surface represents the period for the corresponding parameter pair, c1a (x-axis) and TNFKB (y-axis). The black square represents the original parameter pair. (B) A 2-dimensional projection of the surface in (A), values of the colour bar represent the corresponding period in minutes. Red arrow highlights the direction corresponding to an increase of both the c1a and TNFKB parameters; the black square represents the original parameter pair.

As the two parameters are simultaneously increased the model continues to show a limit cycle with a 100-minute period. The 2-dimensional analysis identified an area in parameter space where the model can maintain a limit cycle with an approximately 100-minute period, as can be seen by the broad flat area in figure 5.3a. Figure 5.3b represents a projection of this surface into 2-dimensions; the red arrow traces the direction along the surface corresponding to an increase of both parameters, akin to over-expression of RelA and I $\kappa$ B $\alpha$ . The direction of this arrow follows the flat area of the surface where the limit cycle period remains approximately 100 minutes. This suggests that in order to oscillate the system requires a balance between the level of NF- $\kappa$ B and expression of I $\kappa$ B $\alpha$ . However, the broad nature of the surface also implies that this is by no means a delicate balance and that the system is insensitive to a degree of variation in the levels. This analysis supports the robust period seen when cells are co-transfected with CMV-RelA-dsRedXP and CMV-I $\kappa$ B $\alpha$ -EGFP. However, not when cells are transfected with CMV-RelA-dsRedXP and NF-I $\kappa$ B $\alpha$ -EGFP.

One consideration in this analysis is the choice of parameter values to represent the experimental perturbation of the system. The RelA and I $\kappa$ B $\alpha$  fluorescent constructs are both driven using the CMV promoter and are therefore constitutively expressed. The choice of the parameter TNFKB to represent RelA level appears sensible as after transfection with the CMV-RelA-dsRedXP plasmid the system will alter to obtain a new steady state with a higher level of RelA in the cell. However, the model assumes that I $\kappa$ B $\alpha$  is only transcribed when RelA is present in the nucleus, which is not true after transfection with a CMV driven I $\kappa$ B $\alpha$  reporter. The model system is better represented by the NF-I $\kappa$ B $\alpha$ -EGFP construct, co-transfection with this construct showed an increase in the period however, the data presented was obtained from only a few cells (n=3) and this is a very artificial promoter. In the next section RelA-I $\kappa$ B $\alpha$  dynamics are analysed using a physiologically relevant expression system.

### 5.2.3 – Characterising NF- $\kappa$ B and I $\kappa$ B $\alpha$ Dynamics Using BAC Constructs

The bacterial artificial chromosome (BAC) system is capable of maintaining human genomic DNA fragments of >350kb (Shizuya *et al.*, 1992). The development of seamless recombination methods (Warming *et al.*, 2005) has allowed expression of fluorescently conjugated genes under the control of large native genomic regions, resulting in normal regulation and sensitivity to all feedback mechanisms. Recombinant BACs have been created to transiently transfect cells with fusion proteins for I $\kappa$ B $\alpha$  and RelA fused at the C-terminus with EGFP and dsRedXP respectively (A. Adamson, R. Awais, *Systems Microscopy Centre, University of Manchester, unpublished*). These constructs contain several thousand kilobases of the regions up and downstream of the I $\kappa$ B $\alpha$  and RelA genes, therefore encompassing much of the promoter and enhancer regions responsible for their transcriptional control. Furthermore, all UTRs, exons and introns have been maintained resulting in properly controlled transcription and RNA processing. This allows for fluorescent imaging of proteins that more accurately represent the level of the endogenous system, with these constructs asynchronous nuclear-cytoplasmic oscillations of I $\kappa$ B $\alpha$  and RelA at the single cell level have been observed (A. Adamson, *unpublished*). Transfection with the I $\kappa$ B $\alpha$ -EGFP construct alone showed oscillations in the cellular level of I $\kappa$ B $\alpha$  fluorescence intensity (figure 5.4a). This construct has demonstrated the cycles of degradation and re-synthesis of I $\kappa$ B $\alpha$  on the single cell level predicted by the Ashall model.

A mixed clonal population of SK-N-AS cells stably transfected with varying copy numbers of the RelA-dsRedXP and I $\kappa$ B $\alpha$ -EGFP BACs were stimulated using 10ng/ml TNF $\alpha$  and imaged approximately every 5 minutes for up to 10 hours using fluorescence confocal microscopy. The imaging data was subsequently analysed using CellTracker to determine the ratio of nuclear to total RelA fluorescence and the period of RelA oscillations. The cells exhibited RelA nuclear-cytoplasmic oscillations with a period of approximately 100 minutes (figure 5.4b). This is not a clonal cell line and therefore within this population there will be cells with varying

copy numbers of the I $\kappa$ B $\alpha$  and RelA constructs. (*Dr A. Adamson, Systems Microscopy Centre, University of Manchester performed Imaging and analysis*).

The number of RelA molecules in the Ashall model is assumed to be  $\sim 100,000$ . This corresponds to a concentration of  $0.08\mu\text{M}$  using the cell volume parameters measure by Ashall *et al.* After equilibration of the model there is approximately  $0.09\mu\text{M}$  of I $\kappa$ B $\alpha$ , indicating that the level of I $\kappa$ B $\alpha$  in unstimulated cells is slightly in excess of RelA, which is in general agreement with existing literature (Carlotti *et al.*, 2000). Fluorescence correlation spectroscopy (FCS) (Hess *et al.*, 2002) has been used to analyse of the level of RelA and I $\kappa$ B $\alpha$  in the non-clonal BAC cells. This method estimated the number fluorescent RelA molecules in these cells to be around 220,000-270,000 and the number of fluorescent I $\kappa$ B $\alpha$  molecules to be similar (*J. Boyd, Centre for Cell Imaging, University of Liverpool*). This is in addition to the endogenous RelA, therefore, these data suggest an approximate 3- to 4-fold increase in expression from the original estimates of Ashall *et al.* These cell lines demonstrate an average period of  $\sim 100$  minutes and therefore support the model prediction (figure 5.3) that the system can tolerate over-expression of RelA and I $\kappa$ B $\alpha$  as long as a balance in their expression levels is maintained.

The NF- $\kappa$ B dynamics were also analysed in clonal SK-N-AS cell lines expressing only the I $\kappa$ B $\alpha$ -EGFP BAC. Three clonal cell lines were analysed each one having a different level of I $\kappa$ B $\alpha$ -EGFP expression. Similarly, these cells were treated with 10ng/ml TNF $\alpha$  and imaged approximately every 5 minutes for up to 10 hours. The resulting imaging data was analysed using CellTracker to quantify the cellular level of I $\kappa$ B $\alpha$  fluorescence. Oscillations with approximately 100-minute period were present in all cell lines, regardless of expression level (figure 5.4b). Immunoblotting did not highlight any change in the endogenous level of RelA. Therefore, it can be hypothesised that the system itself is insensitive to altered levels of I $\kappa$ B $\alpha$  expression, which the model currently does not predict. (*Dr A. Adamson, Systems Microscopy Centre, University of Manchester performed Imaging and analysis*).

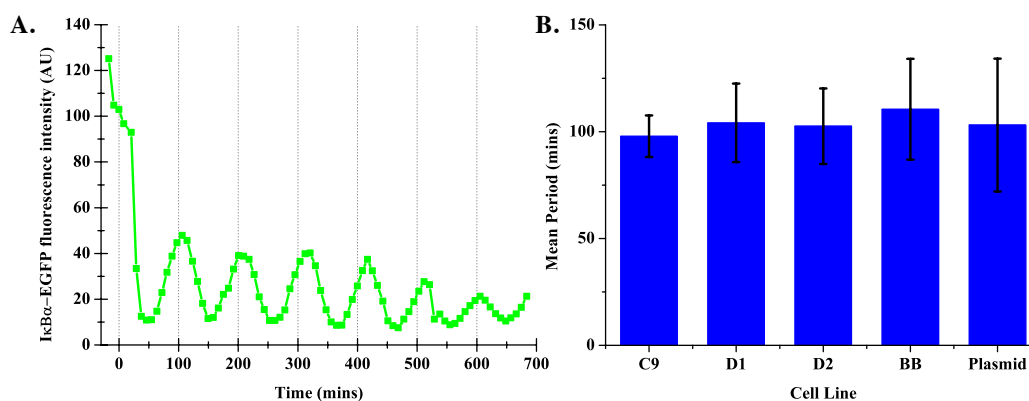


**Figure 5.4** - (A) I $\kappa$ B $\alpha$ -EGFP fluorescence intensity, measured as a whole cell average, for SK-N-AS cells stably transfected with the I $\kappa$ B $\alpha$ -EGFP BAC (cell line C9). Cells were treated with 10ng/ml TNF $\alpha$  at time 0-minutes (A. Adamson, unpublished). (B) Mean period for 5 different NF- $\kappa$ B reporter systems after 10ng/ml TNF $\alpha$  stimulation. C9, D1 and D2 represent three I $\kappa$ B $\alpha$ -EGFP BAC stable SK-N-AS cell lines with different expression levels. C9 low (n=10), D1 medium (n=20), D2 high (n=14). A mixed population of SK-N-AS cells stably transfected with I $\kappa$ B $\alpha$ -EGFP and RelA-dsRedXP BACs at different copy numbers denoted BB (n=42) (A. Adamson, unpublished). Finally, SK-N-AS cells transiently transfected with CMV-RelA-dsRedXP (n=25), data taken from Horton (2006).

#### 5.2.4 – Developing a Model Robust to I $\kappa$ B $\alpha$ Transcription Rate

These clonal cell lines have an increased expression of I $\kappa$ B $\alpha$  but at different levels ranging from a 2.5- to 9- fold increase in expression, measured through immunoblotting (A. Maya-Mendoza, *Systems Microscopy Centre, University of Manchester*). However, the timing of the oscillations is similar for all three clones and consistent with previous estimates of 100 minutes (Ashall *et al.*, 2009, Nelson *et al.*, 2004). An increase in the I $\kappa$ B $\alpha$  transcription rate is the only known perturbation in these cell lines therefore bifurcation analysis with respect to this parameter (c1a) is a sensible starting point to probe this phenomenon. The period bifurcation with respect to this I $\kappa$ B $\alpha$  mRNA synthesis (c1a) is a curve with negative gradients at both tails and an almost stationary point in between these (figure 5.5a). The first way the model can be adapted to fit these data is by increasing the I $\kappa$ B $\alpha$  transcription rate so that the parameter value lies in the interval of the period bifurcation with the smallest gradient (figure 5.5a). To do this the rate of transcription was increased from 10

mRNAs per minute to  $\sim 30$  mRNAs per minute ( $4 \times 10^{-7} \mu\text{Ms}^{-1}$ ); while this rate is high it is still within experimentally measured bounds (Cheong *et al.*, 2006).

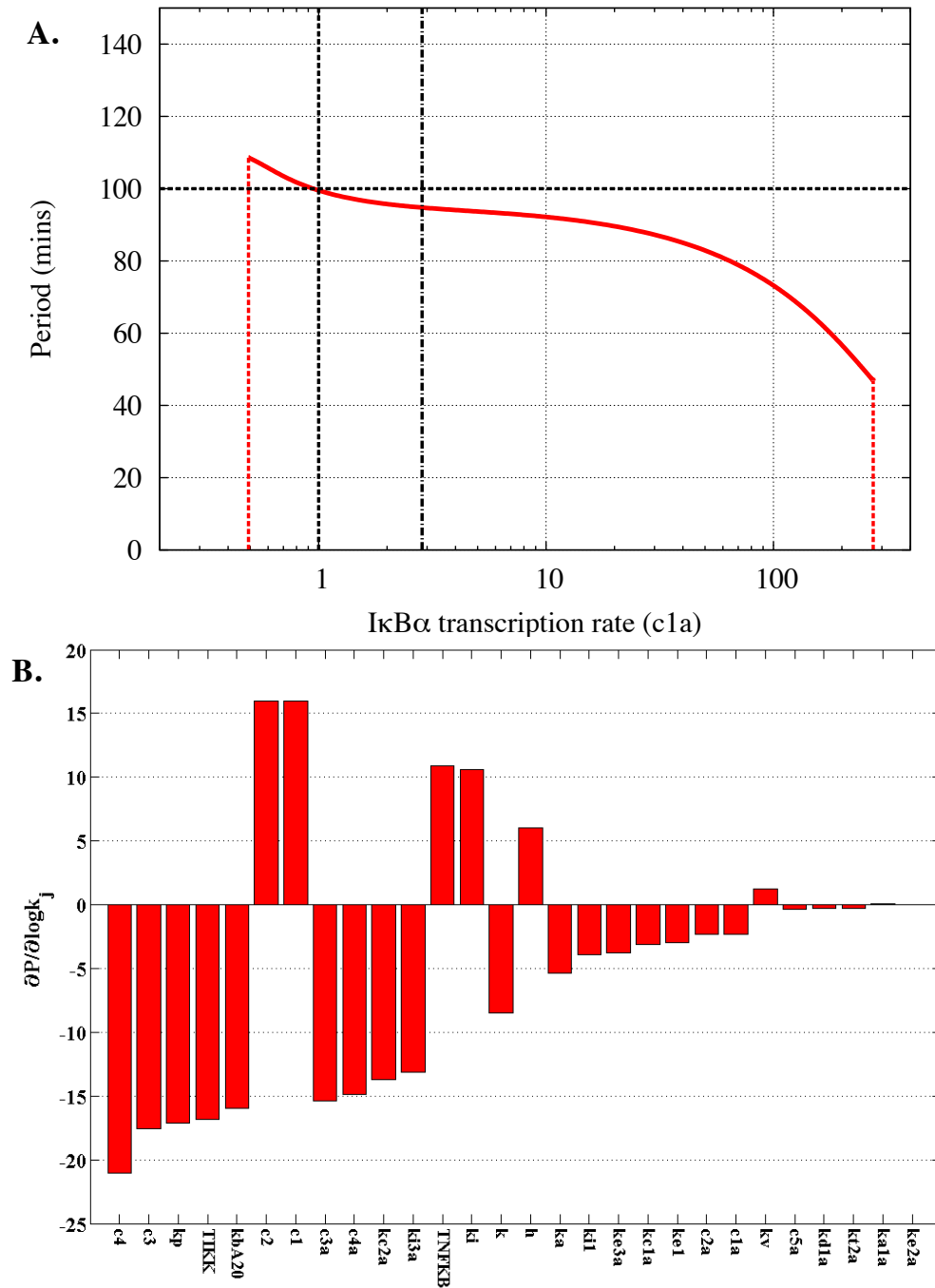


**Figure 5.5** – (A) Period bifurcation for the parameter  $c1a$ , I $\kappa$ B $\alpha$  transcription rate. The parameter values have been normalised to their original value in Ashall *et al.* (2009). The vertical dashed black line at 1 represents the original parameter value ( $1.4 \times 10^{-7}$ ), the vertical dot-dash black line represents the increased parameter value ( $4 \times 10^{-7}$ ) and the horizontal dashed black line represents the period of the original model. (B) Control coefficients for the Ashall model when  $c1a$  is set to  $4 \times 10^{-7}$  (see Chapter 3).

After this re-parameterisation the control coefficient for  $c1a$  is over three times smaller than in the original parameterisation (8.69 vs. 2.31, figure 4.2, Chapter 4 vs. figure 5.5b). A smaller coefficient means that the period is more robust to small perturbations of  $c1a$ . However, in this new parameter set, the period is now reduced (94mins in comparison to 100mins) and the model is only robust to small variations of the transcription rate. To develop this parameter set further, a similar approach to Wang *et al.* (2012a) was undertaken. Wang *et al.* explored the sensitivity of the model to TNF $\alpha$  dose by measuring the change in the Hopf bifurcation with respect to TNF $\alpha$ , as other parameters were varied. A similar approach was used here with the I $\kappa$ B $\alpha$  transcription rate. The period bifurcation for  $c1a$  was analysed as other I $\kappa$ B $\alpha$  related parameters were varied 2-fold. These parameters were  $c3a$ ,  $c4a$ ,  $ke3a$ ,  $ki3a$  and  $c5a$ .

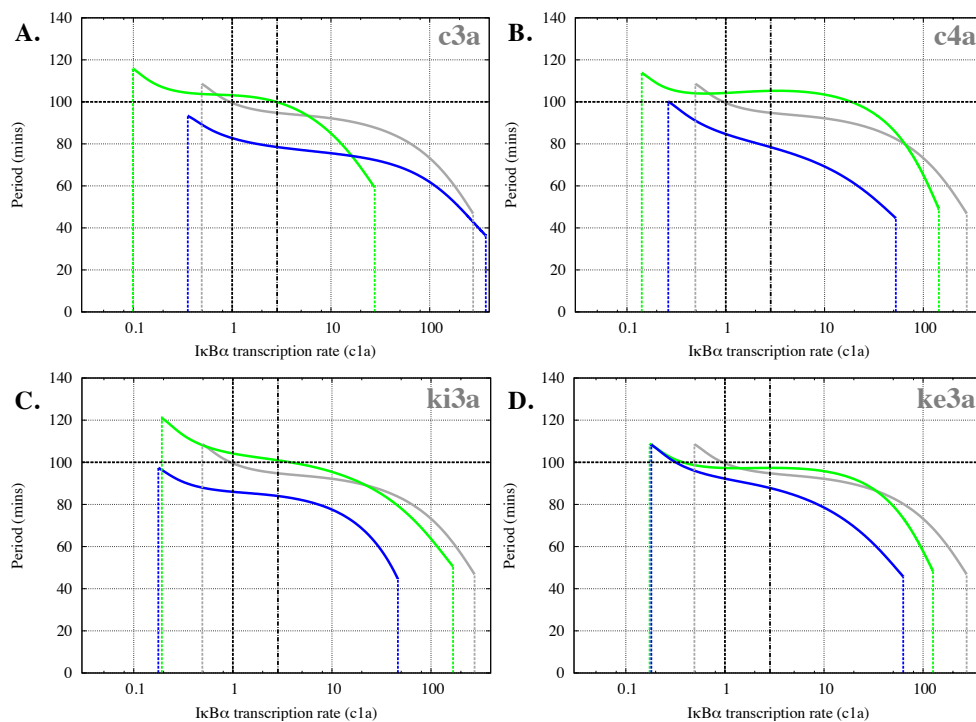
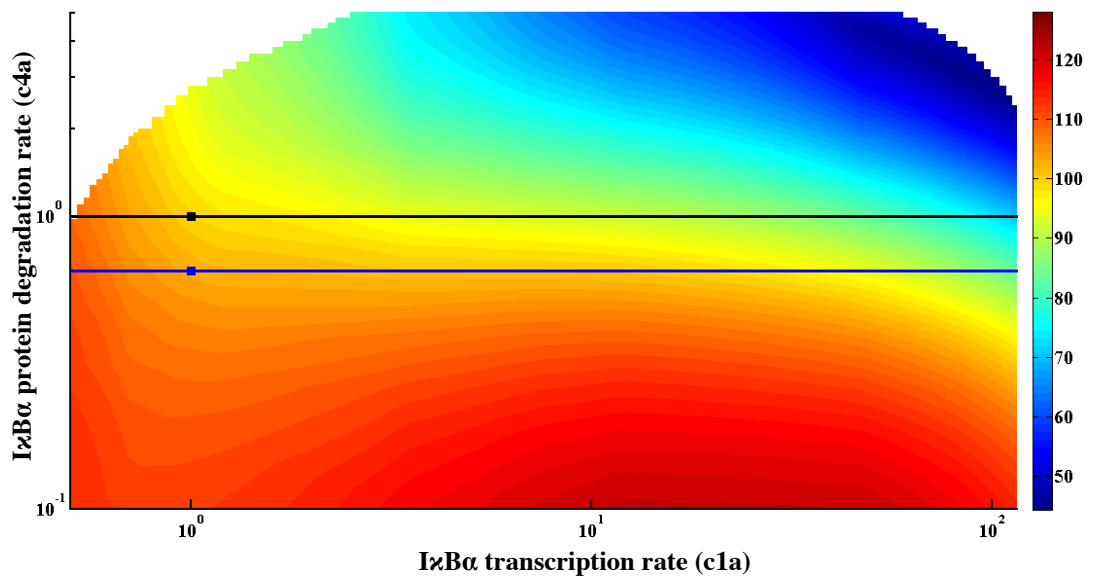


**Figure 5.6** – Exploration of the effect of parameter changes on the period bifurcation with respect to I $\kappa$ B $\alpha$  transcription ( $c1a$ ). Model parameters were altered 2-fold up and down, and the period bifurcation for  $c1a$  calculated. The parameters chosen were  $c3a$ ,  $c4a$ ,  $ki3a$  and  $ke3a$ , (A)-(D) respectively. The green curves represent a 2-fold decrease, the blue curve a 2-fold increase and the grey curve the original  $c1a$  period bifurcation. The parameter values have been normalised to their original value in Ashall *et al.* (2009). The vertical dashed black line at 1 represents the original parameter value ( $1.4 \times 10^{-7}$ ), the vertical dot-dash black line represents the increased parameter value ( $4 \times 10^{-7}$ ) and the horizontal dashed black line represents the period of the original model.



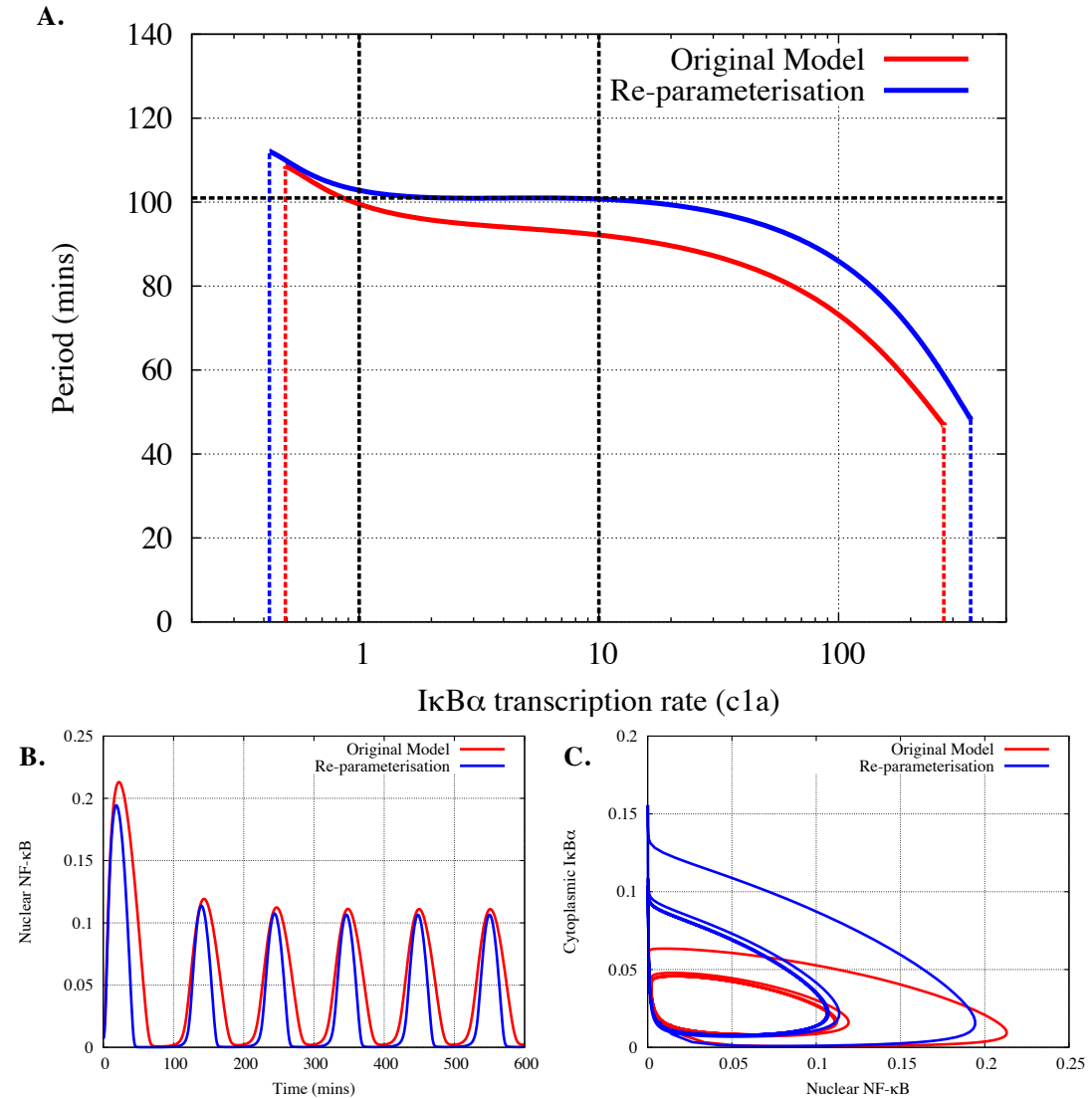
A comparison between the original  $c1a$  period bifurcation and the parameters  $c1a$ ,  $ki3a$  and  $ke3a$  is depicted by figure 5.6, these parameters were chosen due to their direct relation to  $I\kappa B\alpha$ . They represent mRNA and protein degradation, and nuclear import and export. The parameter  $c5a$  was also analysed, however, it has a very small control coefficient (figure 5.5a) and therefore a negligible effect on the  $c1a$  period bifurcation. The parameter  $c2a$  was omitted as previous analysis has demonstrated this is analogous to  $c1a$  (figure 4.8, Chapter 4). This analysis can be used to identify parameter changes that can help to achieve the desired bifurcation structure with respect to  $c1a$ , namely a period of 100 minutes that is robust to changes in the  $I\kappa B\alpha$  transcription rate between 3- and 8-fold (based on the expression levels in the BAC cell lines). Figure 5.6d can be immediately ruled out, as the period is less than 100 minutes except for very slow transcription rates. Analysis of the other curves identifies the parameter  $c4a$  (figure 5.6b) as a suitable candidate for further study. For a 2-fold decrease in this parameter (green curve) the bifurcation has a shallow gradient over a 10-fold range of the original parameter value and the period is close to 100 minutes. The relationship between  $c1a$  and  $c4a$  can further be studied using 2-dimensional bifurcation analysis.

Figure 5.7 shows a projection of the surface representing the periods for possible  $c1a$  and  $c4a$  parameter combinations. A central band of yellow-orange colour can be seen corresponding to model with periods of approximately 100 minutes. The black line highlights the cross-section of the surface for the original  $c4a$  parameter value. It can be seen that this line lies near a precipice before a steep drop into model parameterisations that give markedly shorter periods. By reducing the  $c4a$  parameter it is possible to move the  $c1a$  period bifurcation further into this yellow-orange zone yielding a model parameterisation that is more robust to increasing  $I\kappa B\alpha$  transcription and has a period of approximately 100 minutes. Analysis of the surface based on the identified criteria found a parameter value of  $c4a=0.000325$  resulted in the best fit (figure 5.7, blue line).



**Figure 5.7** – Projection of the 2-dimensional period bifurcation surface for the parameters  $c1a$  and  $c4a$ ,  $\text{I}\kappa\text{B}\alpha$  transcription and protein degradation respectively. The black square represents the parameter values for the model in Ashall *et al.* (2009); the black line highlights the  $c1a$  periods corresponding to the original  $c4a$  parameter value. The blue square represents the parameter values for the re-parameterised model. The blue line highlights the corresponding periods as  $c1a$  is varied for the new  $c4a$  parameter value. Parameter values have been normalised to their nominal values in Ashall *et al.* (2009).

This re-parameterisation caused minimal change to the period and resulted in a model that is robust to  $\text{I}\kappa\text{B}\alpha$  and  $\text{NF-}\kappa\text{B}$  over-expression, and to a 10-fold  $\text{I}\kappa\text{B}\alpha$  over-expression (figure 5.8a). In the Ashall model  $c4a$  was a fitted parameter and this change is within the fitting constraints (Ashall *et al.*, 2009). The resulting model has a comparable period and amplitude, but the shape of the peaks became sharper (figure 5.8b). There was a small increase in the level of  $\text{I}\kappa\text{B}\alpha$  after equilibration ( $0.0931\mu\text{M}$  in comparison to  $0.0915\mu\text{M}$ ), and an increase in the amplitude of  $\text{I}\kappa\text{B}\alpha$  oscillations, which can be seen in the  $\text{I}\kappa\text{B}\alpha$ - $\text{NF-}\kappa\text{B}$  phase plane (figure 5.8c). In addition the model was able to respond correctly to the other fitting criteria of the Ashall model, pulsatile  $\text{TNF}\alpha$  stimulation. The system recapitulated the correct response to all three pulsing frequencies.



**Figure 5.8** – (A) Period bifurcation for the parameter  $c1a$ , I $\kappa$ B $\alpha$  transcription. The red line represents the original model in Ashall *et al.* (2009), the blue line represents the re-parameterised model where  $c5a = 0.000325$ . The rates have been normalised to the value of  $c1a$  in Ashall *et al.* The vertical dashed black line at 1 represents the original parameter value, the vertical dashed black line 10, represents a 10-fold increase in the parameter value, the horizontal dashed black line represents the period of the original model. (B) Time series for the variable nuclear NF- $\kappa$ B, assuming continuous TNF $\alpha$  stimulation, for the model in Ashall *et al.* (red line) and the re-parameterised version (blue line). (C) Phase plane analysis for the variables nuclear NF- $\kappa$ B and cytoplasmic I $\kappa$ B $\alpha$  for the model in Ashall *et al.* (red line) and after re-parameterisation (blue line), assuming continuous TNF $\alpha$  stimulation.

### **5.2.5 – The Effect of A20 Feedback on NF- $\kappa$ B Oscillations**

To determine the effect of increased A20 transcription on the NF- $\kappa$ B dynamics SK-N-AS cells were transiently transfected with an EGFP-A20 reporter driven by a proximal A20 promoter (ppA20-EGFP-A20) and CMV driven RelA-dsRedXP. The A20 construct consists of a short section of the A20 promoter (~250bp) that contains two  $\kappa$ B binding sites driving the expression of EGFP fused to the A20 gene. 24 hours post transfection SK-N-AS cells were stimulated with 10ng/ml TNF $\alpha$  and those visibly expressing both reporters imaged every ~5 minutes for up to 17 hours. Figure 5.9 is a series of representative images from one location in one experiment; the bright field, RelA (red), A20 (green) and a composite of RelA and A20 are displayed. From these images a cytoplasmic localisation of RelA and A20 can be seen prior to stimulation. Following TNF $\alpha$  stimulation RelA nuclear translocations can be seen in cells at 1h46m and 3h31m, while A20 maintains a cytoplasmic localisation throughout the image series. The images also suggest that a portion of the A20 fluorescence is localised in perinuclear speckles.

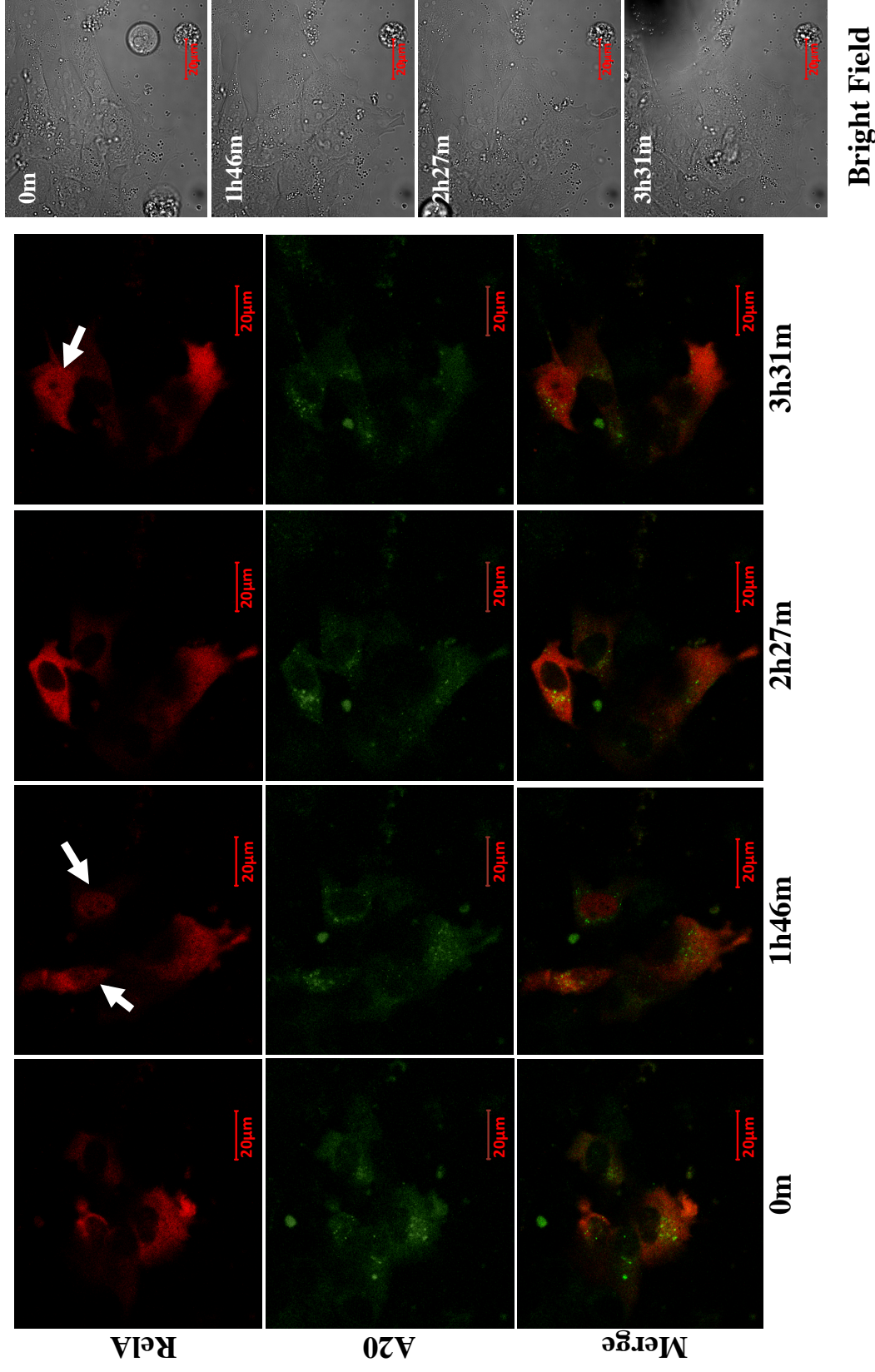


**Figure 5.9** - Fluorescence confocal imaging of SK-N-AS cells transiently transfected with CMV-RelA-dsRedXP and ppA20-EGFP-A20, and stimulated with TNFα (10ng/ml). Representative images are shown at the same location for four time points. Three channels are shown (bright field, red and green) and a composite of the red and green channels. Times are measured post TNFα stimulation, the red scale bar measures 20μm and the white arrows show nuclear translocations within cells.

The resulting imaging data was analysed using CellTracker to quantify the fluorescence in a nuclear region of interest (ROI). A20 maintained a cytoplasmic localisation throughout the experiment, with no significant change in A20 nuclear fluorescence being observed. The cells showed damped and non-damped oscillations in the level of nuclear RelA (figure 5.10a and figure 5.10b). The timing between peaks was analysed from peak 2 onwards, the time between peak one and two was ignored as previously it has been observed to be extended relative to other peaks-to-peak times (Horton, 2006). These data had a mean peak-to-peak time of  $150.4 \pm 47.1$  minutes ( $n=25$ , figure 5.10d), which is longer than seen in SK-N-AS cells transiently transfected with only CMV-RelA-dsRedXP (Ashall *et al.*, 2009, Nelson *et al.*, 2004). These data indicated that cells exhibiting a greater number of peaks have a shorter period, which can be seen from the average oscillation time from peak 6 onwards, however, this was still greater than 100 minutes (figure 5.10d). These data also imply over-expression of A20 results in an extended time to the first and time between the first and second peaks, relative to that observed with only the RelA-dsRedXP transgene (Nelson *et al.*, 2004). The data in figure 5.10c shows the distribution of peak-to-peak times, the majority of times are between 120 and 160 minutes, with a mean of  $\sim 150$  minutes.

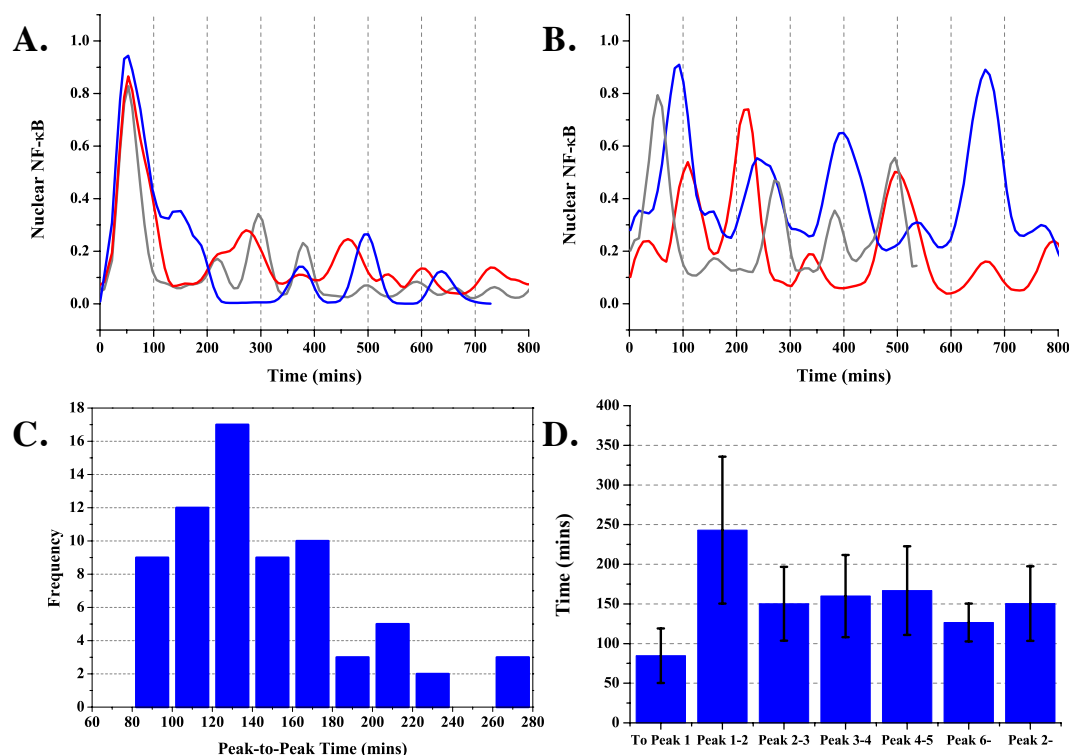


**Figure 5.10** - Analysis of the RelA dynamics seen in cells transiently transfected with CMV-RelA-dsRedXP and ppA20-EGFP-A20. (A) & (B) Quantification of RelA nuclear levels using small-circle CellTracker with a nuclear ROI. (A) Three representative traces showing cells that displayed damped RelA N:C oscillations. (B) Three representative traces of cells showing non-damped RelA N:C oscillations. (C) Histogram of peak-to-peak timings for all cells from peak 2 onwards (25 cells from 3 independent experiments). (D) Summary of peak-to-peak timings for all 25 cells.

### 5.2.6 – One and Two-dimensional Bifurcation Analysis for A20

Figure 5.11 depicts the bifurcation analysis with respect to the parameter  $c_1$ , the rate of transcription of A20 in the Ashall model. These bifurcations suggest that this preliminary data on RelA and A20 dynamics is consistent with the model prediction that increased A20 transcription rate elongates the period of NF- $\kappa$ B oscillations. Again assuming an average copy number in transfected cells of  $\sim 20$  this would result in a 10-fold increase in A20 transcription; from the 1-dimension bifurcation analysis this corresponds to a 30-minute increase in the period. The average period was found to be approximately 150 minutes in these data. However, figure 5.10c shows that the distribution of these timings is skewed towards a longer period and a Shapiro-Wilko normality test identified these data as not normally distributed, therefore analysis of a greater number of cells may result in increased consistency with the model. The

model also predicts a reduction in limit cycle amplitude as the expression of A20 is increased. This is consistent with the damped oscillation seen in some cells (figure 5.10a).

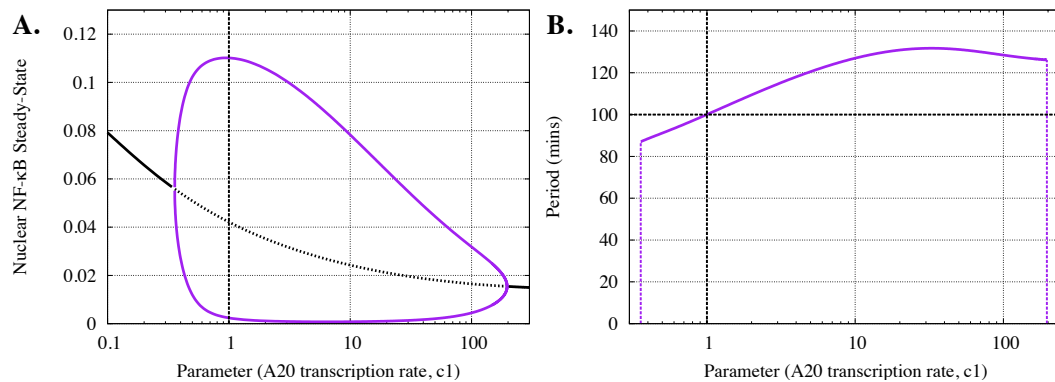


**Figure 5.11** – Bifurcation analysis for the model parameter  $c_1$ , A20 transcription rate. The parameter has been normalised to its nominal value, the vertical black dashed line represents the nominal parameter value. (A) Shows the how the limit cycle amplitude changes between the lower and upper Hopf bifurcation (HB) points. Solid black lines represent a stable steady state, the dashed black line shows the unstable steady state and the purple line represents the max and min of the limit cycle. (B) Period bifurcation showing the limit cycle period between the upper and lower HB points. The horizontal black line shows the normal period of 100-minutes.

Figure 5.12 represents a 2-dimensional analysis for A20 transcription ( $c_1$ ) and the level of NF- $\kappa$ B (TNF $\kappa$ B). These parameters show a markedly different relationship in comparison to  $\text{I}\kappa\text{B}\alpha$  transcription (figure 5.3). This is supported by the different gradients of the A20 and  $\text{I}\kappa\text{B}\alpha$  transcription period bifurcations (figure 5.1). This analysis suggests that simultaneously increasing the level of NF- $\kappa$ B and A20 transcription will increase the period to a maximum of  $\sim 140$ -minutes, consistent with the experimental data (figure 5.10). However, the analysis also suggests that a further increase of the levels  $\sim 100$ -fold will result in a flatter regime where the limit cycle period appears robust to the level of NF- $\kappa$ B and A20 feedback. This phenomenon is difficult to rationalise with the experimental data, as there is no quantification of the level of expression. In addition, the parameter increase required for this behaviour is also in a range, which could be considered physiologically unrealistic.



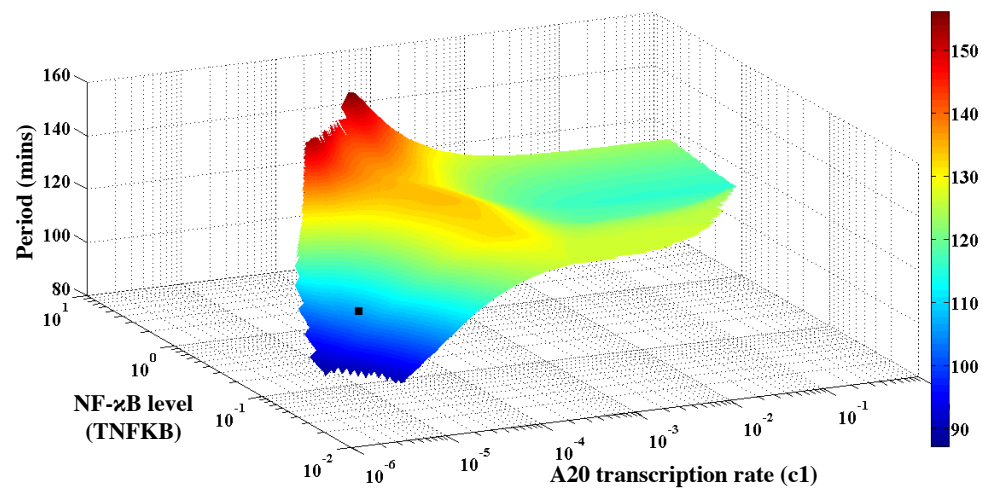


**Figure 5.12** - 2-dimensional bifurcation analysis for the parameters related to A20 transcription ( $c1$ ) and the level of NF- $\kappa$ B (TNFKB). (A) The surface represents the period for the corresponding parameter pair,  $c1$  (x-axis) and TNFKB (y-axis). The black square represents the original location of the parameter pair.

### 5.2.7 – Perinuclear Speckling of A20

Transfection of SK-N-AS cells with ppA20-EGFP-A20 showed a portion of the A20 localised in perinuclear compartments. To understand this phenomenon SK-N-AS cells were imaged using a higher magnification. Cells were transiently transfected with CMV-RelA-dsRedXP and ppA20-EGFP-A20 24 hours prior to imaging. The microscope was focused near the cell membrane. A single image of both RelA and A20 was taken. Then a series of 250 images of the EGFP channel were taken over 5 minutes to follow the short-term dynamics of the speckles. The cells were imaged without stimulation and  $\sim$ 1-hour after stimulation with 10ng/ml TNF $\alpha$  and the speckling phenomenon was present in both stimulated and unstimulated cells. Figure 5.13 shows three example cells after treatment with TNF $\alpha$ , the green channel has been filtered to reduce the background fluorescence. The third column in figure 5.13 shows a stack of the time series; all but the highest intensity fluorescence has been removed, this was done to elucidate any movement of the speckles.

From these images, there appears to be a clear perinuclear localisation of the speckles. This is in accordance with data in the literature that shows co-localisation of A20 with lysosome compartments in HeLa cells (Li *et al.*, 2008). The speckling was present in both stimulated and unstimulated cells, implying that it could be a mechanism to sequester, and degrade or recycle excess A20. Concatenation of the images into a time stack and filtering for only high intensity fluoresces showed the speckles to be relatively stable over the 5-minute time period. This can be seen from predominantly complete lines across the time stack (figure 5.13, third column). There are also some broken traces in the time stack that could be representative of movement or loss of the speckles. This is consistent of the hypothesis that A20 in the lysosome is being recycled, degraded or excreted. It should be noted that there is a degree of overlap between the traces and there will also be blurring due to movement of the cell over the time course, which makes it difficult to infer too much from these data without further analysis.

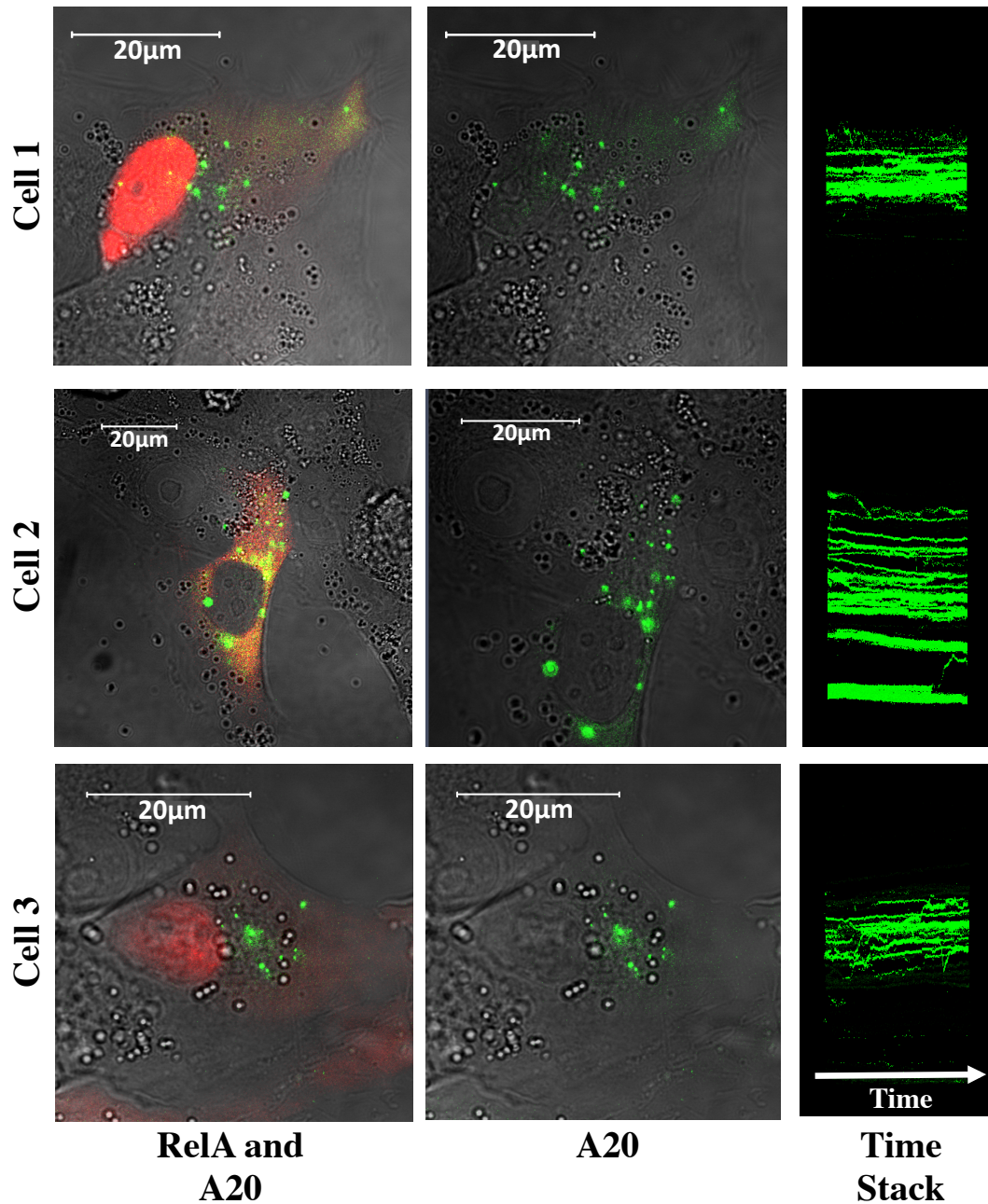


**Figure 5.13** - Analysis of A20 perinuclear speckles for 3 SK-N-AS cells transiently transfected with CMV-RelA-dsRedXP and ppA20-EGFP-A20 and stimulated with 10ng/ml  $\text{TNF}\alpha$ . Images taken ~1-hour post-stimulation. The first column is a composite image of the bright field, RelA and A20 channels; the second column shows the bright field and A20 channels. A series of 250 images of the A20 channel were taken over 5 minutes and the third column shows a time-stack of the A20 speckles. The green channel has been filtered to remove low intensity values to aid detection of the speckles.

CellTracker was used to further elucidate any possible dynamic behaviour in these speckles. A subset of the speckles in each cell were identified with a ROI, the centroid of this ROI could then be followed to track the movement of the speckles. The data in figure 5.14 shows some representative results of this analysis for both unstimulated cells and cells stimulated with 10ng/ml TNF $\alpha$ , the time intervals have been chosen to highlight interesting examples. In all cells, it is possible to identify speckles that appear stable over the time course; they are present for the entire observation period in the same location. The analysis also identified a number of speckles, which after a stationary period move very rapidly around the cell (figure 5.14a,c and d). This rapid motion often happens prior to the disappearance of the speckle (figure 5.14c, dark blue trace). Figure 5.14b demonstrates that during the observation period speckles were observed to disappear (dark blue trace) and appear (grey trace). The presence of these dynamics in both stimulated and unstimulated cells implies that this is most likely a regulatory mechanism associated with A20. The disappearance of speckles supports the hypothesis that the sequestered A20 is being excreted, degraded or recycled. Three phases of movement were consistently seen in this analysis, a stationary phase followed by rapid movement and then disappearance of the speckle. These three phases of movement are consistent with a hypothesis that these A20-containing vesicles are in the exocytotic pathway.

This hypothesis is further strengthened by figure 5.15, a series of images from a cell that demonstrated a clear excretion of A20 over the course of the experiment. These images are from a single location in an experiment where cells were transiently transfected with CMV-RelA-dsRedXP and ppA20-EGFP-A20, and stimulated with 10ng/ml TNF $\alpha$ . The A20 channel (green) shows the formation of speckles of A20 over the course of the experiment. During the experiment the speckles become stuck, while the cell moves away demonstrating that during the time course the A20 has been actively, or passively, excreted from the cell.

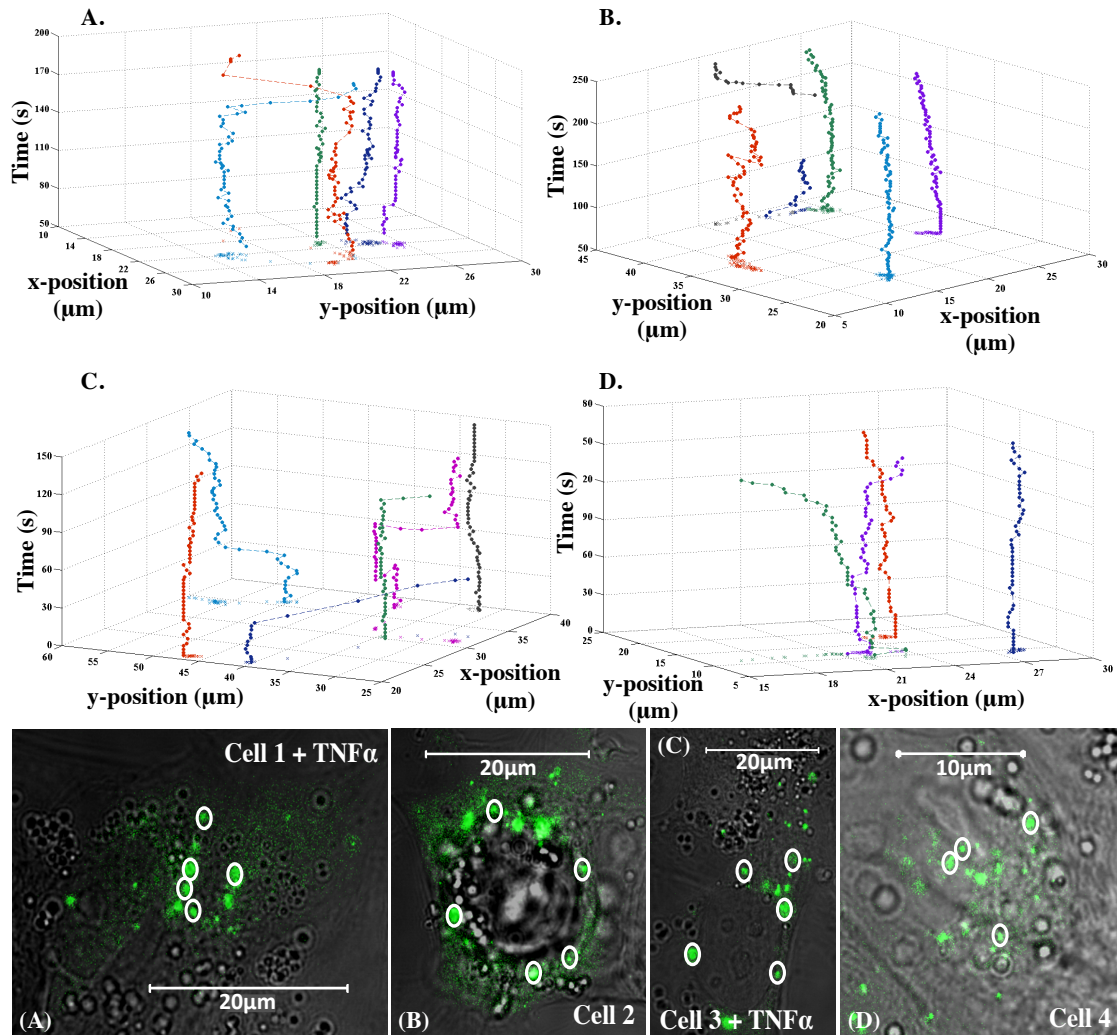


**Figure 5.14** - Dynamics of A20 speckles in SK-N-AS transiently transfected with ppA20-EGFP-A20 and CMV-RelA-dsRedXP. (A) and (C) were imaged after 1h stimulation with  $10\text{ ng/ml TNF}\alpha$ , (B) and (D) are unstimulated. CellTracker was used to follow the movement of the speckles, each point represents the measured location of a speckle. A project into the (x,y)-plane is also shown to demonstrate the distance moved. The distance is measure from the bottom-left corner of the image. Images underneath highlight the speckles analysed, for (B) one speckle was not present at the start of the analysis. (A) represents cell 1 and (B) represents cell 2 from figure 5.13.

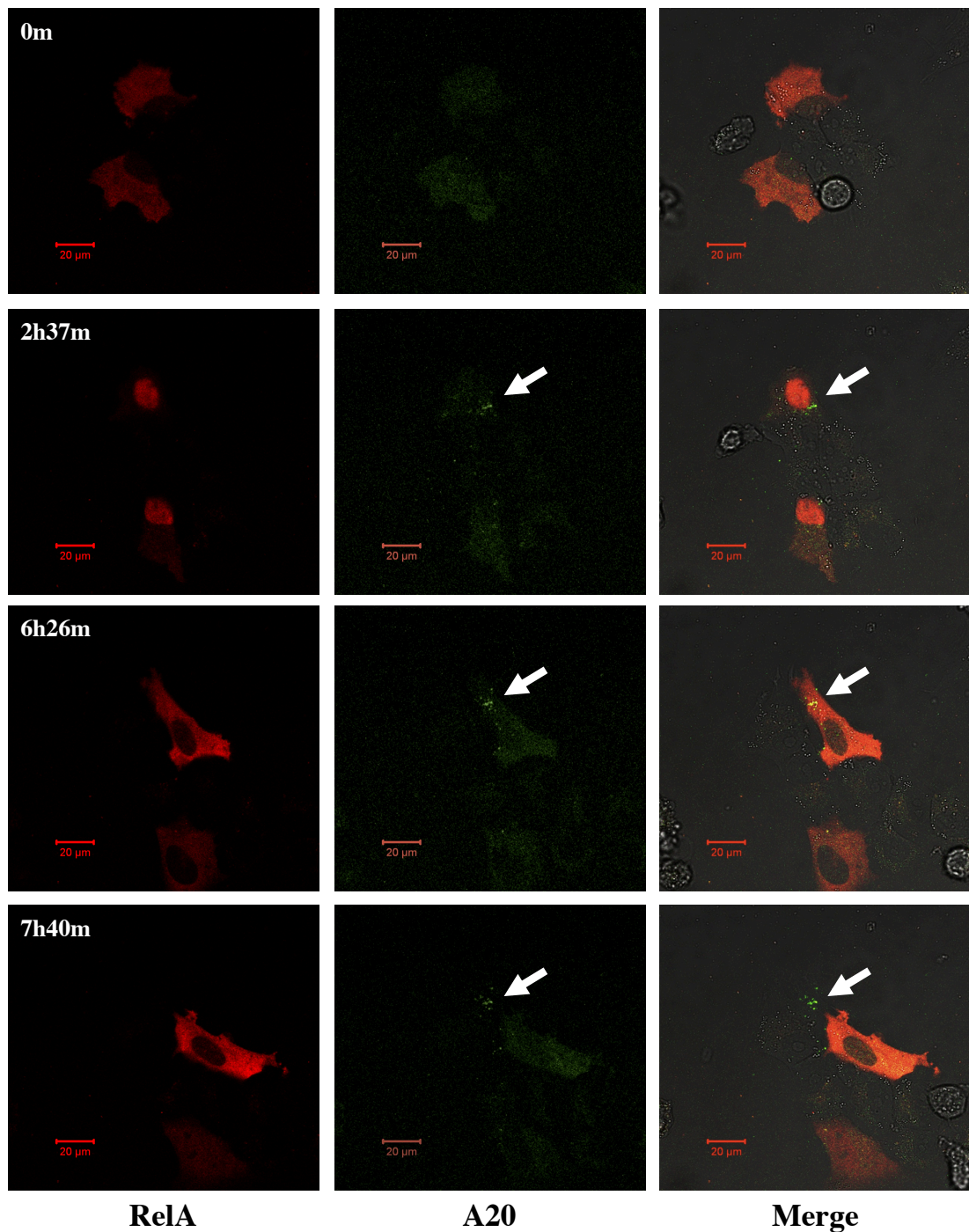


**Figure 5.15** - Excretion of A20 speckles. SK-N-AS cells transiently transfected with CMV-RelA-dsRedXP and ppA20-EGFP-A20 and stimulated with 10ng/ml  $\text{TNF}\alpha$ . Images have been taken from a single location and time is measure from  $\text{TNF}\alpha$  stimulation. The white arrows highlight A20 that has been formed and excreted over the course of the experiment. The red scale bar represents a distance of 20 $\mu\text{m}$ .

## 5.3 – Discussion

### 5.3.1 – Implications of A20 Expression Data on Future Modelling

The Ashall model made several predictions about the effect of A20 over-expression on the NF- $\kappa$ B system. Chiefly, the model predicted that increased transcription of A20 would cause a longer limit cycle period. Bifurcation analysis with respect to A20 transcription rate, and with respect to both A20 transcription and NF- $\kappa$ B level implied that an increase in the rates would result in a longer limit cycle period (figure 5.11 and figure 5.12). The experimental data presented here has served to validate these predictions showing an increase in the period resulting from over-expression of A20 through transient transfection (figure 5.10). These data also identified a portion of A20 to localise in perinuclear compartments; this sequestration is not currently represented in the Ashall model (figure 5.13).

The half-life of A20 in HeLa cells has been measure to be approximately 8 hours through immunoblotting (Werner *et al.*, 2008). In the Ashall model this is significantly higher at ~5 minutes. The parameter is considered representative of the activity of A20, rather than its protein concentration. The A20 feedback loop in this model is further believed to represent other negative feedback inhibitors such as Cylindromatosis and Cezanne (Ashall *et al.*, 2009). The A20 sequestration phenomenon provides an avenue to parameterise the model with a more realistic protein half-life. If it is assumed that sequestered A20 is unable to inhibit TNF $\alpha$  mediated NF- $\kappa$ B signalling, then the parameter  $c4$  actually becomes a sum of two parameters, protein degradation and sequestering. This can be represented as follows,

$$c4 = c4s + c4d , \quad (5.1)$$

where  $c4d$  is the A20 degradation rate and  $c4s$  is the rate of sequestration. If the relationship (5.1) is assumed then the model can be parameterised with the correct A20 degradation rate without altering the dynamics. This results in the inclusion of a second species of A20 representing the sequestered protein in speckles, which is assumed to no longer affect the system. The caveat is that the parameter  $c4s$ , representing sequestering of A20, is unconstrained and possibly physiologically unrealistic. As this parameter now represents A20 activity and other inhibitors of the

TNF $\alpha$  mediated NF- $\kappa$ B signalling. Unfortunately, it is not possible to estimate the parameter  $c_4$ s from the preliminary A20 expression data as the intensity of the speckles are saturated and therefore the amount of sequestered A20 relative to cytoplasmic A20 cannot be calculated.

A second hypothesis resulting from the literature is that A20 can also inhibit TNF $\alpha$  induced NF- $\kappa$ B activity by targeting TRAF2 to the lysosome (Li *et al.*, 2009). This can be incorporated into the model by including a term that inhibits IKK activation or increases IKK inactivation as a function of A20 concentration. This choice depends on whether A20 is assumed to only target activated TRAF2. Both of these actions have an equivalent role in the model as the parameters related to IKK activation ( $k_a$ ) and IKK inactivation ( $k_i$ ) have opposite control coefficients. From the control coefficients (figure 4.1, Chapter 4) it can be seen that both of these actions would elongate the period, consistent with the A20 expression data. However, both are relatively small control coefficients and therefore will not exert a large effect on the limit cycle. It would also be possible to include a nonlinear term to represent the sequestering of A20. However, considering the model currently fits the data and the mechanism is not fully classified, further development does not seem warranted.

### **5.3.2 – General Discussion**

The work in this chapter has combined computational analysis with novel imaging data to better understand the effect of I $\kappa$ B $\alpha$  and A20 negative feedback on NF- $\kappa$ B dynamics. The application of 2-dimensional bifurcation analysis has been heavily exploited to provide an avenue to understand how co-varying two parameters can influence the system. Simultaneous variation of parameters has shown that is possible to achieve a richer range in the dynamics properties of the system than with only one parameter (figure 5.1 vs. figure 5.2a). These changes can have an effect greater than the sum of the individual parameter effects, implying a possible avenue to ‘tune’ NF- $\kappa$ B dynamics.

When performing an analysis of this kind an important consideration is the range of parameter values studied, while it is possible to achieve substantial changes to the limit cycle this often requires parameter values outside experimentally measured



bounds. In the case of I $\kappa$ B $\alpha$  and A20 transcription, limitation of the parameter variation to a physiologically realistic range (5-fold) showed that it was only possible to achieve a period change of approximately 20 minutes (figure 5.2b). This is similar to the variation seen in experimental data (Ashall *et al.*, 2009, Nelson *et al.*, 2004). The next step to support the *in silico* analysis performed in this chapter would be experimental measurement of the NF- $\kappa$ B dynamics after perturbing both negative feedback loops. One possible way to achieve this would be to transfect the stable SK-N-AS cells containing the I $\kappa$ B $\alpha$ -EGFP BAC with the proximal promoter A20 construct. The computational analysis (figure 5.2) predicts that this will increase the period of oscillations. However, at this time both constructs use the same colour fluorescence reporter so this experiment cannot be performed.

To understand the effect of co-transfection with I $\kappa$ B $\alpha$  and NF- $\kappa$ B reporters, 2-dimensional bifurcation analysis was performed for the parameters related to NF- $\kappa$ B level and I $\kappa$ B $\alpha$  transcription. This analysis shows that increasing both I $\kappa$ B $\alpha$  and NF- $\kappa$ B levels maintained the 100-minute period (figure 5.3). Use of the dual transfected BAC cell line also demonstrated a period robust to 3- to 4-fold over-expression, consistent with the model predictions (figure 5.3 and figure 5.4b). One consideration of this analysis is that the Ashall model is fitted to transient transfection data and therefore could already be parameterised to account for a high level of NF- $\kappa$ B and I $\kappa$ B $\alpha$  expression.

Different computational models of the NF- $\kappa$ B system predict different relationships between the period and I $\kappa$ B $\alpha$  transcription rate. The model of Hoffmann *et al.* (2002) predicts that an increase in I $\kappa$ B $\alpha$  transcription will increase the period of NF- $\kappa$ B oscillations, contrary to the prediction of the Ashall model. Preliminary data showed RelA-dsRedXP oscillations with an extended period in HeLa cells co-transfected with I $\kappa$ B $\alpha$ -EGFP driven by a promoter consisting of 5  $\kappa$ B binding sites (Nelson *et al.*, 2004). However, the artificial nature of this promoter could result in an altered level of I $\kappa$ B $\alpha$  expression. To understand the effect of I $\kappa$ B $\alpha$  transcription rate in a physiologically relevant context the NF- $\kappa$ B dynamics was measured using a BAC construct. Clonal cell lines with 2.5- to 9-fold increased expression of I $\kappa$ B $\alpha$  all

showed a 100-minute period (figure 5.4). This suggests that the period is robust to differences in the level of I $\kappa$ B $\alpha$  expression (figure 5.4), in contrast to previous observations (Nelson *et al.*, 2004). As the BACs are much larger than plasmids the reported gene is insulated against site integration effects, which can result in a higher degree of correlation between expression level and copy number (Bian and Belmont, 2010). Therefore, in this context it is more appropriate to assume that different expression levels results from a different number of transgene copies.

Computational analysis of the Ashall model demonstrated that it is possible to find a parameterisation that can simulate NF- $\kappa$ B dynamics and which is robust to a 10-fold increase in the rate of I $\kappa$ B $\alpha$  transcription (figure 5.8). It is unrealistic that this robust property is the result of a single parameter change as implied herein. This analysis was to demonstrate that the Ashall model structure is able to capture the robustness seen in the data, but it is not sufficient to make a prediction about the underlying mechanism. The re-parameterisation did not alter the representation of I $\kappa$ B $\alpha$  transcription yet all three I $\kappa$ B $\alpha$  reporter constructs differ primarily in their transcriptional control, suggesting that the transcription regulation is central to the robust phenotype. This is supported by studies that have highlighted the importance of modelling transcriptional regulation, in the form of a delay, on the oscillatory dynamics (Kerszberg, 2004, Nguyen, 2012). Chapter 6, Section 6.3.2.7 will show the inclusion of a delay in transcription can change the sensitivity structure of a model.

There was very different relationship between A20 and NF- $\kappa$ B level in comparison to I $\kappa$ B $\alpha$  and NF- $\kappa$ B level (figure 5.3 vs. figure 5.12), in the case of A20 and NF- $\kappa$ B increasing the level of both species increased the period. There is a direct inhibition of NF- $\kappa$ B by I $\kappa$ B $\alpha$ , while the A20 feedback loop inhibits NF- $\kappa$ B by acting further upstream in the pathway. The different architecture of the negative feedback loops could cause the markedly different NF- $\kappa$ B dynamics seen in simulation and experiment. This suggests an interesting point regarding the inclusion of multiple feedback loops in oscillatory systems. Moreover, it provides an obvious avenue to pursue when endeavouring to manipulate the dynamics of the system. Studies of models with nested negative feedback structures have shown that in the presence of strong inner loop varying the outer loop significantly changed the period (Nguyen,

2012). These insights can be applied to the NF- $\kappa$ B system, where I $\kappa$ B $\alpha$  and A20 represent the inner and outer loops, respectively. One possible hypothesis for the existence of this topology could be formed as follows. The direct interaction in the NF- $\kappa$ B-I $\kappa$ Bs feedback loop forms the core network and therefore it would be advantageous for the system to be robust to variation. This solid basis would then allow the evolution of additional feedbacks to modulate the NF- $\kappa$ B in response to different conditions or stimuli. The concept of evolution of a system from a core network has been proposed in the literature (Kirschner and Gerhart, 1998).

Through transient transfection of an A20 reporter driven by a proximal promoter this chapter has successfully validated the prediction made by the Ashall model regarding increased A20 transcription. However, this data is in the preliminary stages and a greater number of cells need to be analysed and the expression levels assessed. These data have been compared to previous single-cell NF- $\kappa$ B dynamics (Ashall *et al.*, 2009, Nelson *et al.*, 2004) but for completeness a current control data set should be established. An analysis of the level of A20 expression over time would also be beneficial for further model development. Preliminary analysis suggests that average EGFP level is stable within the cytoplasm, promoting the hypothesis that there exists a stable steady state between synthesis, degradation and sequestration. These data were not appropriate for a rigorous analysis of EGFP levels due to low levels of expression and changes in the focal plane. Quantification of the EGFP fluorescence over the short time-course experiments (figure 5.13), showed a decrease in the level of A20 over the 5-minute period. However, this behaviour was highly consistent between all cells and occurred over a very short time period therefore, it is possible that this result is due to photo bleaching.

The ppA20-EGFP-A20 construct contains only a short segment of the A20 promoter (~250kb), which includes two NF- $\kappa$ B binding sites. The promoter elements identified as primarily controlling A20 expression are the two  $\kappa$ B sites in association with 6xSp-1 binding sites and an ELIE (elongation inhibitory element) (Verstrepen *et al.*, 2010). Sp-1 is required for efficient initiation of transcription and in basal conditions re-initiations are repressed by the E-box protein USF1 bound at the ELIE site. Stimulation causes binding of NF- $\kappa$ B to the promoter, which displaces USF1

and allows for multiple rounds of transcription (Amir-Zilberstein and Dikstein, 2008). All these elements are present in the proximal A20 promoter segment, which suggests this is an appropriate reporter for inducible A20 activity. However, it should be noted that the full endogenous promoter could contain distal regulatory regions that modulate A20 transcription.

These data highlighted the localisation of a proportion of A20 in perinuclear speckles, consistent with studies that show A20 to co-localise with lysosomes in HeLa cells (Li *et al.*, 2008). Li *et al.* used biological fractionation and immunoblotting experiments to show there is a membrane associated A20 component present under basal conditions, which increased after stimulation. They further showed co-localisation of fluorescently tagged A20 with a lysosome marker to build their hypothesis. This study complements the data presented herein, showing perinuclear localisation of A20 speckles before and after TNF $\alpha$  stimulation (figure 5.13 and figure 5.14). To confirm this in SK-N-AS cells similar co-localisation experiments need to be performed using the A20 construct and a fluorescent probe to label the lysosome. The data presented in this chapter also demonstrated movement and disappearance of the speckles (figure 5.14) and in some cases excretion of A20 (figure 5.15), an interesting future direction would be to determine the fate of these speckles. Sequestration could be a mechanism to isolate and degrade excess A20, as such the prevalence of this phenomenon these data might be increased due to high A20 expression in comparison to physiological levels. However, this behaviour has also been shown to have functional implications by targeting TRAF2 to the lysosome, thereby inhibiting TNF $\alpha$ -NF- $\kappa$ B signalling (Li *et al.*, 2009). The functional implications in conjunction with the confirmation of this phenomenon using endogenous A20 suggests that this mechanism plays a role in mediating TNF $\alpha$  induced NF- $\kappa$ B dynamics.

The Ashall model predicts A20 to have a key role in influencing NF- $\kappa$ B dynamics. In addition, other NF- $\kappa$ B models (Mengel *et al.*, 2012) have predicted this relationship. These data motivate several future experiments to help inform model development. One key experiment is to understand the impact of a reduction in A20 transcription rate on the NF- $\kappa$ B oscillation period. A means to accomplish this is

with the use A20 siRNA to knockdown mRNA levels. If this were shown to reduce the period it would be further validation of the relationship demonstrated by figure 5.1. Other experiments that could be used to confirm possible A20 mechanism include characterising the interactions between A20, TRAF2 and the IKK complex. These data would help to elucidate the role of A20 in the NF- $\kappa$ B system and refine computational models.

**Chapter 6 –  
Pharmacological and  
Temperature Perturbations to  
the NF- $\kappa$ B System**

## 6.1 – Introduction

This chapter combines the theoretical analysis of the Ashall model performed in chapters three and four with novel experimental data that show a change in the NF- $\kappa$ B translocation frequency. These changes can result from treatment with a chemical inhibitor or alteration of the temperature of the system. Due to the disparate nature of the perturbations used, this chapter has been subdivided into two sections that each focus on the analysis of an individual data set. Section 6.2 looks at the effect of a pharmacological perturbation to the system resulting from treatment with the compound diclofenac. Section 6.3 investigates the effect of temperature changes on NF- $\kappa$ B dynamics.

## 6.2 – Pharmacological Modulation of the NF- $\kappa$ B System

### 6.2.1 – Pharmacological Introduction

Due to the central role of NF- $\kappa$ B in inflammation and immunity, and its deregulation in many autoimmune diseases and cancers there has been significant investment in exploiting the NF- $\kappa$ B system as a therapeutic target. This has resulted in the identification of numerous chemical inhibitors of its activity. For example, proteasome inhibitors reduce the degradation of the I $\kappa$ Bs resulting in inhibition of NF- $\kappa$ B activity (Rajkumar *et al.*, 2005). The proteasome inhibitor bortezomib, which is now part of chemotherapy treatments for multiple myeloma, has been shown to inhibit NF- $\kappa$ B activity in head and neck squamous cell carcinoma (HNSCC) cells (Sung *et al.*, 2008, Sunwoo *et al.*, 2001). The chemical Bay11-7082 irreversibly inhibits TNF $\alpha$  induced phosphorylation of I $\kappa$ B $\alpha$  (Pierce *et al.*, 1997), thereby preventing the subsequent I $\kappa$ B $\alpha$  degradation and RelA nuclear translocation (Nelson *et al.*, 2002). In SK-N-AS cells high concentrations of these compounds result in the complete suppression of the NF- $\kappa$ B responses (Dr C. Heyward, CCI, unpublished data) and therefore are not useful perturbations to study with respect to their clinical significance. However, other chemicals have a more subtle effect and so facilitate a more involved study. Notably, the cell-permeable peptide SN50 contains the NLS of

NF- $\kappa$ B and therefore competitively inhibits nuclear translocations (Lin *et al.*, 1995). SN50 has been shown to reduce the amplitude of the first NF- $\kappa$ B nuclear translocation without completely aborting the movement (Nelson *et al.*, 2002). Other chemicals have also been shown to alter the period: the compound cryptolepine that intercalates DNA, the p-glycoprotein inhibitor PSC833 and the anti-inflammatory diclofenac (Dr C. Heyward, CCI, unpublished data).

Diclofenac, a non-steroidal anti-inflammatory drug (NSAID), is widely administered to treat pain and rheumatoid arthritis. While the exact mechanism of action is not fully understood its primary action is classically believed to be through inhibition of cyclooxygenase (COX) activity and subsequently prostaglandin biosynthesis (Vane and Botting, 1996). Other mechanisms have also been demonstrated, for example, it inhibits bacterial DNA synthesis suggesting a possible anti-bacterial action (Dastidar *et al.*, 2000). More recently, diclofenac has been shown to affect NF- $\kappa$ B activity in hepatic cells (Fredriksson *et al.*, 2011). Treatment of the human HepG2 cells with diclofenac shows a dose dependent inhibition of TNF $\alpha$ -stimulated NF- $\kappa$ B activity using a luciferase reporter assay and imaging of the HepG2 cells showed an extended time between the first and second nuclear translocation of NF- $\kappa$ B in a population of cells treated with diclofenac. Complementary, Western blot analysis shows a change in the rate of degradation of I $\kappa$ B $\alpha$  and reduction in I $\kappa$ B $\alpha$  phosphorylation at high concentrations of the compound. These data could suggest a novel role for the compound in modulating inflammatory signalling through the NF- $\kappa$ B pathway and motivates a more in-depth analysis of the effect of diclofenac on NF- $\kappa$ B dynamics in single cells.



## 6.2.2 – Pharmacological Results

### 6.2.2.1 - Characterisation of RelA Oscillations After Treatment with Diclofenac

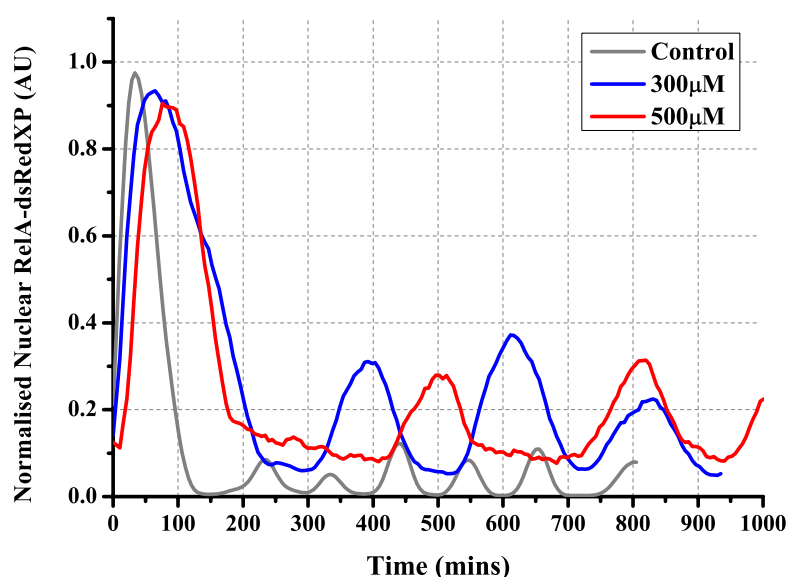


**Figure 6.1** – Representative traces for three SK-N-AS cells treated with different doses of diclofenac 0µM (grey), 300µM (blue) and 500µM (red). Cells were analysed using small circle tracking on a nuclear region of interest (ROI), mean intensity for the ROI was then normalised to the maximum value over the time-course. Data has been smoothed using a moving average of 5 data points.

SK-N-AS cells were transiently transfected with the CMV driven RelA-dsRedXP reporter plasmid. After 24-48 hours of transfection, cells were treated with different doses of diclofenac (300µM or 500µM) for 90 minutes and then imaged using fluorescence confocal microscopy. Cells were stimulated with 10ng/ml TNF $\alpha$  and those visibly expressing RelA imaged approximately every 5 minutes for up to 17 hours. Images of cells showing RelA nuclear-cytoplasmic oscillations were analysed using CellTracker to measure average fluorescence in a nuclear region of interest (ROI). These data were subsequently analysed to determine the period of RelA oscillations. Figure 6.1 shows a representative time-course from each of the experimental conditions, demonstrating an extended period when cells have been

treated with diclofenac. The data has been smoothed using a moving average of 5 data points along the time-course to facilitate detection of peaks. *Imaging data collected and analysed by Dr C. Heyward, CCI, University of Liverpool.*

Figure 6.2a shows the distribution of peak-to-peak timings, the time between peaks in the nuclear intensity of RelA, for each of the diclofenac doses used. The time from the first to second peak has been excluded from this analysis as it generally extended and highly variable (Horton, 2006). The average peak-to-peak time without diclofenac was  $110 \pm 30$  mins ( $n=25$ ), treatment with diclofenac  $300 \mu\text{M}$  and  $500 \mu\text{M}$  diclofenac increased this to  $182 \pm 36$  mins ( $n=25$ ) and  $210 \pm 67$  mins ( $n=15$ ) respectively (figure 6.2b). Figure 6.2a suggests the control and  $300 \mu\text{M}$  data could be from a normal distribution, however, for the  $500 \mu\text{M}$  condition this is less clear, goodness-of-fit tests did not clearly demonstrate the peak-to-peak data to be normally distributed; this is most likely due to a small sample size. Therefore, the non-parametric Mann-Whitney U test was used to compare each of the experimental conditions. The mean peak-to-peak timing for treatment with both  $300 \mu\text{M}$  and  $500 \mu\text{M}$  of diclofenac were significantly longer than that of the control ( $U=286$ ,  $Z=-8.24$ ,  $p<0.0001$  and  $U=75$ ,  $Z=-5.89$ ,  $p<0.0001$  respectively). The difference between the  $300 \mu\text{M}$  and  $500 \mu\text{M}$  doses was less marked, but still significantly different ( $U=438$ ,  $Z=-2.07$ ,  $p=0.03817$ ). There was also a significant difference in the time to the first peak between the control and  $300 \mu\text{M}$  condition ( $U=1$ ,  $Z=-6.57$ ,  $p<0.0001$ ). These data strongly indicated that treatment with diclofenac increased the period of RelA oscillations and imply it happens in a dose dependent manner, to confirm dose dependence a larger sample size is required. There are fewer cells analysed for the  $500 \mu\text{M}$  condition, which contributes to the lack of clarity in the data, this is partially due to increased cytotoxicity at higher doses of the compound.

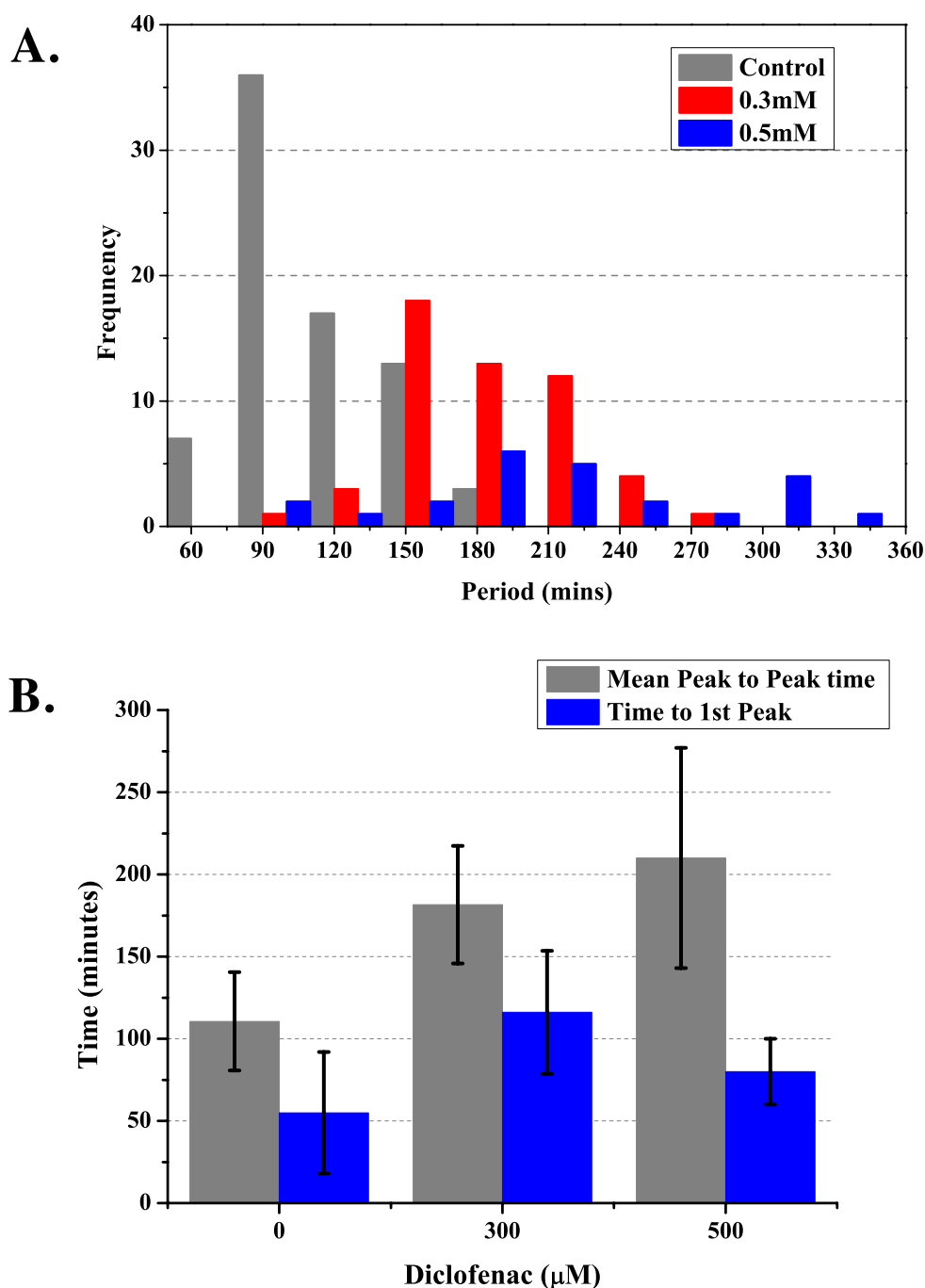


**Figure 6.2** – Summary of periodicity data for SK-N-AS cells transiently transfected with RelA-dsRedXP, treated with different concentrations of diclofenac for 90 minutes and then stimulated with TNF $\alpha$  (10ng/ml). Concentrations of diclofenac used were: 0 $\mu$ M (25 cells), 300 $\mu$ M (25 cells) and 500 $\mu$ M (15 cells). (A) Distributions of peak-to-peak timings for all cells for all peaks from peak 2 onwards. (B) Mean peak-to-peak timing from peak 2 onwards for all cells and the mean time to the first peak, error bars represent the standard deviation.

### **6.2.2.2 – The Effect of Diclofenac Treatment on the Degradation and Phosphorylation of I $\kappa$ B $\alpha$**

To further understand the effect of diclofenac on the system, western blot analysis was performed to assay the I $\kappa$ B $\alpha$  phosphorylation and degradation rate in SK-N-AS cells (figure 6.3). Cells were treated with appropriate dose of diclofenac for 90 minutes and subsequently stimulated with 10ng/ml TNF $\alpha$  for the durations shown. Following TNF $\alpha$  stimulation the cells were lysed and analysed by immunoblot, probing with the I $\kappa$ B $\alpha$  and phospho-I $\kappa$ B $\alpha$  antibodies, figure 6.3a and figure 6.3b show representative blots for I $\kappa$ B $\alpha$  and phospho-I $\kappa$ B $\alpha$  respectively. Treatment with diclofenac resulted in a delayed degradation and resynthesis of I $\kappa$ B $\alpha$  (figure 6.3c); this is evidenced by the higher level of I $\kappa$ B $\alpha$  protein after 5 minutes of stimulation in cells treated with diclofenac. Moreover, resynthesis of I $\kappa$ B $\alpha$  can be seen after 30 minutes in the control condition but is delayed until 45 minutes when treated with diclofenac (figure 6.3c). The later time points in figure 6.3d also suggest that there is a reduction in the level of phosphorylated I $\kappa$ B $\alpha$  in cells treated with diclofenac (30-120 minutes, figure 6.3d). However, this is not apparent at the 5-minute time point where all conditions show a comparable level of phosphorylation. These data are in broad agreement with Fredriksson *et al.* (2011), which showed reduced I $\kappa$ B $\alpha$  phosphorylation at higher doses of diclofenac. From these data and those in the literature it is reasonable to hypothesis that treatment with diclofenac affects the phosphorylation and degradation of I $\kappa$ B $\alpha$  in SK-N-AS cells.

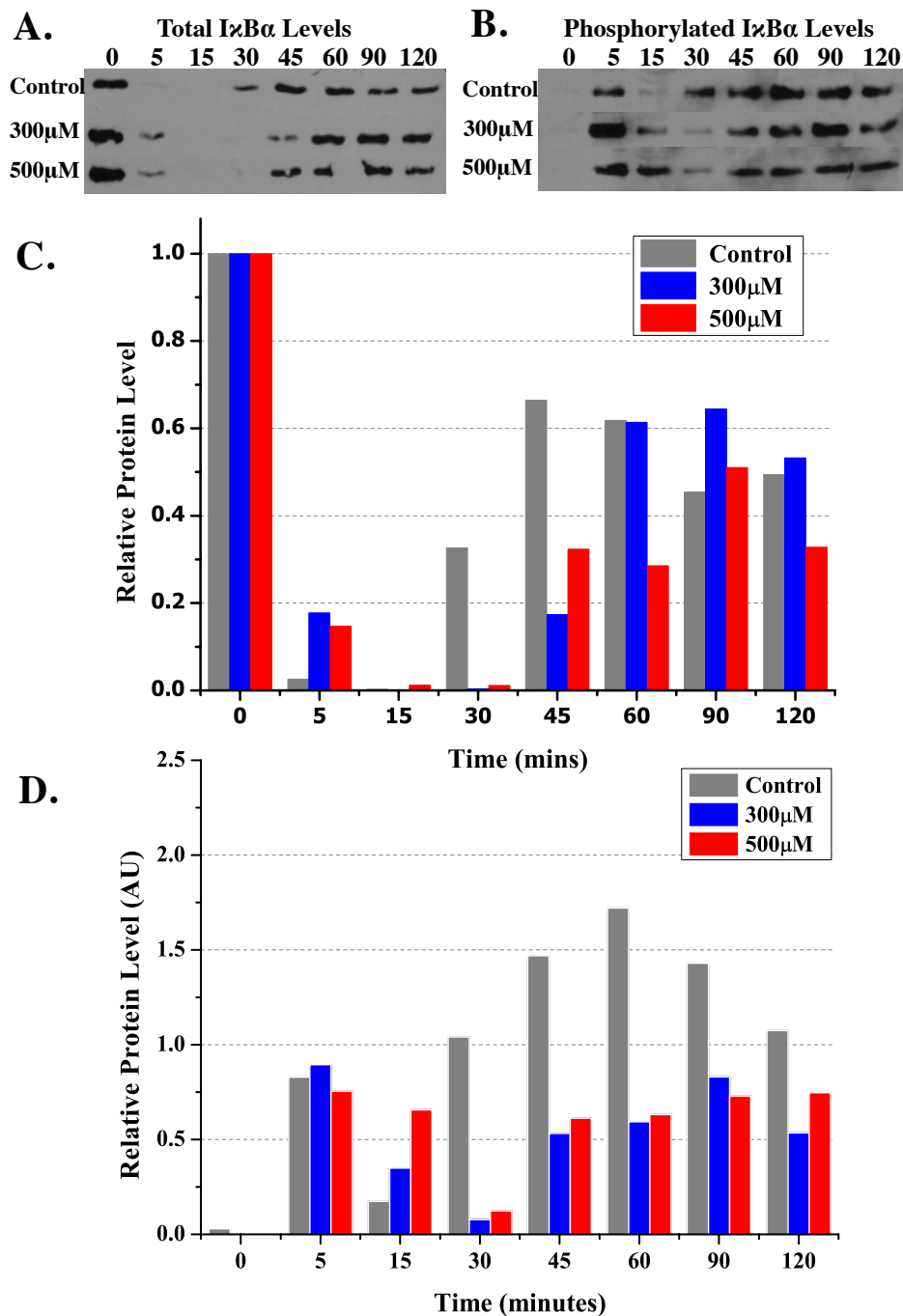


**Figure 6.3** – The phosphorylation status and degradation rate of I $\kappa$ B $\alpha$  was measured through western blot analysis in SK-N-AS cells. Cells were treated with the different doses of diclofenac shown for 90 minutes before adding 10ng/ml TNF $\alpha$ . Actin was used as a loading control (not shown), protein concentration in the lysate was assayed and 35 $\mu$ g loaded into each well. This figure shows representative blots from two independent repeats. (A & B) Example blots for I $\kappa$ B $\alpha$  and phosphorylated I $\kappa$ B $\alpha$ , (A) and (B) respectively. (C & D) Quantification of the I $\kappa$ B $\alpha$  and phospho-I $\kappa$ B $\alpha$  blots, (C) and (D) respectively. Fold changes in (C) represent the change in protein expression compared to 0 minutes TNF $\alpha$ . Fold changes in (D) represent the change in protein expression compared to a control well using the 5-minute TNF $\alpha$  time-point.

### 6.2.2.3 – Computational Analysis of the IKK Module

The data presented in section 6.2.2 demonstrates that in SK-N-AS cells treatment with diclofenac significantly extends the NF- $\kappa$ B oscillatory period. The change in I $\kappa$ B $\alpha$  phosphorylation and degradation seen in immunoblotting leads to the hypothesis that diclofenac is acting at or upstream of the IKK complex. Moreover, these data imply that the IKK activity is altered; this is evidenced by the change in I $\kappa$ B $\alpha$  phosphorylation, which is a result of IKK activity. These hypotheses are further supported by studies that have shown other NSAIDs to inhibit IKK activity, such as aspirin and sulindac, or to reduce I $\kappa$ B $\alpha$  phosphorylation, such as sulfasalazine (Krakauer, 2004).

Bifurcation analysis with respect to the IKK related parameters ( $k_a$ ,  $k_i$ ,  $k_p$  or  $k_{c2a}$ ) shows it is possible to achieve a maximum period increase of approximately 25 minutes by only changing one parameter (figure 4.4, Chapter 4), even less if the parameter change is restricted to a 3-fold range (figure 4.6, Chapter 4). This corresponds to a period increase of 25% at most, however, the experimental data demonstrated that treatment with 300 $\mu$ M diclofenac results in a period change of approximately 64% and larger changes are seen with higher doses of the compound (figure 6.2).

In Chapter 5 it was shown that by altering two-parameters it is possible to achieve greater changes in the limit cycle period. Therefore, 2-dimensional bifurcation analysis was performed for the parameters related to the IKK complex (figure 6.4). Figure 6.4a represents the analysis for the parameters identified to have the largest control coefficients, these were IKK complex recycling ( $k_p$ ) and IKK phosphorylation of I $\kappa$ B $\alpha$  ( $k_{c2a}$ ). By co-varying the parameters it was only possible to find a limit cycle period similar to that attained by altering just a single parameter ~25% (figure 6.4a, maximum of the heat map 124.75 minutes). Chapters 4 and 5 have also highlighted that the effect of multiple parameter changes can be non-additive. Therefore, other IKK related parameter combinations were analysed to determine if it was possible find a solution with a greater increase in the limit cycle period (figure 6.4). The combination of  $k_a$  (IKK activation) and  $k_{c2a}$  gave a similar

maximum period increase (figure 6.4c, maximum of the heat map 126.75). The combination  $k_a$  and  $k_p$  resulted in the greatest period change  $\sim 34\%$  (figure 6.4b) yet, this was still of a much smaller magnitude than the changes seen in the experimental data. This parameter combination also results in a substantial reduction in the amplitude and a solution that was not comparable to NF- $\kappa$ B dynamics.

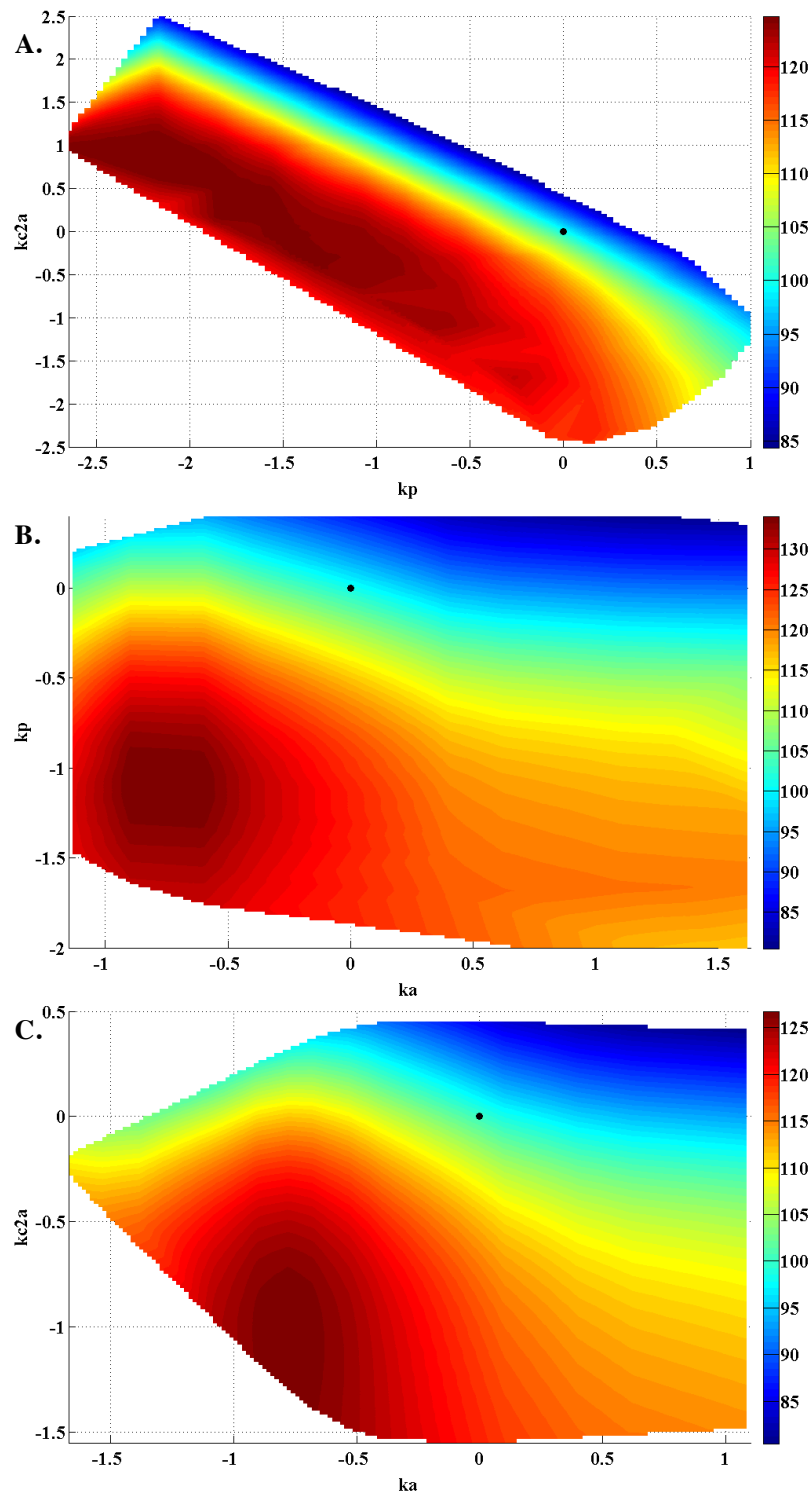


**Figure 6.4** - 2-dimensional bifurcation analysis of the IKK module. Parameters have been normalised to their nominal value and the logarithm taken, colour represents the period (mins) that corresponds to each parameter pair, the black dot represents the original parameter values. (A) Analysis for the parameters  $kp$  and  $kc2a$  (IKK recycling and IKK phosphorylation of  $I\kappa B\alpha$ ), (B) analysis for the parameter pair  $ka$  and  $kp$  (IKK activation and recycling), (C) analysis for the parameters  $ka$  and  $kc2a$ .



A series of parameter scans were performed using the IKK-related parameters to determine if it was possible to achieve the desired period change through re-parameterisation of the IKK module. The parameters chosen were I $\kappa$ B $\alpha$  phosphorylation parameter (kc2a), the three IKK parameters (ka, ki and kp), and the NF- $\kappa$ B nuclear import parameter (ke1) was also included. The parameter ke1 was included in this analysis as studies have shown that the IKK $\beta$  subunit can phosphorylate RelA at certain serine residues (Viatour *et al.*, 2005). Moreover, it has been suggested that nuclear translocation of NF- $\kappa$ B might be regulated by phosphorylation, as this is true for the NF- $\kappa$ B homolog in *Drosophila melanogaster* (Schmitz *et al.*, 2001) therefore, altered kinase activity of IKK might change the nuclear import of NF- $\kappa$ B. The scans were performed to cover a 2-, 5- and 10-fold range of the parameter space with an increasingly coarse step-size.

Initially, a scan of the parameter space defined by these five parameters over a 2-fold interval was performed. A mesh of 11 equally spaced points sampling 2-fold above and below each parameter value was used, these points define a lattice in the 5-dimensional hypercube related to these parameters which can be used to search parameter space. All permutations of these values were then simulated and the resulting solutions analysed to determine the period. Of these 161015 simulations only 1442 (0.9%) had periods over 120 minutes with the maximum being 130.22 minutes. This search was expanded to cover 5- and 10-fold ranges of the parameter values, in each case using a coarser mesh to save computational time. Using a 5-fold interval with 9 equally spaced points, one parameterisation gave a period change of 60 minutes. This parameterisation had a 5-fold reduction in I $\kappa$ B $\alpha$  phosphorylation (kc2a) and RelA nuclear import (ke1). The solution relating to this parameterisation was not ideal as there was a reduction in the amplitude of the limit cycle. The parameter range explored was further expanded, sampling at 2-, 4-, 6-, 8- and 10-fold above and below the original value. In this case 6626 parameterisations (4%) were found that gave model solutions greater than 160-minutes. Of these 5442 (82%) had reduced I $\kappa$ B $\alpha$  phosphorylation and all of them had reduced RelA nuclear import (figure 6.5), further supporting the reduced kinase activity hypothesis. This analysis suggests a large change in the parameter values is required to achieve the desired

period change. The IKK parameters  $k_a$ ,  $k_i$  and  $k_p$  are fitted and therefore such a large change could be considered reasonable but, the parameters  $k_{c2a}$  and  $k_{i1}$  were constrained and the change required to alter the period sufficiently moves these parameter values beyond the fitting constraints.

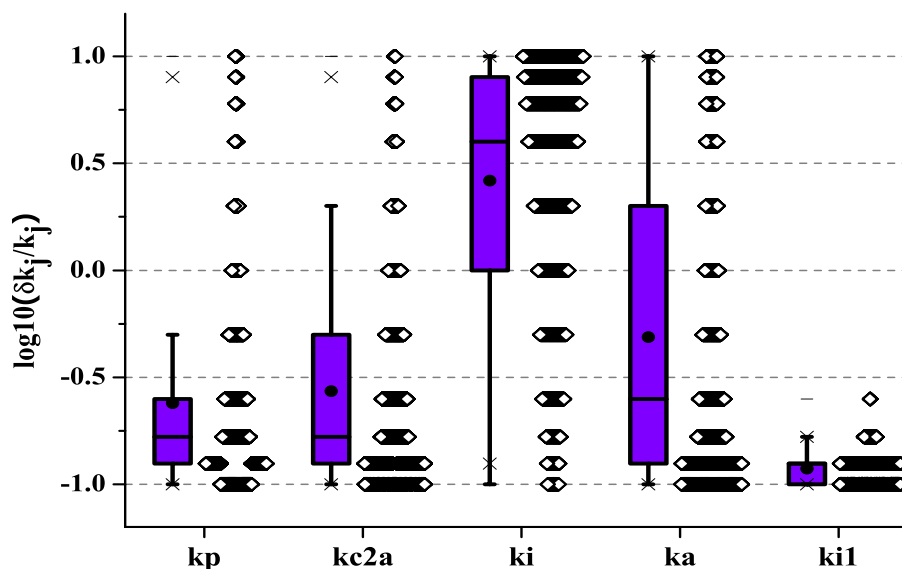


**Figure 6.5** - Analysis of the parameter values that resulted in solutions with a limit cycle period  $>160$  minutes. The parameters were altered 2-, 4-, 6-, 8- and 10-fold above and below the original value and all possible permutations of the parameters simulated. The distributions of the parameter values that gave periods  $>160$  minutes are shown. Boxes show the 2<sup>nd</sup> and 3<sup>rd</sup> quartiles, whiskers show 1<sup>st</sup> and 4<sup>th</sup>, crosses show outliers, black dots show the mean value and the line in the boxes shows the median.

#### 6.2.2.4 – Delayed Activation of IKK

The data regarding diclofenac treatment also implies an alternative hypothesis. The increased time to the first peak of NF- $\kappa$ B nuclear occupancy (figure 6.2b) could suggest a delay in the activation of the IKK complex (figure 6.3). This hypothesis is further evidenced by the western blot data that shows a delay in the degradation of  $I\kappa B\alpha$ , which could be a result of delayed phosphorylation by the IKK module (figure 6.3a). Phosphorylation of  $I\kappa B\alpha$  is the result of a cascade of signals from binding of TNF $\alpha$  to the extracellular domain of the TNF-R1 receptor, to phosphorylation by the IKK complex (Chen and Goeddel, 2002). TNF $\alpha$  mediated NF- $\kappa$ B activation is achieved through the binding of TNF $\alpha$  trimers to the extracellular domain of the

TNF-R1 receptor, which causes the recruitment of the TNF receptor associated death domain (TRADD). This causes the recruitment of other adaptor proteins, such as the receptor-interacting protein (RIP), TNF-R associated factor 2 (TRAF2) and the Fas-associated death domain (FADD) (Chen and Goeddel, 2002). RIP is central to IKK activation; recent studies have suggested this is due to polyubiquitination of TAK1 by RIP is causing IKK activation (Ea *et al.*, 2006). If diclofenac acts upstream of the IKK complex it is reasonable to assume that it can inhibit one of these steps, resulting in a delay in the formation of the active IKK complex.

To capture this hypothesis in the model, a delay was introduced in the activation of IKK, using a method of linear chains (Smith, 2011). For a system of  $n$  ODEs,

$$\frac{dx_i}{dt} = f_i(x_1, \dots, x_n), \quad (6.1)$$

where  $i = 1, \dots, n$ . To include a delay in the transition of the variable  $x_j$  a linear chain of  $p$  equations can be included using the following differential equations:

$$\dot{g}_1 = \theta(x_j - g_1) \quad (6.2)$$

$$\dot{g}_2 = \theta(g_1 - g_2) \quad (6.3)$$

$\vdots$

$$\dot{g}_p = \theta(g_{p-1} - g_p), \quad (6.4)$$

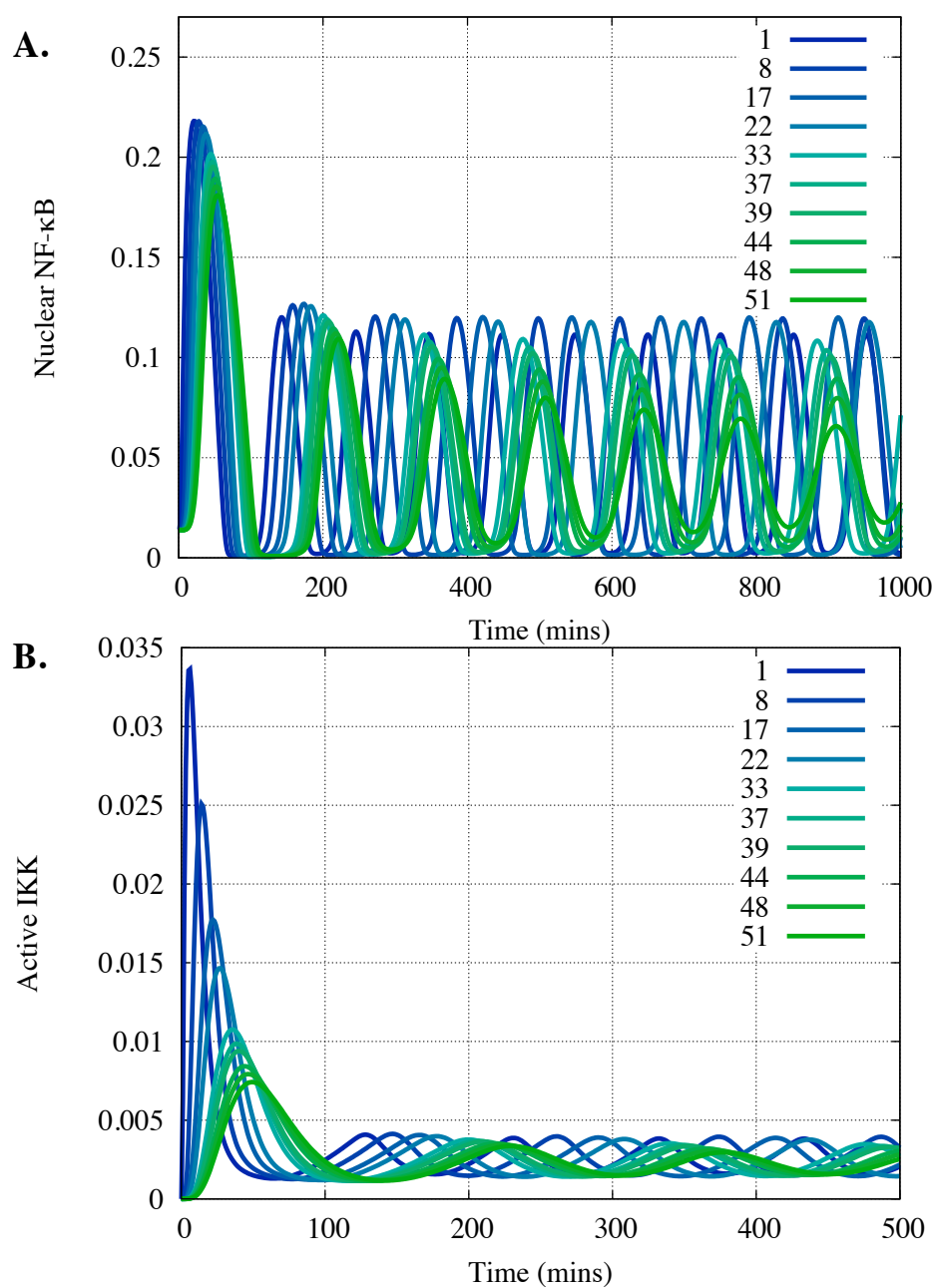
where  $\theta$  is a scalar parameter representing the probability of transition. Then (6.1) becomes a system of  $N + p$  equations as follows,

$$\frac{dx_i}{dt} = f_i(x_1, \dots, x_{j-1}, g_p, x_{j+1}, \dots, x_n), \text{ for } i = 1, \dots, j - 1, j + 1, \dots, n, \quad (6.5)$$

$$\frac{dx_j}{dt} = f_j(x_1, \dots, x_n), \quad (6.6)$$

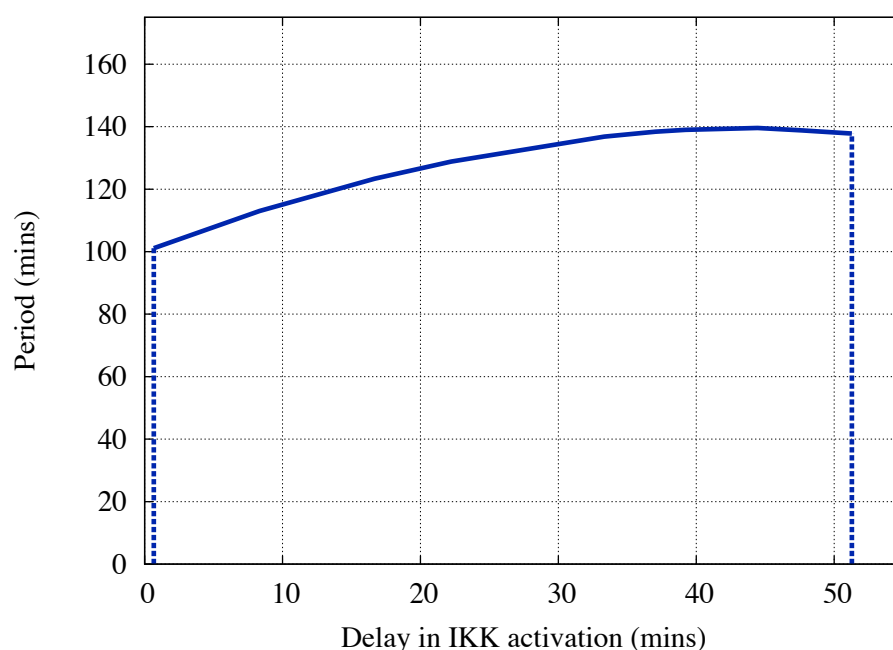
and the equations defined by  $\dot{g}_1, \dots, \dot{g}_p$ . This introduces a delay in the transition of  $x_j$  that is approximately equivalent to  $\theta/p$ .

In short, this method introduces several intermediary states between the neutral and active IKK species. A proportion of the neutral IKK species then moves to the active species, through the intermediaries with a certain probability defined by a delay parameter (Smith, 2011), thus delaying the time until the IKK species becomes active and able to phosphorylate I $\kappa$ B $\alpha$ . While this is predominantly a mathematical device to introduce a delay into a system of differential equations without the need to solve delay differential equations (DDEs), in this context it is also possible to ascribe some biological meaning to it. These intermediate states could be considered to correspond to the steps between receptor binding and IKK activation, such as the binding of TRADD, TRAF2, FADD and RIP.



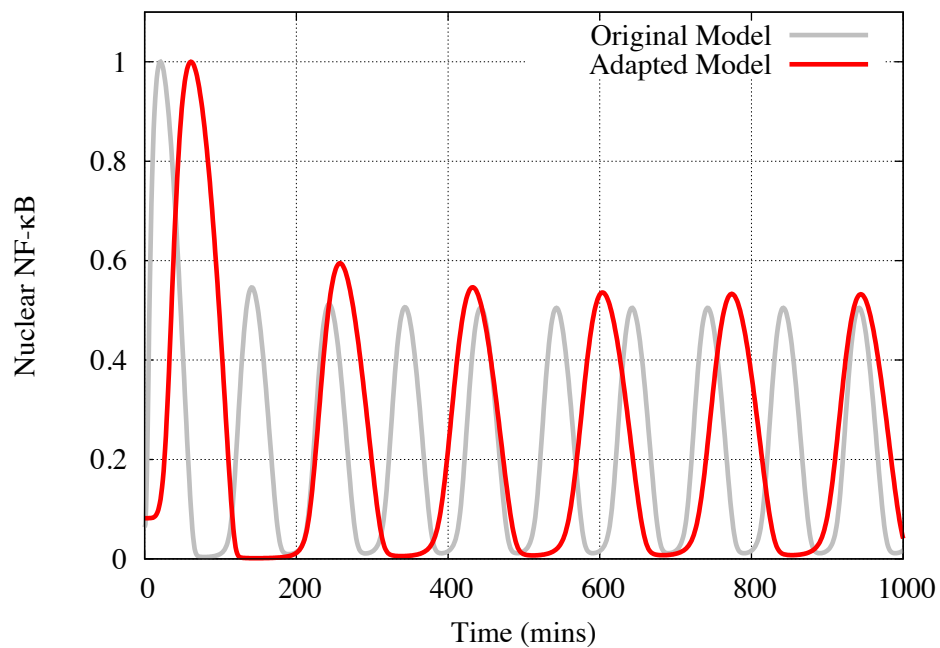
**Figure 6.6** – The effect of delayed IKK activation on the NF- $\kappa$ B system. (A) The nuclear NF- $\kappa$ B solution as the delay in IKK activation is increased. (B) The active IKK solution as the delay in IKK activation is increased. For both plots, the values in the legend correspond to the delay in time in minutes to reach maximal IKK activation in comparison to the original system.

Figure 6.6 demonstrates the effect on the model solutions for nuclear NF- $\kappa$ B and active IKK as the delay in IKK activation is increased, the legend represents the time to maximal IKK activity. Increasing the delay does cause a lengthening of the period while maintaining the qualitative nature of the solution. The relationship between period and delay does not appear monotonic and there is an “optimal” delay in the IKK activation to achieve the maximum period (figure 6.7), further increase of the delay (>50mins) caused a reduction in amplitude and loss of the limit cycle. By including a delay of 39 minutes to the maximal IKK activation, to represent treatment with diclofenac, it was possible to gain a ~40% change in the model period (figure 6.7). IkB $\alpha$  phosphorylation can be seen at 5 minutes in the western blot analysis, which suggests that this is greater than the physiological delay, should it exist. Quantification of the IKK kinase activity would be required to provide a more realistic parameterisation of the model.



**Figure 6.7** – Summary of the effect of altering the delay in IKK activation on the model period. Values on the x-axis correspond to the delay in reaching maximal IKK activation in comparison to the original system.

This approach was not sufficient to solely recapitulate the NF- $\kappa$ B dynamics seen in response to diclofenac treatment. However, inclusion of delayed IKK activation and reduction of the IKK-related parameters by 2-fold resulted in a model that was able to recreate the effects seen with diclofenac treatment. Inclusion of the IKK delay resulted in a model that recapitulated the delayed first peak seen in the experimental data and the magnitudes of the parameter changes required to fit the data were smaller and nearer the measured bounds. The model period was extended by approximately 70% and the first peak delayed. Figure 6.8 shows a comparison between this developed model and its predecessor, showing an agreement with the experimental data in figure 6.1. For model equations and parameters see Appendix 3.1.



**Figure 6.8** – Comparison of the original model presented in Ashall et al. (2009) with the model that has been adapted to include a delay in the activation of IKK and a scaling of the rates of IKK recycling and phosphorylation to recapitulate co-treatment with diclofenac.

### 6.2.3 – Conclusions & Future Outlook

Treatment with diclofenac appears to be a novel means to alter the NF- $\kappa$ B response to TNF $\alpha$  stimulation. Use of the compound showed a significant increase in the period of oscillations (figure 6.2) and there was an increase in the time to the first peak in NF- $\kappa$ B nuclear occupancy. This analysis was performed using a transiently transfected reporter, where the number of ectopically expressed transgenes is highly variable, repetition of these data in a stably transfected cell line would serve to eliminate any variation that might be a result of changing expression level. These data also suggested that this effect was dose-dependent but to validate this hypothesis a greater amount of data for cells treated with the 500 $\mu$ M concentration of diclofenac needs to be collected. Currently only a small number of cells have been analysed and the data set has a large deviation (figure 6.2a). It must also be noted that larger doses of diclofenac resulted in a greater amount of cell death and this should be properly quantified to establish an appropriate range of concentrations to work with. To elucidate the functional implications of this effect an analysis of NF- $\kappa$ B-dependent gene expression is required. This can be preliminarily achieved using quantitative RT-PCR probing for known responsive genes such as I $\kappa$ B $\alpha$ , I $\kappa$ B $\epsilon$ , A20, MCP1 and RANTES. However, a global analysis of diclofenac's effect on the transcriptome should also be conducted.

The change in the timing of the first peak of NF- $\kappa$ B nuclear occupancy (figure 6.2), and the altered I $\kappa$ B $\alpha$  degradation and phosphorylation (figure 6.3) were in accordance with the hypothesis that diclofenac is acting on or upstream of the IKK complex. This hypothesis was further strengthened by studies that have shown other NSAIDs to affect IKK activity (Krakauer, 2004). These data suggested that diclofenac treatment could result in altered activity of the IKK complex. To test this hypothesis parameter searches were performed to determine if it was possible to alter the period through changing of the IKK-related parameters. Parameter space searches demonstrated that it was possible to achieve a suitable re-parameterisation by altering five IKK-related parameters by a larger amount. This was an unsophisticated search of parameter space and the qualitative nature of the solution



was not ideal; this analysis was only to demonstrate that it is possible to achieve the magnitude of period change seen in the data. However, with the application of more refined fitting methods it may be possible to find an ideal parameterisation. It is also possible that other parameters are altered by treatment with diclofenac that have not been included in this search and likewise, the parameters included in this search might not be changed by diclofenac.

All the parameterisations that resulted in a period change comparable to that seen experimentally required a large reduction in NF- $\kappa$ B nuclear import (5-fold or greater). This parameter was included in the search as there is evidence to suggest nuclear import can be affected by IKK phosphorylation, for example phosphorylation of S536 by IKK $\beta$  can alter the nuclear translocation of RelA (Kennedy, 2010, Mattioli *et al.*, 2004). In addition to S536 there are a number of identified and potential phosphorylation sites where the functionality and kinase is unknown, these could also potentially affect NF- $\kappa$ B translocation. However, if no such residue exists, then the importance of this parameter to fitting the data could suggest that the IKK activity hypothesis is invalid.

The data also supported an alternative hypothesis that the activation of the IKK module is delayed by treatment with diclofenac; this hypothesis is evidenced by the delay in the first peak of nuclear NF- $\kappa$ B (figure 6.1 and figure 6.2). Inclusion of this delay in the Ashall model resulted in an extended period, while maintaining the qualitative nature of the limit cycle (figure 6.6). The delay was included using a method of linear chains, this method includes a number of intermediary steps between the neutral IKK species becoming active. These steps could be representative of the stages between binding of TNF $\alpha$  to the extracellular receptor and activation of the IKK complex (Cho *et al.*, 2003). The inclusion of a linear chain gave a model with a solution that was qualitatively in agreement with the data but not quantitatively (figure 6.6); the period of the solution was shorter than observed experimentally (figure 6.2). A combination of the two hypotheses was successful in producing model that could reproduce both experimental observations: the period change and the delay in the first peak (figure 6.8). The inclusion of a delay limited the  $ki1$  parameter change required to 2-fold, which is within the experimentally

measured bounds (Ashall *et al.*, 2009). That no single approach suitably fits the data could imply that the model is too robust, motivating the development of a more accurate representation of the NF- $\kappa$ B system upstream of the IKK module. More interestingly, it could support the hypothesis that diclofenac is not only delaying the activation of the IKK complex but also reducing its kinase activity.

To validate or disprove the existence of a delay in the activation of the IKK complex a measure of the IKK kinase activity following TNF $\alpha$  stimulation is needed. Previous assays have found the peak of IKK activity to be approximately 5 to 15 minutes after stimulation in response to high doses of TNF $\alpha$  (Cheong *et al.*, 2006, Werner *et al.*, 2008), a delay in the time of this peak after treatment with diclofenac would be in accordance with the delayed IKK activation hypothesis. If the temporal profile was unchanged but the relative level of activity was reduced this would support the hypothesis that the amplitude of IKK kinase activity is being altered not the temporal profile. If both of these characteristics were present it could suggest that diclofenac has a more complex effect on the system.

A further explanation for the inability of the Ashall model to capture the dynamics seen is that the altered IKK activation is changing the temporal expression of NF- $\kappa$ B-dependent feedbacks. This could imply that the system is being changed on two levels. A delay in IKK activation is responsible for the delay in the time to the first peak but a change in the expression of the NF- $\kappa$ B dependent feedbacks is responsible for the significantly extended limit cycle period. It must also be noted that this behaviour may not be related to the IKK complex, the proteasome is responsible for I $\kappa$ B $\alpha$  degradation and a delay in the degradation could also be due to proteasome inhibition. Moreover, proteasome inhibition can have a knock-on effect on NF- $\kappa$ B nuclear import, which could explain the re-parameterisation necessary to capture the data. Currently, the Ashall model does not sufficiently represent this pathway to be able to explore this hypothesis *in silico*, if no change in the IKK activity were found this could provide an alternative avenue to explore.

## 6.3 – The Effect of Temperature on the NF- $\kappa$ B System

### 6.3.1 – Temperature Introduction

*Calor* (increased heat) is one of the cardinal symptoms of inflammation (Tracy, 2006) and many anti-inflammatory treatments have antipyretic effects causing a reduction in body temperature, thus relieving fever (Whitehouse, 2005). In a physiological context many studies have demonstrated a relationship between *calor* and the NF- $\kappa$ B system. The induction of inflammation in prostate cancer through the TNF $\alpha$  treatment has been shown to increase the tumour's susceptibility to cryosurgery (destruction by the application of extreme cold) (Chao *et al.*, 2004). In neutrophils increased temperature has been seen to inhibit NF- $\kappa$ B activation in response to TNF $\alpha$  (Salanova *et al.*, 2005) and moreover, blocking NF- $\kappa$ B activation has been shown to result in antipyresis (Lee *et al.*, 2003). The deeply woven association between inflammation, NF- $\kappa$ B and pyresis motivated an analysis of the effect of temperature changes on the single-cell dynamics of this transcription factor.

Atoms and molecules are continually in motion; temperature is a description of the intensity of kinetic motion of these atoms and molecules (Cossins and Bowler, 1987). The influence of temperature changes on enzymatic reactions has been extensively studied. Numerous relationships have been defined, both empirically and from first principles, which endeavour to describe how a change in the rate of a reaction corresponds to a change in temperature (Cossins and Bowler, 1987). One of the most notable of these is the Arrhenius equation, which relates a rate constant for a reversible reaction in equilibrium to temperature. These relationships can be used to predict the effect of temperature changes on a system in computational models (Akman *et al.*, 2008).

A consideration when using temperature to perturb a system is the occurrence of adaptive changes in the rate of biological processes as a result of temperature change. Temperature compensation has been extensively studied in processes such as metabolism (Fry, 1958) and circadian rhythms (Gardner and Feldman, 1981). Circadian clocks maintain their period over a wide range of physiological temperatures - this property is referred to as temperature compensation (Rensing and

Ruoff, 2002). Without this property it has been proposed that daily biological timekeeping would be highly unreliable, running too fast at warm temperatures and too slow at colder temperatures (Mattern *et al.*, 1982). The design principles underlying circadian oscillations have many parallels with those defining NF- $\kappa$ B oscillations. Similarly to the NF- $\kappa$ B system, the core molecular representation of the circadian clock employs a delayed negative feedback loop to drive sustained oscillations (Goldbeter, 2002). However, the complete structure is far more complicated with multiple interlocking positive and negative feedback loops (Rand *et al.*, 2004). Studies have demonstrated that components of circadian clock are differentially altered in response to temperature changes, resulting in a balancing of feedbacks that leads to temperature compensation (Gould *et al.*, 2006).

Both the NF- $\kappa$ B system and circadian clock exhibit robust oscillatory dynamics where the timing of these oscillations is important for appropriate cellular responses. Their networks have many similarities in their fundamental design principles both consisting of multiple feedback loops that drive their dynamic behaviour. The many parallels between the circadian clock and NF- $\kappa$ B system highlight the need for a systems level analysis to explain the effect of temperature changes on the NF- $\kappa$ B dynamics.

## 6.3.2 – Temperature Results

### 6.3.2.1 – Characterisation of RelA Oscillations at Different Temperatures

SK-N-AS cells were transiently transfected with the CMV driven RelA-dsRedXP reporter plasmid. After 24-48 hours of transfection cells were treated with 10ng/ml TNF $\alpha$  and those visibly expressing RelA imaged approximately every 5 minutes for up to 10 hours using fluorescent confocal microscopy. Images of cells showing RelA nuclear-cytoplasmic oscillations were analysed using CellTracker to determine the nuclear to cytoplasmic ratio (N:C) of RelA fluorescence. These data were subsequently analysed to determine the period of RelA oscillations. Figure 6.9 shows a single-cell time-course from each of the experimental conditions, these data showed an increased frequency of RelA N:C oscillations with increasing temperature. *Imaging data collected and analysed by Dr C. Harper, Systems Microscopy Centre, University of Manchester.*

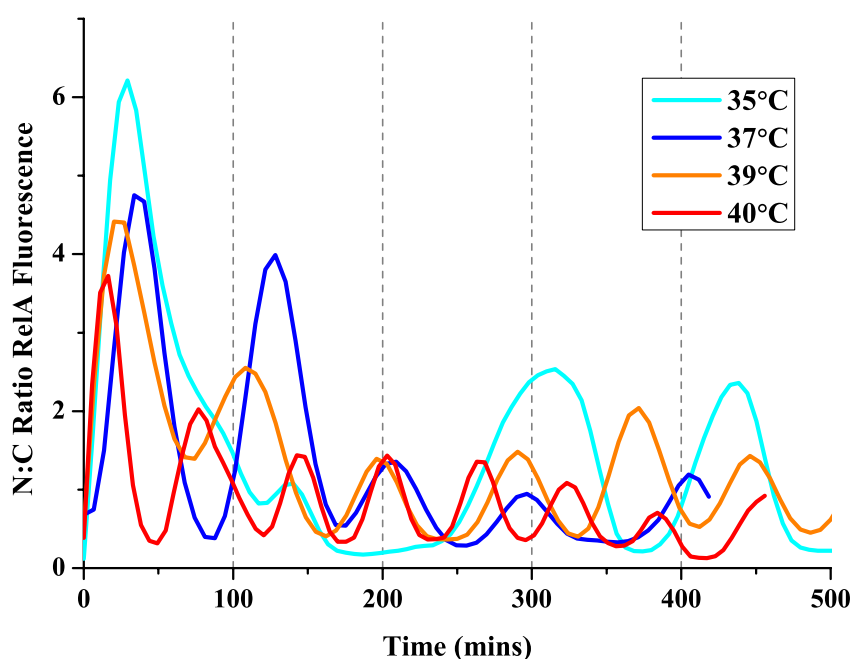


**Figure 6.9** – Single cell examples of SK-N-AS RelA oscillations at different temperatures following stimulation with 10ng/ml TNF $\alpha$ . Cells were analysed using whole-cell tracking and the resulting quantification of the N:C ratio of RelA fluorescence has been plotted. The data has been smoothed using a moving average of 5 data points. These data show an increased frequency of RelA oscillations at higher temperatures.

Table 6.1 and figure 6.10 give a summary of the RelA-dsRedXP peak-to-peak timings (the time taken between each peak of nuclear occupancy) for each of the temperatures. These do not include the time between the first and second peaks, as this is highly variable (Horton, 2006). At 37°C the results showed a period of 102±17mins, in agreement with previously published data (Ashall *et al.*, 2009, Nelson *et al.*, 2004). In comparison, the period at a lower temperature (35°C) was 120±17mins, while at higher temperatures (39°C and 40°C) the period was 84±19mins and 75±17mins respectively. A nonparametric statistical analysis, using a Mann-Whitney U test, showed a significant difference between the average peak-to-peak time at 37°C and the other temperatures ( $p < 0.001$ ). These data demonstrated a clear relationship between the temperature and oscillatory period. It is interesting to note that this relationship also appears to be highly linear, which is a surprising result for a nonlinear system. Comparing temperature with average peak-to-peak time showed that there was approximately a 9-minute change in period per degree change in temperature (table 6.1).

**Table 6.1** – Summary of the data for RelA-dsRedXP oscillations in transiently transfected SK-N-AS cells at different temperatures. For each condition the number of replicates, cells analysed and peaks detected is listed along with the resulting average peak-to-peak time ± the standard deviation of the pooled data.

Temperature (°C)	Replicates	Number of Cells	Number of Peaks	Average Peak-to-Peak timing (mins)
35	3	21	88	120±27
37	2	30	66	102±17
39	4	43	152	84±19
40	2	24	98	75±17

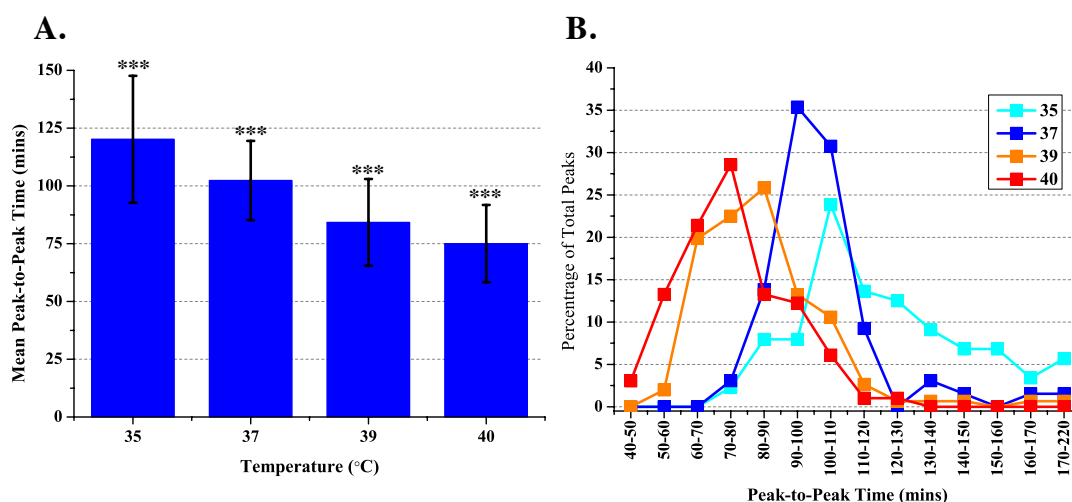


**Figure 6.10** – Summary of RelA-dsRedXP peak-to-peak timings at different temperatures for SK-N-AS cells transiently transfected with RelA-dsRedXP and stimulated with 10ng/ml TNF $\alpha$ . (A) Average peak-to-peak timing for each of the four temperatures, measured from the second peak onwards. Horizontal black line shows the nominal 100-minute period. Asterisk denotes a significant difference from the 37°C condition (using a Mann-Whitney U test,  $p < 0.001$ ). (B) Distribution of peak-to-peak timings for each of the temperature, measured from the second peak onwards.

### 6.3.2.2 – Understanding the Temperature influence on NF-κB

#### Dynamics Using the Balance Equations

It is possible to derive a relationship between the period of oscillation and temperature (Ruoff, 1992, Ruoff, 1994), this relationship assumes the temperature dependence of the model parameters is similar to the temperature dependence of rate constants in chemical reactions. This dependence is expressed by the Arrhenius equation (6.7), which relates the rate,  $k_j$ , of the  $j^{\text{th}}$  reaction to the temperature T and activation energy for that reaction  $E_j$ , where R is the gas constant ( $R=8.314472JK^{-1}mol^{-1}$ ) and  $A_j$  is a constant specific to the parameter  $k_j$  (Akman *et al.*, 2008). It should be noted that temperature units of Kelvin should be used in this calculation.

$$k_j = A_j e^{-E_j/RT} \quad (6.7)$$

Using the Arrhenius equation and the application of the chain rule to the derivative of the period with respect to time enables the derivation of this relationship between the change in temperature and the change in period, and is given as,

$$\frac{dP}{dT} = \frac{P}{RT^2} \sum_j c_j E_j \quad (6.8)$$

where  $c_j = \partial \log P / \partial \log k_j$  (Akman *et al.*, 2008). This relationship can be applied to determine if the Ashall model is able to explain the change in period by faster reaction rates due to increased energy in the system.

For this evaluation, it is convenient to rewrite (6.8) as,

$$P^{-1} RT^2 \frac{dP}{dT} = \sum_j c_j E_j. \quad (6.9)$$

From figure 6.10 and table 6.1 it can be seen that in the NF-κB system  $dP/dT \approx -9$  and that at 37°C (310K) the period is approximately 100 minutes ( $P \approx 100$ ). Using these data and the gas constant the LHS of (6.9) is  $\approx -71873$ .

The  $c_j$ 's can be calculated using the global sensitivity analysis software (Rand, 2008). For this system they are shown in figure 6.11 and it can be seen that the largest coefficient is approximately  $-0.2$ . The activation energies for biological reactions are assumed to be in the range of  $1-150 \text{ kJmol}^{-1}$  (Akman *et al.*, 2008). As there are 28 parameters in the model if it is assumed that  $|c_j| \leq 0.2 \forall j$  and  $E_j \leq 150 \forall j$ , then it is possible to compute a bound for the RHS of (6.9) as follows:

$$\sum_j |c_j| E_j \leq 150 \sum_j |c_j| \leq 150(0.2n) \lesssim 840. \quad (6.10)$$

However, considering the modulus of the LHS gives,

$$\left| P^{-1} RT^2 \frac{dP}{dT} \right| \approx 71873 \not\leq 840. \quad (6.11)$$

In reality this inequality will be greater as this analysis has assumed that all parameters exert the same and equally strong influence on the period. They have been assumed to have the same influence as the strongest parameter (c4), which is in fact an amalgamation of multiple negative feedbacks (Chapter 1, Section 1.5.3). Other terms in the equation (6.8) that might change with temperature to balance this



inequality include the  $1/T^2$  term and the  $E_j s$ . However, as temperature is represented in Kelvin for the  $1/T^2$  term this is a difference between  $1/310^2$  and  $1/313^2$  at the maximum temperature change, which would not account for a significant change. The  $E_j s$  have been represented close to the observed upper level ( $150\text{kJmol}^{-1}$ ) therefore to increase them to account for a difference of two orders of magnitude would require unrealistically high activation energies. This analysis strongly suggests that in the Ashall model the parameters do not exert a sufficient influence on the period to be able to explain the period change solely due to a change in the level of thermodynamic energy in the system.

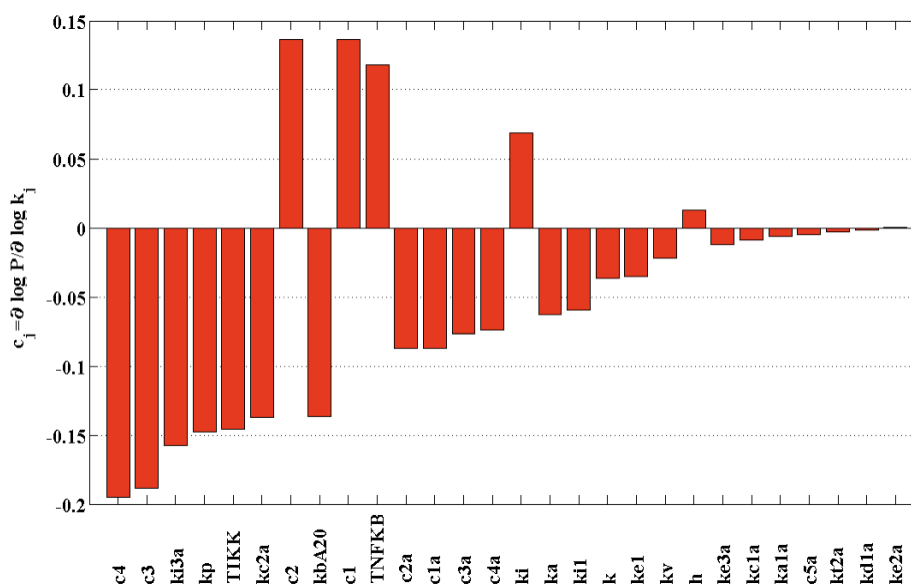


**Figure 6.11** - Derivative of the model period with respect to the log change in a parameter for the Ashall model, calculated using the Global Sensitivity Analysis Software (Rand, 2008). Values are presented as  $\partial \log P / \partial \log k_j$  to be compatible with (6.2).

### **6.3.2.3 – I $\kappa$ B $\alpha$ and A20 mRNA Expression Profiles at Different Temperatures**

Microarray analysis was performed at 37°C and 40°C to investigate the effect of temperature on NF- $\kappa$ B dependent gene expression. SK-N-AS cells were stimulated with 10ng/ml TNF $\alpha$  for following time periods, 0, 30, 130, 230 and 430 minutes, lysed and the mRNA expression profile analysed. The resulting data was analysed to find genes that were differentially expressed between the different temperatures. (*Dr C. Harper, Systems Microscopy Centre, University of Manchester performed this experiment. Dr B. Noyvert, Systems Biology Centre, University of Warwick performed data analysis.*)

Temperature did not appear to alter the expression of many of the genes in the canonical NF- $\kappa$ B pathway, especially those represented in the Ashall model; figure 6.12 shows the results for the genes: RelA, I $\kappa$ B $\alpha$ , I $\kappa$ B $\epsilon$  and A20. The data indicates that RelA, I $\kappa$ B $\alpha$  and I $\kappa$ B $\epsilon$  expression levels were comparable at both the 37°C and 40°C temperatures (figure 6.12a-c). The data for A20 transcription showed an increased expression level, of approximately 2-fold, after 30 minutes at 40°C in comparison to the 37°C condition (figure 6.12b). However, from 130 minutes onwards the A20 expression profiles reached a similar steady state levels (figure 6.12c).

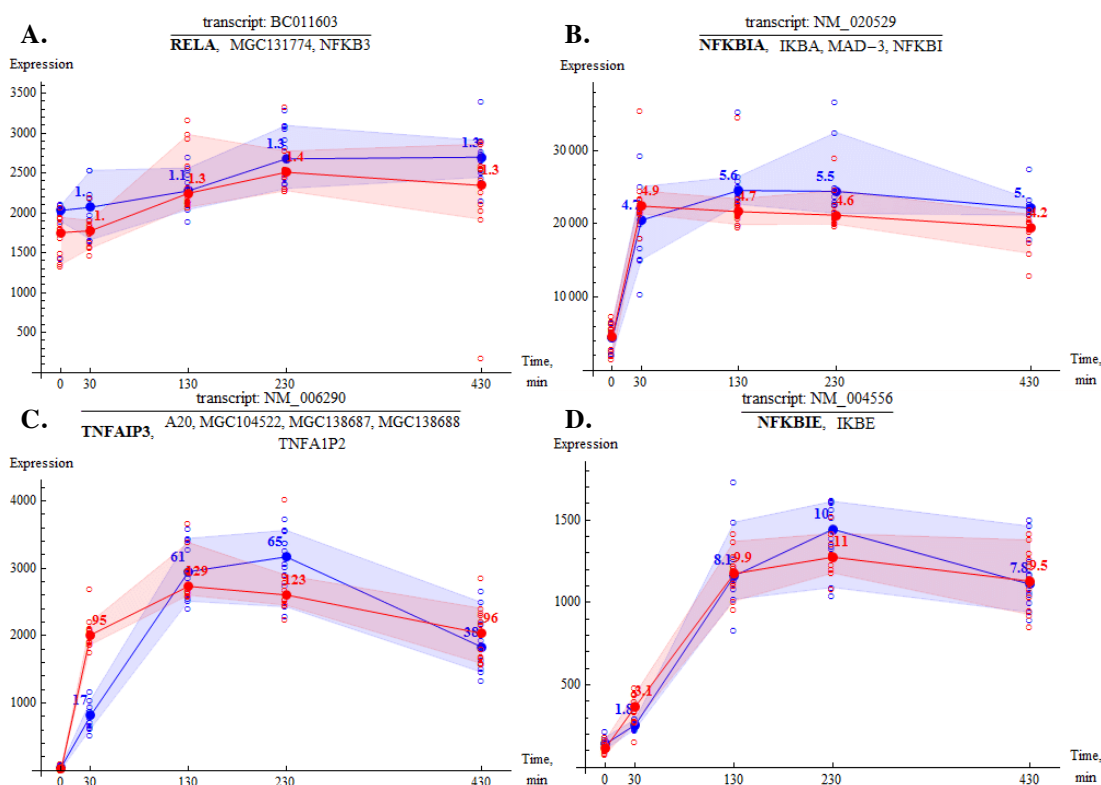


**Figure 6.12** – RelA, I $\kappa$ B $\alpha$ , A20 and I $\kappa$ B $\epsilon$  expression profiles at 37°C and 40°C, blue and red respectively. SK-N-AS cells were incubated at the appropriate temperature, stimulated with 10ng/ml TNF $\alpha$  for the appropriate duration, then lysed. The mRNA was then extracted, converted to cDNA and hybridised to a NimbleGen<sup>TM</sup> array. A representative transcription has been shown for: RelA (A), I $\kappa$ B $\alpha$  (B), A20 (C) and I $\kappa$ B $\epsilon$  (D). The x-axis shows time in minutes. Solid lines show the median of four biological replicates. Translucent bands show the spread of the data, excluding the maximum and minimum points. *Graphs were originally generated by Dr B. Noyvert, Systems Biology Centre, University of Warwick.*

#### 6.3.2.4 – A Temperature Sensitive NF- $\kappa$ B Model

The different A20 mRNA expression level at 30 minutes between the temperatures is uncharacteristic of other genes in the system. These data coupled with the high sensitivity of the model to A20 related parameters (figure 6.11 and Chapter 4) makes further investigation warranted. I $\kappa$ B $\alpha$  and A20 are both classed as early genes but they show markedly different expression profiles. I $\kappa$ B $\alpha$  attains a maximum expression level very quickly at ~30 minutes while A20 is slower to do so, peaking between 130 and 230 minutes. The profile of A20 is qualitatively more similar to that of I $\kappa$ B $\epsilon$ , a middle gene with a known transcriptional delay (Paszek *et al.*, 2010b). These similarities in profiles lead to a hypothesis that there is a similar, albeit shorter, delay in the mechanism of A20 transcription. Moreover, the fact that A20 expression is different at 30 minutes but reaches similar levels at later times, could suggest that the delay in the initiation A20 transcription is changing with temperature. This delayed response is not fully approximated by the Hill function representing A20 transcription in the Ashall model, which shows an initiation of transcription in less than 5 minutes (figure 6.13a). An inaccurate representation of A20 transcription could explain why the model is not able to capture the change in NF- $\kappa$ B dynamics seen at different temperatures.

There is also evidence of a delay in A20 expression from the literature. Analysis of A20 and I $\kappa$ B $\alpha$  mRNA expression using a semi-quantitative RT-PCR method over a finer time resolution shows an induction of I $\kappa$ B $\alpha$  but not A20 mRNA after 15 minutes following a 5-minute pulse of TNF $\alpha$  (Ashall *et al.*, 2009). This is further supported by western blot analysis, which showed expression of the A20 protein in HeLa cells 1 hour after TNF $\alpha$  but no band was present at 50 minutes (Werner *et al.*, 2008). In comparison, figure 6.3 showed resynthesis of I $\kappa$ B $\alpha$  in basal conditions after 30 minutes, however, this was in SK-N-AS cells. These data and the sensitivity analysis imply that inclusion of a delay in the transcriptional representation of A20 in the model is a reasonable hypothesis to test.

To include a delay in the transcription of A20 the linear chain method was applied (see section 6.2.2.4). A parameterisation of the model was then found based upon the following fitting criteria: a limit cycle with a 100-minute period after the inclusion of a transcriptional delay, the ability to reduce this period to between 75-80 minutes by reduction of the delay, and a  $\sim$ 2-fold difference in the level of A20 mRNA at 30 minutes for these two parameterisations. A suitable parameter set was determined without moving any parameters outside of the intervals defined by their fitting criteria. To adjust for temperature change the delay parameter was altered to suitably change the model period while all other parameters were kept fixed; this corresponded to a  $\sim$ 5-minute change in the A20 transcriptional delay, (figure 6.13a). In reality the other parameters would be expected to change with increased thermal energy however, this would affect the period considerably less. The resulting model and parameters can be found in Appendix 3.2. Figure 6.13b shows the solution of this model with the delay parameter adjusted to represent the two temperatures (at 40°C the period is 80 minutes). For the new model the average level of A20 mRNA was calculated after a limit cycle was achieved (200 minutes onwards) at the 37°C and 40°C parameterisations, these were  $6.26 \times 10^{-5}$  and  $6.19 \times 10^{-5}$ , respectively. The similarity in these levels is consistent with the microarray data, which shows similar levels of A20 expression after 430 minutes (figure 6.12).

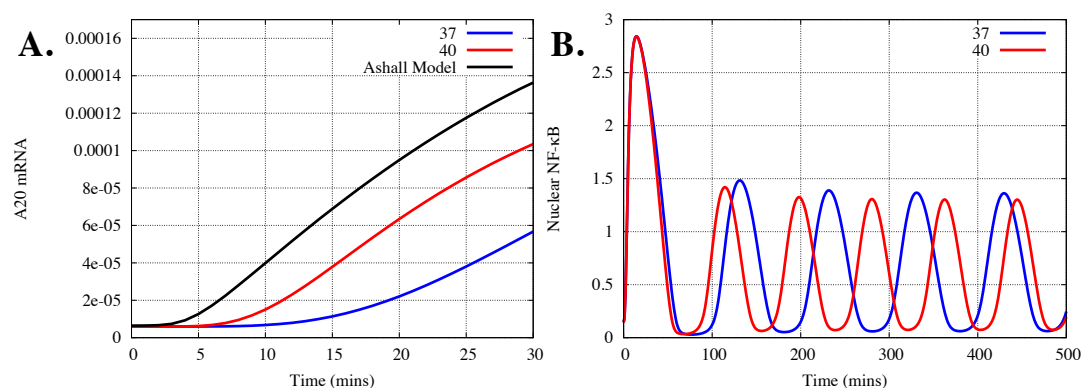


**Figure 6.13** - Analysis of the model with altered A20 transcriptional representation. (A) The solution of A20 mRNA over 30-minutes comparing the Ashall model (black) and the model with a delay in A20 transcription parameterised to recapitulate the microarray data for 37°C and 40°C (blue and red respectively). (B) Comparison of the solution for Nuclear NF- $\kappa$ B normalised to total NF- $\kappa$ B in the altered model parameterised to 37°C and 40°C (blue and red respectively).

### 6.3.2.5 – Validating the Temperature Sensitive NF- $\kappa$ B Model

To validate the existence of a delay in the transcription of A20, quantitative RT-PCR was performed on SK-N-AS cells at 37°C and 40°C over a fine time resolution. SK-N-AS cells were stimulated with 10ng/ml TNF $\alpha$  at 2.5-minute intervals between 0 and 15 minutes, and 5-minute intervals between 15 and 30 minutes. (*Dr L. Ashall, Systems Microscopy Centre, University of Manchester performed these experiments.*)

A comparison of the A20 transcription at 37°C and 40°C can be seen in figure 6.14b. The transcription of A20 after 30 minutes is approximately three times higher at 40°C. The shape of the A20 profile is in much better agreement with the delay model in comparison to the Ashall model where there is a sharp increase in transcription ~2.5-minutes after stimulation (figure 6.13a). Firstly, these data suggests that the Ashall model does not accurately capture the transcription of A20 however, figure 6.14a does not fully confirm the delay hypothesis. Figure 6.14a represents the results for I $\kappa$ B $\alpha$  transcription, which also showed over a 2-fold increase in transcription at 30 minutes and 40°C in contradiction to the microarray data.

Figure 6.14c and figure 6.14d show a more detailed analysis of the data between 0 and 20 minutes. In this case the individual data points have been depicted and not the average. Quantitative RT-PCR data points are independent of each other within the experiment and between experiments, therefore this method is a more accurate way to visualise the data. Figure 6.14d, showing A20, suggests that A20 mRNA levels are increased relative to the basal time-point after 7.5 minutes at 40°C and 12.5 minutes at 37°C; this is especially pronounced at the 10-minute time-point. It would also suggest that the rate of transcription is higher at 40°C, indicating that A20 transcription is occurring earlier at 40°C with an increased rate. In figure 6.14c, showing I $\kappa$ B $\alpha$ , the relationship is less clear. The transcription of I $\kappa$ B $\alpha$  remains near basal for the first 5 minutes in both conditions, which is currently not in agreement with the Ashall model however, both transcripts seem to be higher at the 7.5-minute time point and this is definitely apparent after 10 minutes.

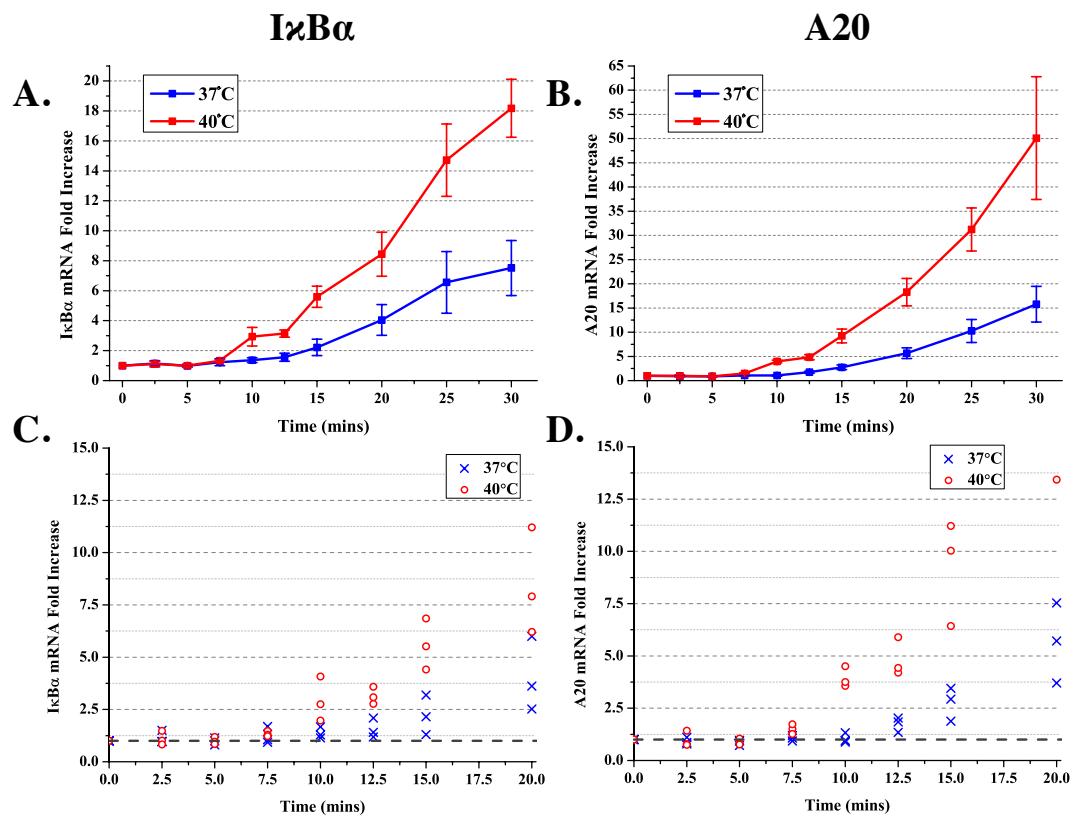


**Figure 6.14** - Quantitative RT-PCR measurement for the I $\kappa$ B $\alpha$  and A20 genes. SK-N-AS cells, 24-hours post-plating, were incubated at either 37°C or 40°C for 1-hour prior to stimulation and then stimulated with 10ng/ml TNF $\alpha$  for the time periods shown. The cells were lysed, mRNA extracted, converted to cDNA and quantitative RT-PCR performed with primers for I $\kappa$ B $\alpha$  and A20. Data was analysed using the  $2^{-\Delta\Delta CT}$  method, using cyclophilin A as the endogenous control and time point 0 as the calibrator. (A) and (B) compare the average of triplicates for each gene at different temperatures, I $\kappa$ B $\alpha$  and A20 respectively. (C) and (D) show the results for the individual experiments and is zoomed to the window 0-20 minutes.

### 6.3.2.6 – Refinement of the Temperature Sensitive Model

To try and unravel the complexities of the quantitative RT-PCR and rationalise these data with the sensitivity and microarray analyses, the model was altered to include a delayed transcriptional mechanism for only I $\kappa$ B $\alpha$  transcription, or both I $\kappa$ B $\alpha$  and A20 transcription. This analysis gives an insight into how different representations of the transcriptional mechanism of the feedback genes influence the system, not only with respect to temperature but in general. Studies have highlighted the importance of including transcriptional delay for correct representation of the system dynamics (Kerszberg, 2004) and moreover, the length of delay in negative feedback loops can markedly alter the period (Nguyen, 2012). Again the method of linear chains was applied and the model parameters fitted so that the classic limit cycle period of 100 minutes was present and the transcriptional profiles of I $\kappa$ B $\alpha$  and A20 were similar to those seen in the quantitative RT-PCR data at 37°C. The delay parameter was then adjusted to give a limit cycle period of 80 minutes for the 40°C condition. For model equations and parameters see Appendix 3.3 and 3.4.

Analysis of these models identified that inclusion of delayed transcription in either of the species to have a similar effect on the limit cycle period when the length of delay is decreased. Reducing the duration of the delay resulted in a reduced period (figure 6.15c). Inclusion of a delay in both species increased the model's sensitivity to the delay parameter (figure 6.15d), as a result it was straightforward to adjust the delay parameter to recapitulate the NF- $\kappa$ B dynamics seen at the 37°C and 40°C temperatures in the dual delay model (both I $\kappa$ B $\alpha$  and A20 transcription delayed). Again the average A20 mRNA levels were very similar (<2% different) for both temperatures, consistent with the microarray data. However, when increasing the delay to simulate lower temperatures, a markedly different effect on the period is seen dependent upon which variable contains the delay. For A20, there is an increased period with increased delay however, in the case of I $\kappa$ B $\alpha$ , sufficiently large delays cause a decrease in the limit cycle period and it is only possible to obtain periods of ~100-minutes or less by variation of the delay parameter. These results suggest that by only including a delay in I $\kappa$ B $\alpha$  transcription it would not be possible to recapitulate the dynamics seen at 35°C where the period was ~120 minutes (table



6.1). This supports the hypothesis that period modulation of the system is primarily conferred through the A20 feedback loop.

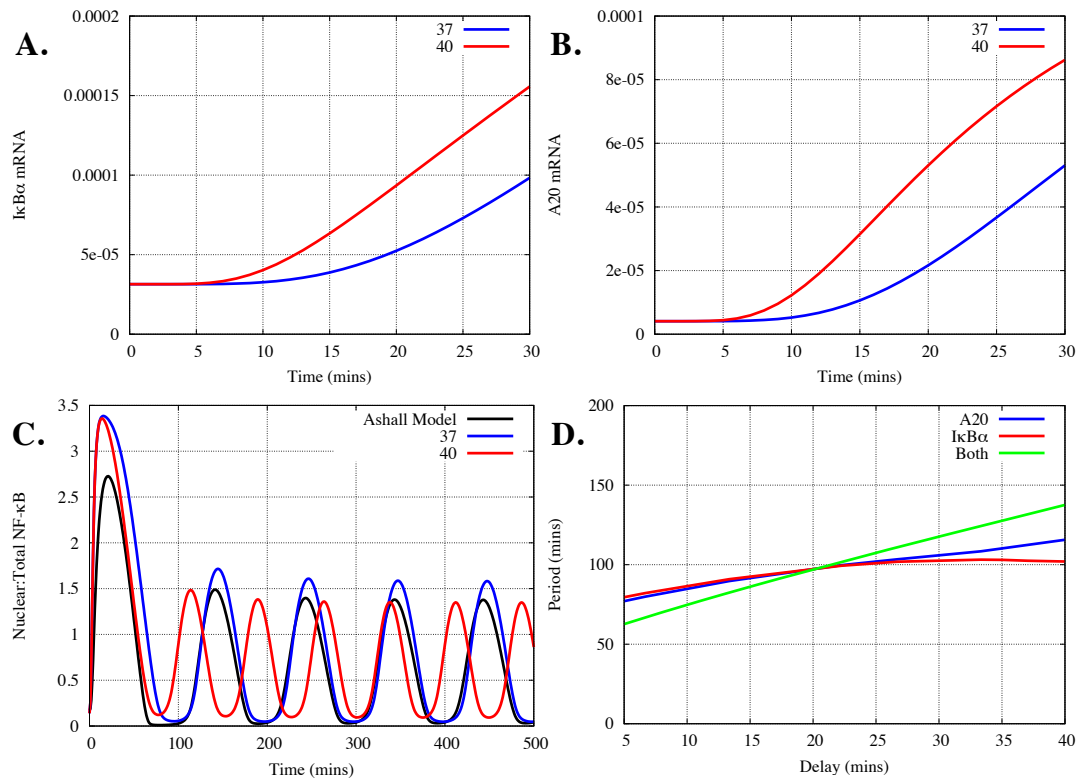


**Figure 6.15** - Analysis of the model where a delay has been included in A20 and I $\kappa$ B $\alpha$  transcription. (A) and (B) solutions for I $\kappa$ B $\alpha$  and A20 mRNA, respectively. The delay has been altered to recapitulate the RT-PCR data in figure 6.14, red traces correspond to 40°C and blue traces to 37°C. (C) Comparison of the model solution for nuclear NF- $\kappa$ B normalised to total NF- $\kappa$ B at 37°C and 40°C (blue and red respectively). (D) Comparison of the effect of altering the delay on the period of oscillations, where the delay has been applied to A20 transcription (blue), I $\kappa$ B $\alpha$  transcription (red), or both species (green).

Figure 6.15d shows that altering the transcriptional mechanism of both species results in a highly linear period bifurcation, which is in agreement with the linear effect seen when perturbing the temperature. Altering both A20 and I $\kappa$ B $\alpha$  transcription resulted in a high sensitivity of the period to the delay parameter making it possible to find parameterisation that could recapitulate the NF- $\kappa$ B dynamics seen at all the temperatures used in the experimental analysis (table 6.2).

**Table 6.2** - Summary of the delay parameters required to recapitulate the NF- $\kappa$ B dynamics seen at different temperatures.

Temperature (°C)	Delay Parameter Value	Delay (mins)	Period (mins)
40	0.0080	8.33	74.13
39	0.0055	12.12	84.28
37	0.0036	18.51	100.34
35	0.0025	27.78	122.5

### 6.3.2.7 – The Effect of Pulsatile and Low Dose TNF $\alpha$ Stimulation on the Dual Delay Model

The Ashall model was also designed to fit data regarding pulsatile stimulation of the NF- $\kappa$ B system (Ashall *et al.*, 2009), these data show an entrainment of NF- $\kappa$ B oscillations to 60-, 100- and 200-minute frequencies resulting from stimulation by 5-minute pulses of TNF $\alpha$  at those frequencies. To address if the model with altered transcription of I $\kappa$ B $\alpha$  and A20 (dual delay model) is able to capture these data the system was simulated using a pulsed TNF $\alpha$  input.

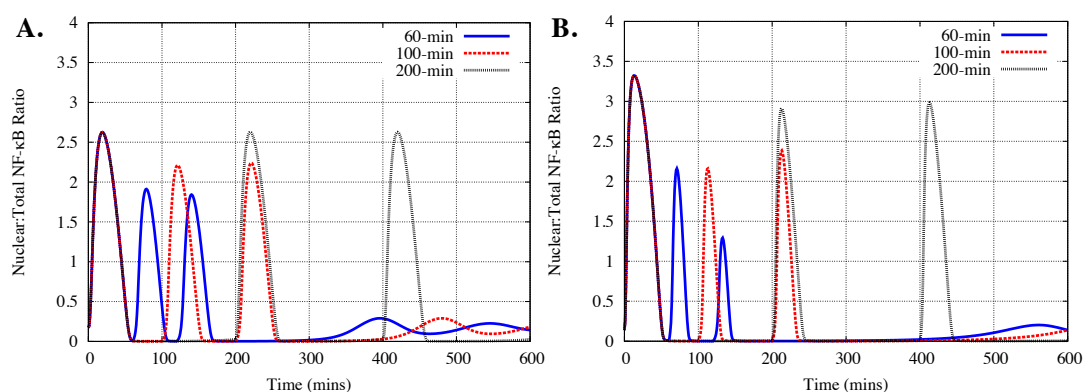


**Figure 6.16** - The effect of pulsatile TNF input on the Ashall Model (A) and dual delay Model (B). The system was stimulated with three 5-minute pulses of TNF $\alpha$  (TR=1), every 60 (blue), 100 (red) or 200 (grey) minutes, for all other times TR=0. The solution is shown for nuclear NF- $\kappa$ B normalised to the total level of NF- $\kappa$ B (0.08 $\mu$ M).

Figure 6.16b demonstrates that the model is able to produce oscillations of NF- $\kappa$ B entrained to the pulse frequency. There are qualitative differences between the two models. In the dual delay model the first translocation is of higher amplitude. Quantification of the ratio of RelA nuclear to total cell fluorescence for the first peak in SK-N-AS cells was approximately  $3 \pm 0.8$  (Horton, 2006), therefore this increase is well within the experimentally measured bounds. Subsequent translocations also appear to be sharper with a reduced period of nuclear occupancy. For the 60-minute condition there is a reduction in the ratio of amplitudes between peaks two and three, this pattern is more consistent with the experimental observations (Ashall *et al.*, 2009). The dual delay model is also able to recapitulate the data without A20 inhibition being dependent on the presence of TNF $\alpha$  stimulation, which was an unsubstantiated hypothesis to aid in fitting of the Ashall model to the pulsatile data and was removed by Turner *et al.* (2010) to fit data regarding low dose TNF $\alpha$  stimulation.

RelA has also been shown to oscillate in SK-N-AS cells in response to a 1000-fold range of TNF $\alpha$  doses (Tay *et al.*, 2010, Turner, 2010). Turner *et al.* (2010) presented a development of the Ashall model that was able to respond to a greater range of TNF $\alpha$  concentrations. To represent different doses of TNF $\alpha$  in the Ashall model it was assumed that a parameter value of 1 for TR (TNF $\alpha$  dose) corresponded to the saturating dose of TNF $\alpha$  (10ng/ml) therefore, a parameter value of 0.1 is equivalent to a dose of 1ng/ml and so on. The Ashall model had a Hopf Bifurcation (HB) with respect to TR at 0.36 below which there was no limit cycle, suggesting that the system could only respond to high doses of TNF $\alpha$  (>3.6ng/ml). The model was altered by the removal of the TNF $\alpha$  dependence on A20 inhibition of IKK and changing of the A20 inhibition concentration (kbA20). This resulted in a model with a HB 10-fold lower (0.045) and limit cycle period that changed from 100 and 120 minutes as the TR parameter value was decreased from 1. Figure 6.17 summarises the effect of changing TNF $\alpha$  dose on the Ashall model, the low dose model presented by Turner *et al.* and the dual delayed negative feedback mode presented here. The dual delay model has a HB with respect to the parameter TR 10-fold lower still at 0.0014, that the model of Turner *et al.* and the period is between 100 and 120

minutes for a  $\sim 10$ -fold reduction in TR from 1 similar to Turner's model (figure 6.17b). Further reduction of the parameter value resulted in an increase in the period, which is consistent with Turner *et al.* (2010) who demonstrated a larger standard deviation of the period at the lower doses of TNF $\alpha$ .

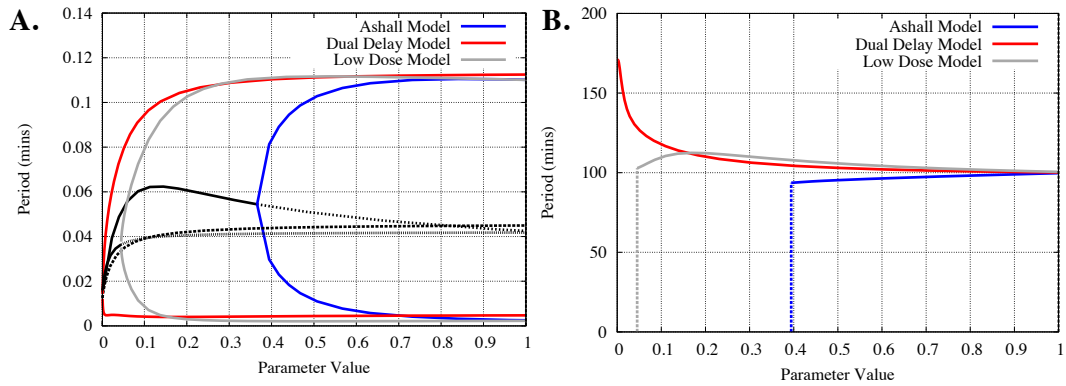


**Figure 6.17** - The effect of low dose TNF $\alpha$  stimulation on the Ashall model, the model of Turner *et al.* and the dual delayed negative feedback temperature sensitive model. Bifurcation analysis was performed with respect to the parameter representing TNF $\alpha$  stimulation (TR). (A) The effect on limit cycle amplitude. The solid black line shows a stable steady state, dashed black lines represent unstable steady state, red, grey and blue lines show the max and min on the limit cycle. (B) The effect on period as TR is reduced from 0 to 1. Horizontal black dashed line shows the nominal period of 100 minutes. Analysis performed using XPPAUT.

### 6.3.2.8 – The Role of I $\kappa$ B $\alpha$ and A20 Feedback in the Dual Delay Model

Chapter 5 has shown that the negative feedbacks I $\kappa$ B $\alpha$  and A20 have different effects on the period and that manipulation of these feedbacks can be used as a means to modulate the period. With the inclusion of a new mechanism to represent transcription of these feedback genes it is a reasonable question to ask how this has affected the previously established relationships. To address this, period bifurcations were found for the parameters related to I $\kappa$ B $\alpha$  and A20 transcription rate,  $c1a$  and  $c1$  respectively.

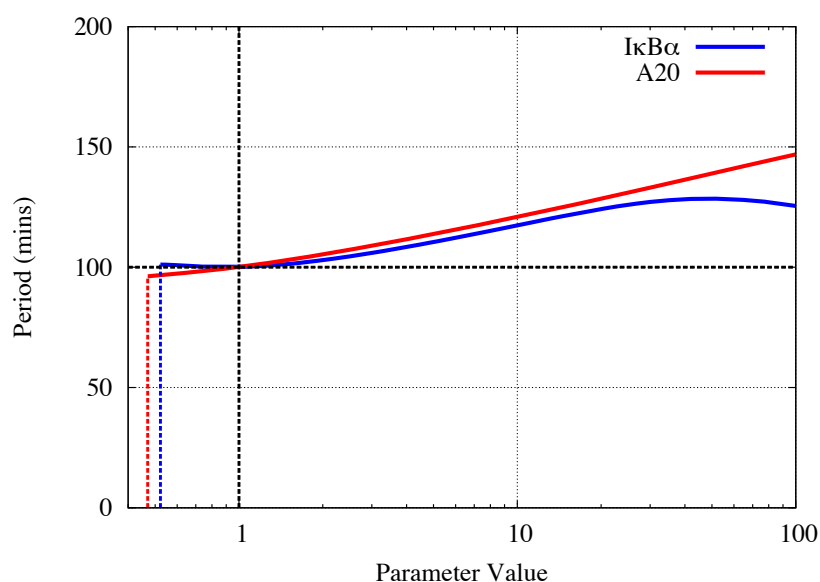


**Figure 6.18** - Period bifurcations with respect to I $\kappa$ B $\alpha$  transcription rate ( $c1a$ ) and A20 transcription rate ( $c1$ ), blue and red respectively, for the model where a delay has been included in their transcriptional mechanism. Parameter values have been normalised to their nominal value, the vertical black dashed line corresponds to the nominal value, and the horizontal black dashed line corresponds to the nominal 100-minute period. Analysis performed in XPPAUT.

Figure 6.18 shows the period dependence of the dual delay model for the parameters related to I $\kappa$ B $\alpha$  and A20 transcription,  $c1a$  and  $c1$  respectively. The dependence on A20 showed a similar qualitative relationship to the dependence in the Ashall model (figure 5.1, Chapter 5), increased A20 transcription resulted in an increased limit cycle period. However, the effect of the I $\kappa$ B $\alpha$  transcription rate has changed and the dependence is now opposite with increased transcription increasing the period. Moreover, this dependence is no longer monotonic, with the bifurcation curve attaining a minimum around the nominal parameter value. Previously it was shown that the shape of the I $\kappa$ B $\alpha$  bifurcation could be exploited to recapitulate the robustness to increased I $\kappa$ B $\alpha$  transcription seen in experiments. While this feature is now less apparent, there is still an interval for which the I $\kappa$ B $\alpha$  bifurcation curve has a small gradient, from 0.5 to 1.3. This suggests that the robust quality is still present for a 6- to 7-fold increase in I $\kappa$ B $\alpha$  expression. However, the model now predicts that a large over-expression of I $\kappa$ B $\alpha$  would increase the period.

This is an interesting phenomenon that suggests that the delay in activation of a reaction could alter the sensitivity structure of the system. To endeavour to understand if this was a feature of the NF- $\kappa$ B system or one that could be more generally be applied to oscillatory systems a similar analysis was performed on the minimal NF- $\kappa$ B model  $z_0 p_0 y_0 s_0 v_0 w_1$ . This model was chosen as it has been simplified to only include the core network topology and therefore can be considered more representative of a general motif of some oscillatory systems. A delay was included in the transcription of I $\kappa$ B $\alpha$  and the effect on the period of increasing the I $\kappa$ B $\alpha$  transcription rate was investigated for different lengths of this delay. Figure 6.19 shows the results of this analysis; the blue and green lines correspond to a very short or no delay in the initiation of transcription and it can be seen that there is a decrease in the period as the rate is increased. As the length of delay increases the effect of transcription rate on the period reverses and moreover, there appears to be an “optimal” delay where the period is extremely robust to any increase in transcription rate (figure 6.19, yellow line).

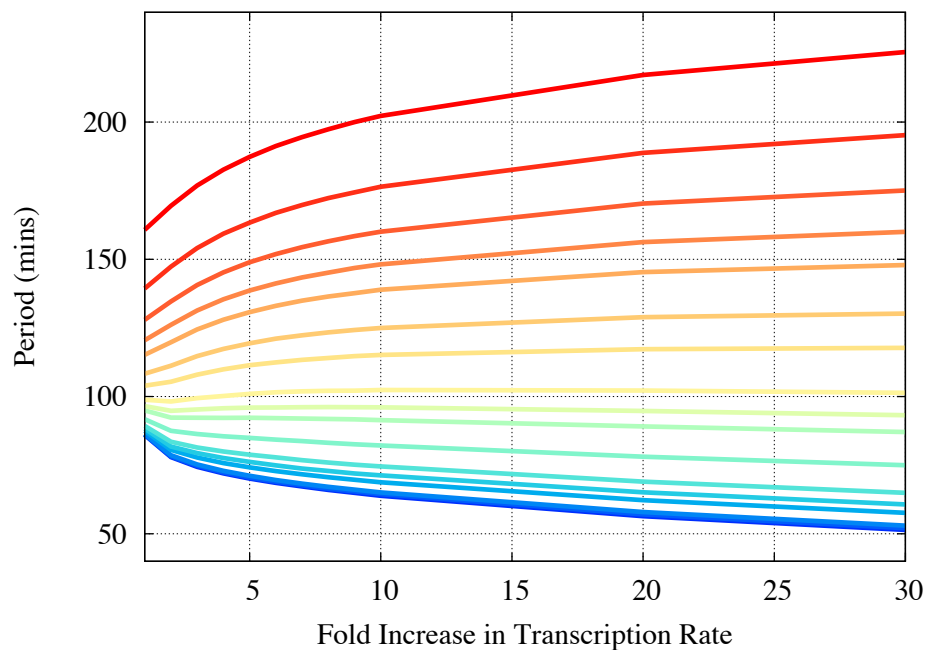


**Figure 6.19** - Period bifurcations with respect to  $\text{I}\kappa\text{B}\alpha$  transcription rate for increasing durations of transcriptional delay calculated using the  $z_0 p_0 y_0 s_0 v_0 w_1$  minimal model (Chapter 3).  $\text{I}\kappa\text{B}\alpha$  transcription rate ( $c1a$ ) was increased up to 30-fold and the corresponding limit cycle period found. Each line corresponds to a different delay in the initiation of transcription, from no delay (blue) to a 25-minute delay (red).

### 6.3.3 – Conclusions & Future Outlook

This work was motivated by physiological relationship between inflammation and fever. NF-κB is a key regulator of the inflammatory response and analysis of single-cell NF-κB dynamics at different temperatures showed varying oscillation frequencies (figure 6.10). The NF-κB network and circadian clock share many similarities in their design principles, but while the circadian clock has evolved to have a robust period in response to varying temperature, the NF-κB system appears to have done quite the opposite. A few degrees change in temperature appears to be sufficient to result in a significant change in the period of oscillations (table 6.1). The  $Q_{10}$  temperature coefficient measures the change a reaction rate for a 10°C temperature change. For oscillatory system the  $Q_{10}$  is a ratio between frequencies and can be calculated by

$$Q_{10} = (f_2/f_1)^{10/T_2-T_1}, \quad (6.12)$$

where  $f_1$  and  $f_2$  are the oscillatory frequencies at the temperatures  $T_1$  and  $T_2$ , respectively (Ruoff *et al.*, 1997). Therefore, in temperature compensated system the  $Q_{10}$  would be expected to be  $\sim 1$ , which is true of the circadian clock (Reyes *et al.*, 2008). For biochemical reactions the  $Q_{10}$  is  $\sim 2$  (Ruoff *et al.*, 1997), these data suggest that the NF-κB system has a  $Q_{10}$  of  $\sim 2.6$  (assuming a 9 minute change per °C) highlighting the temperature dependence of the NF-κB system.

The simplest explanation for this dependence is the increased thermodynamic energy in the system. Using the balance equations the Ashall model was analysed to determine if the period change could be explained in this way. This method of analysis has previously been used to understand temperature compensation in the circadian clock (Akman *et al.*, 2008). This analysis demonstrated that the current representation of the model was insufficient to explain the effect of temperature on the NF-κB dynamics. The predicted change in the period as a result of altered reaction rates was markedly less than the experimentally observed change (equation 6.11). This analysis made two key assumptions, that the Arrhenius relationship is true for the temperature range studied and the activation energies are comparable to



those that have previously been measured. If these assumptions are believed to be fair then there are two possible explanations for this discrepancy: there is a temperature-sensitive mechanism within the NF- $\kappa$ B network or the Ashall model is not a sufficiently accurate representation of the system to be able to capture the effect of temperature.

A microarray analysis was performed to determine if there were any differences in the NF- $\kappa$ B-dependent feedbacks at the different temperatures. While this analysis showed similar profiles for the I $\kappa$ B $\alpha$  and I $\kappa$ B $\epsilon$  feedbacks, A20 expression was increased 2-fold after 30 minutes of TNF $\alpha$  stimulation. Comparisons of these expression profiles lead to the hypothesis that there could be a delay in the transcription of A20. Sensitivity analyses of the Ashall model have demonstrated A20 feedback to be a key regulator of the limit cycle period (figure 6.11). Therefore, a change in the temporal dynamics of A20 transcription could have a large effect on the period. Inclusion of a delay in the transcription of A20 was sufficient to recapitulate the dynamics seen at 37°C and 40°C (figure 6.13).

In basal conditions RNA polymerase II (Pol II) is already bound to the A20 promoter and controlled by the transcription factor SP1 (Ainbinder *et al.*, 2002). The re-initiation of A20 transcription is inhibited by the presence of the factor USF1 on the promoter, which causes the DRB sensitivity-inducing factor (DSIF) to inhibit elongation of the transcript accounting for low basal expression of A20. Following TNF $\alpha$  stimulation, NF- $\kappa$ B binds to the promoter, displacing USF1 and taking over control of DSIF (Verstrepen *et al.*, 2010); NF- $\kappa$ B also recruits the positive elongation factor b (p-TEFb). These events cause elongation of the transcript and multiple rounds of A20 transcription (Amir-Zilberstein and Dikstein, 2008). This recruitment and reorganisation of factors at the promoter could provide a biological explanation for the delayed transcription hypothesis. The frequency of the re-initiation of transcription could also be responsible for the observed change in rate (figure 6.14).

Quantitative RT-PCR analysis for A20 mRNA did not conclusively prove or disprove the existence of a transcriptional delay (figure 6.14). These data suggested there could be an approximate 5-minute change in the initiation of A20 transcription

(figure 6.14d) but further analysis would be required before any definite statement could be made. It must also be noted that an increase in A20 mRNA does not necessarily correlate to an increase in the level of the protein. Western blot analysis would be a sensible next step; this would help to identify any differences in the temporal profile of the protein at different temperatures. This analysis could help to elucidate if there is a change in the level of A20 protein or the time at which it becomes detectable. However, western blot analysis would not give a true indication of the activity or spatial availability of the A20 protein (see Section 5.2.7, Chapter 5).

There was also a discrepancy between the RT-PCR and microarray data for I $\kappa$ B $\alpha$  mRNA. In the microarray analysis the I $\kappa$ B $\alpha$  mRNA levels at 37°C and 40°C are comparable at the 30-minute time-point (figure 6.12b). However, in the RT-PCR data I $\kappa$ B $\alpha$  shows a 2-fold increase after 30 minutes at 40°C (figure 6.14a). One explanation is that there appears to be a large degree of variation in the replicates in the microarray (figure 6.12b). It could also be a result of a non-ideal experimental design, the short interval between time points makes it difficult to maintain a constant temperature in the incubator due to the frequent access required for stimulation and lysing. This experiment could be better conducted in a sealed workstation, similar to a hypoxic workstation, where the cells can be accessed without disruption of the internal environment.

The quantitative RT-PCR data did suggest that the current representation of transcription of A20 and I $\kappa$ B $\alpha$  in the Ashall model is not representative of the endogenous system. In the Ashall model transcription of both I $\kappa$ B $\alpha$  and A20 occurs less than 5-minutes after stimulation, however, the data indicates at least a 5-minute delay before transcription occurs (figure 6.13 vs. figure 6.14). As a result the transcription representation of both species was altered, this resulted in a model that was able to recapitulate the NF- $\kappa$ B dynamics at both lower and higher temperatures through altering the delay in the transcription (table 6.2). Theoretical studies have demonstrated the central role transcriptional delay can play in generating oscillations (Kerszberg, 2004).

The dual delay model makes several assumptions that may not be justified, primarily the existence of a delay in the transcription of these species. However, if such a delay exists then the model also assumes the delay to be affected by temperature changes and similarly affected for both I $\kappa$ B $\alpha$  and A20. It is possible to separate this relationship by including different delay parameters for the two variables. It is interesting to note that inclusion of the delay in both I $\kappa$ B $\alpha$  and A20 results in a highly linear relationship between transcriptional delay and the period (figure 6.15d), comparable to that seen in the experimental data. It should be further noted that due to the highly linear relationship between transcription and translation in the Ashall model (figure 4.8, Chapter 4), this representation could also be equivalent to a delay in the translation of the mRNA, which has yet to be investigated.

While this altered model is not necessarily representative of the endogenous system it does provide a means to address several hypotheses about the NF- $\kappa$ B system, namely, the effect of a transcriptional delay on the period. The inclusion of a delay in transcription results in a dramatically altered relationship between the limit cycle period and I $\kappa$ B $\alpha$  transcription rate (figure 6.18). This relationship has been key question when assessing the validity of the Ashall model, the previous relationship showed a decrease in period with increased transcription rate (figure 5.1, Chapter 5) that was in contradiction to other published NF- $\kappa$ B models (Hoffmann *et al.*, 2002) and published data (Nelson *et al.*, 2004). To understand this, a deeper analysis of the effect of transcriptional delay on the period bifurcation was performed (figure 6.19). This analysis used the minimal NF- $\kappa$ B model with a linear chain included in the I $\kappa$ B $\alpha$  mRNA variable. The minimal model represents the core network topology responsible for NF- $\kappa$ B oscillations therefore, analysis of this model can more easily be generalised to other systems that contain this circuit in their topology. The analysis demonstrated that by altering the delay it was possible to invert the effect of transcription rate on the period. Moreover, there was an “optimal” delay time, which resulted in a system that was robust to a 30-fold increase in transcription rate. This implies that the delay in transcription changes the sensitivity structure of the model. This is in accordance with recent theoretical studies that have shown the inclusion of intermediary steps can change the effect of the feedback loop on the system

dynamics (Nguyen, 2012). Data presented in Chapter 5 promoted the hypothesis that the period of the NF- $\kappa$ B system is robust to a 8-fold over-expression of I $\kappa$ B $\alpha$ , this analysis has identified a potential mechanism in the design of the I $\kappa$ B $\alpha$ -NF- $\kappa$ B feedback loop that can explain this phenomenon.

The inclusion of this delay mechanism in the transcription in the Ashall model has resulted in a model that is able to qualitatively recreate the dynamics seen in response to changing temperature, pulsatile and low dose TNF $\alpha$  stimulation (figure 6.16 and figure 6.17). While the existence of a delay at the transcriptional level has not been conclusively proved, it has been demonstrated in the case of A20 there is a series of events that occur between NF- $\kappa$ B entering the nucleus and transcription of the mRNA. The inclusion of a linear chain is a crude method to include these events in the model, this can similarly be argued for the events between mRNA synthesis and the active protein. This analysis demonstrates that by increasing the complexity in the model's representation of the system it is possible to recapitulate the experimental results. Increased complexity would result in more parameters, each with a control coefficient and associated activation energy, which would help to address the imbalance in equation (6.11). This leads to the hypothesis that a finer-grained model is required to gain the necessary sensitivity to thermodynamic changes. This hypothesis draws parallels with Svante Arrhenius' first study into the effects of temperature on rate. He noted that the observed increase in kinetic energy in a product was too great to be accounted for by the increased energy of the constitutive molecules. This led to the introduction of the concept of "activated state" to define intermediary complexes within a reaction (Cossins and Bowler, 1987). An interesting future development would be to apply the minimal model algorithm (Chapter 3) to this expanded model to address the timescale of these intermediary reactions and determine if it is possible to gain a minimal temperature-sensitive model.

## 6.4 – Discussion

This chapter has shown two possible ways to alter the period of NF- $\kappa$ B oscillations. Application of the NSAID diclofenac resulted in a lengthening of the period. Further analysis is required here to determine any functional implication from treatment with the compound. One issue with the use of diclofenac as a perturbation is that its mechanism is not fully understood, computational analysis has narrowed down the possible targets to the IKK complex and components upstream of this. However, further investigation is required to confirm or disprove this hypothesis.

Another compound that has been shown to alter NF- $\kappa$ B dynamics is the SN50 peptide, which inhibits NF- $\kappa$ B nuclear translocation. Treatment of cells with SN50 showed a reduction in amplitude of the first NF- $\kappa$ B translocation (Nelson *et al.*, 2002). However, cells were only imaged for 40 minutes so there is no quantification of the peptide's effect on the oscillatory period. An interesting future line of research would be to analyse the NF- $\kappa$ B dynamics after treatment with SN50. Bifurcation analysis of the Ashall model with respect to the NF- $\kappa$ B nuclear import parameter ( $ki1$ ) shows a reduction in amplitude when  $ki1$  is decreased, in agreement with the published data. Moreover, reduction of  $ki1$  in the model predicts an extension of the period (figure 4.1, Chapter 4). Unlike diclofenac, SN50's mechanism of action is better understood and therefore this could prove a more useful modulator of the system.

The experimental data suggested there is a linear relationship between the temperature changes and the period and computational analysis showed alteration of the transcriptional representation of the negative feedback could give a model that is able to capture these data. This could suggest there is a delay in the transcription of A20 that changes with temperature; while this is an interesting hypothesis the experimental investigation was inconclusive. The delay included in the Ashall model could equally be considered a representation of translational delay, providing an alternative hypothesis that has yet to be investigated. From a modelling perspective, these findings suggest that a finer-grained model is required to fit these data.

Ultimately, substantial further analysis is required to determine which of these theoretical hypotheses is justified.

Diclofenac, like many anti-inflammatories, is a potent antipyretic (Gehanno *et al.*, 2003, Polman *et al.*, 1981). Therefore, the ability of temperature to shorten the period and diclofenac to extend it is compatible with diclofenac's antipyretic effects. An interesting future direction would be to understand the effect of these two perturbations together. A key question would be whether the combined effects of the two perturbations are additive, super-additive or less than additive with one dominating the other. The data presented herein shows diclofenac to have a far greater magnitude of effect than temperature changes. Therefore, treatment with diclofenac could dwarf the effect of increased temperature; this would be fitting with diclofenac's strong effect on pyresis.

It might be more sensible to compare perturbations that have similar magnitudes of effect, for example, A20 ectopic expression (Chapter 5) and increased temperature. This could yield some interesting insights into the hypotheses generated in this chapter about the transcriptional regulation of A20. Bifurcation analysis with respect to nuclear import ( $ki1$ ) predicts a period increase of approximately 15 minutes for a 2-fold reduction (figure 4.4, Chapter 4), indicating the potential effect of SN50 on the period. If this effect were shown to be true it provides another antagonist to increased temperature.

An understanding of how to fine-tune NF- $\kappa$ B dynamics in conjunction with a characterisation of the changes in NF- $\kappa$ B dependent gene synthesis could mark the beginning of a paradigm shift in approaching NF- $\kappa$ B as a therapeutic target. "Tuning" of the NF- $\kappa$ B dynamic in contrast to inhibition to restore physiological NF- $\kappa$ B function.

# **Chapter 7 – Final Discussion**

## 7.1 – Introduction

The network topology that defines biological signalling networks often involves numerous components and nonlinear interactions. In addition, biological systems often display emergent properties that are a result of the interactions of multiple components. Therefore, it can be difficult to understand the overall behaviour of these systems using a reductionist approach. The NF- $\kappa$ B system is a prime example of a complex, nonlinear, biological network that shows emergent properties - in this case oscillations. Systems biology provides an avenue to further our understanding of these systems; through the consideration of the multiple interactions within a network and how these give rise to the overall function of the system. One key facet of systems biology is the combination of experimental data with computational models. These computational models provide a powerful tool to analyse the system in a dynamic context. Over the last 10 years a great deal of effort has been invested in the development of computational models that can elucidate the mechanisms responsible for NF- $\kappa$ B function.

The NF- $\kappa$ B system is central in controlling inflammation and the immune response. Dysregulation of NF- $\kappa$ B has been related to a number of autoimmune dysfunctions, such as lupus, inflammatory diseases, such as arthritis, and cancers (Baud and Karin, 2009, Makarov, 2001, Sun and Andersson, 2002). This vast and ever growing list of diseases in which NF- $\kappa$ B is dysregulated has made this one of the most intensely studied eukaryotic transcription factors. A key focus of this has been drug discovery and the exploitation of NF- $\kappa$ B as a therapeutic target. However, due to the scale, diversity and conflicting nature of the cellular processes that NF- $\kappa$ B regulates this is no simple task. Key components of the network that have been targeted by drug discovery to inhibit NF- $\kappa$ B signalling include the IKK $\alpha$  and IKK $\beta$  subunits, the proteasome and ubiquitin ligases (Baud and Karin, 2009, Karin *et al.*, 2004). However, the NF- $\kappa$ B system is connected to other cellular processes, such as cell cycle and development, and can interact with other signalling pathways (Perkins, 2007). Therefore NF- $\kappa$ B inhibition can often have unwanted side effects (Karin *et al.*, 2004). The primary goal now is to develop drugs that inhibit NF- $\kappa$ B with higher



specificity, several inhibitors are currently being used to treat autoimmune disorders, which specifically neutralise a given stimuli. For example, infliximab, etanercept and adalimumab are used to inhibit TNF $\alpha$  signalling (Wong *et al.*, 2008) and canakinumab to inhibit IL-1 $\beta$  (Dhimolea, 2010). Further downstream in the pathway, focus is on the inhibition of specific kinases, such as IKK $\beta$  (Karin *et al.*, 2004).

The frequency of NF- $\kappa$ B nuclear-cytoplasmic oscillations has been demonstrated to alter the expression profiles of NF- $\kappa$ B dependent genes (Ashall *et al.*, 2009). Recent studies have highlighted an alternative route to explore when considering NF- $\kappa$ B as a therapeutic target. An understanding of how to change NF- $\kappa$ B dynamics in a physiological context could provide a new path to exploit the system for clinical gain without the unwanted side effects that can stem from inhibition. To this aim, this work has endeavoured to use a Systems Biology approach to understand the complex and nonlinear interactions that govern the NF- $\kappa$ B dynamics. The ultimate goal was to understand how the period of NF- $\kappa$ B oscillations could be altered through activation or inhibition of key nodes in the network.

## **7.2 - Reflection on Project Aims**

To characterise the effect on the NF- $\kappa$ B dynamics of each component of the network an in-depth analysis was performed of the Ashall model; this involved three analysis methods. The first was the development of a minimal model to identify the core network topology in the Ashall model. This analysis resulted in the definition of a general algorithm that can be used to reduce the dimension of many biochemical models in order to gain an insight into the core network topology. Secondly, classic sensitivity analysis tools were applied to derive a relationship between the parameters and the period of the limit cycle. Finally an in-depth bifurcation analysis of the model parameters was performed to complement the sensitivity analysis. A central focus in these three analyses was to understand how the different negative feedbacks in the Ashall model, namely I $\kappa$ B $\alpha$  and A20, influence the system both independently and synergistically. These analyses resulted in a measure of how each

of the parameters affects the solution of the Ashall model locally and over the entire range for which the limit cycle exists, both individually and for some parameters in combination. Further analysis was also conducted to address the validity of these results when multiple parameters were changed. Ultimately, these analyses provided a basis which enabled the formation of a number of hypotheses about the NF- $\kappa$ B system; specific attention was given to the effect of altering the negative feedbacks on the dynamics.

With this computational framework in place this work moved on to rationalise the Ashall *et al.* representation of the NF- $\kappa$ B system with new experimental data regarding NF- $\kappa$ B oscillations. These data were generated using live single-cell imaging of RelA, I $\kappa$ B $\alpha$  and A20 fluorescent fusion proteins. These data include new information to guide model refinement with regard to the effect of the negative feedbacks, temperature and pharmacological perturbations on the oscillation frequency. This information was used to develop the mathematical representation of the NF- $\kappa$ B system so that it was sufficient to recapitulate this new experimental data. These changes generated new predictions about the topology and function of the NF- $\kappa$ B system, which now required experimental investigation. Moreover, the model development and analysis in this work has created some interesting insights that have applications for general biochemical oscillators.

### **7.3 – Computational Methods for Analysis of Biological Models**

The dynamic systems that describe biochemical reaction networks are often extremely complex. These systems can be highly nonlinear, having a high dimensional state space, and depended on a large number of parameters. Therefore analysis methods, such as sensitivity and bifurcation analyses, as well as model reduction approaches, are key tools to aid in the comprehension of these models. A full characterisation of the dependence of the dynamic system's solution on its parameters is integral to facilitate model validation, development and hypothesis

generation. One of the primary focuses of this work was the application of these methods to a recent model of the NF- $\kappa$ B system (Ashall *et al.*, 2009). The application of several analysis methods helped to identify their strengths and limitations.

The first technique employed was a model reduction algorithm based on Tikhonov's theorems (Tikhonov, 1952). This method exploited the fact that biological reactions occur on markedly different timescales. An algorithm was developed to enable the identification of 'fast' reactions and replace them with quasi-steady state approximations (Chapter 3). Reduction of the Ashall model identified the key reactions and variables responsible for NF- $\kappa$ B oscillations. The Ashall model was designed to reproduce different solutions in response to continuous or pulsatile input. The use of this algorithm with these different input solutions resulted in different reduced models from the same originator, highlighting the importance of different phases of the IKK complex activation in controlling the response to pulsatile or continuous stimulation. This demonstrates a novel application of a model reduction method to systems that exhibit a range of dynamics. If the application of the method to different solutions results in different minimal models, then the points where they do not overlap can provide insight into the design principles.

Model reduction techniques become extremely important as the number of components in a system increases, they are useful to identify the core variables and reactions responsible for a system's dynamics. The algorithm developed herein is very general and could be applied to a number of biochemical models. The efficacy of this and other reduction methods will depend on the system represented; this algorithm's effectiveness is limited by the separation of timescale or 'stiffness' in the system. Model reduction techniques are associated with eliminating complexity and as such they are less useful for understanding the effect of individual reactions on the system's behaviour.

Sensitivity and bifurcation analyses methods provide another means to analyse computational models. These methods can be applied on a parameter-by-parameter basis and therefore it is possible to determine the effect of each reaction on the system's solution. Here, several sensitivity analyses were applied to the Ashall

model. First, the control coefficients (Rand, 2008) were calculated, these describe the effect of a small change in the parameter on the period. In addition, a bifurcation analysis was performed to determine the scale of period change predicted by the model. Each analysis method has its merits and limitations. Calculation of the control coefficients is relatively straightforward and can be performed for all parameters simultaneously, whereas bifurcation analysis is more time consuming and most software requires the computation of one bifurcation at a time. However, control coefficients only consider a small range of the parameter values and assume parameters have a linear effect. Bifurcation analysis does not make this assumption and can be extended over the whole range of parameter values for which a stable limit cycle exists. There was a high level of agreement between all three analysis methods, especially on a local range moreover, the control coefficients defined by Rand *et al.* and sensitivity measure defined herein are analogous for sufficiently small intervals of the parameter values. In practice it seems most sensible to calculate the control coefficients for all parameters and then perform bifurcations for particularly interesting ones. A key point highlighted in this theoretical analysis is the non-additive effects seen when multiple parameters are changed (Chapter 4). This is an important consideration when using these sensitivity analyses to guide model development and make predictions.

Another consideration in the application of sensitivity analysis methods is the choice of a local or global method. Local and global can refer to the range of parameter values considered or the number of parameter changes considered at one time. As has been seen with bifurcation analysis it is possible to extend this analysis to consider a larger parameter range. However, both the sensitivity and bifurcation methods discussed in Chapter 4 are essentially local as they are primarily concerned with single parameter changes. Global sensitivity analysis methods have also been developed and applied to biochemical models (Marino *et al.*, 2008). However, varying all possible combinations of parameters for a wide range of values can be computationally unfeasible for large models (van Riel, 2006). Similarly, bifurcation analysis can be extended into higher dimensions of parameter space (Chapter 5), however this becomes difficult past 3-dimensions. Ultimately, the choice of analysis method will depend upon the question asked and the time available.

## 7.4 – The Importance of Negative Feedbacks in Oscillatory Systems

In order to generate stable oscillation, such as those seen in the NF- $\kappa$ B system, the presence of a negative feedback is a necessary requirement. The oscillations of NF- $\kappa$ B are a result of the I $\kappa$ B $\alpha$  negative feedback, which is sufficiently delayed due to transcription and translation. The model reduction method identified the feedback from I $\kappa$ B $\alpha$  and A20 as integral for NF- $\kappa$ B dynamics (Chapter 3). In reality, there are other I $\kappa$ B isoforms, such as I $\kappa$ B $\epsilon$ , which are dependent on NF- $\kappa$ B (Kearns *et al.*, 2006). Therefore, I $\kappa$ B $\alpha$  in the Ashall model is representative of numerous I $\kappa$ Bs. Likewise, A20 is representative of numerous negative feedbacks that can inhibit the NF- $\kappa$ B pathway; these include CYLD and Cezanne (Enesa *et al.*, 2008, Jono *et al.*, 2004).

The different negative feedbacks displayed very different effects of the NF- $\kappa$ B dynamics. The data suggested that I $\kappa$ B $\alpha$  is central to generating oscillations but has a relatively weak influence on the period. This could be extended to other I $\kappa$ Bs, which share a similar network topology. In contrast, computational analysis showed A20 to have a strong effect on the period. Similarly, this could be extended to other feedbacks that act higher up in the pathway. For I $\kappa$ B $\epsilon$ , the timing of the negative feedback has been shown to influence the dynamics (Paszek *et al.*, 2010b). This leads to a hypothesis that the numerous feedbacks acting on different points in the pathway or limit cycle are required to control the NF- $\kappa$ B dynamics; this could be in response to different stimuli or environmental conditions. Previous studies have identified that that interplay between positive and negative feedbacks can tune the period of oscillations (Tsai *et al.*, 2008). These analyses demonstrate that negative feedbacks can also control oscillations by acting at different points in the pathway or at different times. This concept has been demonstrated in a recent study by Nguyen (2012), which showed that the existence of dual negative feedback loops could control characteristics of the limit cycle, such as period and amplitude.

Analysis of the model showed that length of delay in a negative feedback influences the solution's dependence on the production rate of this feedback (Chapter 6). This would be an interesting hypothesis to pursue in general models of oscillators. This could be achieved by analysis of the relationship between the length of delay and the parameter bifurcations for the simplest possible oscillator. The delay in a negative feedback has previously been hypothesised to be important in mediating the system's dynamic behaviour. Theoretical simulations have shown that transcriptional delay in negative feedbacks has a strong bearing on oscillations (Kerszberg, 2004). Further studies have shown the inclusion of intermediary steps markedly changes the negative feedback's effect on dynamics. Therefore if time delay is significant it "should be considered in the model for faithful representation of the system" (Nguyen, 2012). This was demonstrated in Chapter 6 where the inclusion of transcriptional delay resulted in a model that could recreate the NF- $\kappa$ B dynamics seen in response to a number of experimental conditions, namely temperature, low dose and pulsatile stimulation. In addition to negative feedbacks, NF- $\kappa$ B can induce the transcription of a number of pro-inflammatory cytokines, including TNF $\alpha$  (Tian *et al.*, 2005). Therefore, within the system there is possibility of positive feedback loops that can signal in a paracrine or autocrine fashion (Yde *et al.*, 2011). The Ashall model does not include any representation of these loops, which could also influence the oscillatory dynamics.

## **7.5 – Modulation of the NF- $\kappa$ B Period**

Many cellular networks exhibit the property of multitasking – the ability to generate different dynamics according to their operating context. For example, the p53 pathway can display multiple pulses of p53 or a single pulse in response to ionising or UV-radiation, respectively (Wong *et al.*, 2012). Multitasking networks have been proposed to have developed through expansions of pre-existing core processes, an evolutionarily plausible route to generate novel biological responses (Kirschner and Gerhart, 1998). Computational models of these networks often require different parameter sets to recreate these distinct dynamics – this has been defined as "tension"

(Wong *et al.*, 2012). In the NF- $\kappa$ B system this concept can be applied to explain the parameter alterations required for a single model to be able to recreate the NF- $\kappa$ B dynamics seen in different cell lines, or in response to different stimuli. This has already been demonstrated for pulsatile TNF $\alpha$  stimulation (Wong *et al.*, 2012). Another application could be in explaining the damped NF- $\kappa$ B oscillations seen in HeLa cells when compared to those observed in SK-N-AS cells (Nelson *et al.*, 2004). These dynamics could be achieved through alteration of the parameter sets without changing the underlying network topology. In this thesis the magnitude of period change seen in response to diclofenac was difficult to capture without the alteration of multiple parameters; this could demonstrate another example of tension (Chapter 6). This concept would be interesting to probe further by the measurement of reaction rates in cell lines that display different NF- $\kappa$ B dynamics, for example in MEF cells where the average time between peaks appears to be shorter than in SK-N-AS cells (Ashall *et al.*, 2009).

The relationship between system dynamics and function has been shown in signalling systems such as Calcium signalling and more recently the p53 pathway. In this pathway the treatment of cells with a chemical inhibitor to alter p53 dynamics from oscillatory to constitutive in response to the same stimulus resulted in altered cell fate, namely senescence (Purvis *et al.*, 2012). These studies further support the hypothesis that altered NF- $\kappa$ B dynamics can change cell function. Two perturbations were identified that changed the NF- $\kappa$ B oscillation frequency: diclofenac treatment and temperature changes. These data promoted some interesting hypotheses, however, they are still preliminary and require substantial further investigation.

Treatment with the NSAID diclofenac caused an extended period and the data promoted the hypothesis that this was due to altered IKK activity (Chapter 6). To validate these hypotheses, analysis of the IKK kinase activity after treatment with diclofenac is required. Other NSAIDs have been shown to inhibit NF- $\kappa$ B, such as salicylates, sulindac and sulphasalazine (Karin *et al.*, 2004). Their inhibitory effects are due to the inhibition of IKK activity or I $\kappa$ B $\alpha$  phosphorylation (Krakauer, 2004), in accordance with the hypothesis made herein. Therefore, it could also be interesting to characterise the NF- $\kappa$ B response after treatment with other anti-inflammatory

drugs. The analysis of differentially expressed genes after treatment with NSAIDs that alter NF- $\kappa$ B dynamics could help to inform the development drugs that target the NF- $\kappa$ B system. In addition to anti-inflammatory drugs there are other known inhibitors of NF- $\kappa$ B activity, these can influence nuclear import, the proteasome or NF- $\kappa$ B transcriptional activity (Karin *et al.*, 2004). A quantification of their effect on NF- $\kappa$ B dynamics and gene expression profiles could provide further information when considering the pathway in a clinical context.

The oscillation frequency was also shown to be sensitive to temperature changes; this result is interesting in itself as other oscillatory systems, such as the circadian clock have been shown to be temperature-compensated (Rensing and Ruoff, 2002). There is a fundamental relationship between pyresis and inflammation; the change in NF- $\kappa$ B dynamics in response to increased temperature could be advantageous as it heightens the anti-inflammatory response. This is evidenced by the increased production of chemokines and cytokines in the microarray performed at 40°C in comparison to 37°C (Dr C. Harper and Dr L. Ashall, SMC, unpublished data). This proposes an interesting hypothesis about distinctive evolutionary paths, to compensate for or to exploit environmental changes depending on how these changes affect cell fate.

Anti-inflammatory drugs, including diclofenac, have also been show to be effective as antipyretic drugs (Gehanno *et al.*, 2003), and NF- $\kappa$ B activation has been linked to pyresis (Salanova *et al.*, 2005). These studies coupled with the complementary effects of reduced temperature and diclofenac treatment on the oscillation period could suggest a mechanism in part responsible for their antipyretic effects. An interesting future direction would be to experiment with multiple period perturbations and determine if it is possible to rescue a normal phenotype through the application of multiple effectors; for example, treatment with diclofenac to slow oscillations at higher temperatures. This analysis could also be extended to unrelated perturbations to demonstrate how to target aspects of the pathway for clinical gain. For example, the model predicts SN50 to have a similar but lesser effect to diclofenac (Chapter 6). A combination of SN50 and temperature experiments could show a novel anti-inflammatory target, namely nuclear import.



NF- $\kappa$ B dynamics are context-dependent, varying for different cell types or in response to different stimuli, recently a study has shown the NF- $\kappa$ B response to depend upon the cell's point in the cell cycle (*Dr J. Ankers, CCI, University of Liverpool, publication in progress*). The coupling between dynamic cellular processes such as cell cycle, NF- $\kappa$ B and p53 represents a way for cells to make cell fate decisions based on their intra- and extracellular context. Crosstalk has been identified between p53 and NF- $\kappa$ B and simultaneous activation and inhibition of these antagonistic pathways has been proposed as a means to increase efficacy of cancer treatments (Dey *et al.*, 2008), in addition cell cycle location can affect tolerance to cancer therapies (Levi *et al.*, 2010). Therefore, an understanding of the interaction between coupled processes could be beneficial in future drug development, moreover, this understanding requires a systems level approach.

## **7.6 – Future Perspective**

The key role of A20 in the NF- $\kappa$ B system was demonstrated several times in this thesis. Over-expression of A20 increased the period of oscillations (Chapter 5); this analysis also demonstrated a perinuclear localisation of A20. Computational analysis highlighted the importance of A20-related parameters in controlling the frequency of oscillations. Moreover, microarray analysis demonstrated a differential expression in A20 between temperatures. These observations highlight the A20 feedback loop as an important area for future study. The single-cell dynamics of A20 are still preliminary, further analysis is required to confirm the magnitude of the period change for ectopic expression. It would also be interesting to determine if specific inhibition of A20 mRNA production using RNA interference also alters the oscillation period. Other live cell microscopy experiments could also help to elucidate the function of A20. These include co-localisation experiments to determine the function of A20 sequestration. Fluorescent Correlation Spectroscopy can identify binding of A20 to components of the signalling pathway. These data could help to elucidate the inhibitory function of this protein *in cellulo*.

Numerous avenues can be explored to develop the model presented in Ashall *et al.* (2009) but they will require the production of experimental data in order to constrain model parameters. The prediction regarding diclofenac inspires a more thorough representation of the pathway upstream of the IKK complex. This could provide insight into the effect of this and other NSAIDs on the NF- $\kappa$ B system. In addition, it could also help to test predications regarding the function of A20 as more experimental data is generated. Some A20 parameters are not constrained by experimental measurements, such as protein half-life. This could motivate the inclusion of other negative feedbacks to de-convolve the function of A20. The Ashall model is also limited in its representation of transcription and translation; this analysis has shown the inclusion of more non-linearity in these terms can result in a single model with the ability to fit a larger spectrum of experimental data (Section 6.3.2.7, Chapter 6).

Beyond a representation of the core network there are other possible developments such as stochastic and spatial models, which could help to address questions regarding noise, paracrine and autocrine signalling. The choice of model development will depend on the question being addressed. Each addition can increase the complexity of the model and there will be a point where a single model becomes impractical. In practice, a series of working models is required where each performs a different function. This could include a fine-grained representation to address questions regarding the network topology in the single cell. Minimal models with the addition positive feedbacks can be derived from this for the simulation of multi-cellular models. Stochastic representation could also be developed for either the full or minimal model to address the effect of noise in the system.

This work has primarily considered the timing of NF- $\kappa$ B translocations to be the key factor in controlling gene expression. However, in practice this is a more complex process. NF- $\kappa$ B subunits are subject to a number of different post-translational modifications, including phosphorylation and acetylation. These modifications have been shown to affect the transactivation and translocation of NF- $\kappa$ B dimers in response to different stimuli (Perkins, 2006). Therefore an understanding of the effect of the post-translational modification will also help to inform the use of NF-

$\kappa$ B as a therapeutic target. Inhibition or activation of kinases, phosphatases, acetyltransferases and deacetyltransferases could provide an additional means to control NF- $\kappa$ B function. Inclusion of different functional NF- $\kappa$ B species could be a future development of the model however, there is not currently enough data regarding the regulation of posttranslational modifications to represent these in a non-trivial fashion.

The key focus of the analysis was on the period, for the ease of hypothesis generation NF- $\kappa$ B activation was considered a digital process and the effect of the translocation amplitude on gene expression was largely ignored. There is very little quantification in the literature about the effect of amplitude on NF- $\kappa$ B-dependent synthesis, while frequency has been demonstrated to have a profound impact. The amplitude of  $\text{Ca}^{2+}$  oscillations has been shown to be important (Berridge *et al.*, 1998), this might also be the case for the NF- $\kappa$ B system. The bifurcation analysis presented here could easily be adapted to identify parameters that have a strong impact on NF- $\kappa$ B amplitude. If it were possible to prove these effects *in vivo* or *in cellulo*, this would highlight a novel and complementary avenue to explore in the NF- $\kappa$ B system. However, the current experimental protocol shows variable amplitudes of NF- $\kappa$ B translocation before normalisation (Nelson *et al.*, 2004), most likely due to the differences in copy number resulting from transient transfection. The use of stable cells lines will be key in investigating amplitude. In addition, the endogenous NF- $\kappa$ B protein is also present in the cells analysed and therefore there is a proportion of nuclear NF- $\kappa$ B that is not quantified.

## **7.7 – Final Comment**

The work presented herein has generated some new insights into the NF- $\kappa$ B system. These include, preliminary quantification of the effect of A20 ectopic expression and diclofenac treatment on the system. In the case of diclofenac, this could have interesting implications for NSAIDs in general. This work has also resulted in the development of new analysis tools that can be applied to other biochemical models,

such as the sensitivity analysis (Chapter 4) or model reduction algorithm (Chapter 3). Moreover, the application of these has resulted in some intuitions that could be useful for computational modelling in general. For example, the non-additive effects of multiple parameter changes (Chapter 4) or the relationship between delay and production rate in negative feedback motifs (Chapter 6).

To understand the data presented in this thesis a number of computational analysis methods were employed. This in turn led to the development of several updated NF- $\kappa$ B models in order to explain the results, in some cases the analysis method itself generated a new NF- $\kappa$ B model. This reinforces the idea that a series of models are required for a Systems approach. In biological experimentation no single technique is sufficient to address all hypotheses. Likewise, no single model will be sufficient, or practical, to address all *in silico* predictions.

Several compounds have been identified that can or potentially could influence NF- $\kappa$ B dynamics. This has included existing pharmaceuticals that were not designed to target the NF- $\kappa$ B system. The next step in the exploration of the motivating hypothesis is to determine the differences in NF- $\kappa$ B output in response to these perturbations. A way to recreate this differential output with a high fidelity is also required; this could be through the application of single or multiple effectors. If these questions can be addressed then it could represent a new paradigm for the exploitation of NF- $\kappa$ B as a drug target – ‘fine-tuning’ rather than inhibition.

This work only represents one turn of the Systems Biology cycle. The data presented led to the proposal of a number of hypotheses about the structure and function of the NF- $\kappa$ B system. The next step is to validate these hypotheses in experimental models. This will no doubt lead to some surprises and a new batch of interesting and non-intuitive data, which will require further computational modelling to understand.

# **Chapter 8 – Bibliography**

- AGGARWAL, B. B. 2004. Nuclear factor-kappaB: the enemy within. *Cancer Cell*, 6, 203-8.
- AINBINDER, E., REVACH, M., WOLSTEIN, O., MOSHONOV, S., DIAMANT, N. & DIKSTEIN, R. 2002. Mechanism of rapid transcriptional induction of tumor necrosis factor alpha-responsive genes by NF-kappaB. *Mol Cell Biol*, 22, 6354-62.
- AKMAN, O. E., LOCKE, J. C., TANG, S., CARRE, I., MILLAR, A. J. & RAND, D. A. 2008. Isoform switching facilitates period control in the *Neurospora crassa* circadian clock. *Mol Syst Biol*, 4, 164.
- ALBERTS, B. 2002. *Molecular biology of the cell*, New York, Garland Science.
- ALON, U. 2007. *An introduction to systems biology : design principles of biological circuits*, Boca Raton, FL, Chapman & Hall/CRC.
- ALON, U., SURETTE, M. G., BARKAI, N. & LEIBLER, S. 1999. Robustness in bacterial chemotaxis. *Nature*, 397, 168-171.
- AMIR-ZILBERSTEIN, L. & DIKSTEIN, R. 2008. Interplay between E-box and NF-kappaB in regulation of A20 gene by DRB sensitivity-inducing factor (DSIF). *J Biol Chem*, 283, 1317-23.
- ARENZANA-SEISDEDOS, F., TURPIN, P., RODRIGUEZ, M., THOMAS, D., HAY, R. T., VIRELIZIER, J. L. & DARGEMONT, C. 1997. Nuclear localization of I kappa B alpha promotes active transport of NF-kappa B from the nucleus to the cytoplasm. *J Cell Sci*, 110 ( Pt 3), 369-78.
- ASHALL, L., HORTON, C. A., NELSON, D. E., PASZEK, P., HARPER, C. V., SILLITOE, K., RYAN, S., SPILLER, D. G., UNITT, J. F., BROOMHEAD, D. S., KELL, D. B., RAND, D. A., SEE, V. & WHITE, M. R. 2009. Pulsatile stimulation determines timing and specificity of NF-kappaB-dependent transcription. *Science*, 324, 242-6.
- BAEUEERLE, P. A. & BALTIMORE, D. 1988. Activation of DNA-binding activity in an apparently cytoplasmic precursor of the NF-kappa B transcription factor. *Cell*, 53, 211-7.
- BALDWIN, A. S., JR. 1996. The NF-kappa B and I kappa B proteins: new discoveries and insights. *Annu Rev Immunol*, 14, 649-83.
- BAUD, V. & KARIN, M. 2009. Is NF-kappaB a good target for cancer therapy? Hopes and pitfalls. *Nat Rev Drug Discov*, 8, 33-40.
- BEG, A. A. & BALDWIN, A. S. 1993. The I-Kappa-B Proteins - Multifunctional Regulators of Rel/Nf-Kappa-B Transcription Factors. *Genes & Development*, 7, 2064-2070.
- BEG, A. A. & BALTIMORE, D. 1996. An essential role for NF-kappaB in preventing TNF-alpha-induced cell death. *Science*, 274, 782-4.
- BEG, A. A., SHA, W. C., BRONSON, R. T. & BALTIMORE, D. 1995. Constitutive NF-kappa B activation, enhanced granulopoiesis, and neonatal lethality in I kappa B alpha-deficient mice. *Genes Dev*, 9, 2736-46.
- BERNABEU, M. O., BORDAS, R., PATHMANATHAN, P., PITT-FRANCIS, J., COOPER, J., GARNY, A., GAVAGHAN, D. J., RODRIGUEZ, B., SOUTHERN, J. A. & WHITELEY, J. P. 2009. CHASTE: incorporating a novel multi-scale spatial and temporal algorithm into a large-scale open source library. *Philosophical Transactions of the Royal Society a-Mathematical Physical and Engineering Sciences*, 367, 1907-1930.

- BERRIDGE, M. J., BOOTMAN, M. D. & LIPP, P. 1998. Calcium - a life and death signal. *Nature*, 395, 645-648.
- BHALLA, U. S. & IYENGAR, R. 1999. Emergent properties of networks of biological signaling pathways. *Science*, 283, 381-7.
- BIAN, Q. A. & BELMONT, A. S. 2010. BAC TG-EMBED: one-step method for high-level, copy-number-dependent, position-independent transgene expression. *Nucleic Acids Res*, 38.
- BIKTASHEVA, I. V., SIMITEV, R. D., SUCKLEY, R. & BIKTASHEV, V. N. 2006. Asymptotic properties of mathematical models of excitability. *Philos Transact A Math Phys Eng Sci*, 364, 1283-98.
- BIRBACH, A., GOLD, P., BINDER, B. R., HOFER, E., DE MARTIN, R. & SCHMID, J. A. 2002. Signaling molecules of the NF-kappa B pathway shuttle constitutively between cytoplasm and nucleus. *Journal of Biological Chemistry*, 277, 10842-10851.
- BOLOURI, H. & DAVIDSON, E. H. 2002. Modeling transcriptional regulatory networks. *Bioessays*, 24, 1118-1129.
- BORISUK, M. T. & TYSON, J. J. 1998. Bifurcation analysis of a model of mitotic control in frog eggs. *Journal of Theoretical Biology*, 195, 69-85.
- BOX, G. E. P. & DRAPER, N. R. 1987. *Empirical model-building and response surfaces*, New York, Wiley.
- BRADY, C. A., JIANG, D., MELLO, S. S., JOHNSON, T. M., JARVIS, L. A., KOZAK, M. M., KENZELMANN BROZ, D., BASAK, S., PARK, E. J., MCLAUGHLIN, M. E., KARNEZIS, A. N. & ATTARDI, L. D. 2011. Distinct p53 transcriptional programs dictate acute DNA-damage responses and tumor suppression. *Cell*, 145, 571-83.
- BRITTON, N. F. 2003. *Essential mathematical biology*, London ; New York, Springer.
- BRUGGEMAN, F. J., BLUTHGEN, N. & WESTERHOFF, H. V. 2009. Noise management by molecular networks. *PLoS Comput Biol*, 5, e1000506.
- CARLOTTI, F., DOWER, S. K. & QWARNSTROM, E. E. 2000. Dynamic shuttling of nuclear factor kappa B between the nucleus and cytoplasm as a consequence of inhibitor dissociation. *J Biol Chem*, 275, 41028-34.
- CHANCE, B., GHOSH, A. & ESTABROOK, R. W. 1964. Damped Sinusoidal Oscillations of Cytoplasmic Reduced Pyridine Nucleotide in Yeast Cells. *Proc Natl Acad Sci U S A*, 51, 1244-&.
- CHAO, B. H., HE, X. & BISCHOF, J. C. 2004. Pre-treatment inflammation induced by TNF-alpha augments cryosurgical injury on human prostate cancer. *Cryobiology*, 49, 10-27.
- CHEN, G. & GOEDDEL, D. V. 2002. TNF-R1 signaling: a beautiful pathway. *Science*, 296, 1634-5.
- CHEN, L. F. & GREENE, W. C. 2004. Shaping the nuclear action of NF-kappaB. *Nat Rev Mol Cell Biol*, 5, 392-401.
- CHEONG, R., BERGMANN, A., WERNER, S. L., REGAL, J., HOFFMANN, A. & LEVCHENKO, A. 2006. Transient IkappaB kinase activity mediates temporal NF-kappaB dynamics in response to a wide range of tumor necrosis factor-alpha doses. *J Biol Chem*, 281, 2945-50.
- CHEONG, R., HOFFMANN, A. & LEVCHENKO, A. 2008. Understanding NF-kappaB signaling via mathematical modeling. *Mol Syst Biol*, 4, 192.

- CHO, K. H., SHIN, S. Y., LEE, H. W. & WOLKENHAUER, O. 2003. Investigations into the analysis and modeling of the TNF alpha-mediated NF-kappa B-signaling pathway. *Genome Res*, 13, 2413-22.
- COSSINS, A. R. & BOWLER, K. 1987. *Temperature biology of animals*, London ; New York, Chapman and Hall.
- DADA, J. O. & MENDES, P. 2011. Multi-scale modelling and simulation in systems biology. *Integrative Biology*, 3, 86-96.
- DASTIDAR, S. G., GANGULY, K., CHAUDHURI, K. & CHAKRABARTY, A. N. 2000. The anti-bacterial action of diclofenac shown by inhibition of DNA synthesis. *Int J Antimicrob Agents*, 14, 249-51.
- DEY, A., TERGAONKAR, V. & LANE, D. P. 2008. Double-edged swords as cancer therapeutics: simultaneously targeting p53 and NF-kappaB pathways. *Nat Rev Drug Discov*, 7, 1031-40.
- DHIMOLEA, E. 2010. Canakinumab. *MAbs*, 2, 3-13.
- DHOOGHE, A., GOVAERTS, W. & KUZNETSOV, Y. A. 2003. Matcont: A Matlab Package for Numerical Bifurcation Analysis of Odes. *Acm Transactions on Mathematical Software*, 29, 141-164.
- DOEDEL, E., PAFFENROTH, R. C., CHAMPNEYS, A. R., FAIRGRIEVE, T. F., KUZNETSOV, Y. A., SANDSTEDTE, B. & WANG, X. 2000. AUTO2000: Continuation and bifurcation software for ordinary differential equations (with HomCont). California Institute of Technology.
- DU, C. J., MARCELLO, M., SPILLER, D. G., WHITE, M. R. & BRETSCHNEIDER, T. 2010. Interactive segmentation of clustered cells via geodesic commute distance and constrained density weighted Nystrom method. *Cytometry A*, 77, 1137-47.
- DUBITZKY, W. 2006. Understanding the computational methodologies of systems biology. *Briefings in Bioinformatics*, 7, 315-7.
- EA, C. K., DENG, L., XIA, Z. P., PINEDA, G. & CHEN, Z. J. 2006. Activation of IKK by TNFalpha requires site-specific ubiquitination of RIP1 and polyubiquitin binding by NEMO. *Molecular Cell*, 22, 245-57.
- EISSING, T., KUEPFER, L., BECKER, C., BLOCK, M., COBOEKEN, K., GAUB, T., GOERLITZ, L., JAEGER, J., LOOSEN, R., LUDEWIG, B., MEYER, M., NIEDERALT, C., SEVESTRE, M., SIEGMUND, H. U., SOLODENKO, J., THELEN, K., TELLE, U., WEISS, W., WENDL, T., WILLMANN, S. & LIPPERT, J. 2011. A computational systems biology software platform for multiscale modeling and simulation: integrating whole-body physiology, disease biology, and molecular reaction networks. *Front Physiol*, 2, 4.
- ENESA, K., ZAKKAR, M., CHAUDHURY, H., LUONG, L. A., RAWLINSON, L., MASON, J. C., HASKARD, D. O., DEAN, J. L. E. & EVANS, P. C. 2008. NF-kappa B suppression by the deubiquitinating enzyme Cezanne - A novel negative feedback loop in pro-inflammatory signaling. *Journal of Biological Chemistry*, 283, 7036-7045.
- ERMENTROUT, B. 2002. *Simulating, analysing, and animating dynamical systems: a guide to XPPAUT for researchers and students.*, SIAM.
- FEMINO, A., FAY, F. S., FOGARTY, K. & SINGER, R. H. 1998. Visualization of single RNA transcripts in situ. *Science*, 280, 585-590.
- FENICHEL, N. 1979. Geometric Singular Perturbation-Theory for Ordinary Differential-Equations. *Journal of Differential Equations*, 31, 53-98.



- FREDRIKSSON, L., HERPERS, B., BENEDETTI, G., MATADIN, Q., PUIGVERT, J. C., DE BONT, H., DRAGOVIC, S., VERMEULEN, N. P., COMMANDEUR, J. N., DANEN, E., DE GRAAUW, M. & VAN DE WATER, B. 2011. Diclofenac inhibits tumor necrosis factor-alpha-induced nuclear factor-kappaB activation causing synergistic hepatocyte apoptosis. *Hepatology*, 53, 2027-41.
- FRIESEN, W. O. & BLOCK, G. D. 1984. What Is a Biological Oscillator. *American Journal of Physiology*, 246, R847-R851.
- FRY, F. E. 1958. Temperature compensation. *Annu Rev Physiol*, 20, 207-24.
- GARDNER, G. F. & FELDMAN, J. F. 1981. Temperature Compensation of Circadian Period Length in Clock Mutants of *Neurospora crassa*. *Plant Physiol*, 68, 1244-8.
- GARG, A. & AGGARWAL, B. B. 2002. Nuclear transcription factor-kappaB as a target for cancer drug development. *Leukemia*, 16, 1053-68.
- GEHANNO, P., DREISER, R. L., IONESCU, E., GOLD, M. & LIU, J. M. 2003. Lowest effective single dose of diclofenac for antipyretic and analgesic effects in acute febrile sore throat. *Clin Drug Investig*, 23, 263-71.
- GERARD, C., GONZE, D. & GOLDBETER, A. 2009. Dependence of the period on the rate of protein degradation in minimal models for circadian oscillations. *Philos Transact A Math Phys Eng Sci*, 367, 4665-83.
- GERONDAKIS, S., GROSSMANN, M., NAKAMURA, Y., POHL, T. & GRUMONT, R. 1999. Genetic approaches in mice to understand Rel/NF-kappaB and IkappaB function: transgenics and knockouts. *Oncogene*, 18, 6888-95.
- GEVA-ZATORSKY, N., ROSENFELD, N., ITZKOVITZ, S., MILO, R., SIGAL, A., DEKEL, E., YARNITZKY, T., LIRON, Y., POLAK, P., LAHAV, G. & ALON, U. 2006. Oscillations and variability in the p53 system. *Mol Syst Biol*, 2, 2006 0033.
- GHOSH, S., MAY, M. J. & KOPP, E. B. 1998. NF-kappa B and Rel proteins: evolutionarily conserved mediators of immune responses. *Annu Rev Immunol*, 16, 225-60.
- GILLESPIE, D. T. 2007. Stochastic simulation of chemical kinetics. *Annual Review of Physical Chemistry*, 58, 35-55.
- GOLDBETER, A. 1995. A Model for Circadian Oscillations in the *Drosophila* Period Protein (Per). *Proceedings of the Royal Society of London Series B-Biological Sciences*, 261, 319-324.
- GOLDBETER, A. 2002. Computational approaches to cellular rhythms. *Nature*, 420, 238-45.
- GOLDBETER, A. & LEFEVER, R. 1972. Dissipative Structures for an Allosteric Model - Application to Glycolytic Oscillations. *Biophysical Journal*, 12, 1302-&.
- GOULD, P. D., LOCKE, J. C., LARUE, C., SOUTHERN, M. M., DAVIS, S. J., HANANO, S., MOYLE, R., MILICH, R., PUTTERILL, J., MILLAR, A. J. & HALL, A. 2006. The molecular basis of temperature compensation in the *Arabidopsis* circadian clock. *Plant Cell*, 18, 1177-87.
- HAEFNER, J. 2005. Modeling Biological Systems. *Models of Systems*. Springer US.
- HALE, J. K. & KOÇAK, H. S. 1991. *Dynamics and bifurcations*, New York, Springer-Verlag.

- HARPER, C. V., FINKENSTADT, B., WOODCOCK, D. J., FRIEDRICHSEN, S., SEMPRINI, S., ASHALL, L., SPILLER, D. G., MULLINS, J. J., RAND, D. A., DAVIS, J. R. E. & WHITE, M. R. H. 2011. Dynamic Analysis of Stochastic Transcription Cycles. *Plos Biology*, 9.
- HAYDEN, M. S. & GHOSH, S. 2008. Shared principles in NF-kappaB signaling. *Cell*, 132, 344-62.
- HESS, S. T., HUANG, S., HEIKAL, A. A. & WEBB, W. W. 2002. Biological and chemical applications of fluorescence correlation spectroscopy: a review. *Biochemistry*, 41, 697-705.
- HODGKIN, A. L. & HUXLEY, A. F. 1952. A Quantitative Description of Membrane Current and Its Application to Conduction and Excitation in Nerve. *Journal of Physiology-London*, 117, 500-544.
- HOFFMANN, A. & BALTIMORE, D. 2006. Circuitry of nuclear factor kappaB signaling. *Immunol Rev*, 210, 171-86.
- HOFFMANN, A., LEVCHENKO, A., SCOTT, M. L. & BALTIMORE, D. 2002. The IkappaB-NF-kappaB signaling module: temporal control and selective gene activation. *Science*, 298, 1241-5.
- HORTON, C. A. 2006. *Computational Modelling of Cell Signalling Pathway Dynamics*. PhD, University of Liverpool.
- HUTTI, J. E., TURK, B. E., ASARA, J. M., MA, A., CANTLEY, L. C. & ABBOTT, D. W. 2007. IkappaB kinase beta phosphorylates the K63 deubiquitinase A20 to cause feedback inhibition of the NF-kappaB pathway. *Mol Cell Biol*, 27, 7451-61.
- IDEKER, T., GALITSKI, T. & HOOD, L. 2001. A new approach to decoding life: systems biology. *Annu Rev Genomics Hum Genet*, 2, 343-72.
- IHEKWABA, A. E., BROOMHEAD, D. S., GRIMLEY, R., BENSON, N., WHITE, M. R. & KELL, D. B. 2005. Synergistic control of oscillations in the NF-kappaB signalling pathway. *Syst Biol (Stevenage)*, 152, 153-60.
- IHEKWABA, A. E., BROOMHEAD, D. S., GRIMLEY, R. L., BENSON, N. & KELL, D. B. 2004. Sensitivity analysis of parameters controlling oscillatory signalling in the NF-kappaB pathway: the roles of IKK and IkappaBalpha. *Syst Biol (Stevenage)*, 1, 93-103.
- IRVING, A. D. 1992. Stochastic Sensitivity Analysis. *Applied Mathematical Modelling*, 16, 3-15.
- JONO, H., LIM, J. H., CHEN, L. F., XU, H. D., TROMPOUKI, E., PAN, Z. X. K., MOSIALOS, G. & LI, J. D. 2004. NF-kappa B is essential for induction of CYLD, the negative regulator of NF-kappa B - Evidence for a novel inducible autoregulatory feedback pathway. *Journal of Biological Chemistry*, 279, 36171-36174.
- JORDAN, J. D., LANDAU, E. M. & IYENGAR, R. 2000. Signaling networks: the origins of cellular multitasking. *Cell*, 103, 193-200.
- KARIN, M. 1999. How NF-kappaB is activated: the role of the IkappaB kinase (IKK) complex. *Oncogene*, 18, 6867-74.
- KARIN, M., YAMAMOTO, Y. & WANG, Q. M. 2004. The IKK NF-kappa B system: a treasure trove for drug development. *Nat Rev Drug Discov*, 3, 17-26.
- KEARNS, J. D., BASAK, S., WERNER, S. L., HUANG, C. S. & HOFFMANN, A. 2006. IkappaBepsilon provides negative feedback to control NF-kappaB

- oscillations, signaling dynamics, and inflammatory gene expression. *J Cell Biol*, 173, 659-64.
- KELL, D. B. 2006. Systems biology, metabolic modelling and metabolomics in drug discovery and development. *Drug Discov Today*, 11, 1085-92.
- KENNEDY, S. M. 2010. *Imaging cell arrays*, Liverpool, Thesis Ph.D.
- KERSZBERG, M. 2004. Noise, delays, robustness, canalization and all that. *Curr Opin Genet Dev*, 14, 440-5.
- KHOLODENKO, B. N. 2006. Cell-signalling dynamics in time and space. *Nat Rev Mol Cell Biol*, 7, 165-76.
- KIELHOFER, H. R. 2003. *Bifurcation theory : an introduction with applications to PDEs*, New York, Springer.
- KIRSCHNER, M. & GERHART, J. 1998. Evolvability. *Proc Natl Acad Sci U S A*, 95, 8420-7.
- KITANO, H. 2002a. Computational systems biology. *Nature*, 420, 206-210.
- KITANO, H. 2002b. Systems biology: A brief overview. *Science*, 295, 1662-1664.
- KLIPP, E. & LIEBERMEISTER, W. 2006. Mathematical modeling of intracellular signaling pathways. *BMC Neurosci*, 7 Suppl 1, S10.
- KLONOWSKI, W. 1983. Simplifying Principles for Chemical and Enzyme Reaction-Kinetics. *Biophysical Chemistry*, 18, 73-87.
- KOLCH, W., CALDER, M. & GILBERT, D. 2005. When kinases meet mathematics: the systems biology of MAPK signalling. *FEBS Lett*, 579, 1891-1895.
- KRAKAUER, T. 2004. Molecular therapeutic targets in inflammation: cyclooxygenase and NF-kappaB. *Curr Drug Targets Inflamm Allergy*, 3, 317-24.
- KRIKOS, A., LAHERTY, C. D. & DIXIT, V. M. 1992. Transcriptional activation of the tumor necrosis factor alpha-inducible zinc finger protein, A20, is mediated by kappa B elements. *J Biol Chem*, 267, 17971-6.
- KRISHNA, S., JENSEN, M. H. & SNEPPEN, K. 2006. Minimal model of spiky oscillations in NF-kappaB signaling. *Proc Natl Acad Sci U S A*, 103, 10840-5.
- KUZNETSOV, I. U. A. 2004. *Elements of applied bifurcation theory*, New York, Springer.
- LAHAV, G., ROSENFELD, N., SIGAL, A., GEVA-ZATORSKY, N., LEVINE, A. J., ELOWITZ, M. B. & ALON, U. 2004. Dynamics of the p53-Mdm2 feedback loop in individual cells. *Nat Genet*, 36, 147-50.
- LAM, S. H. & GOUSSIS, D. A. 1994. The Csp Method for Simplifying Kinetics. *International Journal of Chemical Kinetics*, 26, 461-486.
- LEE, E. G., BOONE, D. L., CHAI, S., LIBBY, S. L., CHIEN, M., LODOLCE, J. P. & MA, A. 2000. Failure to regulate TNF-induced NF-kappaB and cell death responses in A20-deficient mice. *Science*, 289, 2350-4.
- LEE, J. J., HUANG, W. T., SHAO, D. Z., LIAO, J. F. & LIN, M. T. 2003. Blocking NF-kappaB activation may be an effective strategy in the fever therapy. *Jpn J Physiol*, 53, 367-75.
- LEV BAR-OR, R., MAYA, R., SEGEL, L. A., ALON, U., LEVINE, A. J. & OREN, M. 2000. Generation of oscillations by the p53-Mdm2 feedback loop: a theoretical and experimental study. *Proc Natl Acad Sci U S A*, 97, 11250-5.

- LEVI, F., OKYAR, A., DULONG, S., INNOMINATO, P. F. & CLAIRAMBAULT, J. 2010. Circadian Timing in Cancer Treatments. *Annual Review of Pharmacology and Toxicology*, 50, 377-421.
- LEVINS, R. 1966. Strategy of Model Building in Population Biology. *American Scientist*, 54, 421-&.
- LI, L., HAILEY, D. W., SOETANDYO, N., LI, W., LIPPINCOTT-SCHWARTZ, J., SHU, H. B. & YE, Y. 2008. Localization of A20 to a lysosome-associated compartment and its role in NF-kappaB signaling. *Biochim Biophys Acta*, 1783, 1140-9.
- LI, L., SOETANDYO, N., WANG, Q. & YE, Y. 2009. The zinc finger protein A20 targets TRAF2 to the lysosomes for degradation. *Biochim Biophys Acta*, 1793, 346-53.
- LI, Q. & VERMA, I. M. 2002. NF-kappaB regulation in the immune system. *Nat Rev Immunol*, 2, 725-34.
- LIN, Y. Z., YAO, S. Y., VEACH, R. A., TORGERSON, T. R. & HAWIGER, J. 1995. Inhibition of nuclear translocation of transcription factor NF-kappa B by a synthetic peptide containing a cell membrane-permeable motif and nuclear localization sequence. *J Biol Chem*, 270, 14255-8.
- LIPNIACKI, T., PASZEK, P., BRASIER, A. R., LUXON, B. & KIMMEL, M. 2004. Mathematical model of NF-kappaB regulatory module. *J Theor Biol*, 228, 195-215.
- LIPNIACKI, T., PASZEK, P., BRASIER, A. R., LUXON, B. A. & KIMMEL, M. 2006. Stochastic regulation in early immune response. *Biophysical Journal*, 90, 725-742.
- LIPNIACKI, T., PUSZYNSKI, K., PASZEK, P., BRASIER, A. R. & KIMMEL, M. 2007. Single TNF alpha trimers mediating NF-kappa B activation: stochastic robustness of NF-kappa B signaling. *BMC Bioinformatics*, 8.
- MA, W., TRUSINA, A., EL-SAMAD, H., LIM, W. A. & TANG, C. 2009. Defining network topologies that can achieve biochemical adaptation. *Cell*, 138, 760-73.
- MACAL, C. M. & NORTH, M. J. 2010. Toward Teaching Agent-Based Simulation. *Proceedings of the 2010 Winter Simulation Conference*, 268-277.
- MAEDA, Y., PAKDAMAN, K., NOMURA, T., DOI, S. & SATO, S. 1998. Reduction of a model for an Onchidium pacemaker neuron. *Biological Cybernetics*, 78, 265-276.
- MAKAROV, S. S. 2001. NF-kappa B in rheumatoid arthritis: a pivotal regulator of inflammation, hyperplasia, and tissue destruction. *Arthritis Res*, 3, 200-6.
- MARINO, S., HOGUE, I. B., RAY, C. J. & KIRSCHNER, D. E. 2008. A methodology for performing global uncertainty and sensitivity analysis in systems biology. *Journal of Theoretical Biology*, 254, 178-196.
- MATTERN, D. L., FORMAN, L. R. & BRODY, S. 1982. Circadian rhythms in *Neurospora crassa*: a mutation affecting temperature compensation. *Proc Natl Acad Sci U S A*, 79, 825-9.
- MATTIOLI, I., SEBALD, A., BUCHER, C., CHARLES, R. P., NAKANO, H., DOI, T., KRACHT, M. & SCHMITZ, M. L. 2004. Transient and selective NF-kappa B p65 serine 536 phosphorylation induced by T cell costimulation is mediated by I kappa B kinase beta and controls the kinetics of p65 nuclear import. *J Immunol*, 172, 6336-44.

- MCADAMS, H. H. & ARKIN, A. 1999. It's a noisy business! Genetic regulation at the nanomolar scale. *Trends Genet*, 15, 65-9.
- MCKANE, A. J. & NEWMAN, T. J. 2004. Stochastic models in population biology and their deterministic analogs. *Physical Review E*, 70.
- MENG, T. C., SOMANI, S. & DHAR, P. 2004. Modeling and simulation of biological systems with stochasticity. *In Silico Biol*, 4, 293-309.
- MENGEL, B., KRISHNA, S., JENSEN, M. H. & TRUSINA, A. 2012. Nested feedback loops in gene regulation. *Physica a-Statistical Mechanics and Its Applications*, 391, 100-106.
- MEYER, T. & STRYER, L. 1988. Molecular-Model for Receptor-Stimulated Calcium Spiking. *Proc Natl Acad Sci U S A*, 85, 5051-5055.
- MONK, N. A. M. 2003. Oscillatory expression of Hes1, p53, and NF-kappa B driven by transcriptional time delays. *Current Biology*, 13, 1409-1413.
- MOROHASHI, M., WINN, A. E., BORISUK, M. T., BOLOURI, H., DOYLE, J. & KITANO, H. 2002. Robustness as a measure of plausibility in models of biochemical networks. *Journal of Theoretical Biology*, 216, 19-30.
- MURRAY, J. D. 2002. *Mathematical biology*, New York, Springer.
- NELSON, D. E., IHEKWABA, A. E., ELLIOTT, M., JOHNSON, J. R., GIBNEY, C. A., FOREMAN, B. E., NELSON, G., SEE, V., HORTON, C. A., SPILLER, D. G., EDWARDS, S. W., MCDOWELL, H. P., UNITT, J. F., SULLIVAN, E., GRIMLEY, R., BENSON, N., BROOMHEAD, D., KELL, D. B. & WHITE, M. R. 2004. Oscillations in NF-kappaB signaling control the dynamics of gene expression. *Science*, 306, 704-8.
- NELSON, G., PARAOAN, L., SPILLER, D. G., WILDE, G. J., BROWNE, M. A., DJALI, P. K., UNITT, J. F., SULLIVAN, E., FLOETTMANN, E. & WHITE, M. R. 2002. Multi-parameter analysis of the kinetics of NF-kappaB signalling and transcription in single living cells. *J Cell Sci*, 115, 1137-48.
- NGUYEN, L. K. 2012. Regulation of oscillation dynamics in biochemical systems with dual negative feedback loops. *J R Soc Interface*, 9, 1998-2010.
- NOVAK, B. & TYSON, J. J. 2004. A model for restriction point control of the mammalian cell cycle. *J Theor Biol*, 230, 563-79.
- NOVAK, B. & TYSON, J. J. 2008. Design principles of biochemical oscillators. *Nat Rev Mol Cell Biol*, 9, 981-91.
- OREN, M. 1999. Regulation of the p53 tumor suppressor protein. *J Biol Chem*, 274, 36031-4.
- PASZEK, P., JACKSON, D. A. & WHITE, M. R. 2010a. Oscillatory control of signalling molecules. *Curr Opin Genet Dev*, 20, 670-6.
- PASZEK, P., RYAN, S., ASHALL, L., SILLITOE, K., HARPER, C. V., SPILLER, D. G., RAND, D. A. & WHITE, M. R. 2010b. Population robustness arising from cellular heterogeneity. *Proc Natl Acad Sci U S A*, 107, 11644-9.
- PERKINS, N. D. 2006. Post-translational modifications regulating the activity and function of the nuclear factor kappa B pathway. *Oncogene*, 25, 6717-30.
- PERKINS, N. D. 2007. Integrating cell-signalling pathways with NF-kappaB and IKK function. *Nat Rev Mol Cell Biol*, 8, 49-62.
- PFÄFFL, M. W., HORGAN, G. W. & DEMPFLER, L. 2002. Relative expression software tool (REST) for group-wise comparison and statistical analysis of relative expression results in real-time PCR. *Nucleic Acids Res*, 30, e36.

- PIERCE, J. W., SCHOENLEBER, R., JESMOK, G., BEST, J., MOORE, S. A., COLLINS, T. & GERRITSEN, M. E. 1997. Novel inhibitors of cytokine-induced IkappaBalpha phosphorylation and endothelial cell adhesion molecule expression show anti-inflammatory effects in vivo. *J Biol Chem*, 272, 21096-103.
- PITT-FRANCIS, J., PATHMANATHAN, P., BERNABEU, M. O., BORDAS, R., COOPER, J., FLETCHER, A. G., MIRAMS, G. R., MURRAY, P., OSBORNE, J. M., WALTER, A., CHAPMAN, S. J., GARNY, A., VAN LEEUWEN, I. M. M., MAINI, P. K., RODRIGUEZ, B., WATERS, S. L., WHITELEY, J. P., BYRNE, H. M. & GAVAGHAN, D. J. 2009. Chaste: A test-driven approach to software development for biological modelling. *Computer Physics Communications*, 180, 2452-2471.
- POLMAN, H. A., HUIJBERS, W. A. & AUGUSTEIJN, R. 1981. The use of diclofenac sodium (Voltaren) suppositories as an antipyretic in children with fever due to acute infections: a double-blind, between-patient, placebo-controlled study. *J Int Med Res*, 9, 343-8.
- PURVIS, J. E., KARHOHS, K. W., MOCK, C., BATCHELOR, E., LOEWER, A. & LAHAV, G. 2012. p53 Dynamics Control Cell Fate. *Science*, 336, 1440-1444.
- PUSZYNSKI, K., HAT, B. & LIPNIACKI, T. 2008. Oscillations and bistability in the stochastic model of p53 regulation. *Journal of Theoretical Biology*, 254, 452-465.
- RAJKUMAR, S. V., RICHARDSON, P. G., HIDESHIMA, T. & ANDERSON, K. C. 2005. Proteasome inhibition as a novel therapeutic target in human cancer. *J Clin Oncol*, 23, 630-9.
- RAND, D. A. 2008. Mapping global sensitivity of cellular network dynamics: sensitivity heat maps and a global summation law. *J R Soc Interface*, 5 Suppl 1, S59-69.
- RAND, D. A., SHULGIN, B. V., SALAZAR, D. & MILLAR, A. J. 2004. Design principles underlying circadian clocks. *J R Soc Interface*, 1, 119-30.
- REIJENGA, K. A., VAN MEGEN, Y. M. G. A., KOOI, B. W., BAKKER, B. M., SNOEP, J. L., VAN VERSEVELD, H. W. & WESTERHOFF, H. V. 2005. Yeast glycolytic oscillations that are not controlled by a single oscillator: a new definition of oscillator strength. *Journal of Theoretical Biology*, 232, 385-398.
- RENSING, L. & RUOFF, P. 2002. Temperature effect on entrainment, phase shifting, and amplitude of circadian clocks and its molecular bases. *Chronobiol Int*, 19, 807-64.
- REYES, B. A., PENDERGAST, J. S. & YARNAZAKI, S. 2008. Mammalian peripheral circadian oscillators are temperature compensated. *J Biol Rhythms*, 23, 95-98.
- RUOFF, P. 1992. Introducing Temperature-Compensation in Any Reaction Kinetic Oscillator Model. *Journal of Interdisciplinary Cycle Research*, 23, 92-99.
- RUOFF, P. 1994. General Homeostasis in Period-Compensated and Temperature-Compensated Chemical Clock Mutants Formed by Random Selection Conditions. *Naturwissenschaften*, 81, 456-459.
- RUOFF, P., RENSING, L., KOMMEDAL, R. & MOHSENZADEH, S. 1997. Modeling temperature compensation in chemical and biological oscillators. *Chronobiol Int*, 14, 499-510.

- SAEZ-RODRIGUEZ, J., KREMLING, A., CONZELMANN, H., BETTENBROCK, K. & GILLES, E. D. 2004. Modular analysis of signal transduction networks. *Ieee Control Systems Magazine*, 24, 35-52.
- SALANOVA, B., CHOI, M., ROLLE, S., WELLNER, M., SCHEIDEREIT, C., LUFT, F. C. & KETTRITZ, R. 2005. The effect of fever-like temperatures on neutrophil signaling. *FASEB J*, 19, 816-8.
- SCHMITZ, M. L., BACHER, S. & KRACHT, M. 2001. I kappa B-independent control of NF-kappa B activity by modulatory phosphorylations. *Trends Biochem Sci*, 26, 186-90.
- SCHNEIDER, K. R. & WILHELM, T. 2000. Model reduction by extended quasi-steady-state approximation. *Journal of Mathematical Biology*, 40, 443-450.
- SCHRODINGER, E. 1948. *What is life? : the physical aspect of the living cell*, Cambridge, Cambridge University Press.
- SHEN, H., NELSON, G., NELSON, D. E., KENNEDY, S., SPILLER, D. G., GRIFFITHS, T., PATON, N., OLIVER, S. G., WHITE, M. R. & KELL, D. B. 2006. Automated tracking of gene expression in individual cells and cell compartments. *J R Soc Interface*, 3, 787-94.
- SHIZUYA, H., BIRREN, B., KIM, U. J., MANCINO, V., SLEPAK, T., TACHIIRI, Y. & SIMON, M. 1992. Cloning and stable maintenance of 300-kilobase-pair fragments of human DNA in Escherichia coli using an F-factor-based vector. *Proc Natl Acad Sci U S A*, 89, 8794-7.
- SKAUG, B., CHEN, J. Q., DU, F. H., HE, J., MA, A. & CHEN, Z. J. J. 2011. Direct, Nucleolytic Mechanism of IKK Inhibition by A20. *Molecular Cell*, 44, 559-571.
- SKERKER, J. M., PERCHUK, B. S., SIRYAPORN, A., LUBIN, E. A., ASHENBERG, O., GOULIAN, M. & LAUB, M. T. 2008. Rewiring the specificity of two-component signal transduction systems. *Cell*, 133, 1043-54.
- SMITH, H. 2011. Distributed Delay Equations and the Linear Chain Trick. *An Introduction to Delay Differential Equations with Applications to the Life Sciences*. New York: Springer.
- SUCKLEY, R. & BIKTASHEV, V. N. 2003. Comparison of asymptotics of heart and nerve excitability. *Physical Review E*, 68.
- SUN, L., YANG, G. Z., ZAIDI, M. & IQBAL, J. 2008. TNF-induced gene expression oscillates in time. *Biochemical and Biophysical Research Communications*, 371, 900-905.
- SUN, S. C. 2011. Non-canonical NF-kappa B signaling pathway. *Cell Research*, 21, 71-85.
- SUN, S. C., GANCHI, P. A., BALLARD, D. W. & GREENE, W. C. 1993. NF-kappa B controls expression of inhibitor I kappa B alpha: evidence for an inducible autoregulatory pathway. *Science*, 259, 1912-5.
- SUN, Z. & ANDERSSON, R. 2002. NF-kappaB activation and inhibition: a review. *Shock*, 18, 99-106.
- SUNG, M. H., BAGAIN, L., CHEN, Z., KARPOVA, T., YANG, X., SILVIN, C., VOSS, T. C., MCNALLY, J. G., VAN WAES, C. & GORDON, L. 2008. Dynamic Effect of Bortezomib on Nuclear Factor-kappa B Activity and Gene Expression in Tumor Cells. *Molecular Pharmacology*, 74, 1215-1222.

- SUNG, M. H., SALVATORE, L., DE LORENZI, R., INDRAWAN, A., PASPARAKIS, M., HAGER, G. L., BIANCHI, M. E. & AGRETI, A. 2009. Sustained oscillations of NF-kappaB produce distinct genome scanning and gene expression profiles. *PLoS One*, 4, e7163.
- SUNWOO, J. B., CHEN, Z., DONG, G., YEH, N., CROWL BANCROFT, C., SAUSVILLE, E., ADAMS, J., ELLIOTT, P. & VAN WAES, C. 2001. Novel proteasome inhibitor PS-341 inhibits activation of nuclear factor-kappa B, cell survival, tumor growth, and angiogenesis in squamous cell carcinoma. *Clin Cancer Res*, 7, 1419-28.
- SUROVTSOVA, I., SIMUS, N., LORENZ, T., KONIG, A., SAHLE, S. & KUMMER, U. 2009. Accessible methods for the dynamic time-scale decomposition of biochemical systems. *Bioinformatics*, 25, 2816-2823.
- TAKAHASHI, K., ARJUNAN, S. N. V. & TOMITA, M. 2005. Space in systems biology of signaling pathways - towards intracellular molecular crowding in silico. *FEBS Lett*, 579, 1783-1788.
- TAY, S., HUGHEY, J. J., LEE, T. K., LIPNIACKI, T., QUAKE, S. R. & COVERT, M. W. 2010. Single-cell NF-kappa B dynamics reveal digital activation and analogue information processing. *Nature*, 466, 267-U149.
- TERGAONKAR, V. 2006. NFkappaB pathway: a good signaling paradigm and therapeutic target. *Int J Biochem Cell Biol*, 38, 1647-53.
- THANOS, D. & MANIATIS, T. 1995. Nf-Kappa-B - a Lesson in Family Values. *Cell*, 80, 529-532.
- TIAN, B., NOWAK, D. E. & BRASIER, A. R. 2005. A TNF-induced gene expression program under oscillatory NF-kappaB control. *BMC Genomics*, 6, 137.
- TIKHONOV, A. N. 1952. Systems of differential equations with small parameters at the derivatives. *USSR Mathematics Sbornik*, 31, 575-586.
- TRACY, R. P. 2006. The five cardinal signs of inflammation: Calor, Dolor, Rubor, Tumor ... and Penuria (Apologies to Aulus Cornelius Celsus, De medicina, c. A.D. 25). *J Gerontol A Biol Sci Med Sci*, 61, 1051-2.
- TSAI, T. Y. C., CHOI, Y. S., MA, W. Z., POMERENING, J. R., TANG, C. & FERRELL, J. E. 2008. Robust, tunable biological oscillations from interlinked positive and negative feedback loops. *Science*, 321, 126-129.
- TURNER, D. 2010. *An investigation into the dynamics of NF-kappaB following physiological levels of cytokine stimulation in single living cells*. PhD, University of Liverpool.
- TURNER, D. A., PASZEK, P., WOODCOCK, D. J., NELSON, D. E., HORTON, C. A., WANG, Y., SPILLER, D. G., RAND, D., WHITE, M. R. & HARPER, C. V. 2010. Physiological levels of TNFalpha stimulation induces stochastic dynamics of NF-kappaB response in single living cells. *J Cell Sci*.
- TYSON, J. J., HONG, C. I., THRON, C. D. & NOVAK, B. 1999. A simple model of circadian rhythms based on dimerization and proteolysis of PER and TIM. *Biophysical Journal*, 77, 2411-2417.
- TYSON, J. J. & NOVAK, B. 2001. Regulation of the eukaryotic cell cycle: molecular antagonism, hysteresis, and irreversible transitions. *J Theor Biol*, 210, 249-63.



- VAN RIEL, N. A. 2006. Dynamic modelling and analysis of biochemical networks: mechanism-based models and model-based experiments. *Briefings in Bioinformatics*, 7, 364-74.
- VANE, J. R. & BOTTING, R. M. 1996. Mechanism of action of anti-inflammatory drugs. *Scand J Rheumatol Suppl*, 102, 9-21.
- VERSTREPEN, L., VERHELST, K., VAN LOO, G., CARPENTIER, I., LEY, S. C. & BEYAERT, R. 2010. Expression, biological activities and mechanisms of action of A20 (TNFAIP3). *Biochemical Pharmacology*, 80, 2009-2020.
- VIATOUR, P., MERVILLE, M. P., BOURS, V. & CHARIOT, A. 2005. Phosphorylation of NF-kappaB and IkappaB proteins: implications in cancer and inflammation. *Trends Biochem Sci*, 30, 43-52.
- VRIES, G. D. 2006. *A course in mathematical biology : quantitative modeling with mathematical and computational methods*, Philadelphia, PA, Society for Industrial and Applied Mathematics.
- WALKER, D. C. & SOUTHGATE, J. 2009. The virtual cell-a candidate co-ordinator for 'middle-out' modelling of biological systems. *Briefings in Bioinformatics*, 10, 450-461.
- WANG, Y., PASZEK, P., HORTON, C. A., YUE, H., WHITE, M. R., KELL, D. B., MULDOON, M. R. & BROOMHEAD, D. S. 2012a. A systematic survey of the response of a model NF-kappaB signalling pathway to TNFalpha stimulation. *J Theor Biol*, 297, 137-47.
- WANG, Y. J., PASZEK, P., HORTON, C. A., YUE, H., WHITE, M. R. H., KELL, D. B., MULDOON, M. R. & BROOMHEAD, D. S. 2012b. A systematic survey of the response of a model NF-kappa B signalling pathway to TNF alpha stimulation. *Journal of Theoretical Biology*, 297, 137-147.
- WARMING, S., COSTANTINO, N., COURT, D. L., JENKINS, N. A. & COPELAND, N. G. 2005. Simple and highly efficient BAC recombineering using galK selection. *Nucleic Acids Res*, 33, e36.
- WEBSTER, G. A. & PERKINS, N. D. 1999. Transcriptional cross talk between NF-kappaB and p53. *Mol Cell Biol*, 19, 3485-95.
- WENG, G., BHALLA, U. S. & IYENGAR, R. 1999. Complexity in biological signaling systems. *Science*, 284, 92-6.
- WERNER, S. L., BARKEN, D. & HOFFMANN, A. 2005. Stimulus specificity of gene expression programs determined by temporal control of IKK activity. *Science*, 309, 1857-61.
- WERNER, S. L., KEARNS, J. D., ZADOROZHNYAYA, V., LYNCH, C., O'DEA, E., BOLDIN, M. P., MA, A., BALTIMORE, D. & HOFFMANN, A. 2008. Encoding NF-kappaB temporal control in response to TNF: distinct roles for the negative regulators IkappaBalpha and A20. *Genes Dev*, 22, 2093-101.
- WERTZ, I. E., O'ROURKE, K. M., ZHOU, H. L., EBY, M., ARAVIND, L., SESHAGIRI, S., WU, P., WIESMANN, C., BAKER, R., BOONE, D. L., MA, A., KOONIN, E. V. & DIXIT, V. M. 2004. De-ubiquitination and ubiquitin ligase domains of A20 downregulate NF-kappa B signalling. *Nature*, 430, 694-699.
- WHITEHOUSE, M. W. 2005. Drugs to treat inflammation: a historical introduction. *Curr Med Chem*, 12, 2931-42.
- WHITELEY, J. P. 2010. Model reduction using a posteriori analysis. *Mathematical Biosciences*, 225, 44-52.

- WILDERMUTH, M. C. 2000. Metabolic control analysis: biological applications and insights. *Genome Biology*, 1.
- WILKINSON, D. J. 2009. Stochastic modelling for quantitative description of heterogeneous biological systems. *Nature Reviews Genetics*, 10, 122-133.
- WONG, J. V., LI, B. & YOU, L. 2012. Tension and robustness in multitasking cellular networks. *PLoS Comput Biol*, 8, e1002491.
- WONG, M., ZIRING, D., KORIN, Y., DESAI, S., KIM, S., LIN, J., GJERTSON, D., BRAUN, J., REED, E. & SINGH, R. R. 2008. TNFalpha blockade in human diseases: mechanisms and future directions. *Clin Immunol*, 126, 121-36.
- WU, W. H., WANG, F. S. & CHANG, M. S. 2008. Dynamic sensitivity analysis of biological systems. *BMC Bioinformatics*, 9.
- YDE, P., MENGEL, B., JENSEN, M. H., KRISHNA, S. & TRUSINA, A. 2011. Modeling the NF-kappaB mediated inflammatory response predicts cytokine waves in tissue. *BMC Syst Biol*, 5, 115.
- YUE, H., BROWN, M., KNOWLES, J., WANG, H., BROOMHEAD, D. S. & KELL, D. B. 2006. Insights into the behaviour of systems biology models from dynamic sensitivity and identifiability analysis: a case study of an NF-kappaB signalling pathway. *Mol Biosyst*, 2, 640-9.

**Appendix 1 –  
Ashall Model  
Representations**

## A1.1 – Ashall Model Equations and Parameters

The model consists of 14 ODEs:

$$\frac{d}{dt} IKKn(t) = kp \times \frac{kbA20}{kbA20 + TR \times A20(t)} \times IKKi(t) - TR \times ka \times IKKn(t) \quad (A1.1a)$$

$$\frac{d}{dt} IKKa(t) = TR \times ka \times IKKn(t) - ki \times IKKa(t) \quad (A1.1b)$$

$$\frac{d}{dt} IKKi(t) = ki \times IKKa(t) - kp \times \frac{kbA20}{kbA20 + TR \times A20(t)} \times IKKi(t) \quad (A1.1c)$$

$$\begin{aligned} \frac{d}{dt} NF\kappa B(t) &= kd1a \times (I\kappa B\alpha: NF\kappa B)(t) - ka1a \times I\kappa B\alpha(t) \times NF\kappa B(t) \\ &\quad - ki1 \times NF\kappa B(t) + ke1 \times nNF\kappa B(t) \\ &\quad + kt2a \times (pI\kappa B\alpha: NF\kappa B)(t) + c5a \times (I\kappa B\alpha: NF\kappa B)(t) \end{aligned} \quad (A1.1d)$$

$$\begin{aligned} \frac{d}{dt} nNF\kappa B(t) &= kd1a \times (nI\kappa B\alpha: nNF\kappa B)(t) \\ &\quad - ka1a \times nI\kappa B\alpha(t) \times nNF\kappa B(t) + ki1 \times kv \times NF\kappa B(t) \\ &\quad - ke1 \times kv \times nNF\kappa B(t) \end{aligned} \quad (A1.1e)$$

$$\begin{aligned} \frac{d}{dt} I\kappa B\alpha(t) &= kd1a \times (I\kappa B\alpha: NF\kappa B)(t) - ka1a \times I\kappa B\alpha(t) \times NF\kappa B(t) \\ &\quad + c2a \times tI\kappa B\alpha(t) - c4a \times I\kappa B\alpha(t) - ki3a \times I\kappa B\alpha(t) \\ &\quad + ke3a \times nI\kappa B\alpha(t) - kc1a \times IKKa(t) \times I\kappa B\alpha(t) \end{aligned} \quad (A1.1f)$$

$$\begin{aligned} \frac{d}{dt} nI\kappa B\alpha(t) &= kd1a \times (nI\kappa B\alpha: nNF\kappa B)(t) \\ &\quad - ka1a \times nI\kappa B\alpha(t) \times nNF\kappa B(t) - c4a \times nI\kappa B\alpha(t) \\ &\quad + ki3a \times kv \times I\kappa B\alpha(t) - ke3a \times kv \times nI\kappa B\alpha(t) \end{aligned} \quad (A1.1g)$$

$$\frac{d}{dt} A20(t) = c2 \times tA20(t) - c4 \times A20(t) \quad (A1.1h)$$

$$\frac{d}{dt} tIkB\alpha(t) = c1a \times \frac{nNF\kappa B^h(t)}{nNF\kappa B^h(t) + k^h} - c3a \times tIkB\alpha(t) \quad (A1.1i)$$

$$\frac{d}{dt} tA20(t) = c1 \times \frac{nNF\kappa B^h(t)}{nNF\kappa B^h(t) + k^h} - c3 \times tA20(t) \quad (A1.1j)$$

$$\frac{d}{dt} pIkB\alpha(t) = kc1a \times IKKa(t) \times I\kappa B\alpha(t) - kt1a \times pIkB\alpha(t) \quad (A1.1k)$$

$$\begin{aligned} \frac{d}{dt} (pIkB\alpha: NF\kappa B)(t) & \quad (A1.1l) \\ & = kc1a \times IKKa(t) \times (I\kappa B\alpha: NF\kappa B)(t) \\ & \quad - kt2a \times (pIkB\alpha: NF\kappa B)(t) \end{aligned}$$

$$\begin{aligned} \frac{d}{dt} (I\kappa B\alpha: NF\kappa B)(t) & \quad (A1.1m) \\ & = ka1a \times I\kappa B\alpha(t) \times NF\kappa B(t) - kd1a (I\kappa B\alpha: NF\kappa B)(t) \\ & \quad - c5a \times (I\kappa B\alpha: NF\kappa B)(t) + ke2a \times (nI\kappa B\alpha: nNF\kappa B)(t) \\ & \quad - kc2a \times IKKa(t) \times (I\kappa B\alpha: NF\kappa B)(t) \end{aligned}$$

$$\begin{aligned} \frac{d}{dt} (nI\kappa B\alpha: nNF\kappa B)(t) & \quad (A1.1n) \\ & = ka1an \times nI\kappa B\alpha(t) \times nNF\kappa B(t) \\ & \quad - kd1a (nI\kappa B\alpha: nNF\kappa B)(t) \\ & \quad - ke2a \times kv \times (nI\kappa B\alpha: nNF\kappa B) \end{aligned}$$

The variables and parameters are described below. The initial conditions were found by setting  $I\kappa B\alpha: NF-\kappa B$  and  $IKKn$  to be 0.08,  $TR=0$ , and allowing the system to equilibrate for 4000 minutes. The initial conditions are also listed.

Variables		I.C.'s
NFκB	Cytoplasmic NF-κB	$3.81 \times 10^{-3}$
IκBα	Cytoplasmic IκBα	$1.58 \times 10^{-2}$
nNFκB	Nuclear NF-κB	$9.79 \times 10^{-3}$
nIκBα	Nuclear IκBα	$5.44 \times 10^{-3}$
tIκBα	IκBα mRNA	$2.07 \times 10^{-5}$

IKK <sub>n</sub>	Neutral IKK	0.08
IKK <sub>a</sub>	Active IKK	0
tA20	A20 mRNA	$6.49 \times 10^{-6}$
A20	A20 protein	$7.19 \times 10^{-4}$
pI $\kappa$ B $\alpha$ NF $\kappa$ B	Phospho I $\kappa$ B $\alpha$ complexed with NF- $\kappa$ B	0
IKK <sub>i</sub>	Inactive IKK	0
pI $\kappa$ B $\alpha$	Phosphorylated I $\kappa$ B $\alpha$	0
nI $\kappa$ B $\alpha$ :nNF $\kappa$ B	Nuclear I $\kappa$ B $\alpha$ complexed with NF- $\kappa$ B	$7.95 \times 10^{-4}$
I $\kappa$ B $\alpha$ :NF $\kappa$ B	Cytoplasmic I $\kappa$ B $\alpha$ complexed with NF- $\kappa$ B	$7.30 \times 10^{-2}$

<b>Parameters</b>		
<i>kv</i>	Ratio of nuclear to cytoplasmic volume	3.3
<i>ka1a</i>	I $\kappa$ B $\alpha$ and NF- $\kappa$ B association in cytoplasm	$0.5\mu\text{Ms}^{-1}$
<i>ka1an</i>	I $\kappa$ B $\alpha$ and NF- $\kappa$ B association in the nucleus	$0.5\mu\text{Ms}^{-1}$
<i>kd1a</i>	I $\kappa$ B $\alpha$ and NF- $\kappa$ B disassociation	$0.0005\text{s}^{-1}$
<i>c1a</i>	I $\kappa$ B $\alpha$ transcription	$1.4 \times 10^{-7}\mu\text{M}^{-1}\text{s}^{-1}$
<i>c2a</i>	I $\kappa$ B $\alpha$ mRNA translation	$0.5\text{s}^{-1}$
<i>c3a</i>	I $\kappa$ B $\alpha$ mRNA degradation	$0.0003\text{s}^{-1}$
<i>c4a</i>	I $\kappa$ B $\alpha$ protein degradation	$0.0005\text{s}^{-1}$
<i>c5a</i>	I $\kappa$ B $\alpha$ protein degradation when bound to NF- $\kappa$ B	$0.000022\text{s}^{-1}$
<i>c1</i>	A20 transcription	$1.4 \times 10^{-7}\mu\text{M}^{-1}\text{s}^{-1}$
<i>c2</i>	A20 mRNA translation	$0.5\text{s}^{-1}$
<i>c3</i>	A20 mRNA degradation	$0.00048\text{s}^{-1}$
<i>c4</i>	A20 protein degradation	$0.0045\text{s}^{-1}$
<i>ki3a</i>	I $\kappa$ B $\alpha$ nuclear import	$0.00067\text{s}^{-1}$
<i>ke3a</i>	I $\kappa$ B $\alpha$ nuclear export	$3.35 \times 10^{-4}\text{s}^{-1}$
<i>ke2a</i>	I $\kappa$ B $\alpha$ complexed with NF- $\kappa$ B nuclear export	$0.01\text{s}^{-1}$
<i>ki1</i>	NF- $\kappa$ B nuclear import	$0.0026\text{s}^{-1}$
<i>ke1</i>	NF- $\kappa$ B nuclear export	$0.00052\text{s}^{-1}$
<i>kc1a</i>	I $\kappa$ B $\alpha$ phosphorylation by IKK	$0.074\text{s}^{-1}$
<i>kc2a</i>	I $\kappa$ B $\alpha$ :NF- $\kappa$ B phosphorylation by IKK	$0.185\text{s}^{-1}$
<i>kt1a</i>	Phospho-I $\kappa$ B $\alpha$ degradation	$0.1\text{s}^{-1}$
<i>kt2a</i>	Phospho-I $\kappa$ B $\alpha$ :NF- $\kappa$ B degradation	$0.1\text{s}^{-1}$
<i>kp</i>	IKK recycling	$0.0006\text{s}^{-1}$
<i>kbA20</i>	A20 inhibition rate	$0.0018\mu\text{M}$
<i>ka</i>	IKK activation	$0.004\text{s}^{-1}$
<i>ki</i>	IKK inactivation	$0.003\text{s}^{-1}$
<i>TR</i>	TNF $\alpha$ stimulation	1/0
<i>k</i>	Order of the Hill function for transcription	$0.065\mu\text{M}$
<i>h</i>	Hax-max constant of the Hill function	2

## A1.2 – 11-Variable Representation of the Ashall Model

This is a system of 11 ODEs that is equivalent to the Ashall model (Chapter 3 and Wang *et al.* (2010)). The same variable and parameters as described in A1.1 are used, the model contains and two additional parameters to represent the total level of NF- $\kappa$ B and IKK. Similarly, the initial conditions were found by setting all variable concentrations to be equal to 0, TR=0 and allowing the system to equilibrate for 4000 minutes.

$$\begin{aligned} \frac{d}{dt} IKKn(t) = & kp \times (TIKK - IKKn(t) - IKKi(t)) \\ & \times \frac{kbA20}{kbA20 + TR \times A20(t)} - TR \times ka \times IKKn(t) \end{aligned} \quad (A1.2a)$$

$$\frac{d}{dt} IKKa(t) = TR \times ka \times IKKn(t) - ki \times IKKa(t) \quad (A1.2b)$$

$$\begin{aligned} \frac{d}{dt} NF\kappa B(t) = & kd1a \times (I\kappa B\alpha: NF\kappa B)(t) - ka1a \times I\kappa B\alpha(t) \times NF\kappa B(t) \\ & - ki1 \times NF\kappa B(t) + ke1 \times nNF\kappa B(t) \\ & + kt2a \\ & \times \left( TNF\kappa B - NF\kappa B(t) - (I\kappa B\alpha: NF\kappa B)(t) \right. \\ & \left. - \frac{(nNF\kappa B(t) + (nI\kappa B\alpha: nNF\kappa B)(t))}{kv} \right) \\ & + c5a \times (I\kappa B\alpha: NF\kappa B)(t) \end{aligned} \quad (A1.2c)$$

$$\begin{aligned} \frac{d}{dt} nNF\kappa B(t) = & kd1a \times (nI\kappa B\alpha: nNF\kappa B)(t) \\ & - ka1a \times nI\kappa B\alpha(t) \times nNF\kappa B(t) + ki1 \times kv \times NF\kappa B(t) \\ & - ke1 \times kv \times nNF\kappa B(t) \end{aligned} \quad (A1.2d)$$

$$\begin{aligned} \frac{d}{dt} I\kappa B\alpha(t) = & kd1a \times (I\kappa B\alpha: NF\kappa B)(t) - ka1a \times I\kappa B\alpha(t) \times NF\kappa B(t) \\ & + c2a \times tI\kappa B\alpha(t) - c4a \times I\kappa B\alpha(t) - ki3a \times I\kappa B\alpha(t) \\ & + ke3a \times nI\kappa B\alpha(t) - kc1a \times IKK\alpha(t) \times I\kappa B\alpha(t) \end{aligned} \quad (A1.2e)$$

$$\begin{aligned} \frac{d}{dt} nI\kappa B\alpha(t) = & kd1a \times (nI\kappa B\alpha: nNF\kappa B)(t) \\ & - ka1a \times nI\kappa B\alpha(t) \times nNF\kappa B(t) - c4a \times nI\kappa B\alpha(t) \\ & + ki3a \times kv \times I\kappa B\alpha(t) - ke3a \times kv \times nI\kappa B\alpha(t) \end{aligned} \quad (A1.2f)$$

$$\frac{d}{dt} A20(t) = c2 \times tA20(t) - c4 \times A20(t) \quad (A1.2g)$$

$$\frac{d}{dt} tI\kappa B\alpha(t) = c1a \times \frac{nNF\kappa B^h(t)}{nNF\kappa B^h(t) + k^h} - c3a \times tI\kappa B\alpha(t) \quad (A1.2h)$$

$$\frac{d}{dt} tA20(t) = c1 \times \frac{nNF\kappa B^h(t)}{nNF\kappa B^h(t) + k^h} - c3 \times tA20(t) \quad (A1.2i)$$

$$\begin{aligned} \frac{d}{dt} (I\kappa B\alpha: NF\kappa B)(t) & \\ = & ka1a \times I\kappa B\alpha(t) \times NF\kappa B(t) - kd1a (I\kappa B\alpha: NF\kappa B)(t) \\ & - c5a \times (I\kappa B\alpha: NF\kappa B)(t) + ke2a \times (nI\kappa B\alpha: nNF\kappa B)(t) \\ & - kc2a \times IKK\alpha(t) \times (I\kappa B\alpha: NF\kappa B)(t) \end{aligned} \quad (A1.2j)$$

$$\begin{aligned} \frac{d}{dt} (nI\kappa B\alpha: nNF\kappa B)(t) & \\ = & ka1an \times nI\kappa B\alpha(t) \times nNF\kappa B(t) \\ & - kd1a (nI\kappa B\alpha: nNF\kappa B)(t) \\ & - ke2a \times kv \times (nI\kappa B\alpha: nNF\kappa B) \end{aligned} \quad (A1.2k)$$

The additional parameters were:

Parameters		
<i>TNFκB</i>	Total conserved amount of NF-κB	0.08μM
<i>TIKK</i>	Total conserved amount of IKK	0.08μM



# **Appendix 2 – Minimal Models**

## A2.1 – Equations for the $z_0 p_I y_I v_I s_I w_I$ Model

The model consists of four ODEs:

$$\frac{dq}{dt} = -k_4 q \bar{p}(q, r, x) + k_6 u - k_8 q - k_{13} q + k_{14} \bar{s}(q, r) - k_{17} \bar{w}(r, x) q, \quad (\text{A2.1a})$$

$$\frac{dr}{dt} = k_{15} k_1 \bar{p}(q, r, x) - k_4 \bar{s}(q, r) r - k_{16} k_1 r, \quad (\text{A2.1b})$$

$$\frac{du}{dt} = k_5 \frac{r^h}{r^h + k^h} - k_7 u, \quad (\text{A2.1c})$$

$$\frac{dx}{dt} = k_9 \frac{r^h}{r^h + k^h} - k_{11} u, \quad (\text{A2.1d})$$

where the functions in the right-hand side are defined by

$$w_0(x) = \frac{k_{24} k_{22} k_{20} k_{21} k_{12} k_3}{(k_{20} k_{21} k_{12} + k_{24} k_{22} k_{21} k_{12} + k_{24}^2 k_{22} k_{10} x) k_{23}}, \quad (\text{A2.2a})$$

$$w_1(x) = \frac{k_{24}^3 k_{22}^2 k_{20} k_{21} k_{12} k_3 k_{10} \left( \frac{k_9 r^h}{r^h + k^h} - k_{11} x \right)}{(k_{20} k_{21} k_{12} + k_{24} k_{22} k_{21} k_{12} + k_{24}^2 k_{22} k_{10} x)^2 k_{23}^2}, \quad (\text{A2.2b})$$

$$\bar{w}(r, x) = w_0(x) + w_1(r, x), \quad (\text{A2.2c})$$

$$\bar{y}(r, x) = \frac{k_{10} x}{k_{12}} - \frac{k_{12} \left( \frac{k_9 r^h}{r^h + k^h} - k_{11} x \right)}{k_{10}^2}, \quad (\text{A2.2d})$$

$$v_0(r, x) = \frac{k_3 k_{20} k_{21}}{k_{20} k_{21} + k_{21} k_{22} k_{24} + k_{24}^2 k_{22} \bar{y}(r, x)}, \quad (\text{A2.2e})$$

$$v_1(r, x) = \frac{-k_{20}^2 k_{24} k_{10} k_3 k_{21}^2 \left( \frac{k_9 r^h}{r^h + k^h} - k_{11} x \right)}{k_{12} \left( \frac{k_{20} k_{21}}{k_{21} + k_{24} \bar{y}(r, x)} + k_{24} k_{22} \right) \left( \frac{k_{20} k_{21}}{k_{21} + k_{24} \bar{y}(r, x)} - k_{24} k_{22} \right)^2 (k_{21} + k_{24} \bar{y}(r, x))^3}, \quad (\text{A2.2f})$$

$$\bar{v}(r, x) = v_0(r, x) + v_1(r, x), \quad (\text{A2.2g})$$

$$p_0(q, r, x) = \frac{k_{16}r + k_{18}\bar{w}(r, x) \left(k_3 - \frac{r}{k_1}\right)}{k_4q + k_{15} + k_{18}\bar{w}(r, x)}, \quad (\text{A2.2h})$$

$$s_\alpha(q) = k_1k_{13}q, \quad (\text{A2.2i})$$

$$s_\beta(r) = k_4r + k_1k_{14} + k_{12}, \quad (\text{A2.2j})$$

$$s_\delta(q, r, x) = k_1k_{15}p_0(q, r, x) - k_1k_{16}r, \quad (\text{A2.2k})$$

$$s_\gamma(q, r, x) = -k_4qp_0(q, r, x) - k_{13}q - k_8q + k_6u - k_{17}\bar{w}(r, x)q, \quad (\text{A2.2l})$$

$$\bar{s}(q, r, u, x) = \frac{s_\alpha(q)s_\beta^2(r) - k_4s_\delta(q, r, x)s_\alpha(q) - k_1k_{13}s_\gamma(q, r, u, x)s_\beta(r)}{k_4^2s_\alpha(q)r + s_\beta^3(r) + k_1k_{13}k_{14}s_\beta(r)}, \quad (\text{A2.2m})$$

$$\alpha_p(r, x) = k_1k_{16}r + k_{18}\bar{w}(r, x)(k_1k_3 - r), \quad (\text{A2.2n})$$

$$\beta_p(q, r, x) = k_1(k_4q + k_{15} + k_{18}\bar{w}(r, x)), \quad (\text{A2.2o})$$

$$q_\alpha(q, r, u, x) = k_6u - k_{13}q - k_8q + k_{14}s - k_{17}\bar{w}(r, x)q, \quad (\text{A2.2p})$$

$$q_\beta(q) = -k_4q, \quad (\text{A2.2q})$$

$$r_\alpha(q, r, u, x) = -r(k_4\bar{s}(q, r, u, x) + k_{16}k_1), \quad (\text{A2.2r})$$

$$r_\beta = k_1k_{15}, \quad (\text{A2.2s})$$

$$p_\delta(r, q) = k_1(k_4q_\alpha(q, r, u, x) + k_{18}(k_{24}k_{22}\bar{v}(r, x) - k_{23}\bar{w}(r, x))), \quad (\text{A2.2t})$$

$$p_\gamma(q) = k_1k_4q_\beta(q), \quad (\text{A2.2u})$$

$$p_\varepsilon(q, r, u, x) = k_{16}k_1r_\alpha(q, r, u, x) - k_{18}\bar{w}(r, x)r_\alpha(q, r, u, x) + k_{18}(k_{24}k_{22}\bar{v}(r, x) - k_{23}\bar{w}(r, x))(k_1k_3 - r), \quad (\text{A2.2v})$$

$$p_\zeta(r, x) = (k_1k_{16} - k_{18}\bar{w}(r, x))r_\beta, \quad (\text{A2.2w})$$

$$\bar{p}(q, r, u, x) = \frac{\beta_p^3 \alpha_p + \alpha_p p_\delta - \beta_p p_\varepsilon}{\beta_p^3 - \alpha_p p_\gamma + \beta_p p_\zeta}. \quad (\text{A2.2x})$$

## A2.2 – Equations for the $z_0p_0y_0v_0$ Model

Dynamic equations for the 6-variable model,  $z_0p_0y_0v_0$ , reduced using a representative solution for continuous TNF $\alpha$  stimulation ( $k_{24} \equiv 1$ ):

$$\frac{dq}{dt} = -k_4q\bar{p}(q, r, w) + k_6u - k_8q - k_{13}q + k_{14}s - k_{17}wq, \quad (\text{A2.3a})$$

$$\frac{dr}{dt} = k_{15}k_1\bar{p}(q, r, w) - k_4sr - k_{16}k_1r, \quad (\text{A2.3b})$$

$$\frac{ds}{dt} = k_{13}k_1\bar{p}(q, r, w) - k_4sr - k_8s - k_{14}k_1s, \quad (\text{A2.3c})$$

$$\frac{du}{dt} = k_5 \frac{r^h}{r^h + k^h} - k_7u, \quad (\text{A2.3d})$$

$$\frac{dw}{dt} = k_{24}k_{22}\bar{v}(y) - k_{23}w \quad (\text{A2.3e})$$

$$\frac{dx}{dt} = k_9 \frac{r^h}{r^h + k^h} - k_{11}u, \quad (\text{A2.3f})$$

$$\bar{p}(q, r, w) = \frac{k_{16}r + k_{18}w \left(k_3 - \frac{r}{k_1}\right)}{k_4q + k_{15} + k_{18}w}, \quad (\text{A2.3g})$$

$$\bar{y}(x) = \frac{k_{10}x}{k_{12}}, \quad (\text{A2.3h})$$

$$\bar{v}(x) = \frac{k_2k_{20}k_{21}}{k_{21}k_{22}k_{24} + k_{24}^2k_{22}\bar{y}(x) + k_{20}k_{21}}, \quad (\text{A2.3i})$$

# **Appendix 3 – Delay Models**

### A3.1 – Delayed IKK Activation

For this system the same variable and parameter notations as in Appendix 1 has been used. This model is a system of 15 ODEs consisting of:

$$\begin{aligned} \frac{d}{dt} IKKn(t) = & kp \times (TIKK - IKKn(t) - IKKi(t)) \\ & \times \frac{kbA20}{kbA20 + TR \times A20(t)} - TR \times ka \times IKKn(t) \end{aligned} \quad (A3.1a)$$

$$\frac{d}{dt} IKKa(t) = TR \times ka \times IKKn(t) - ki \times IKKa(t) \quad (A3.1b)$$

$$\begin{aligned} \frac{d}{dt} NF\kappa B(t) = & kd1a \times (I\kappa B\alpha: NF\kappa B)(t) - ka1a \times I\kappa B\alpha(t) \times NF\kappa B(t) \\ & - ki1 \times NF\kappa B(t) + ke1 \times nNF\kappa B(t) \\ & + kt2a \times IKK1(t) \\ & \times \left( TNF\kappa B - NF\kappa B(t) - (I\kappa B\alpha: NF\kappa B)(t) \right. \\ & \left. - \frac{(nNF\kappa B(t) + (nI\kappa B\alpha: nNF\kappa B)(t))}{kv} \right) \\ & + c5a \times (I\kappa B\alpha: NF\kappa B)(t) \end{aligned} \quad (A3.1c)$$

$$\begin{aligned} \frac{d}{dt} nNF\kappa B(t) = & kd1a \times (nI\kappa B\alpha: nNF\kappa B)(t) \\ & - ka1a \times nI\kappa B\alpha(t) \times nNF\kappa B(t) + ki1 \times kv \times NF\kappa B(t) \\ & - ke1 \times kv \times nNF\kappa B(t) \end{aligned} \quad (A3.1d)$$

$$\begin{aligned} \frac{d}{dt} I\kappa B\alpha(t) = & kd1a \times (I\kappa B\alpha: NF\kappa B)(t) - ka1a \times I\kappa B\alpha(t) \times NF\kappa B(t) \\ & + c2a \times tI\kappa B\alpha(t) - c4a \times I\kappa B\alpha(t) - ki3a \times I\kappa B\alpha(t) \\ & + ke3a \times nI\kappa B\alpha(t) - kc1a \times IKK1(t) \times I\kappa B\alpha(t) \end{aligned} \quad (A3.1e)$$

$$\begin{aligned} \frac{d}{dt} nI\kappa B\alpha(t) = & kd1a \times (nI\kappa B\alpha: nNF\kappa B)(t) \\ & - ka1a \times nI\kappa B\alpha(t) \times nNF\kappa B(t) - c4a \times nI\kappa B\alpha(t) \\ & + ki3a \times kv \times I\kappa B\alpha(t) - ke3a \times kv \times nI\kappa B\alpha(t) \end{aligned} \quad (A3.1f)$$

$$\frac{d}{dt} A20(t) = c2 \times tA20(t) - c4 \times A20(t) \quad (A3.1g)$$

$$\frac{d}{dt} tIkB\alpha(t) = c1a \times \frac{nNF\kappa B^h(t)}{nNF\kappa B^h(t) + k^h} - c3a \times tIkB\alpha(t) \quad (A3.1h)$$

$$\frac{d}{dt} tA20(t) = c1 \times \frac{nNF\kappa B^h(t)}{nNF\kappa B^h(t) + k^h} - c3 \times tA20(t) \quad (A3.1i)$$

$$\frac{d}{dt} (IkB\alpha: NF\kappa B)(t) \quad (A3.1j)$$

$$\begin{aligned} &= ka1a \times I\kappa B\alpha(t) \times NF\kappa B(t) - kd1a (IkB\alpha: NF\kappa B)(t) \\ &- c5a \times (IkB\alpha: NF\kappa B)(t) + ke2a \times (nIkB\alpha: nNF\kappa B)(t) \\ &- kc2a \times IKK1(t) \times (IkB\alpha: NF\kappa B)(t) \end{aligned}$$

$$\frac{d}{dt} (nIkB\alpha: nNF\kappa B)(t) \quad (A3.1k)$$

$$\begin{aligned} &= ka1an \times nIkB\alpha(t) \times nNF\kappa B(t) \\ &- kd1a (nIkB\alpha: nNF\kappa B)(t) \\ &- ke2a \times kv \times (nIkB\alpha: nNF\kappa B) \end{aligned}$$

with the inclusion of the linear chain:

$$\frac{d}{dt} IKK1(t) = delay \times (IKK2(t) - IKK1(t)) \quad (A3.1l)$$

$$\frac{d}{dt} IKK2(t) = delay \times (IKK3(t) - IKK2(t)) \quad (A3.1m)$$

$$\frac{d}{dt} IKK3(t) = delay \times (IKK4(t) - IKK3(t)) \quad (A3.1n)$$

$$\frac{d}{dt} IKK4(t) = delay \times (IKKa(t) - IKK4(t)) \quad (A3.1o)$$



The parameterization to give the solution as in *Figure 6.X* is:

<b>Parameters</b>			
<i>TNFκB</i>	0.08μM	<i>c1</i>	1.4 x10 <sup>-7</sup> μMs <sup>-1</sup>
<i>TIKK</i>	0.08μM	<i>c2</i>	0.5 s <sup>-1</sup>
<i>kv</i>	3.3	<i>c3</i>	0.00048 s <sup>-1</sup>
<i>ka1a</i>	0.5μMs <sup>-1</sup>	<i>c4</i>	0.0045 s <sup>-1</sup>
<i>ka1an</i>	0.5μMs <sup>-1</sup>	<i>ki3a</i>	0.00043 s <sup>-1</sup>
<i>kd1a</i>	0.0005s <sup>-1</sup>	<i>ke3a</i>	0.000335 s <sup>-1</sup>
<i>ke2a</i>	0.01s <sup>-1</sup>	<i>ki1</i>	0.0013 s <sup>-1</sup>
<i>c1a</i>	1.4x10 <sup>-7</sup> μMs <sup>-1</sup>	<i>ke1</i>	0.000052 s <sup>-1</sup>
<i>c2a</i>	0.5s <sup>-1</sup>	<i>kc1a</i>	0.074s <sup>-1</sup>
<i>c3a</i>	0.0003 s <sup>-1</sup>	<i>kc2a</i>	0.185 s <sup>-1</sup>
<i>c4a</i>	0.0005 s <sup>-1</sup>	<i>kt2a</i>	0.1 s <sup>-1</sup>
<i>c5a</i>	0.000022 s <sup>-1</sup>	<i>kbA20</i>	0.0018μM
<i>kp</i>	0.0003 s <sup>-1</sup>	<i>TR</i>	1/0
<i>ka</i>	0.002 s <sup>-1</sup>	<i>k</i>	0.065μM
<i>ki</i>	0.0015 s <sup>-1</sup>	<i>h</i>	2
<i>delay</i>	0.0017		

Similarly, the initial conditions were found by setting all variable concentrations to equal 0, TR=0 and allowing the system to equilibrate for 4000-minutes.

### A3.2 – Delayed A20 Transcription

For this system the same variable and parameter notations as in Appendix 1 has been used. This model is a system of 15 ODEs consisting of:

$$\begin{aligned} \frac{d}{dt} IKKn(t) = & kp \times (TIKK - IKKn(t) - IKKi(t)) \\ & \times \frac{kbA20}{kbA20 + TR \times A20(t)} - TR \times ka \times IKKn(t) \end{aligned} \quad (A3.2a)$$

$$\frac{d}{dt} IKKa(t) = TR \times ka \times IKKn(t) - ki \times IKKa(t) \quad (A3.2b)$$

$$\begin{aligned} \frac{d}{dt} NF\kappa B(t) = & kd1a \times (I\kappa B\alpha: NF\kappa B)(t) - ka1a \times I\kappa B\alpha(t) \times NF\kappa B(t) \\ & - ki1 \times NF\kappa B(t) + ke1 \times nNF\kappa B(t) \\ & + kt2a \times IKKa(t) \\ & \times \left( TNF\kappa B - NF\kappa B(t) - (I\kappa B\alpha: NF\kappa B)(t) \right. \\ & \left. - \frac{(nNF\kappa B(t) + (nI\kappa B\alpha: nNF\kappa B)(t))}{kv} \right) \\ & + c5a \times (I\kappa B\alpha: NF\kappa B)(t) \end{aligned} \quad (A3.2c)$$

$$\begin{aligned} \frac{d}{dt} nNF\kappa B(t) = & kd1a \times (nI\kappa B\alpha: nNF\kappa B)(t) \\ & - ka1a \times nI\kappa B\alpha(t) \times nNF\kappa B(t) + ki1 \times kv \times NF\kappa B(t) \\ & - ke1 \times kv \times nNF\kappa B(t) \end{aligned} \quad (A3.2d)$$

$$\begin{aligned} \frac{d}{dt} I\kappa B\alpha(t) = & kd1a \times (I\kappa B\alpha: NF\kappa B)(t) - ka1a \times I\kappa B\alpha(t) \times NF\kappa B(t) \\ & + c2a \times tI\kappa B\alpha(t) - c4a \times I\kappa B\alpha(t) - ki3a \times I\kappa B\alpha(t) \\ & + ke3a \times nI\kappa B\alpha(t) - kc1a \times IKKa(t) \times I\kappa B\alpha(t) \end{aligned} \quad (A3.2e)$$

$$\begin{aligned} \frac{d}{dt} nI\kappa B\alpha(t) = & kd1a \times (nI\kappa B\alpha: nNF\kappa B)(t) \\ & - ka1a \times nI\kappa B\alpha(t) \times nNF\kappa B(t) - c4a \times nI\kappa B\alpha(t) \\ & + ki3a \times kv \times I\kappa B\alpha(t) - ke3a \times kv \times nI\kappa B\alpha(t) \end{aligned} \quad (A3.2f)$$

$$\frac{d}{dt} A20(t) = c2 \times tA20a(t) - c4 \times A20(t) \quad (A3.2g)$$

$$\frac{d}{dt} tI\kappa B\alpha(t) = c1a \times \frac{nNF\kappa B^h(t)}{nNF\kappa B^h(t) + k^h} - c3a \times tI\kappa B\alpha(t) \quad (A3.2h)$$

$$\frac{d}{dt} tA20(t) = c1 \times \frac{nNF\kappa B^h(t)}{nNF\kappa B^h(t) + k^h} - c3 \times tA20(t) \quad (A3.2i)$$

$$\frac{d}{dt} (I\kappa B\alpha: NF\kappa B)(t) \quad (A3.2j)$$

$$\begin{aligned} &= ka1a \times I\kappa B\alpha(t) \times NF\kappa B(t) - kd1a(I\kappa B\alpha: NF\kappa B)(t) \\ &- c5a \times (I\kappa B\alpha: NF\kappa B)(t) + ke2a \times (nI\kappa B\alpha: nNF\kappa B)(t) \\ &- kc2a \times IKKa(t) \times (I\kappa B\alpha: NF\kappa B)(t) \end{aligned}$$

$$\frac{d}{dt} (nI\kappa B\alpha: nNF\kappa B)(t) \quad (A3.2k)$$

$$\begin{aligned} &= ka1an \times nI\kappa B\alpha(t) \times nNF\kappa B(t) \\ &- kd1a(nI\kappa B\alpha: nNF\kappa B)(t) \\ &- ke2a \times kv \times (nI\kappa B\alpha: nNF\kappa B) \end{aligned}$$

with the inclusion of the linear chain:

$$\frac{d}{dt} tA20a(t) = delay \times (tA20b(t) - tA20a(t)) \quad (A3.2l)$$

$$\frac{d}{dt} tA20b(t) = delay \times (tA20c(t) - tA20b(t)) \quad (A3.2m)$$

$$\frac{d}{dt} tA20c(t) = delay \times (tA20d(t) - tA20c(t)) \quad (A3.2n)$$

$$\frac{d}{dt} tA20d(t) = delay \times (tA20(t) - tA20d(t)) \quad (A3.2o)$$

The parameterisation is as follows:

<b>Parameters</b>			
<i>TNFκB</i>	0.08μM	<i>c1</i>	1.4 x 10 <sup>-7</sup> μMs <sup>-1</sup>
<i>TIKK</i>	0.08μM	<i>c2</i>	0.25s <sup>-1</sup>
<i>kv</i>	3.3	<i>c3</i>	0.00072s <sup>-1</sup>
<i>ka1a</i>	0.5μMs <sup>-1</sup>	<i>c4</i>	0.0045s <sup>-1</sup>
<i>ka1an</i>	0.5μMs <sup>-1</sup>	<i>ki3a</i>	0.001s <sup>-1</sup>
<i>kd1a</i>	0.0005s <sup>-1</sup>	<i>ke3a</i>	0.0005s <sup>-1</sup>
<i>ke2a</i>	0.01s <sup>-1</sup>	<i>ki1</i>	0.005s <sup>-1</sup>
<i>c1a</i>	1.4x10 <sup>-7</sup> μMs <sup>-1</sup>	<i>ke1</i>	0.0001s <sup>-1</sup>
<i>c2a</i>	0.65s <sup>-1</sup>	<i>kc1a</i>	0.074s <sup>-1</sup>
<i>c3a</i>	0.00024s <sup>-1</sup>	<i>kc2a</i>	0.37s <sup>-1</sup>
<i>c4a</i>	0.0005s <sup>-1</sup>	<i>kt2a</i>	0.1s <sup>-1</sup>
<i>c5a</i>	0.000022s <sup>-1</sup>	<i>kbA20</i>	0.0018μM
<i>kp</i>	0.0003s <sup>-1</sup>	<i>TR</i>	1/0
<i>ka</i>	0.002s <sup>-1</sup>	<i>k</i>	0.065μM
<i>ki</i>	0.0015s <sup>-1</sup>	<i>h</i>	2
<i>delay</i>	0.003 at 37°C 0.0095 at 40°C		

Similarly, the initial conditions were found by setting all variable concentrations to equal 0, TR=0 and allowing the system to equilibrate for 4000-minutes.

### A3.3 – Delayed $I\kappa B\alpha$ Transcription

For this system the same variable and parameter notations as in Appendix 1 has been used. This model is a system of 15 ODEs consisting of:

$$\begin{aligned} \frac{d}{dt} IKKn(t) &= kp \times (TIKK - IKKn(t) - IKKi(t)) \\ &\quad \times \frac{kbA20}{kbA20 + TR \times A20(t)} - TR \times ka \times IKKn(t) \end{aligned} \quad (A3.3a)$$

$$\frac{d}{dt} IKKa(t) = TR \times ka \times IKKn(t) - ki \times IKKa(t) \quad (A3.3b)$$

$$\begin{aligned} \frac{d}{dt} NF\kappa B(t) &= kd1a \times (I\kappa B\alpha: NF\kappa B)(t) - ka1a \times I\kappa B\alpha(t) \times NF\kappa B(t) \\ &\quad - ki1 \times NF\kappa B(t) + ke1 \times nNF\kappa B(t) \\ &\quad + kt2a \times IKKa(t) \\ &\quad \times \left( TNF\kappa B - NF\kappa B(t) - (I\kappa B\alpha: NF\kappa B)(t) \right. \\ &\quad \left. - \frac{(nNF\kappa B(t) + (nI\kappa B\alpha: nNF\kappa B)(t))}{kv} \right) \\ &\quad + c5a \times (I\kappa B\alpha: NF\kappa B)(t) \end{aligned} \quad (A3.3c)$$

$$\begin{aligned} \frac{d}{dt} nNF\kappa B(t) &= kd1a \times (nI\kappa B\alpha: nNF\kappa B)(t) \\ &\quad - ka1a \times nI\kappa B\alpha(t) \times nNF\kappa B(t) + ki1 \times kv \times NF\kappa B(t) \\ &\quad - ke1 \times kv \times nNF\kappa B(t) \end{aligned} \quad (A3.3d)$$

$$\begin{aligned} \frac{d}{dt} I\kappa B\alpha(t) &= kd1a \times (I\kappa B\alpha: NF\kappa B)(t) - ka1a \times I\kappa B\alpha(t) \times NF\kappa B(t) \\ &\quad + c2a \times tI\kappa B\alpha(t) - c4a \times I\kappa B\alpha(t) - ki3a \times I\kappa B\alpha(t) \\ &\quad + ke3a \times nI\kappa B\alpha(t) - kc1a \times IKKa(t) \times I\kappa B\alpha(t) \end{aligned} \quad (A3.3e)$$

$$\begin{aligned} \frac{d}{dt} nI\kappa B\alpha(t) &= kd1a \times (nI\kappa B\alpha: nNF\kappa B)(t) \\ &\quad - ka1a \times nI\kappa B\alpha(t) \times nNF\kappa B(t) - c4a \times nI\kappa B\alpha(t) \\ &\quad + ki3a \times kv \times I\kappa B\alpha(t) - ke3a \times kv \times nI\kappa B\alpha(t) \end{aligned} \quad (A3.3f)$$

$$\frac{d}{dt} A20(t) = c2 \times tA20(t) - c4 \times A20(t) \quad (A3.3g)$$

$$\frac{d}{dt} tI\kappa B\alpha(t) = c1a \times \frac{nNF\kappa B^h(t)}{nNF\kappa B^h(t) + k^h} - c3a \times tI\kappa B\alpha(t) \quad (\text{A3.3h})$$

$$\frac{d}{dt} tA20(t) = c1 \times \frac{nNF\kappa B^h(t)}{nNF\kappa B^h(t) + k^h} - c3 \times tA20(t) \quad (\text{A3.3i})$$

$$\begin{aligned} \frac{d}{dt} (I\kappa B\alpha: NF\kappa B)(t) & \quad (\text{A3.3j}) \\ & = ka1a \times I\kappa B\alpha(t) \times NF\kappa B(t) - kd1a(I\kappa B\alpha: NF\kappa B)(t) \\ & \quad - c5a \times (I\kappa B\alpha: NF\kappa B)(t) + ke2a \times (nI\kappa B\alpha: nNF\kappa B)(t) \\ & \quad - kc2a \times IKKa(t) \times (I\kappa B\alpha: NF\kappa B)(t) \end{aligned}$$

$$\begin{aligned} \frac{d}{dt} (nI\kappa B\alpha: nNF\kappa B)(t) & \quad (\text{A3.3k}) \\ & = ka1an \times nI\kappa B\alpha(t) \times nNF\kappa B(t) \\ & \quad - kd1a(nI\kappa B\alpha: nNF\kappa B)(t) \\ & \quad - ke2a \times kv \times (nI\kappa B\alpha: nNF\kappa B) \end{aligned}$$

with the inclusion of the linear chain:

$$\frac{d}{dt} tI\kappa B\alpha\alpha(t) = delay \times (tI\kappa B\alpha b(t) - tI\kappa B\alpha\alpha(t)) \quad (\text{A3.3l})$$

$$\frac{d}{dt} tI\kappa B\alpha b(t) = delay \times (tI\kappa B\alpha c(t) - tI\kappa B\alpha b(t)) \quad (\text{A3.3m})$$

$$\frac{d}{dt} tI\kappa B\alpha c(t) = delay \times (tI\kappa B\alpha d(t) - tI\kappa B\alpha c(t)) \quad (\text{A3.3n})$$

$$\frac{d}{dt} tI\kappa B\alpha d(t) = delay \times (tI\kappa B\alpha(t) - tI\kappa B\alpha d(t)) \quad (\text{A3.3o})$$

The parameterisation is as follows:

<b>Parameters</b>			
<i>TNFκB</i>	0.08μM	<i>c1</i>	$1.4 \times 10^{-7} \mu\text{Ms}^{-1}$
<i>TIKK</i>	0.08μM	<i>c2</i>	$0.25\text{s}^{-1}$
<i>kv</i>	3.3	<i>c3</i>	$0.00072\text{s}^{-1}$
<i>ka1a</i>	$0.5\mu\text{Ms}^{-1}$	<i>c4</i>	$0.0045\text{s}^{-1}$
<i>ka1an</i>	$0.5\mu\text{Ms}^{-1}$	<i>ki3a</i>	$0.0001\text{s}^{-1}$
<i>kd1a</i>	$0.0005\text{s}^{-1}$	<i>ke3a</i>	$0.00005\text{s}^{-1}$
<i>ke2a</i>	$0.01\text{s}^{-1}$	<i>ki1</i>	$0.0044\text{s}^{-1}$
<i>c1a</i>	$1.4 \times 10^{-7} \mu\text{Ms}^{-1}$	<i>ke1</i>	$0.000088\text{s}^{-1}$
<i>c2a</i>	$0.65\text{s}^{-1}$	<i>kc1a</i>	$0.074\text{s}^{-1}$
<i>c3a</i>	$0.0003\text{s}^{-1}$	<i>kc2a</i>	$0.37\text{s}^{-1}$
<i>c4a</i>	$0.000325\text{s}^{-1}$	<i>kt2a</i>	$0.1\text{s}^{-1}$
<i>c5a</i>	$0.000022\text{s}^{-1}$	<i>kbA20</i>	0.0018μM
<i>kp</i>	$0.0006\text{s}^{-1}$	<i>TR</i>	1/0
<i>ka</i>	$0.006\text{s}^{-1}$	<i>k</i>	0.065μM
<i>ki</i>	$0.003\text{s}^{-1}$	<i>h</i>	2
<i>delay</i>	0.003 at 37°C 0.0095 at 40°C		

Similarly, the initial conditions were found by setting all variable concentrations to equal 0, TR=0 and allowing the system to equilibrate for 4000-minutes.

### A3.4 – Dual Delay Model

For this system the same variable and parameter notations as in Appendix 1 has been used. This model is a system of 19 ODEs consisting of:

$$\begin{aligned} \frac{d}{dt} IKKn(t) = & kp \times (TIKK - IKKn(t) - IKKi(t)) \\ & \times \frac{kbA20}{kbA20 + TR \times A20(t)} - TR \times ka \times IKKn(t) \end{aligned} \quad (A3.4a)$$

$$\frac{d}{dt} IKKa(t) = TR \times ka \times IKKn(t) - ki \times IKKa(t) \quad (A3.4b)$$

$$\begin{aligned} \frac{d}{dt} NF\kappa B(t) = & kd1a \times (I\kappa B\alpha: NF\kappa B)(t) - ka1a \times I\kappa B\alpha(t) \times NF\kappa B(t) \\ & - ki1 \times NF\kappa B(t) + ke1 \times nNF\kappa B(t) \\ & + kt2a \times IKKa(t) \\ & \times \left( TNF\kappa B - NF\kappa B(t) - (I\kappa B\alpha: NF\kappa B)(t) \right. \\ & \left. - \frac{(nNF\kappa B(t) + (nI\kappa B\alpha: nNF\kappa B)(t))}{kv} \right) \\ & + c5a \times (I\kappa B\alpha: NF\kappa B)(t) \end{aligned} \quad (A3.4c)$$

$$\begin{aligned} \frac{d}{dt} nNF\kappa B(t) = & kd1a \times (nI\kappa B\alpha: nNF\kappa B)(t) \\ & - ka1a \times nI\kappa B\alpha(t) \times nNF\kappa B(t) + ki1 \times kv \times NF\kappa B(t) \\ & - ke1 \times kv \times nNF\kappa B(t) \end{aligned} \quad (A3.4d)$$

$$\begin{aligned} \frac{d}{dt} I\kappa B\alpha(t) = & kd1a \times (I\kappa B\alpha: NF\kappa B)(t) - ka1a \times I\kappa B\alpha(t) \times NF\kappa B(t) \\ & + c2a \times tI\kappa B\alpha\alpha(t) - c4a \times I\kappa B\alpha(t) - ki3a \times I\kappa B\alpha(t) \\ & + ke3a \times nI\kappa B\alpha(t) - kc1a \times IKKa(t) \times I\kappa B\alpha(t) \end{aligned} \quad (A3.4e)$$

$$\begin{aligned} \frac{d}{dt} nI\kappa B\alpha(t) = & kd1a \times (nI\kappa B\alpha: nNF\kappa B)(t) \\ & - ka1a \times nI\kappa B\alpha(t) \times nNF\kappa B(t) - c4a \times nI\kappa B\alpha(t) \\ & + ki3a \times kv \times I\kappa B\alpha(t) - ke3a \times kv \times nI\kappa B\alpha(t) \end{aligned} \quad (A3.4f)$$

$$\frac{d}{dt} A20(t) = c2 \times tA20a(t) - c4 \times A20(t) \quad (A3.4g)$$



$$\frac{d}{dt} tIkB\alpha(t) = c1a \times \frac{nNF\kappa B^h(t)}{nNF\kappa B^h(t) + k^h} - c3a \times tIkB\alpha(t) \quad (A3.4h)$$

$$\frac{d}{dt} tA20(t) = c1 \times \frac{nNF\kappa B^h(t)}{nNF\kappa B^h(t) + k^h} - c3 \times tA20(t) \quad (A3.4i)$$

$$\frac{d}{dt} (IkB\alpha: NF\kappa B)(t) \quad (A3.4j)$$

$$\begin{aligned} &= ka1a \times I\kappa B\alpha(t) \times NF\kappa B(t) - kd1a (IkB\alpha: NF\kappa B)(t) \\ &- c5a \times (IkB\alpha: NF\kappa B)(t) + ke2a \times (nIkB\alpha: nNF\kappa B)(t) \\ &- kc2a \times IKKa(t) \times (IkB\alpha: NF\kappa B)(t) \end{aligned}$$

$$\frac{d}{dt} (nIkB\alpha: nNF\kappa B)(t) \quad (A3.4k)$$

$$\begin{aligned} &= ka1an \times nIkB\alpha(t) \times nNF\kappa B(t) \\ &- kd1a (nIkB\alpha: nNF\kappa B)(t) \\ &- ke2a \times kv \times (nIkB\alpha: nNF\kappa B) \end{aligned}$$

with the inclusion of the linear chains:

$$\frac{d}{dt} tA20a(t) = delay \times (tA20b(t) - tA20a(t)) \quad (A3.4l)$$

$$\frac{d}{dt} tA20b(t) = delay \times (tA20c(t) - tA20b(t)) \quad (A3.4m)$$

$$\frac{d}{dt} tA20c(t) = delay \times (tA20d(t) - tA20c(t)) \quad (A3.4n)$$

$$\frac{d}{dt} tA20d(t) = delay \times (tA20(t) - tA20d(t)) \quad (A3.4o)$$

$$\frac{d}{dt} tIkB\alpha\alpha(t) = delay \times (tIkB\alpha b(t) - tIkB\alpha\alpha(t)) \quad (A3.4p)$$

$$\frac{d}{dt} tIkB\alpha b(t) = delay \times (tIkB\alpha c(t) - tIkB\alpha b(t)) \quad (A3.4q)$$

$$\frac{d}{dt}tIkBac(t) = delay \times (tIkBad(t) - tIkBac(t)) \quad (A3.4r)$$

$$\frac{d}{dt}tIkBad(t) = delay \times (tIkBa(t) - tIkBad(t)) \quad (A3.4s)$$

The parameterisation is as follows:

Parameters			
<i>TNFκB</i>	0.08μM	<i>c1</i>	1.1 x 10 <sup>-7</sup> μMs <sup>-1</sup>
<i>TIKK</i>	0.08μM	<i>c2</i>	0.3s <sup>-1</sup>
<i>kv</i>	3.3	<i>c3</i>	0.00072s <sup>-1</sup>
<i>ka1a</i>	0.5μMs <sup>-1</sup>	<i>c4</i>	0.0055s <sup>-1</sup>
<i>ka1an</i>	0.5μMs <sup>-1</sup>	<i>ki3a</i>	0.001s <sup>-1</sup>
<i>kd1a</i>	0.0007s <sup>-1</sup>	<i>ke3a</i>	0.0005s <sup>-1</sup>
<i>ke2a</i>	0.01s <sup>-1</sup>	<i>ki1</i>	0.005s <sup>-1</sup>
<i>c1a</i>	1.1x10 <sup>-7</sup> μMs <sup>-1</sup>	<i>ke1</i>	0.0001s <sup>-1</sup>
<i>c2a</i>	0.65s <sup>-1</sup>	<i>kc1a</i>	0.074s <sup>-1</sup>
<i>c3a</i>	0.0002s <sup>-1</sup>	<i>kc2a</i>	0.37s <sup>-1</sup>
<i>c4a</i>	0.000325s <sup>-1</sup>	<i>kt2a</i>	0.1s <sup>-1</sup>
<i>c5a</i>	0.000033s <sup>-1</sup>	<i>kbA20</i>	0.0019μM
<i>kp</i>	0.0009s <sup>-1</sup>	<i>TR</i>	1/0
<i>ka</i>	0.009s <sup>-1</sup>	<i>k</i>	0.065μM
<i>ki</i>	0.0035s <sup>-1</sup>	<i>h</i>	2

The delay parameter values for each temperature are:

Temperature (°C)	Delay Parameter Value
40	0.0080
39	0.0055
37	0.0036
35	0.0025

Similarly, the initial conditions were found by setting all variable concentrations to equal 0, TR=0 and allowing the system to equilibrate for 4000-minute.